Femtosecond Electron Diffraction: Next generation electron sources for atomically resolved dynamics

Dissertation

zur Erlangung des Doktorgrades

des Department Physik

der Universität Hamburg

vorgelegt von

Dipl. Phys. JULIAN HIRSCHT

aus MINDEN

Hamburg

2015

Gutachter der Dissertation:	Prof. Dr. R.J. Dwayne Miller Prof. Dr. Henry N. Chapman
Gutachter der Disputation:	Prof. Dr. R.J. Dwayne Miller Prof. Dr. Franz X. Kärtner
Datum der Disputation:	16. Juli 2015
Vorsitzender des Prüfungsausschusses:	Prof. Dr. Michael A. Rübhausen
Vorsitzender des Promotionsausschusses:	Prof. Dr. Jan Louis
Dekanin/Dekan der MIN Fakultät:	Prof. Dr. Heinrich Gräner

Meiner ganzen Familie und geliebten Antonia.

PREFACE

I will describe the outcome and core findings of my effort to obtain this doctoral degree. With my arrival in the freshly founded Hamburg group of Prof. R. J. Dwayne Miller at the beginning of 2010, I picked up basic engineering skills to speed up the construction of new setups for electron diffraction in the empty laboratories on the campus of DESY in Hamburg. Initially, two engineers of the university assisted us part-time, but a professorial directive cut their availability to our group shortly after they were engaged. As a consequence I found myself with the tasks of designing and building core elements for a new scientific accelerator, the *Relativistic Electron Gun for Atomic Exploration* (REGAE), to meet our group's obligations to provide previously settled contributions to that machine. I was also in charge of supervising and leading the construction of another compact DC electron diffraction setup, the *E-Gun* 300, becoming the leading engineering scientist for our fast growing group and a interdisciplinary working physicist. The more time I spent engineering the more I learned about cost effective designing and machining that is used for the realization of our experimental needs. This process is still ongoing as we research and apply more techniques and as new developments become available. A pool of knowledge started to grow, which should become the basis for independent ground-breaking machine design at a later period of my PhD work.

During the course of the installation of the first two electron diffraction machines I came to understand the limitations and problems inherent in the commonly employed design of DC operated diffraction setups. We ran into radiation safety concerns as we exceeded a critical electron energy, above which we had to meet x-ray protection and radiation safety requirements. The machines developed by our group were also not working to the full expectation of design, as we increased the electron energy above previous levels. I began to study high voltage and electrical engineering to solve the problem of high voltage breakdowns, which were encountered and subsequently constrained the operation of our compact installations. I started from scratch with the design of a new compact DC operated setup, the *Femtosecond Electron Diffraction CAmera for Molecular Movies* (FED-CAMM). I implemented the high voltage design necessities into this new design, seeing fundamental design aspects always in relation to an optimal design for a femtosecond electron diffraction experiment, which uses the shortest available electron pulses. Working mainly as an engineer for most of my PhD work, I found it nonetheless necessary to possess an in-depth knowledge of physics, which has to be incorporated into the design of these instruments.

Initially I was meant to work on a specific specimen system. The construction of the new setups was supposed to be straight forward and to not take more than a couple of month, leaving sufficient time for the extensive study of the dynamic properties of the assigned specimen system. The initial assumptions regarding the time spans required to

build the new setups proved false, which was also due to a lack of knowledge concerning the difficulties which we were heading into with the new scientific instruments. It took more than 1 and 1/2 years to REGAEs' first electron beam test, and this test did not include any electron diffraction. At least 2 and 1/2 years passed before the preliminary clearance, regulated by DESY radiation safety, was present to test the compact E-Gun 300. Until then no extensive investigation of any specimen system was possible. First preparations concerning the assigned specimen system were made but were unsuccessful. At that time the outcome of my PhD was most uncertain.

The proportion of time required to set up our new instruments required all capacities of my workload throughout my PhD period. In order to transform my duties of engineering into the activities of a scientific work I focused my acquired skills on the evolution of new instruments and postponed the investigation of the assigned specimen system. Outstanding scientific instruments are, by necessity, a prerequisite for the conduction of those prospective and outstanding investigations planned for in the group. Thus I spent time analyzing the current machine limitations as they arose during the course of new setup development and started to work on solutions, which were realizable within the rest of my PhD time. With this refocussing of my PhD work any further delay which occurred during these years and the introduction of new setups was at least part of the development of the new instruments. This was beneficial as any further delay from manufacture belonged to the context of my PhD work; as opposed to having my research delayed due to a dependence on machine function, of which the construction would form a negligible part of my PhD work, despite consuming the majority of my time. Unfortunately, the development of custom experimental setups is often not as appreciated as publications in science journals with high impact factors. However, in experimental physics there is no publication possible without an appropriate experimental installation.

Of all three setups built, the compact FED-CAMM that is operated with static DC electric fields is one of the most promising results of this work and defines the current state-of-the-art, aside from the availability of at least three new instruments for time-resolved electron diffraction directly resulting from my efforts. The FED-CAMM prototype is flexible in many ways, utilizes the most advanced tools for the manufacturing and operates on the edge of physical, but not design limitations. It can keep up with the newest applications for electron diffraction experiments such as investigations of structural dynamics in liquid environments and has sufficient flexibility for future extensions of the setup. Comparing the FED-CAMM to the previous worldwide existing compact setups, the energy is almost tripled, which leads to improved penetration depths of the electrons. The spatial resolution is improved by at least a factor of two, which is due to the finer de Broglie wavelength of 0.02 $\AA$, beam apertures and electron lens improvements, which are incorporated into the setup. There is no other known source,

which is operated with DC fields and possesses a shorter electron pulse duration. A predicted default temporal resolution of 109 femtoseconds (fwhm) is unchallenged, but can be as short as 70 fs (fwhm) with 10^4 electrons per pulse. Even 10^5 electrons can be contained in sub-200 fs (fwhm) electron pulses that are sufficiently bright for structural investigations of various structures with single shots. With this development novel experimental findings can be realized. The improvement of the pulse duration compared to other setups can be obtained, since the electric field gradients can be increased to very intense levels, without an emergence of dark current. Additionally, the electron number per pulse can be decreased to reach pulse durations below 70 fs (fwhm) which is less than the shortest pulse duration that was previously predicted as the lowest limit in literature.

Molecular movies require advanced tools which are now available in various setup of different sizes, from the highly relativistic REGAE to the compact E-Gun 300 and the FED-CAMM. These three new instruments allow the implementation of the long pursued goal of the observation of molecular dynamics with real femtosecond temporal resolution. Especially the compact prototype of the FED-CAMM is guiding future developments in that instrument class and is leading the way for the engineering of advanced and stable DC operated machines. This is because its design incorporates solutions to the high voltage instabilities, which were previously observed with the E-Gun 300 prototype, but which can also be found in other devices that utilize high voltages for the fast acceleration of electrons. Furthermore, the FED-CAMM is free of timing jitter, which is typically inherent to rf-operated electron sources. The energy range of both the FED-CAMM and the REGAE is sufficient to penetrate thicker targets and specimen encapsulations such as liquid cells for solution phase investigations. Currently a maximum of 800 keV could be applied in a compact setup design. More information is given in the specific chapters of this thesis.

This PhD work is a good foundation for a promising and novel class of experiments. These will hold the potential for novel insights into the fundamental processes of nature. The instrument developments also represent the groundwork for future setups and successors in this field, which attempt to unveil ultrafast dynamic structural transformations. The stage is now set for the visualization of ultrafast structural changes, which were not observable in this great detail before.

ABSTRACT

Three instruments for *femtosecond electron diffraction* (FED) experiments were erected, partially commissioned and used for first diffraction experiments. The *Relativistic Electron Gun for Atomic Exploration* (REGAE) was completed by beamline elements including supports, a specimen chamber and dark current or electron beam collimating elements such that the commissioning process, including first diffraction experiments in this context, could be started. The temporal resolution of this machine is simulated to be 25 fs (fwhm) short, while a transverse coherence length of 30 nm (fwhm) is feasible to resolve proteins on this scale. Whether this machine is capable of meeting these predictions or whether the dynamics of the electron beam will stay limited by accelerator components, is not finally determined by the end of this work, because commissioning and improvement of accelerator components is ongoing. Simultaneously, a compact DC electron diffraction apparatus, the E-Gun 300, designed for solid and liquid specimens and a target electron energy of 300 keV, was built. Fundamental design issues of the high potential carrying and beam generating components occurred and are limiting the maximum potential and electron energy to 120 keV. Furthermore, this is limiting the range of possible applications and consequently the design and construction of a brand new instrument began. The *Femtosecond Electron Diffraction CAmera for Molecular Movies* (FED-CAMM) bridges the performance problems of very high electric potentials and provides optimal operational conditions for all applied electron energies up to 300 keV. The variability of gap spacings and optimized manufacturing of the high voltage electrodes lead to the best possible electron pulse durations obtainable with a compact DC setup, that does not comprise of rf-structures. This third apparatus possesses pulse durations just a few tenth femtoseconds apart from the design limit of the highly relativistic REGAE and combines the advantages of simplicity and stability of a compact FED apparatus with the short temporal resolution of femtosecond accelerators, which are operated with or include rf structures. Simulations of the electron beam dynamics and the fact that the apparatus is stable in respect to high voltages and electric field gradients above 27 MV/m allows the conclusion, that a temporal resolution significantly below 100 fs (fwhm), perhaps even shorter than 70 fs, can be achieved. This instrument currently defines the state-of-the-art. Firstly, because high voltage feedthrough for these potentials are commercially still not available, with a subsequent limiting of the potentials and consequent lowering of the electron numbers per pulse as well as the pulse durations and electron penetration. Secondly, this is because research communities focus on photon and rf-based electron sources for the achievement of sub-100 fs pulses, which typically include timing-jitter. Here it is shown that simple DC acceleration can lead to the same, satisfactory pulse duration up to an energy of a few hundred keV, potentially as high as 800 keV.

ZUSAMMENFASSUNG

Drei Instrumente für die Durchführung von *Femtosekunden Elektronen Diffraktionsexperimenten* (FED) wurden gebaut, teilweise kommissioniert und für Diffraktionsexperimente benutzt. Die *Relativistische Elektronen Kanone für Atomare Erforschung* (REGAE) wurde durch Strahlrohre und Gestelle, Probenkammer und Dunkelstrom- bzw. Elektronenstrahl-Kollimationselemente komplettiert, sodass die Kommissionierung beginnen und erste Experimente durchgeführt werden konnten. Die Zeitauflösung dieser Maschine ist laut Simulationen bis zu 25 fs (fwhm) kurz, mit einer transversalen Kohärenzlänge von 30 nm (fwhm), um auch Proteine in dieser Grössenordnung auflösen zu können. Ob diese Anlage die theoretischen Vorhersagen erfüllen kann, oder ob die Dynamik des Elektronenstrahls durch Beschleunigerkomponenten begrenzt bleibt, ist zum Ende dieser Arbeit noch nicht abschliessend geklärt, da die Kommissionierung und Verbesserung von Beschleunigerkomponenten andauern. Zeitgleich wurde ein kompaktes DC Experiment - die E-Gun 300 - gebaut für Proben der Festkörper- und flüssigen Phase und einer Elektronenenergie von 300 keV. Grundlegende Probleme der hochspannungsführenden und strahlerzeugenden Komponenten begrenzen die maximale Betriebsspannung und somit Elektronenenergie auf 120 keV. Da dies die Anwendungsmöglichkeiten beschränkt wurde mit dem Entwurf und Bau einer neuen Anlage begonnen. Die *Femtosekunden Elektronen Beugungskamera für Molekulare Filme* (FED-CAMM) überbrückt die Probleme der Hochspannungsbegrenzung bei sehr hohen Potentialverläufen und bietet optimale Betriebsbedingungen für alle vorhandenen Elektronenenergien bis zu 300 keV. Die Einstellbarkeit des Beschleunigungsspalts und optimierte Herstellungsverfahren der Hochspannungselektroden führen zu jeweils kürzesten Elektronenpulsen, die mit kompakten DC Beschleunigern ohne HF-Strukturen erzeugt werden können. Dieses dritte Experiment liegt in der Zeitauflösung nur wenige zehn Femtosekunden vom Ziel von REGAE entfernt und vereint die Vorteile eines kompakten Aufbaus mit der kurzen Zeitauflösung von relativistischen Beschleunigeranlagen mit HF-Strukturen. Simulationen und die Tatsache, dass die Anlage mit hohen Spannungen und intensiven Feldstärken von mehr als 27 MV/m stabil funktioniert, lassen den Schluss zu, dass eine Zeitauflösung von weit weniger als 100 fs (fwhm), sogar weniger als 70 fs, erreicht werden kann. Die Anlage definiert den Stand der Technik neu. Zum einen, weil kommerzielle Hochspannungsdurchführungen für diese hohen Spannungen nicht verfügbar sind, welches die Betriebsspannung und die Elektronendynamik stark einschränkt. Desweiteren konzentrieren sich Forschergruppen auf Photonen und HF-Elektronenquellen für Lichtpulse kürzer als 100 fs, welche jedoch Zeitungenauigkeiten beinhalten. Hier wird gezeigt, dass DC-Beschleuniger die gleichen Pulsdauern mit Energien von einigen hundert keV, potentiell bis zu 800 keV erzeugen können.

CONTENTS

ACRONYMS

ALS	Advanced Light Source, see http://www-als.lbl.gov/
AS	Australian Synchrotron, see http://www.synchrotron.org.au/
ASTRA	A Space Charge Tracking Algorithm
BESSY	Berliner Elektronenspeicherring-Gesellschaft für Synchrotronstrahlung m.b.H.
CAD	Computer Aided Design
CF	ConFlat, see ISO/TS 3669-2:2007
CFEL	Center for Free Electron Laser Science, see http://www.cfel.de
CLS	Canadian Light Source, see http://www.lightsource.ca/
CNC	Computerized Numerical Control
CSDA	Continuous Slowing Down Approximation
CST	Computer Simulation Technology, see https://www.cst.com/
CTEM	Conventional Transmission Electron Microscope
CUI	Center for Ultrafast Imaging, see http://www.cui.uni-hamburg.de/en/
DC	Direct Current
DESY	Deutsches Electronen SYnchrotron, see http://www.desy.de/
DNA	Deoxyribonucleic acid
DTEM	Dynamic Transmission Electron Microscope
Euratom	European Atomic Energy Community, see http://ec.europa.eu/
FED	Femtosecond Electron Diffraction
FED-CAMM	Femtosecond Electron Diffraction CAmera for Molecular Movies
FEL	Free Electron Laser
FLASH I	Free electron LASer in Hamburg I, see http://flash.desy.de/
FLASH II	Free electron LASer in Hamburg II, see http://flash2.desy.de/
FWHM	Full Width At Half Maximum

GPT	General Particle Tracer, see http://www.pulsar.nl/gpt/
ILC	International Linear Collider, see http://www.linearcollider.org/
ISO	International Organization for Standardization
ISO-K	also ISO-F, see ISO 1609
KF	Kleinflansch, see ISO 2861
LCLS	Stanford Linear Coherent Light Source, see http://lcls.slac.stanford.edu
LINAC	LINear ACcelerator
MC	Monte Carlo
REGAE	Relativistic Electron Gun for Atomic Exploration, see http://regae.desy.de/
PETRA III	Positron Electron Tandem Ring Accelerator III, see http://petra3.desy.de/
RF	also HF, Radiofrequency
RMS	Root Mean Square
RöV	Röntgenschutzverordnung (abbr., German X-Ray Ordinance)
SACLA	Spring-8 Angstrom Compact Free Electron Laser
SASE	Self Amplified Stimulated Emission
SNR	Signal to Noise Ratio
Spring-8	Super Photon Ring 8 GeV, see http://www.spring8.or.jp/
STEP	STandard for the Exchange of Product model data
StrlSchV	Strahlenschutzverordnung (abbr., German Radiation Protection Ordinance)
SwissFEL	Swiss Free Electron Laser, see http://www.psi.ch/swissfel/
TEM	Transmission Electron Microscope
TESLA	Tera Electron Volt Energy Superconducting Linear Accelerator
TTC	TESLA Technology Cooperation, see http://tesla-new.desy.de/
UED	Ultrafast Electron Diffraction
UHV	Ultra-High Vacuum: $\leq 1 \cdot 10^{-8}$ mbar
UV	Ultra-Violet
XFEL	European X-Ray Free Electron Laser, see http://www.xfel.eu/

T	Tera $= 10^{12} = 1,000,000,000,000$
G	Giga $= 10^{9} = 1,000,000,000$
M	Mega $= 10^{6} = 1,000,000$
k	Kilo $= 10^{3} = 1,000$
h	Hecto $= 10^{2} = 100$
da	Deca $= 10^{1} = 10$
d	Deci $= 10^{-1} = 0.1$
c	Centi $= 10^{-2} = 0.01$
m	Milli $= 10^{-3} = 0.001$
μ	Micro $= 10^{-6} = 0.000,001$
n	Nano $= 10^{-9} = 0.000,000,001$
p	Pico $= 10^{-12} = 0.000,000,000,001$
f	Femto $= 10^{-15} = 0.000,000,000,000,001$
a	Atto $= 10^{-18} = 0.000,000,000,000,000,001$

m	Meter
kg	Kilogramm
s	Second
A	Ampere
c	Speed of light in vacuum = $299,792,458$ $\frac{\mathrm{m}}{\mathrm{s}}$
C	Coulomb, 1 C = 1 A·s
Da	Dalton = $1.660538921 \cdot 10^{-27}$ kg
m_e	Mass of electron = $9.1093829140 \cdot 10^{-31}$ kg
Hz	Hertz $\frac{1}{\mathrm{s}}$

J	Joule $\frac{\mathrm{kg\,m^2}}{\mathrm{s^2}}$
N	Newton $\frac{\mathrm{kg \cdot m}}{\mathrm{s^2}}$
V	Volt $\frac{\mathrm{kg\,m^2}}{\mathrm{A\,s^3}}$
e	Elementary charge = $1.602176565 \cdot 10^{-19}$ C
eV	Electron Volt = $1.602176565 \cdot 10^{-19}$ J
W	Watt $\frac{\mathrm{kg\,m^2}}{\mathrm{s^3}}$
γ	Lorentz factor $\gamma = \frac{1}{\sqrt{1-\mathrm{v^2/c^2}}}$

1 INTRODUCTION

New instruments for time-resolved studies in the femtosecond range via electron diffraction were developed in this work. At the beginning of this introduction, the motivation and methods for obtaining molecular movies are outlined [1.1]. Within this chapter, the important concept of the connection of structure with functionality and the significance of the determination of dynamical structural changes is explained together with a relation to the time domains and length scales of interest [1.1.1, 1.1.2, 1.1.3]. The method of gaining structural information via diffraction experiments and the underlying experimental pump-probe setup are explained [1.1.4, 1.1.5] to provide all necessary information on the background to the making of molecular movies. In the following chapter instruments are then introduced to the reader [in particular 2.2 and 2.3] which can potentially resolve fast structural dynamics. The description of electron sources is supplemented by a discourse on the requirements and beam dynamics of electron beams [2.4], which is a important characteristic that constrains and guides instrument design. A review of the two types of radiation which are generally used including the radiation specific interaction and as a consequence thereof, the emerging experiments are discussed [6.4]. The information given up to that point allows for the comparison of existing setups, currently and prospectively in operation, for the purpose of time-resolved diffraction experiments with photons and electrons for the creation of molecular movies to the instruments and developments of this Ph.D. work [chapter 3, 4 and 5]. Section 1.2 provides an overview of the different projects as well as their relative timelines and explains the path taken during this work. A section for the structure and significance of this work [1.4] rounds up the introduction and sketches the outline of the main text.

1.1 MOTIVATION AND METHODS FOR MOLECULAR MOVIES

1.1.1 STRUCTURE-FUNCTION-CORRELATION

The structure and composition determine the function - a fundamental statement in physics, chemistry and biology which is valid on the scale of single atoms, in molecules, in multi-molecular compounds which build up proteins as well as on the scale of cells and large biological systems. To provide an example - it is the arrangement of atoms and the composition of a crystalline compound which leads to the conduction of electrons, semi-conducting behavior or perfect insulating properties. The compositions of materials can be changed to modify their properties. Within this context it is mentioned that even by the temporary manipulation and deformation of lattice structures it is possible to

change the electronic properties of a compound, which for example can be achieved with temperature changes [Ota et al. (2002), Goodson et al. (2003)]. Insulators can be converted into conductive materials as long as the structural deformation is present. Of great interest in this regard is the ongoing research potentially demonstrating that light pulses can trigger conducting and superconducting material states [e.g. Gao et al. (2013), Singla et al. (2013)]. This is a very promising field of research targeting the fabrication of macroscopic systems for wide usage in industries and a revolution of energy transfer. A second example for the structure-function-correlation are the chemical properties of a molecule, which depend on the composition, electronic configuration and three dimensional orientation of the atoms belonging to this molecule in space. The three-dimensional structure and the electronic configuration of a molecule determines the extent to which a molecule is reactive or chemically stable. The description of the physics of electronic properties which determine ground and excited states and eventually describe the contribution of charges to a conduction band in crystalline compounds are closely connected.

A third example is taken from the field of biology. The interaction of ultraviolet radiation with the DNA of skin cells causes local deformations of the DNA structure, which can contribute to mutagen processes and subsequently promote skin cancer. Common photo-products are cyclobutane pyrimidine dimers and $6-4$ photo-products. Pyrimidine dimers are detected by photolytic enzymes, which dock to these sites within fractions of a second to cover the lesion, triggering the repair process that follows. The energy required for the structural rearrangement is provided by the incidence of another UV-photon, which enables the breaking of incorrectly linked molecular bonds and their rearrangement. A prerequisite for this process is the capability to detect a certain anomaly along the DNA. This is achieved by having a distinct shape and hence the functional capabilities that is the result of the composition and structure of the involved molecular machinery. Almost 120 years ago in 1894 a statement in this regard was formulated by Hermann E. Fischer [Fischer (1894)]. He said that an enzyme and its substrate must have complementary structures which fit together like a "lock and key", in order to undergo a chemical reaction. This is also true for other bio-chemical processes on various scales. For his findings he was awarded the second Nobel price in physics [Nobelprize 1902]. An illustration of a possible repair scheme of a $6-4$ photo-product with the photolyase of drosophila melanogaster is shown in figure 1.

A large number of different structures are present in a living cell and an equally large variation of molecular machines must exist which keep the DNA and cell alive and functional, besides the fact that there is a myriad of cell variations. An interpretation of the chemical reaction dynamics cannot be made without the information of the structure and associated physico-chemical properties. This is why there is much interest in mapping all available structures in corresponding facilities. A structure which is present in all

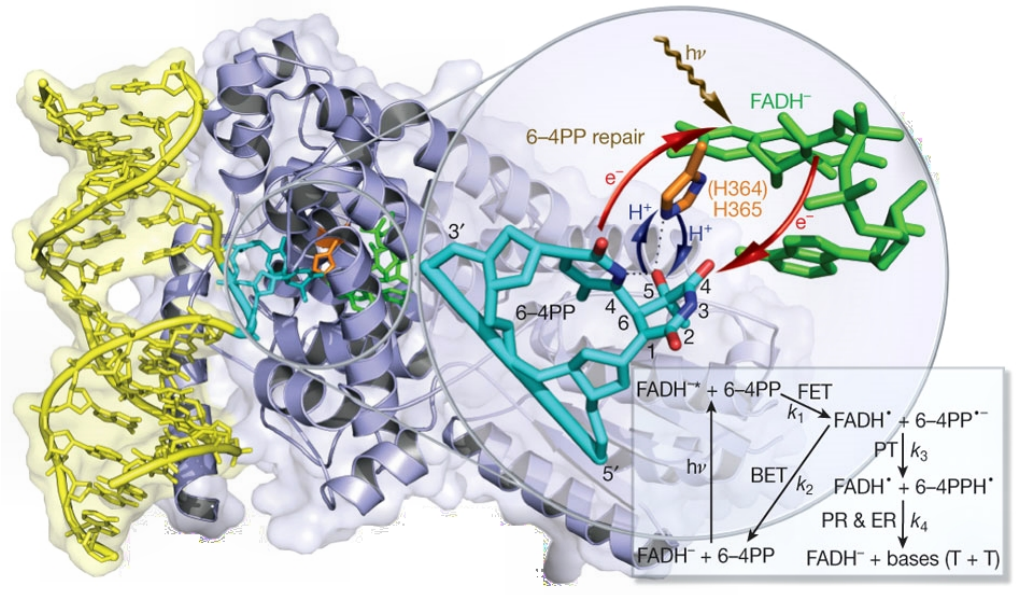

Figure 1: Example of a photolyase enzyme, this one is of the drosophila melanogaster, involved in the repair of a $6-4$ photo-product. Reprinted by permission from Macmillan Publishers Ltd: Nature, Li et al. (2010a). Copyright 2010, rights Managed by Nature Publishing Group.

living cells is the ribosome, which is responsible for the synthesis of polypeptides. A major achievement in this regard was accomplished by Ada E. Yonath, who dedicated decades to the crystallization of ribosomes from various bacteriogenic organisms. In 1986 first diffraction patterns with x-ray radiation were published [Yonath et al. (1986)] and in 2009 she was awarded with the Nobel prize in physics together with Venkatraman Ramakrishan and Thomas Steitz [Nobelprize 2009].

Comparing the third example to the first, we zoom out from the atomic scale to macromolecular systems which have super-structural properties exceeding the configuration of single atoms. We also widen the time span within which processes occur. Electrons change their position in relation to the nuclei and atoms change their state of excitement within attoseconds. Chemical reactions happen in the order of 100 femtoseconds and slower. Biological processes in cells take place in the millisecond timescale. A relation seems to exist between the size and complexity of structures and the speed of structural changes. When structure is directly linked to a function it means that by understanding structures we gain insights into the modus operandi of natures elements on the small, medium and large scale. Furthermore if a fundamental understanding of structure-function correlation is present, it can be aimed at artificially creating structures which possess certain physical, chemical or biological properties. One can consider the design of drugs and agents to cure diseases. For example, exploratory studies on ribosome structures gives hope for the development of new antibiotics [e.g. Schlünzen et al. (2001), Nolan et al. (2010)]. Of course, there are similar important structure-function

relationships in controlling the macroscopic properties of materials from magnetism to degrees of electron conductivity.

1.1.2 DYNAMICAL STRUCTURAL CHANGES

While the complexity of systems scales with their size, it becomes necessary to determine the dynamics and the evolution of changes within a physical transformation, a chemical reaction or biological process. The resolution of static physio-chemical structures alone is no longer sufficient to explain the mechanisms and the functionality of a system. The nature of life itself is dynamic and needs to be investigated in its natural state. The investigation of the chronology of structural transformations clarifies how things evolve, interact and are connected with each other. This in combination with the pure structure analysis forms a crucial part of the jigsaw puzzle that reveals natures secrets. Within the process of interest it is very important that each step is accurately resolved to be correctly understood and linked.

A famous and simple example illustrates how the recording of the structural evolution together with structural determinations contributes to the correct understanding of the process of interest. In the 1870s Eadweard James Muybridge, an English photographer, was invited by Amasa Leland Stanford, the founder of Stanford University, to clarify the details of the horses' trot and gallop. With the poor temporal resolution of the human eye, the answer to the question of whether or not the horses feet were off the ground at the same time or not was not obvious. It was also unclear whether the fore and hind limbs were fully stretched in opposite directions while the feet were off-ground. During that time the motion of various things was generally not well understood and only depicted in cartoons, revealing the contemporary comprehension. Muybridge took a series of photographs with glass-plate cameras next to a horse track in Palo Alto and by 1878 he had developed sufficient mechanics and shutter speed to accurately resolve the motion of the horse to settle this riddle [Muybridge (1887)]. Through his work he further revealed the movements of various other animals as well as details of the motion of the human body. However, the work of Muybridge did not only answer open questions regarding animal and human motions, he had also helped with the evolution of the projection of motion images. His zoopraxiscope may be considered to be the first movie projector.

As the importance of the observation of dynamic structural changes has been underlined, the question is what processes scientists like to look at 130 years after Muybridges dynamic studies of motions of macro-scale living objects, after technology and our general understanding of things have evolved quite a bit in all directions. To answer this question it is easiest to look at the different branches of science and the investigated dimensions, concentrating on those which can be subject to investigations with machines

related to this thesis. In addition, the time domains and length scales will be treated generally in the following subsection [1.1.3].

Starting with small-scale structures, there are atoms which are set into the focus of intense light sources by physicists. The availability of high density, high energy photon beams enables the detailed research of intra-atomic processes and the interaction of matter with light fields through photon absorption and by the detection of emitted photons and ions upon excitation. This gives insight into the changes of electronic configuration and the dynamics of ionization processes [for references see e.g. Bruzzese et al. (1989), Pabst (2013)]. Zooming out from single atoms to molecules, it is intended that all details of chemical transformations are unveiled. While a chemical system undergoes a reaction, it is changing its structure. A dream of chemists is the direct observation of the molecule in the very moment of the transition state - the turning point in a chemical reaction before which the molecule is in the reactant configuration and beyond which it is drifting irrevocably towards the product state configuration [Polanyi and Zewail (1995)]. While the resolution of initial and final structures seems feasible, the resolution of the transition state requires sophisticated instruments and methods for structural reconstruction. The structural transformation occurs along a potential energy surface and the quest is to determine the path of transformation exhibited by nature, as this relates to involved potential energy in the structural rearrangement. The guiding principle within these transformations is the minimization of the final energy of the system, which directly relates to more stable states. Within the process of the reformation, the energy applied for the structural change is constrained and the entire process optimized. In the case of simple and complex structures, only a few key motions are leading and controlling the structural change of the system [Armstrong et al. (2003), Gao et al. (2013)]. Directly, only a very tiny amount of energy is required for macro-scale biological processes, as they are continuously happening within every cell. The third type of processes of interest belong to the investigations of structural biology, a field which investigates every activity inside living cells. These activities are involved in the synthesis and the transport of molecule complexes such as proteins, mechanisms of pathogen-defense, DNA reproduction and more. As a first step the structure of single elements such as the proteins is resolved, before trying to analyze dynamic processes. The last step in this field is understanding the complex interplay of various activities inside living cells. With the possibility to artificially create molecule structures, the synthesis of drugs to suppress or enhance certain processes is based on these findings. While small scale structures up to proteins are typically resolved in reciprocal space, the resolution of structures on the cell scale is conducted in real space. One of the instruments developed in this work shall be used for the resolution of dynamic processes in single cells, which will be floating in a solution and thus be contained in their natural environment. This is achieved by upgrading the accelerator structures with real space

imaging capabilities, as they are known from transmission electron microscopes [see DESY (2014d) for current instrumentation developments of the *Relativistic Electron Gun for Atomic Exploration* REGAE]. With these modifications it is aimed at the observation of macro-scale structures and intra-cellular life in real time.

1.1.3 TIME DOMAINS AND LENGTH SCALES

Nothing is faster than the speed of light. The constant nature of c labels the ultimate speed with which mass-less objects can travel in our universe, according to Albert Einsteins theory of relativity. This is the contemporary understanding and a fundamental constant in physics. Assuming the distance between the surfaces of earth and moon is on average $377,000$ km, it would take a pulse of light 1.25 seconds to travel from one surface to the other. To cross a human head hair (a standardized example) of an average thickness of 0.1 mm it would take light 3 picoseconds $= 3 * 10^{-12}$ s. The time domain which is interesting to chemists who are looking at transition states and the closing and breaking of chemical bonds is at least one to two orders of magnitude smaller. In the range of 100 fs $= 100 * 10^{-15}$ s, bonds between molecules break and their structures start to undergo the change from the reactant into the product configuration. In the time domain of the beginning of these processes the pulse of light would only have traveled through a tiny fraction of a human hair. Two short optical pulses with a 100 fs time delay in between would only be 30 μm apart from each other, which outlines the precision required for the manipulation of light pulses in beam delay paths, as they are required for time-resolved studies. Another comparison which clarifies the ratio between a femtosecond and a second, something we can easily grasp, is the short endurable length of seven minutes compared to the age of the universe, which is estimated to be around 13.8 billion years. Instruments that focus on the resolution of the transition state in chemical reactions require a temporal resolution and stable control of optical and, where applicable, electron pulses on the 100 femtosecond scale or shorter. Atomic vibrational movements happen on the few femtosecond scale, but cannot be resolved due to constraints in contemporary machines, but also due to fundamental uncertainty relations of physics which begin to dominate processes on the atomic scale. Due to the fast pace of technology evolution it is natural to expect that we will be able to resolve some of the fastest atomic and molecular processes in nature within the not so distant future. The most recent technological achievements in the generation of attosecond optical light pulses show the future direction and evolution of technology which will secure and expand ultrafast technological means available for the precise measurement and determination of the fastest processes. In this context, the time domain of intra-atomic electron distribution changes might become observable. The change of the electronic distribution of the atom is happening on the attosecond time-scale, and thus at least another three orders of magnitude smaller than is currently in reach with the latest

femtosecond electron diffraction (FED) setups.

The critical length scale for the understanding of fundamental chemical processes in nature is those of single atoms and molecules. Atomic radii start on the order of $1 * 10^{-10}$ m $= 1$ Å. The covalent radius of the smallest and lightest atom hydrogen is about 25 picometer $= 0.25$ Å and the van der Waals radius measures around 1.2 Å. The unit Å is commonly used among crystallographers to describe not only the dimension of single atoms but also lattice parameters and bond lengths. To visualize this length scale one can imagine that 1 million hydrogen atoms lined up in a row would stretch out to the diameter of a human hair. A protein can have $50 \cdot 10^3$ atoms, depending on its type. A number which relates to the mass of all atoms in a compound is the molecular weight. This refers to the weight of the molecules expressed relative to the weight of hydrogen. With mass spectroscopy, viscosity and light-scattering measurements the mass of molecules and proteins can be determined. The protein with significant appearance in the human blood for example, the immunoglobulin M, has a weight around 150k-Da. This translates to approximately 1000 amino acids. In biological binding processes only a very tiny fraction of these are actively participating. An overview of phenomena subject to investigations with diffraction and imaging techniques is shown in figure 2.

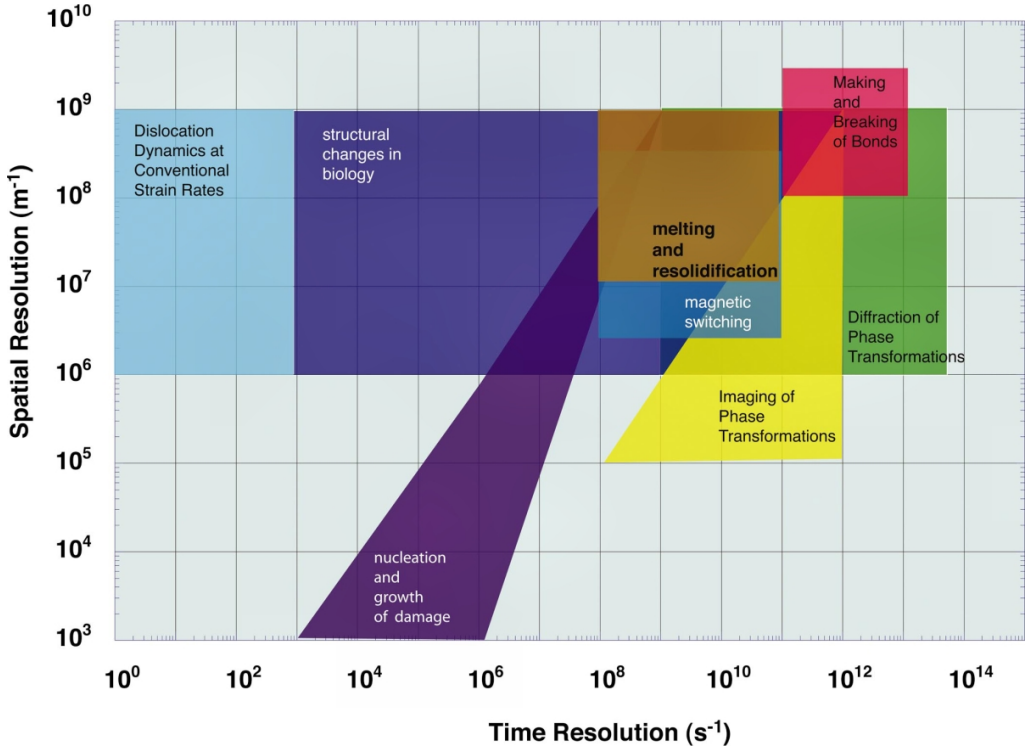

Figure 2: Classification of phenomena of physics, chemistry and biology subject to dynamic structural investigation. Reprinted with permission from AIP Publishing LLC: Journal of Applied Physics, King et al. (2005). Copyright 2005 AIP Publishing LLC.

Due to the inherent wave-like nature of particles it is possible to use electrons just like light to resolve structures which are 1/1000 of the wavelength of visible light and thus we are able to visualize atomic structures. Electrons can be easily generated and accelerated to high energies. They possess in dependence of their total energy a very small de Broglie wavelength in the sub-Å regime, which relates to the wavelength of photons in the hard x-ray range and is used to determine the smallest structures. By position-detection of scattered electrons in diffraction experiments this property of particles can be exploited to determine the atomic positions of the investigated specimens.

1.1.4 STRUCTURE DETERMINATION

The discovery of x-rays by Wilhelm Conrad Röntgen in 1895, the theories of Max von Laue, William Henry and William Lawrence Bragg from 1912 and the theory of Louis de Broglie, published in his PhD thesis in 1924, who postulated a relationship between the energy of a particle and the particle-inherent wavelength, build the basis for crystallographic and diffractive imaging techniques, which can be used for structural investigations (see equation 2.4). In transmission microscopy as well as coherent diffractive imaging experiments, a pencil beam of the radiation of choice (which can be photons, electrons or neutrons) is shot through a thin slice or micro-crystal of the specimen system. In x-ray crystallography crystals are rotated within the x-ray beam to reconstruct three dimensional structures. The incident particles change their direction of propagation due to the interaction with the atoms in the specimen system, and this actual change in relation to the initial direction manifests itself in a diffraction pattern recorded on a specific plane. The experiment can be a tedious endeavor and the following structural reconstruction is equally challenging.

The diffraction data recorded with a detector behind the diffractive volume relates to a probability distribution of coherent and presumably elastically scattered radiation. The observed diffraction spots fulfill the Bragg- or Laue-condition respectively, meaning that constructive interference of the photons or electrons from different scattering centers within the transmitted specimen system is observed at those points. While both of these conditions describe the total probability of the appearance of diffraction spots observed under a certain angle in reference to the primary central beam axis and the crystal lattice plane orientation, these conditions cannot be used to describe the diffraction intensities as the intensity distribution of the diffraction image relates to a structure which is associated with the lattice points in real and reciprocal space. A material dependent structure, which is associated with an underlying lattice type, is contained in the basis of the lattice. Therein the arrangement of material specific atoms of the crystal in the unit cell which form the crystal lattice is described, and this basis directly determines the detected diffraction intensities observed at a certain angle. The position of the atoms of

the basis is also directly correlated with the electron density, which is important for the interaction of photons and used to position the atomic cores into the centers of increased electron densities. The image which is recorded with the detector is best described by a time average of the amplitude of all incoming waves, for particulate radiation and single-particle detectors this signal directly correlates to the detected particles in a specific bin or pixel. Any phase information describing the particle or photon wave in respect to the remaining field and the origin of scatter is lost in the moment the particle or photon is measured at a certain position. Since the phase differences of the incoming waves cannot be measured in sheer particle detection, the direct re-transformation and correlation of the diffraction spots to the scattering structure is not possible.

The structure factor determines atomic and electron densities within the integrated scattering volumes, which are weighted with the phase differences of each wave to the angle of observation. If the structure factors themselves were observable on the detector, one could directly calculate the electron densities and positions of the atomic cores and thus gain the structure of the investigated scattering system. Since only the squared values of the structure factors are available, which are directly proportional to the detected intensities, iterations and estimations have to be made, and various methods such as phase retrieval algorithms or Patterson maps can be used to regain this information. Most likely an atomic structure of a specimen system will be simulated and its virtual diffraction pattern compared to the experiment. With iterations on the virtual atomic structure it is possible to achieve a match of simulated and measured diffraction patterns, leading to the desired information on the structure of the specimen. Once initial and final structures of a structural transformation, which occur during physical, chemical and biological processes are solved, it is possible to consider the single steps of the structural transformation. At all times the simulated structures have to be matched with experimentally observed diffraction patterns. Using the experimental data of the transition states, it will be possible to accurately observe changes in atom positions.

1.1.5 TIME-RESOLVED EXPERIMENTS

To create a continuous record of a complete structural transformation one can deflect an electron pulse, that takes longer to pass the specimen than the observed structural transformation, over the imaging area. This single streaked pulse then contains all diffraction patterns of all time points during the presence of the electron pulse [Li et al. (2010c)]. The separation of the changes observed in the smeared diffraction pattern is more difficult as multiple diffraction patterns are overlaid with each other. But as long as the specimen survives illumination with the charged particles of the pulse, assuming a sufficient brightness or electron density, it is possible to record the dynamics of the

structural change with a single illuminating shot.

The other and probably most utilized method is the animation of the structural change based on multiple short illuminations of the specimen, each one probing the structure at a different time-point after the structural change started to occur. This is a stroboscopic method, but often the only applicable methodology. Especially for x-ray pulses, this is the only option, when intense photon light pulses cause total devastation of the specimen by ionization within a single pulse. Depending on the brightness of the beam, each time point requires multiple shots before the combined diffraction patterns unveil the structure of the investigated moment, and for each time point of the structural transformation this series of experiments has to be repeated. Consequently a large amount of specimens is typically required for experiments using high intensity x-ray pulses, which can be greatly reduced with electron based structural probes. Due to the much larger scattering cross section of electrons only little charge in each pulse is required, and the specimen is typically conserved due to dominant elastic scattering and minimal energy transfer onto the system. Therefore even biological specimens can be studied as long as the overall transmitted energy is kept below a certain threshold, which can be achieved in single shot electron diffraction experiments by keeping the electron numbers and exposing pulses low. With a larger scattering cross section, electrons provide a better signal on the detector, hence fewer illuminations per time point are required. This reduces the total number of charge and illuminations by orders of magnitude. The best case scenario would be a manipulable specimen system, which can cycle many times in between different phases and structural configurations [e.g. Irie (2010)].

To produce a stroboscopic animation two beams are applied to the system. One to excite the specimen, the pump pulse, and one to look at its structure, the probe pulse. This is equally true for solely optical beam experiments. The probe pulse is shot at different time spans after the arrival of the pump pulse through the specimen and provides the structural information contained within a diffraction pattern. A controlled delay between the arrival difference of pumping and probing pulses enables a precise time dependent scan of the structure, when stable beam conditions are assumed. The effect of the excitation of a structural change by a laser pulse can also be induced by the application of heat to the system, which will have different structures between low and high temperature phases. The complexity of the time delay system scales with the size of the machine and requires elaborate and expensive electronic synchronization in the case of rf accelerator based methods. This leads to timing jitter problems and reduces the overall temporal resolution of those machines for time-resolved studies. Clearly, a compact simple to use source for the structural probe of the dynamics is highly desirable. Illustrations of pump-probe setups are available at various sources, e.g. in Rousse et al. (2001), where additional information on the method and background is provided.

1.2 DEVELOPMENTS OF THIS WORK

1.2.1 E-GUN 300 - A COMPACT 120 KEV SOURCE FOR FEMTOSECOND ELECTRON DIFFRACTION

At the start of this work not a single experiment was present nor any lab that would see an end of a renovation in the near future, everything had to be organized and built from scratch. Also due to a lack of manpower the work associated with the majority of constructions fell within the responsibility of this PhD work. The first project that fell into this thesis was the construction of a compact 300 kV apparatus for femtosecond electron diffraction. Two identical electron guns were built, with different specimen chamber designs for solid state and gas phase experiments, the latter setup being further developed by a another group member. The original design for this compact setup was drafted by senior scientists of the former group in Toronto, but it became necessary to change the design plans to build the setup. Figure 3 illustrates the E-Gun 300 setup for solid state experiments.

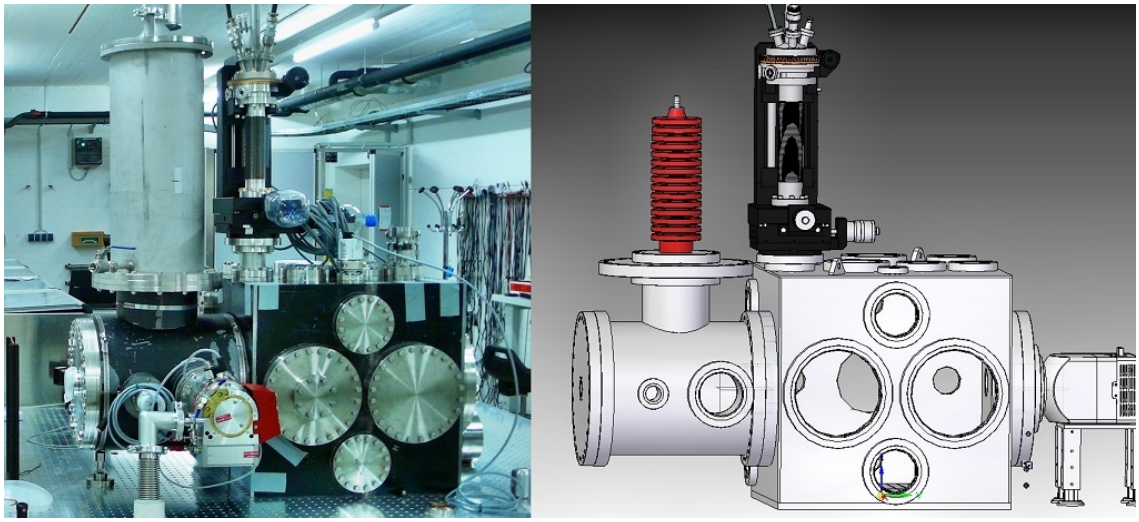

Figure 3: Construction (left) and design (right) of a compact FED apparatus - afterwards named the *E-Gun* 300.

In this project two noteworthy aspects were characteristic and had a big impact on the following proceedings. First of all it was very difficult to get a commercial company to build a feedthrough for the desired energy of 300 kV; which in total took more than 1.5 years for its final delivery. Finally it turned out that the design and manufacturing was simply inappropriate to be operated at this high voltage level, despite of what the engineers of this company claimed. A test of the feedthrough on different setups followed by various modifications to the high voltage adapters and parts demonstrated, that physical damages caused by electric breakdown will be seen above an energy of

120 to 150 kV. Secondly, as we were raising the electron energy compared to previous generations of setups, which were being operated at 50 to 95 kV, we ran into serious radiation safety concerns. When we finally had received the feedthrough for the compact instrument, which had already delayed the project by almost a year, we were not allowed to test the setup for another year. It was mandatory to build a radiation hutch made of lead around the experiment, to meet certain radiation safety regulations. The concerns of the radiation safety department in charge were based on worst case radiation calculations, in which instrument-wise impossible operating conditions were assumed. This has also led to long delays of our test runs and further development of this compact apparatus back at a time where debugging might still have been possible. The observation that up to today not a single radiation event from the setup was measured with radiation detectors located inside the hutch might be resultant of the electric potential constraint at approximately 120 kV, allowing only unstable operational conditions in this regime. The assumptions that were guiding the radiation safety measures were also inappropriate for this apparatus design. Instead of just a few months it took 2.5 years until we had first results on the performance of this compact electron gun design and certainty that it could not be operated at the desired energy. The occurred problems were crucial for a later period of this PhD work [chapter 5 - the *Femtosecond Electron Diffraction CAmera for Molecular Movies* (FED-CAMM)]. Major aspects of this project are outlined in chapter 4.

1.2.2 dark current collimators for the relativistic electron gun for atomic exploration (regae)

Shortly after the start of this PhD work another interesting project commenced, namely the design of dark current collimators for the larger *relativistic electron gun for atomic exploration* REGAE. With a rf-driven cavity for the acceleration of electrons and another series of cavities for the further acceleration and bunching of the electron pulses it was expected to see a significant background of dark current electrons caused by high electric field gradients inside of these cavities. This could potentially outplay the signals from the diffraction experiment. Thus it was aimed at the total suppression of the background rising from the dark current electrons to maintain a good signal to noise ratio.

The dark current collimators were mounted by the end of 2012, having been delayed by the availability of materials, the requirements of the DESY vacuum and complications which arose during manufacture. The design of the manipulators came from DESY engineer M. Lemke, who was temporarily exclusively working on this project, but only after another long delay. The leaf design and estimation of material and thickness specifications was conducted as part of this work [see subsection 3.2.4]. Today the dark current collimators are consistently used to improve the signal to noise ratio and urgently required due to the large amount of dark current, which is indeed generated in

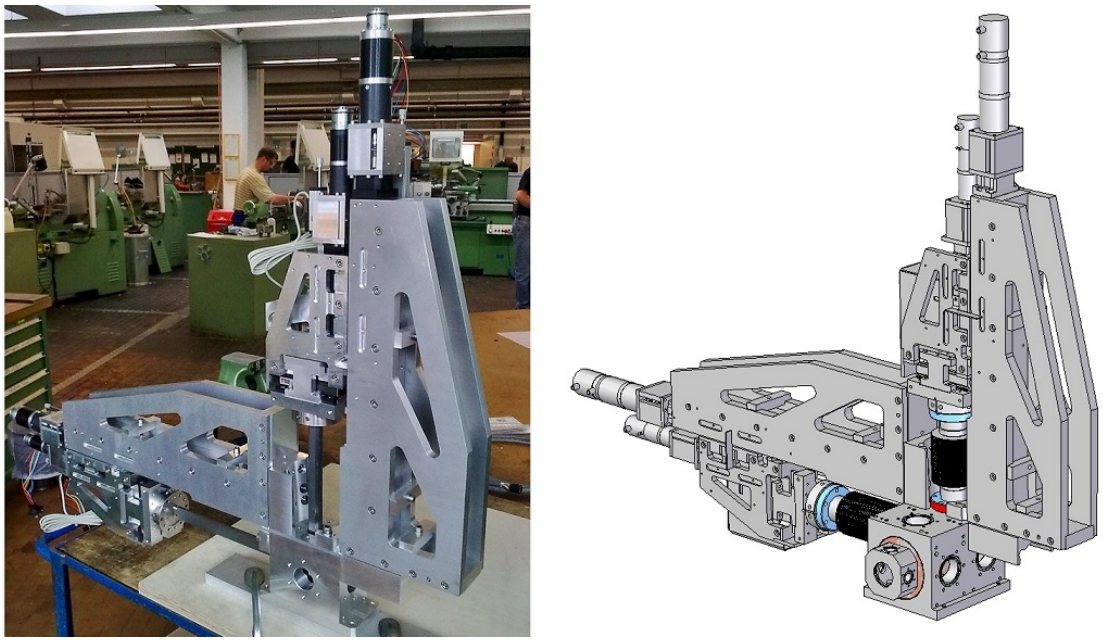

Figure 4: Construction (left) and design (right) of pairs of dark current collimators.

the rf-cavities. Most of the dark current electrons can be shielded properly with these collimators except for the dark current electrons flying on the design orbit of the electron beam. Details on this project are outlined in subsection 3.2.4.

1.2.3 SPECIMEN CHAMBER, SUPPORTS AND BEAMLINES FOR THE RELATIVISTIC ELECTRON GUN FOR ATOMIC EXPLORATION

Also included in the obligations of our group was the provision of all beamline elements and units like the specimen chamber and all connecting elements, such as a beam guiding system for the laser pulses for the excitation of the photo-cathode and the specimen from the floor below. The design of the specimen chamber [see subsection 3.2.2] was conducted in October 2010 in collaboration with Dr. G. Moriena from the group in Toronto, specific designed to house the largest experiment which would be applied to this machine, namely the ponderomotive experiment [Siwick et al. (2005); Hebeisen et al. (2006, 2008) and as illustrated in figure 14]. By January 2011 the chamber was under manufacture in local workshops, accompanied with the construction and installation of an appropriate chamber socket. Following right after was the design and installation of all connecting beamline elements up to the final electron detection stage. The development of the beam guiding system for the laser excitation pulses was supervised until completion, its current design was finally drafted and implemented by the former engineer of DESY J. Gonschior [see figure 15]. By October 2011 the electron beamline of the REGAE machine was completely installed and operational, allowing the observation of the first electron beam on the last detection stage in the following weeks. Figure 5 shows a part of the experimental section of REGAE with the specimen chamber in the front. Figure 6 shows

the entire experimental installation of REGAE, including the arrangement of the E-Gun 300 and the common laser system, which spreads across two floors. Further details are provided in subsection 3.2.2, subsection 3.2.3, in Manz et al. (2015) and DESY (2014d).

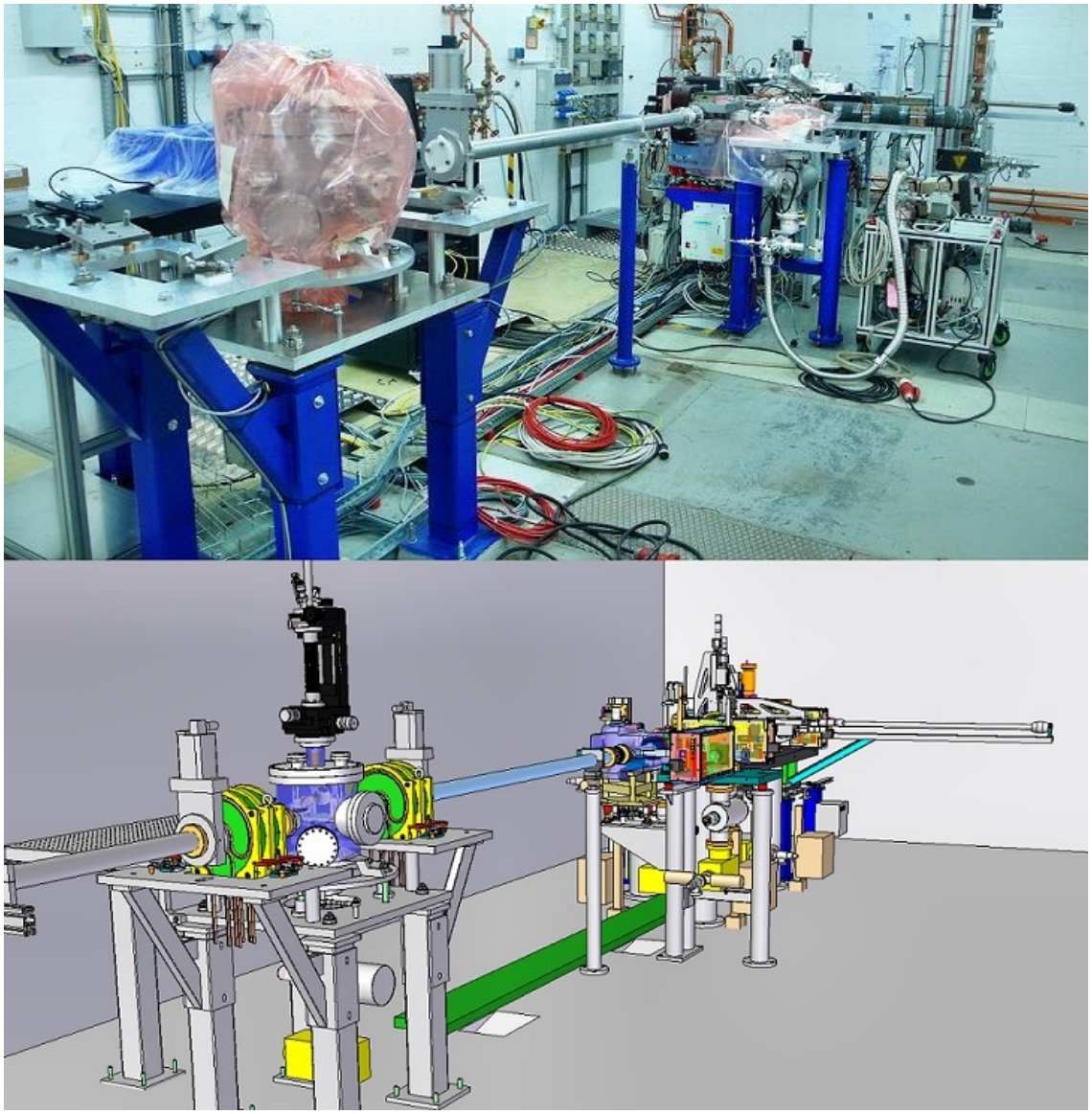

Figure 5: Construction and design of the REGAE specimen chamber including supports and further beamline elements to connect to and complete the main accelerator.

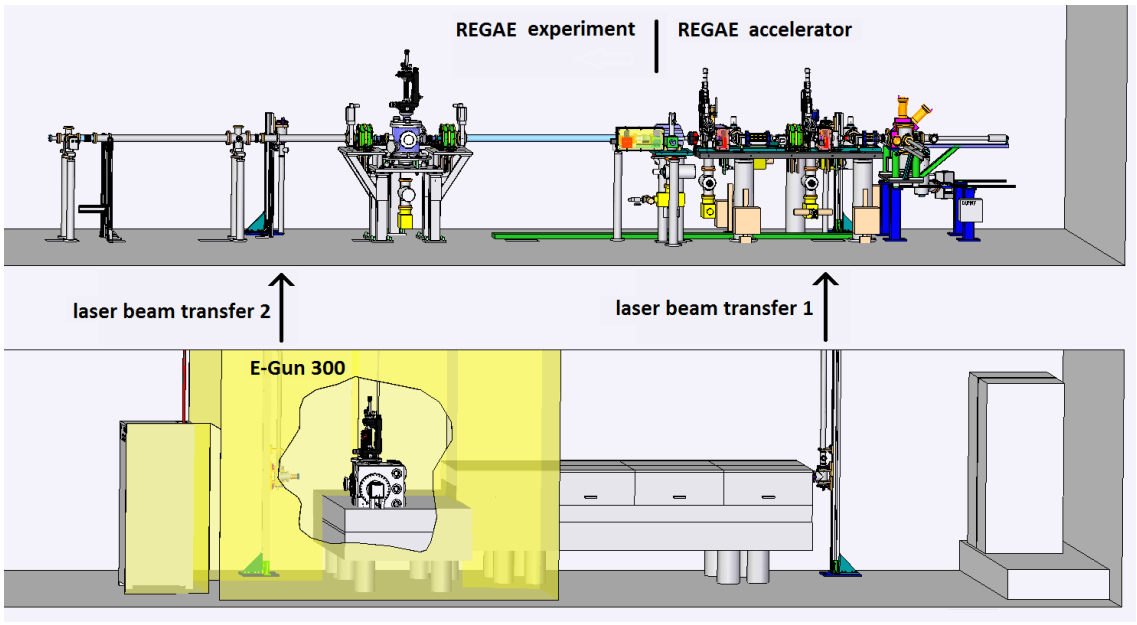

Figure 6: Overview of the compact FED experiment inside a lead hutch and the connection of the common laser system to the REGAE accelerator one floor above. The REGAE experimental section as shown in this illustration was completely developed within this PhD work, as well as the most parts of the compact E-Gun 300 setup and the according parts of a the clone setup for gas phase diffraction.

1.2.4 The femtosecond electron diffraction camera for molecular movies (FED-CAMM)

By the third quarter of 2012 it had become clear that the performance of both the compact setups and the REGAE was not as initially anticipated, and a long period of debugging and enhancing the machine parameters concerning the REGAE apparatus was still required. A time-resolved experiment on the preferred few ten femtosecond scale could not be conducted with the REGAE within the time span of this PhD work. My proposal to work on the design and construction of a new compact apparatus to solve the experienced problems of the high voltage instabilities found in the previously built compact FED setups was fortunately accepted. For this purpose I developed an electric feedthrough design for high voltages, ranging up to multiple hundred kV. The prototype version of a flexible high voltage feedthrough assembly found its way into the apparatus, which I called *Femtosecond Electron Diffraction CAmera for Molecular Movies* FED-CAMM. This development combines the features of compact FED instruments, which are a reduction of size and costs in combination with the provision of stable operation, working at a moderate electron energy which compares well to the energy of commercial transmission electron microscopes, with the advantages of very short electron pulses from relativistic and rf-driven accelerators such as the REGAE. The design of the FED-CAMM had begun by the end of 2012. By the summer 2014 the self designed high voltage feedthrough assembly was installed, initiating first high voltage tests. The design of the feedthrough

is applicable to much higher voltages than those provided by our current 300 kV high voltage power supplies and a patent application was filed to protect this development. By late summer 2014 the high voltage of the new FED-CAMM apparatus was successfully tested in respect of the maximum of the sustainable kinetic electron energy and intense electric field gradients, which are the key parameter for very short electron pulses.

The operational parameter space of this machine comprises the shortest achievable electron pulse durations at various electron energies, which are within the capabilities of DC driven setups. The FED-CAMM currently easily exceeds 250 keV with continuous improvement in the maximal electric field gradients due to further improvements to the photo-cathode and electrodes. The operation of high voltages in this setup is absolutely stable. Short electron pulses are provided without the need for electron pulse compression by for example rf-components. The simulations of electron pulses with 10^4 electrons return a pulse duration around 109 fs (fwhm) throughout all targeted electron energies. Using less electrons per pulse, which is adjustable by the laser intensity of the excitation pulses, the fundamental pulse duration of compact DC driven FED-setups can be reached. The FED-CAMM is operating at the edges of physical as opposed to design limitations, receptive for a new class of experiments. The fastest structural transitions can be captured, even within thicker specimens. The technical developments of this apparatus are of benefit for the entire FED community as well for other fields of research and fundamentally support the access of ultra-short electron pulses. Figure 7 illustrates the prototype as of spring 2014. Chapter 5 provides further information on components and the underlying electron beam dynamics.

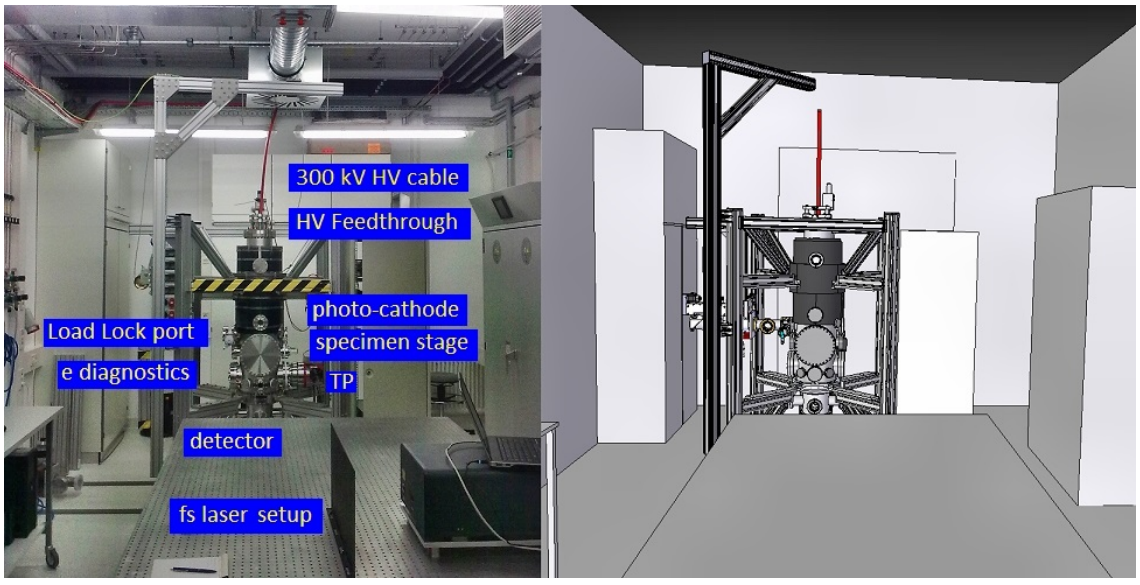

Figure 7: The FED-CAMM experiment in early 2014.

1.2.5 TIMELINE OF PHD PROJECTS

Figure 8 shows the timeline of the different projects that were processed in this PhD work. The consistent work relates to the instrument development of the REGAE, E-Gun 300 and the FED-CAMM and closely related work in the sphere of these experiments, as well as to the preparation of a specimen system, that was initially supposed to be the major focus of investigation.

The assumption that the construction of two new compact FED setups of the type E-Gun 300 would be quick and be straight forward, intended to bridge the gap until the REGAE was operational, proved wrong. The E-Gun 300 could not be tested due to concerns of the DESY radiation group D3. The similar clone was similarly not operational to its full extend of design. It becomes clear from these timelines, that the first test of the compact E-Gun 300 roughly lined up with the first basic diffraction experiments conducted at the REGAE. This was 2 and 1/2 years after this PhD work was started. At the end of 2012, the outcomes of PhD related efforts were at a most indeterminate point.

The preparations of a specimen system for the conduction of FED experiments was conducted in parallel with the by then remaining engineering and construction work of the first experimental installations. Unfortunately, the endeavors in this matter were not successful, which is not unusual. Since no appropriate temporal resolution or operational machine was present within the first half of this work, the preparation and studies of specimen systems were postponed to the day, where a femtosecond electron diffraction instrument with real femtosecond temporal resolution is available for experimental investigations on the ultrafast timescale. This day has come by the end of my work.

As previously mentioned, my proposal to draft a new setup that solves all previously occurred problems and would perform with high voltages and specifically short electron pulse durations, was luckily accepted. It was proven by the end of this work that this new development of the FED-CAMM was indeed successful and may be the most significant outcome of this PhD work. In total three new instruments with different temporal resolutions are now available, ranging from 900 fs (fwhm) of the REGAE down to 80 fs (fwhm) of the FED-CAMM. This outcome is remarkable, as it is the reverse order of what was initially expected to occur.

Out of those instruments being constructed, the FED-CAMM apparatus appears to be most promising. This machine is the foundation for further pioneering developments, as is this development itself. The preparation and manufacturing of high voltage feedthrough is in both of the herein included compact setups marked with a green bar to illustrate the time spans, which were actually involved to the first delivery for the E-Gun

300 and the construction of a working prototype for the FED-CAMM. The E-Gun 300 first had to be completed by a led hutch, which had to be built before the instrument could be tested in respect of the high voltage for the first time. Despite initial concerns raised by DESY, no x-ray radiation was ever detected. This is surely due to the restriction of voltage, at which this machine is operated, due to failure of its components at higher voltage. Additional milestones of each of the developed instruments are equally marked in the following figure 8.

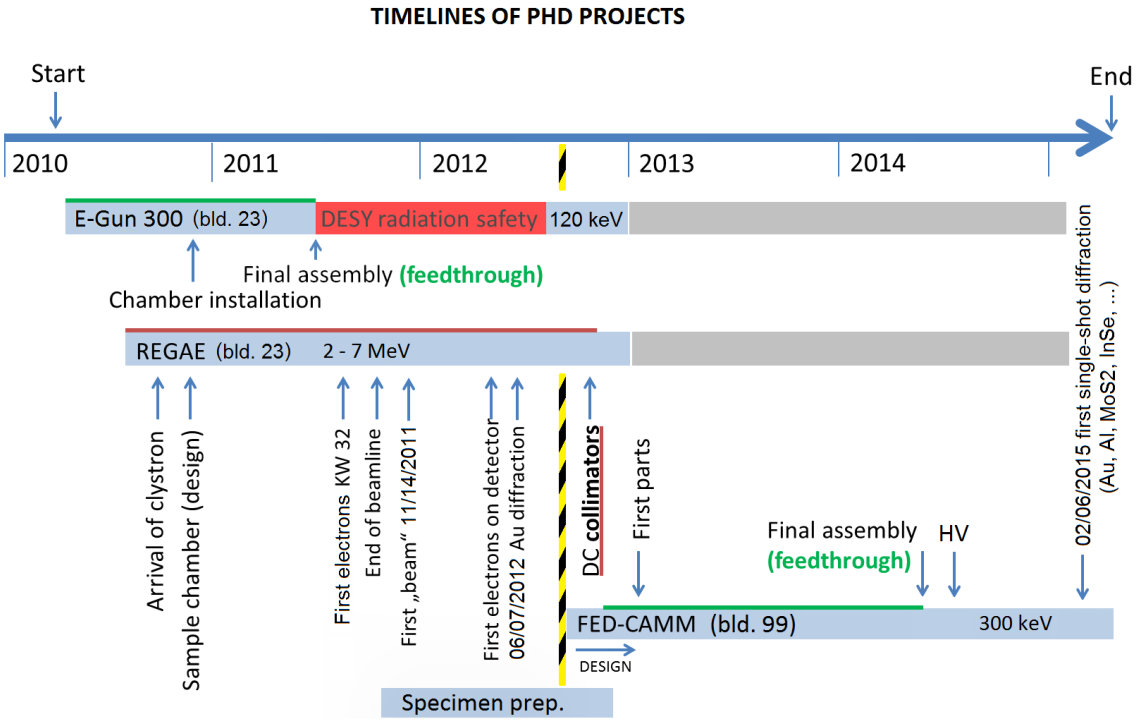

Figure 8: Timeline of PhD related projects and developments. The key developments started by the end of 2012, when it turned out, that the compact E-Gun 300 installation was not operating at its specifications and that REGAE would still have years of commissioning ahead. Further, the preparations of the envisaged specimen system were stalled. First diffraction in February 2015 and prior successful tests of the high voltage validate the decision to start from scratch with the development and construction of a new setup for time-resolved electron diffraction by the end of 2012.

1.3 METHODS AND MATERIALS

1.3.1 SOFTWARE

CAD PROGRAM

For the design of accelerator structures and diffraction setups the use of 3D CAD programs is an essential tool which grants unlimited virtual space for the layout and development of new sources and helps to improve prospective new instruments even before the very start of the production of a first prototype. Based on its wide usage on DESY campus and on my initial decision to support the engineers of the University of Hamburg, who had initially worked for us, I acquired the skills to use Solid Edge V20 and later on version ST3 [PLM (2012)]. Up to now this software package is used and proves extremely helpful. For related tasks that cannot be executed with the CAD program, additional tools are required to cover remaining and important fields of study. In the later period of this PhD work, the interplay in between various programs developed into an iterative process which went back and forth in between the different aspects of machine design. The optimized results were then built within the workshops on the ground of DESY Hamburg.

ASTRA SIMULATIONS

The program *A Space Charge Tracking Algorithm* [ASTRA, Flöttmann (1997)] allows the tracking of micro and macro-particles under the inclusion of space charge effects that occur within a pulse of charged particles through a virtual accelerator consisting of various beamline elements. ASTRA was used by Klaus Floettmann to determine the best theoretical working parameter of the REGAE before the start of this PhD work. ASTRA consists of a few program modules, namely a generator for the generation of charge distributions, the core program ASTRA, which tracks the particle distribution through the accelerator geometry, and programs to visualize various distribution properties along the beamline.

GPT SIMULATIONS

The program *General Particle Tracer* [De Loos and Van Der Geer (2006)] comprises the same capability as ASTRA to track particles through an accelerator geometry, but unlike ASTRA it is not freely available. GPT was used to determine the beam dynamics properties of the FED-CAMM apparatus, since the implementation of the geometry, especially of the static electric fields of DC setups, is much easier compared to the ASTRA package.

MONTE CARLO SIMULATIONS

Unlike ASTRA and GPT, Monte Carlo simulations typically only allow the propagation of single particles through an accelerator geometry, and are not capable of space charge calculations. Thus, they are inappropriate to calculate beam dynamics. For the investigation of the dark current collimators for REGAE EGS5 [SLAC (2005)] was used to simulate the absorption and transmission ratios of various materials in the energy range of the REGAE machine. For a very similar purpose FLUKA [Ferrari et al. (2005), Böhlen et al. (2014)], another Monte Carlo code package, which is also used in the DESY radiation safety group D3, was utilized to confirm the shielding calculations for 300 kV electron diffraction setups.

STATIC ELECTRICAL FIELD SIMULATIONS

To complement the work that was done with Solid Edge, a tool for the simulation of static electric fields was used to optimize the shape of the conducting and charged setup components of the compact electron diffraction instruments. This resulted in electrode shapes, which were optimized for maximized electric fields and the avoidance of geometry based field enhancements in regions where they would cause problems. Historic theories for optimal electrode shaping and experimental findings on electrode behavior found in literature from the past few decades did also find their way into this program. The program *CST Studio Suite* [CST (2014)], which was used to perform these static electrical field simulations, is available on two servers on DESY campus with corresponding permission. The simulations of electric fields helped to avoid mistakes as they can be found in literature and to obey what is already present as advice from various sources.

1.3.2 MACHINING

DESY INFRASTRUCTURE

Working on DESY campus and collaborating with various DESY organs involved multiple resources ranging from DESY measurement services, production facilities to hardware installation teams. The collaboration started with the erection of the REGAE accelerator and the first compact electron diffraction setup, the E-Gun 300, and lasted to the manufacture of parts for the FED-CAMM apparatus. The tools, instruments, the people, their knowledge, skills and experience on DESY campus had built a rich and very helpful environment for successful construction of new instruments, as every aspect of a company that produces commercial products are present within this non-profit research organization. DESY workshops and methods to set up optimal machine operation conditions proved also critical for the successful installation of the final compact setup of this PhD work, the FED-CAMM apparatus.

FOLLOW-UP TREATMENT OF HIGH VOLTAGE ELECTRODES

The follow-up treatment of electrodes was optimized by a series of tests to find the optimal machining and hence optimal surface qualities for best breakdown behavior, i.e. to suppress electric breakdowns from sources from which it would easily occur. Different tools for machining electrode parts were tested, followed by extensive manual polishing periods after the CNC manufacturing processes, concluded by electric polishing. Tests of electric breakdown of various manufacturing stages helped to evaluate the most ideal approaches. More information on this matter is given in the latter parts of section 5.4.

1.4 SIGNIFICANCE AND STRUCTURE OF THIS WORK

The three instruments for femtosecond electron diffraction which evolved during the course of this PhD work pursue different approaches for the generation of ultra-short electron pulses. The large REGAE [chapter 3] uses rf cavities for the acceleration and compression of electron pulses, the compact instruments E-Gun 300 [chapter 4] and the FED-CAMM [chapter 5] have the identical underlying concept of quick acceleration of electrons in DC electric fields and immediate use of the accelerated pulses without additional compression. The main focus of this PhD work came to existence as a consequence of the anticipated problems seen with the REGAE and the E-Gun 300. Initially focused on structural dynamics, the scope of the PhD work changed into the development of appropriate machines. In the end, these valuable developments led to a novel compact electron diffraction setup, the FED-CAMM, which is breaking the 100 fs (fwhm) window as a compact robust platform. Its design and developed electric components pursue the concepts of simplicity and reliability and open up many new possibilities for structural investigations.

A prerequisite to film transitions of atomic and molecular structures in real time is a very good spatial and temporal resolution, as previously described [please consider the relevant publications in this context, which all provide a detailed introduction into the subject: Dwyer et al. (2006), Dwyer et al. (2007), Baum and Zewail (2007), Miller et al. (2010), Barty et al. (2013), Miller (2014a) and Miller (2014b)]. This prerequisite is now achievable and the increasing demands on the characteristics of instruments used for the generation of state of the art molecular movies can be met with compact electron diffraction devices. The major outcome of this work is based on the successful treatment of anticipated high voltage and radiation safety problems. As a final result, a setup design including a full prototype version of a compact DC driven electron diffraction setup with less than 100 fs temporal resolution came into existence. The work on the REGAE project is negligible in this sense, though it was the completion of the accelerator to its first fully operational state, which was most helpful in guiding the designing and machining procedures on the new, compact machines for electron

diffraction. Measured with existing and previously proposed setups it was proven that non trivial rf-acceleration and re-compression techniques are not urgently required for gaining sub 100 fs pulses. This is an important result, as most of all interesting chemical bond breaking and making processes happen on this temporal order and can now be resolved using compact and inexpensive machines. The new small compact electron diffraction design proves reliable and is unbeaten in its capability to create molecular movies in respect to its simplicity. It forms a very promising instrument which could see widespread use in order to realize this new potential for significant scientific discoveries within many research groups worldwide.

The temporal resolution of the compact FED-CAMM competes well with the pulse duration of rf-based compressed relativistic electron pulses, though the electron energy seems more ideal in the FED-CAMM instrument regime, as specimen damages due to inelastic scattering events are reduced when compared to MeV electron beams. Also the structural images of diffraction patterns show up more clearly with energies of 100 up to a few hundred keV. Besides a novel development of a high voltage electric feedthrough, the FED-CAMM apparatus reaches the extreme conditions of very high electric field gradients that can be experimentally obtained in DC electric setups with high voltage electrodes. With a further reduction of electron numbers in each pulse, albeit sufficient for single shot structure determination, the total electron pulse lengths emanating from this setup may well compete with the newest of the fourth generation light sources, while it also benefits from not having the typical component related timing jitter problems. This is beneficial for the total temporal resolution in the study of ultrafast structural changes on the few tens fs timescale.

In the main text of this thesis, each project and involved tasks are described to a level of detail which is necessary to present the efforts of this PhD work. Chapter 3 describes the REGAE project and the core tasks which were undertaken within this PhD work. The following chapters 4 and 5 concentrate on the compact installations. They are completed with simulations concerning the beam dynamics of each machine, which are of major interest and used to outline the outstanding capabilities of the more advanced FED-CAMM apparatus. The results are compared with the REGAE and other existing machines, which are introduced and discussed in the following chapter 2 to allow a direct comparison of the PhD projects to the state of the art in the directly competing machines using x-rays and electrons for time-resolved diffraction. In the last chapters, this PhD work is summarized, discussed, conclusions are given with a finishing outlook on upcoming developments.

It is a natural development to extend and upgrade the existing machines within ones group. However, after the first proof of principle experiments and first compact electron

installations ranging up to the voltage level of 95 kV within the first fifteen years of electron diffraction research, the physics of operation of strong electric DC fields became much more difficult and demanding with higher voltages. Previous advances in electron energies were not much higher than already utilized. The electron pulse properties can be significantly improved by an order of magnitude with an increase in the applied kinetic energy even by small factors, but the modifications to the structures which further accelerate these electrons up to the new pace, were tremendously profound and required a complete restructuring of the electron diffraction setup to meet the physics requirements. The many engineering and challenges in understanding the physics of the required structures delayed progress. The advances made in this PhD work can be used for ground-breaking science comparable to that at the very modern fourth generation photon sources. Especially the experiments concerning structural biology can be properly treated with compact ultrafast electron sources. With the availability of compact electron diffraction setups, that perform comparably, it is standing to reason to have a more widespread usage of the inexpensive and compact electron diffraction apparatuses that may open up a new era of instrumentation for the study of the ultrafast but highly interesting nano-cosmos of nature over a wide range of topics.

2 PHOTON (X-RAY) AND ELECTRON SOURCES FOR FEMTOSECOND DIFFRACTION STUDIES

The discourse of the projects of this work is aligned with the order of their occurrence. Before the specific projects are discussed in the following chapters, a brief discussion on instrumental approaches for femtosecond diffraction studies and then explicitly existing machines for femtosecond electron diffraction experiments is given here. This background information is required to set the developments of this work into the context of existing machines in this field of research. The basics and most important beam parameters of photon and electron beams are discussed to provide the necessary background knowledge. These are compared to emphasize the advantages and disadvantages for each source type.

2.1 INTRODUCTION

The investigation of ultrafast processes on the femtosecond timescale requires probe pulses, which have a temporal duration along their axis of propagation smaller than the smallest increment of time required to probe the structural change. More clearly the transition time of the probe pulse through the specimen directly refers to the shutter speed of the experimental setup; the shorter the pulses are, the quicker the processes that can be investigated with the apparatus. As illustrated in figure 2 the most basic processes in physics and chemistry happen on the order of 100 fs. Below this timescale the lattice motions themselves, if we assume crystalline arrangements, seem frozen during the illumination with ultra-short probe pulses. In this setting, transition states, the breaking and making of chemical bonds, become visible. As for the probing pulses themselves, two different sources can be utilized.

X-rays and electrons are the two sources of choice currently used world-wide in research centers to investigate molecular structures and dynamic structural changes. Their character, generation and interaction with matter is fundamentally different from each other, while their behavior is partially identical with respect to probing structures. The range of applications varies with the predetermined interaction with matter that they undergo. The production and demands on the beam of whatever choice directly determine the size and the costs of the beam producing instrument, while the interaction determines the type of experiment which can be conducted using this or that source. Other particles with rest-masses exist which can be used to determine the structure of the systems of interest, but they are presently less frequently used. The communities

focus on photons [Spence et al. (2012)] and electrons [Sciaini and Miller (2011)], with the latter type receiving less popularity though harboring great potential, as advanced by this work. We will start with a brief discussion about photons, as they will be directly compared to the capabilities of electrons within this thesis. They are also of interest, since a vast number of new research facilities for photon light production are presently under construction, which pursue the same vision of imaging the dynamics of matter on the femtosecond timescale as first made accessible with electrons.

2.2 PHOTON LIGHT SOURCES

Photons are particles without rest-mass and by preference interact with the electrons of atoms. They can be generally generated as a mechanism of energy loss of charged particles which experience a deflection from their initial axis of propagation. This deflection can be caused by a magnet along an evacuated beam-tube, or triggered by an atom of a target material. This latter process is known from the creation of bremsstrahlung by the inelastic interaction with materials. Copper, carbon and tungsten are widely used in x-ray tubes in various devices for (medical) diagnostics. The first process is of further interest in the context of structural investigations using high energy accelerators, among others synchrotrons. These are ring accelerators originally designed for the long term storage of particles for experiments concerning particle collisions. The discovery of synchrotron radiation from this so called first generation light source led to the further investigation and distinct usage of synchrotrons as photon light sources.

The emission of photon radiation from synchrotrons for structural investigations is actively triggered by a sequence of magnets, which induce periodic deflections of the stored electrons. As this is easily achieved using small mass charged particles, electrons are perfectly suited. The condensed undulated movement of the charged particles leads to an intense emission of light in the x-ray range. The photon-spectrum generally depends on a few parameters, as will be outlined shortly. The second generation light sources contains further development of the used magnetic arrangements named wigglers to more accurately generate the x-rays. These do not only consist of permanent magnets, electromagnetic coils with iron cores were also used. These early deflecting structures were optimized over time and are now commonly referred to as undulators within third and fourth generation light sources. Besides differences in construction there are differences in the produced photon spectrum. Thus the elements of major importance for all photon light sources are briefly explained.

A Wiggler produces a continuous spectrum of photon energies. This is due to larger deflections of the electrons off their circular track and a weak interaction between the different emission cones of different sections of the wiggler. A direct consequence is

that the average photon energies are higher but a self-modulation of the electron and photon fields is missing. This in turn leads to a less coherent photon beam. Undulators with overall smaller deflections of the electrons yield a different spectrum. The photon energies are consequently lower, unless more kinetic energy is applied to the electron beam or the magnetic field strength is increased. At a certain length of the undulator a self-modulation based on the interaction of the bunch electrons with the emitted photon field leads to a micro-bunching of the distribution of the electron pulse, while the pulse propagates through the undulator. This process is known as *self-amplified stimulated emission* (SASE) and leads to a very distinct photon spectrum. This spectrum contains a fundamental resonance wavelength and its higher harmonics. The wavelength λ is described by the undulator-equation [Winick (1997)]

$$\lambda = \frac{\lambda_u}{2\,\gamma^2}\left(1 + \frac{K^2}{2} + \Theta^2\gamma^2\right) \tag{2.1}$$

with

$$K = \frac{e\;B\;\lambda_u}{2\;\pi\;m_e\;c}. \tag{2.2}$$

In here λ_u denotes the undulator period, γ the Lorentz factor and Θ the opening angle of the resultant radiation. K denotes the undulator strength parameter, in which B denotes the magnetic field strength, e and m_e the elementary electronic charge and electron mass and c the speed of light in vacuum. The difference between wigglers and undulators is conventionally made by values of $K > 1$ for wigglers and $K \leq 1$ for undulators. Since the deflection in undulators remains compact, more magnetic transitions can be included in the undulating element. This leads directly to a larger number of photons and increased brightness of the photon beam; the undulator period λ_u is thus generally smaller for undulators. The brightness is defined as photons ΔN per time t , unit area A , solid angle $\Delta\Omega$, and spectral range $\frac{\Delta\lambda}{\lambda}$ and reflects one of the most important parameters of photon sources:

$$B = \frac{\Delta N}{t \cdot A \cdot \Delta\Omega \cdot \frac{\Delta\lambda}{\lambda}}. \tag{2.3}$$

The brightness of both types of deflecting elements scales with the number of magnetic periods and is quadratically proportional for wigglers and increased by another factor for undulators due to the high level of self-modulation.

Based on the historic development of photon light producing machines, the different generations of light sources label advances in the brightness of the machine, which was each time increased by orders of magnitude, through the development of improved accelerator components or enhanced undulators. Third and fourth generation light sources exclusively rely on undulators, which mostly carry a series of permanent magnets. Another difference between third and fourth generation light sources is found in the accelerator layout. While in modern synchrotrons the photons are produced in small

straight sections in between the bending magnets of the ring accelerator, most fourth generation light sources form approximately a straight line. At their beginning stands a *linear accelerator* (linac), which is ideally driven by superconducting rf-cavities to provide higher electron energies and lower beam emittances. The final section typically consists of diagnostic stations and at least a few undulator arrays, which produce the photons. The electrons are typically dumped at the end while the photons are further processed in beamlines for scientific experiments. The following table shows the decades in which each generation was born and used, according to Winick (1997) and Saldin et al. (2008).

Generation	Core operation	Type
0	1950 - 1970	Synchrotrons for particle physics research
1		Improved synchrotrons provide stabilized SR
2	after 1970	Dedicated synchrotron rings for SR research
	after 1978	First use of wigglers and undulators
3	1990 - today	Reduced emittance and increased brightness
4	since 1997	SASE lasing from ring and linac sources

Table 1: Overview of contemporary light source generations

To account for smaller photon energies from undulators, the energy of the electron beam is increased to again increase the energy of the emitted photons. The energy of the electron beam sent through the undulators must range in the GeV regime to yield photon wavelengths of a few nanometer or less. This is one major reason for fourth generation light sources, also known as free electron lasers, being so immensely huge and expensive. New sources which are presently under construction aim for atomic resolution, increased orders of brightness, increased numbers of photon pulses per time increment and shorter pulse duration. Overall the kilometer long constructions typically cost several billion Euro.

The following listing reflects a short summary of modern light sources which already do or will have the potential to provide the beam conditions required for time-resolved studies on the few ten femtosecond time-scale. A more complete list of photon sources can be found online, for example at http://www.lightsources.org, which includes 13 sources as of the end of 2014. The state of the art fourth generation sources are listed first, then a brief and more condensed overview of modern synchrotron sources is given, as they can not totally be neglected.

2.2.1 THE FREE ELECTRON LASER IN HAMBURG (FLASH)

The free electron laser in Hamburg is based on the former TESLA Test Facility (TTF). TTF was an experimental installation of the TELSA Technology Cooperation and a test-bed for highly relativistic electron acceleration realized by superconducting niobium cavities. Proof-of-principle experiments concerning SASE processes of undulating magnetic arrays followed. FLASH I was an extension to the existing TTF and the soft x-ray radiation that is generated by this machine has been used by international scientists since 2005 for structural analysis. The key parameters of the FLASH I are summarized in table 2. Information taken from DESY (2014b) and http://flash.desy.de/. Brilliance and brightness are equivalent notations.

FLASH I parameters		
e^- energy	0.38 - 1.25	GeV
e^- pulse duration	50 - 100	fs, fwhm
photon energy	0.028 - 0.295	keV
photon wavelength	45.0 - 4.2	nm
photon pulse duration	30 - 300	fs, fwhm
photons per pulse	1	$\cdot 10^{11}$ - 10^{13}
photon pulses	1 - 8,000	1/s, macro- to micropulses
average brilliance	10^{17} - 10^{21}	$\frac{photons}{s \cdot mrad^2 \cdot mm^2 \cdot 0.1\%bw}$
peak brilliance	10^{29} - 10^{31}	

Table 2: Key parameters of the FLASH I.

The initial six beamline installations inside the experimental hall of FLASH I are now being expanded with another six beamlines in a second experimental hall. The additional beamlines of FLASH II are powered by a branch from the original accelerator using a junction that is placed after the main accelerator and before the undulating magnets of FLASH I. One focus in FLASH II is set on the generation of seeded FEL laser light with wavelengths in the range of 10 to 40 nm.

2.2.2 STANFORD LINEAR COHERENT LIGHT SOURCE (LCLS)

The LCLS is part of the former Stanford Linear Accelerator Center (SLAC) and was the first FEL producing photons in the hard x-ray regime. User operation first started in 2009. The information contained in table 3 is taken from SLAC (2014), listed under the LCLS FAQ page. To keep up with worldwide competitors LCLS is seeing an upgrade with a new linac including a separate injector, which will be independently operated to LCLS I.

LCLS parameters		
e^- energy	4.54 - 14.35	GeV
e^- pulse duration	> 25	fs, fwhm
photon energy	0.27 - 9.50	keV
photon wavelength	15 - 1.5	nm
photon pulse duration	50 - 400	fs, fwhm
photons per pulse	0.2 - 20	$\cdot 10^{12}$
photon pulses	120	1/s
average brilliance	0.2 - 2.7 $\cdot 10^{22}$	$\frac{photons}{s \cdot mrad^2 \cdot mm^2 \cdot 0.1\% bw}$
peak brilliance	0.64 - 8.50 $\cdot 10^{32}$	

Table 3: Key parameters of the LCLS.

The key points of LCLS II are the provision of soft x-ray photons independent of the provision of hard x-rays, an increase of the maximum photon energy to 18 keV, an increase in brightness by three orders of magnitude and an increase of the average pulse energy by one order of magnitude besides a smaller bandwidth of the photon spectrum. Another feature of LCLS II is a potential reduction of the hardware synchronization down to 10 femtoseconds. This is a significant enhancement for the overall timing capability of the machine which would enable the facility to compete with the fastest photon sources [Arthur et al. (2012)].

2.2.3 European X-ray free electron laser (XFEL)

Based on the technological progress and successfully conducted research programs of the TTF, a new free electron laser concept was drafted. It exceeds the parameters of the FLASH by orders of magnitude in certain aspects, extends the spectral range of produced photon light and realizes design aspects of the previously planned *International Linear Collider* (ILC). The prospective key parameters of the future XFEL are summarized in table 4 [DESY (2014c)]. The XFEL measures 3.4 km in length and is meant to start user operation in 2017.

Prospective XFEL parameters		
e^- energy	0.5 - 20.0	GeV
e^- pulse duration	80	fs, fwhm
photon energy	0.2 - 12.4	keV
photon wavelength	6.0 - 0.1	nm
photon pulse duration	≤ 100	fs, fwhm
photons per pulse	1.1 - 430	$\cdot 10^{12}$
photon pulses	10/27,000	1/s, macro-/micropulses
average brilliance	$1.60 - 0.03 \cdot 10^{25}$	$\frac{photons}{s \cdot mrad^2 \cdot mm^2 \cdot 0.1\%bw}$
peak brilliance	$5.4 - 0.06 \cdot 10^{33}$	

Table 4: Key parameters of the XFEL.

2.2.4 SWISS FREE ELECTRON LASER (SWISSFEL)

An outstanding FEL with a prospective first user operation in 2016 is the Swiss free electron laser. It is built from scratch and not based on any existing linac structure. It is the smallest of the presented FELs with an overall length of only 750 m. Its anticipated photon pulse duration and peak brilliance as well as the photon energy range is comparable to the other hard x-ray sources. The key performance characteristics are extracted from the SwissFEL website [SwissFEL (2014a)].

SwissFEL parameters		
e^- energy	2.1 - 5.8	GeV
e^- pulse duration	≥ 60	fs, fwhm
photon energy	0.18 - 12.4	keV
photon wavelength	7.0 - 0.1	nm
photon pulse duration	25 - 140	fs, fwhm
photon pulses	(2x) 100	1/s
peak brilliance	$1.3 \cdot 10^{33}$	$\frac{photons}{s \cdot mrad^2 \cdot mm^2 \cdot 0.1\%bw}$

Table 5: Key parameters of the SwissFEL.

The SwissFEL focuses on the major research activities which are equally pursued at the other FEL facilities. These are electron spin and magnetization dynamics on the sub-picosecond timescale, catalysis and solution chemistry. Coherent diffraction by nanocrystals [as done at the LCLS by Chapman et al. (2011)] is made possible by a

significant transverse coherence length of the FEL sources. Studies of biochemistry and correlated electron materials are generally proposed [SwissFEL (2014b)].

2.2.5 SYNCHROTRONS

Structural investigations with photons were first conducted at synchrotron sources. The content of this work focuses on time-resolved structural resolution. The synchrotrons are thus highlighted for another reason. The electron beam in the ring-like structure of synchrotrons is pulsed. The driving forces in these accelerators are rf-cavities, highly similar to those used in other modern GeV and TeV accelerator systems such as the FELs. Rf-waves condensed in these cavities accelerate electrons to their final energy. They further compensate the energy losses, which occur during the intentional production of the synchrotron radiation and the intrinsic deflections of the electron beam in the bending sections of the accelerator. Due to the alternating field gradients in the cavities, the occurrence of the beam at a given point of the beamline is bunched. The bunch durations range from the regime of micro- to picoseconds, primarily determined by the employed rf-fields and secondarily by further applied techniques to the beams. It is common practice to mechanically select single pulses or fractions of a pulse for time-resolved experiments. This technique further reduces the time resolution of synchrotrons [Schoenlein et al. (2000), Wulff et al. (2003) and Pfeifer et al. (2006)]. For this reason, a synchrotron can serve as a pulsed light source for time-resolved experiments down to the picosecond or potentially few-hundred femtosecond realm, with even sub-100 fs pulse duration. Beam slicing beamlines may however have x-ray photon numbers too low for most applications of interest.

The pulsed electron beam of synchrotrons is sent through undulating structures for the production of photon light-pulses, typically wiggler and undulators. The photon pulses are tangentially leaving the ring-accelerator through straight sections that are directed towards experimental stations. Due to a higher curvature of the electrons inside undulators, specifically for the generation of higher photon energies, the generated x-ray pulses are less coherent. The peak brightness of synchrotrons is also reduced as a consequence of reduced electron densities and missing SASE effects. The photon pulse duration is longer and the photon spectrum is different to fourth generation light sources. Synchrotrons can clearly not compete with the time-resolved instruments developed in this work or with fourth generation light sources. Studies of irreversible structural changes on sub-ps timescales require single-shot structure determination, for which only the brightest electron and x-ray sources suffice. However, these modified modes of synchrotron operation are commonly used for structural determinations, including dynamic developments on the available timescales. The following table 6 is listing contemporary beam parameters available at synchrotron sources. The range of parameters is given

by the number of synchrotrons considered for this table, among those the Advanced Light Source ALS [ALS (2014)], Diamond Light Source [Diamond (2014)], Petra III [DESY (2014a)], Spring-8 [RIKEN (2014)], Bessy-II [Helmholtz-Zentrum (2014)], Canadian Light Source CLS [CLS-Inc. (2014)] and the Australian Snychrotron AS [Australian-Synchrotron (2014)].

Synchrotron parameters		
electron energy	1 - 8	GeV
photon energy	$1 \cdot 10^{-7}$ - 150	keV
photon wavelength	0.1 - $2 \cdot 10^{3}$	nm
photon pulse duration	≥ 30	ps, fwhm

Table 6: Key parameters of synchrotrons.

In terms of static diffraction and slower structural transformations (> 100 ps) synchrotrons can compete well with free electron lasers. They have similar photon energy ranges and certain wavelengths at various beamlines are dedicated to specific experiments. Only SASE effects are missing, which reduce the peak brightness of synchrotron sources by several orders of magnitude compared to the 4th generation light sources. The only other downside of 3rd generation light sources is the absent potential of resolving dynamics on the femtosecond scale with high photon fluxes due to typically extended photon pulse durations, which are a direct consequence of the gathering of electrons in the rf-fields of these particle storage rings.

The above brief discussion gives the present status of photon sources. These facilities are well justified for the science they open up. However, they do require sophisticated and huge electron accelerators which provide large quantities of energetic photons with sufficiently small wavelengths and overall short pulse durations of photons bunches. For time-resolved studies fourth generation light sources are particularly important as they have the potential to reach the dynamics hidden within the 100 fs window.

An alternative for probing the structure of matter has always been the use of electrons, which interact strongly with matter and are easily deflected by atomic cores. Electron scattering is dominated by the spatially varying electrostatic potential. Electrons are less sensitive to valence electrons but are very sensitive to charge distribution by associated atomic position. For structural investigations electrons can be considered the source of choice and the according reasons are now outlined.

(i) It is inexpensive to generate electrons. Simple sources such as hot filaments are present in old televisions, in any x-ray generating tube and microscopes. Electron microscopes can investigate both the surfaces in real space and the structure of thin layers via diffraction in reciprocal space of various specimens ranging from the micro- to the nano-cosmos. Another commonly employed mechanism for the generation of electrons is the photoelectric excitation of photo-active materials. This mechanism avails a simple means to control the time structure of electron sources. Photo-cathodes are employed in various shapes and material compositions. They further provide the basis for the advanced electron sources developed in the present PhD work. The only significant cost factor that could be assigned to photo-cathodes in the context of ultrafast diffraction is a femtosecond laser system, which triggers the photo-electric effect. These laser systems tend to be quite expensive. Otherwise electrons cost nothing (except the monthly electricity bill) and the diffraction setups employing electrons are generally table top, which adds great flexibility in terms of overall machine design.

(ii) Due to the small mass of electrons, they are easily accelerated by electric fields to very high energies and are generally easily manipulable by electromagnetic lenses, bending magnets, and deflection devices. This enables the various imaging modes with *Transmission Electron Microscopes* (TEM), such as bright- and dark-field imaging, magnified real- and reciprocal space diffraction. The manipulation of photon pulses proves very difficult in contrast to this property of electrons.

(iii) An inherent property of electrons is the associated de-Broglie wavelength. The wavelengths of photons produced by fourth generation light sources are easily achieved with relatively low energy electron sources (1 keV) and can be exceeded by over two orders of magnitude shorter at conventional energies used for diffraction (> 100 keV). The much shorter wavelength equals to higher spatial resolution (see table 7).

Evident from table 7 is the approximation of the ultimate speed of light starting around energies of a few MeV. This is an electron energy level which is generally still easily accessible using for example GHz rf-waves. The spatial resolution of electron

Thesis related energy dependent electron parameters				
Instrument	E_{kin} [MeV]	γ	v [v/c]	λ [pm]
E-Gun 300 / FED-CAMM	0.1	1.19	0.54	3.70
	0.2	1.39	0.69	2.50
	0.3	1.58	0.78	1.97
REGAE	1.0	2.95	0.94	0.87
	2.0	4.91	0.97	0.50
	3.0	6.87	0.98	0.35
	4.0	8.82	0.99	0.28
	5.0	10.78	0.99	0.23
	6.0	12.74	0.99	0.19

Table 7: Electron parameters of accelerators developed herein.

driven instruments can resolve fractions of inter-atomic distances in the diffraction mode. To account for the significant enhancement of the electron-mass, the de-Broglie wavelengths relating to these energies require relativistic treatment (starting at electron velocities exceeding 10% of the speed of light, as indicated by the γ-values in table 7). The de-Broglie wavelength λ_e is given by [Reimer and Kohl (2010)]

$$\lambda_e = \frac{\hbar\, c}{\sqrt{2\, E\, E_0 + E^2}}, \tag{2.4}$$

with $\hbar$ denoting Planck's constant, c the speed of light in vacuum, E and E_0 the energy and rest mass energy of the electron, respectively.

(iv) The scattering cross-section for electrons is typically six orders of magnitude larger than the cross-section of photons at similar wavelengths, thus allowing the use of less electrons per pulse for the same *Signal to Noise Ratio* (SNR) as yielded by photons. The ratio of elastic to inelastic scattering events is by a factor of three better compared to x-rays [Henderson (1995)]. Both of these facts are beneficial for the investigation of biological specimens in real- and reciprocal-space imaging [for a review, see for example Cosslett (1978)]. The effect of heating by transmission of kinetic energy into the specimen can be further reduced by the reduction of electron pulses per time interval and prior cooling of the specimen.

The previous advantages of electrons leave only one disadvantage to mention. The property most different to photon radiation is the electric charge of electrons, which on the first hand enables probing the atomic details due to the electric interaction with the core, but on the other hand is complicating the generation and maintenance of electron pulses on the 100 fs range. The inherent Coulomb repulsion between electrons leads in

the context of electron pulses to a broadening of the particle distribution in space and hence time, generally known as space-charge broadening effect. This pulse broadening is most apparent in the axis of propagation and builds a linear chirp in the electron distribution [Siwick et al. (2002), Reed (2006)]. The space-charge broadening effect at the electron pulse duration directly determines the machine concepts that have to be followed by *Femtosecond Electron Diffraction* (FED) setups. The effects of space-charge broadening can be greatly reduced once the electrons reach the highly relativistic MeV regime. The approaches for the generation and maintenance of sub-100 fs pulses are outlined and compared in the following subsections.

2.3.1 DC ACCELERATORS

The simplest acceleration of electrons is achieved by static electric fields. Most setup designs include a source for electrons which is positioned opposite to a plane at a different (positive) potential. Due to the previously mentioned effect of space-charge broadening, it is important to keep the acceleration time and propagation times minimized, to prevent excessive pulse-broadening prior to the interaction with the specimen of interest. Simply stated, the longer the time it takes the pulse to arrive at the specimen, the more space-charge induced pulse-broadening will occur and the longer the electron pulse. It is essential to keep the electron pulse as short as possible to probe the dynamics of interest. For this reason, the electric fields have to be maximized, while the acceleration distance has to be minimized.

For higher voltages (> 150 keV) it proves difficult to provide excessive electric field strengths in a condensed space. For this reason, voltage divisions are commonly used in compact electron accelerators, which operate at electron energies exceeding a few ten keV. In TEMs, stacked electrodes with potential differences of only a few keV to tens of keV are used to reach the final electron energy (up to 300 keV). Since the acceleration in these devices is spatially stretched for the purpose of minimized electrical stress, TEMs are of no use for femtosecond studies, although suited for dynamic changes on the micro- to picosecond time-scale. There it needs to be noted that time and space resolution are related to the electron bunch density. Recent improvements of *Dynamic Transmission Electron Microscopes* (DTEM) have pushed this space-time limit with high bunch charge electron pulses to the nanometer spatial with nanosecond time resolution and hope to achieve the sub-ns realm [Armstrong et al. (2007); Barwick et al. (2008); LaGrange et al. (2012)]. During the course of this PhD work, it was realized that the physics and in particular the engineering required for compact high voltage DC accelerators was not well enough understood. This work lays the foundation for the highest electric field gradients that can be achieved with DC accelerator concepts to achieve the shortest, most intense electron sources possible - within the simplest accelerator concept possible

[details are provided in section 4.3.1 and section 5.5.2].

An obvious question to be asked and which is of greater interest in the context of this work aims at the fundamental time resolution that can be achieved with DC-FED setups, which do not utilize further re-compression elements for the electron pulses. To deal with this question we need to consider all factors which contribute to the initial electron pulse duration prior and until the specimen. One of the factors is the pulse broadening within the acceleration gap. As discussed in Gahlmann et al. (2008) and Aidelsburger et al. (2010), the time broadening factor in the acceleration gap can be expressed by

$$t_{acc} = \frac{m_e \, \Delta v}{e \, E_{acc}}, \tag{2.5}$$

where Δv denotes the initial energy spread of the electron pulse distribution, E_{acc} the electric field strength in the gap and the remaining physical constants of the electron. A similar formula is found in [King et al. (2005)]. This simple equation which describes the slope of a straight line emphasizes the importance of a minimal energy spread for best results. The electric fields strength in this regard seems to be less important for the overall broadening of the electron pulse in between the cathode and anode. Further, the total initial bunch length at the position of the counter-electrode can be approximated by the inclusion of the laser pulse length.

Aidelsburger et al. (2010) investigated the dependency of the laser pulse spectrum on the initial time broadening of the electron pulse. It is stated that the electron pulse duration reaches a minimum by using a laser pulse spectrum not too narrow in bandwidth to improve the initial electron energy spread and sacrifice the laser pulse duration, and not too large as to prevent an extensive initial electron pulse length from the energy spread after acceleration. This optimum, according to their work, is found around 70 fs, assuming $E_{acc} = 10$ MV/m and a laser pulse duration of 40 fs. For physical FED setups other factors need to be considered, which further increase the electron pulse durations of a FED apparatus. Most important of those factors is any timing jitter related to electronic circuits or the stability of the power supply and eventually velocity mismatches [Williamson and Zewail (1993)], which are related to the differences in the transmission times of electron and optical pulses through the specimen. These effects add in quadrature [Cao et al. (2003), Lu et al. (2012)]:

$$t_{pulse} = \sqrt{t_{laser} + t_{acc} + t_{electronics} + t_{vm}}. \tag{2.6}$$

This expression gives a good first approximation of the fundamental timing capability the best FED setup could possess. Unfortunately most sources of literature do not yet account for the timing jitter of electronics included in this formula, probably due to the fact that this is not a factor within the regime of longer probe-pulses (> 1 ps) and thus did not have a significant impact there. For femtosecond pulse durations it is indispensable

to account for this factor. Table 8 lists prior art DC electron diffraction setups where the parameters of energy and temporal resolution could be identified from literature. Partially it is not possible to determine whether the pulse duration is provided in terms of *root mean square* (rms) or *full width at half maximum* (fwhm) values, which makes a relevant difference.

Williamson et al. (1992) apply potentials of 15 keV but do not specify the pulse duration. They assume electron pulses of picosecond duration and claim the feasibility of fs-pulses with modifications on their setup at the time. Park et al. (2005b) only specify the pulse duration with 450 fs. Apparent from the following summary of publications is the constancy of the applied electric potential over the years. Except for Ischenko et al. (1983), who only mention the available voltages of the utilized power supply, and recently Waldecker et al. (2015), no DC-FED-apparatus commonly implies electron energies at the 100 keV energy level. Prior to this PhD work, there were no published reports in which electron energies of compact DC-FED instruments exceeded 60 keV. One of the reasons surely is the missing basis of commercial high voltage feedthroughs, which forces scientific groups to develop their own solutions, if they aim at high voltages. Furthermore, the maximum applicable electric field strength is restricted to the threshold of vacuum breakdown, which is further reduced by imperfections of the electrode and cathode materials that are used in the instruments. It is plausible that these electric limits were already achieved at the energy ranges of the prior state-of-the-art compact setups. Two excellent DC-operated setups are those of Sciaini et al. (2009) and Lahme et al. (2014). The applied conditions in these setups are electric field gradients of ≈ 9 MV/m, due to the application of 55 kV on a 6 mm gap in the first setup [Hebeisen et al. (2008)] and 4 MV/m in the second setup [Lahme et al. (2014)]. The laser pulse durations were 50 fs at 500 nm in Sciaini et al. (2009), and 60 fs at 400 nm in Lahme et al. (2014). In both cases two-photon absorption processes for the generation of electron pulses was exploited. Both sources claim the pulses were characterized with less than 400 fs (fwhm) values. Waldecker et al. (2015) limit the electrons per pulse to at most $5 \cdot 10^3$ to achieve sub-100 fs electron pulses in a compact setup layout. In terms of source brightness, this is at least one order in electrons per pulse less than the other two previously mentioned sources.

The more profound advances in compact FED setups in the past decades have arguably been made in the development of new laser sources and improved electronic circuits, which may also be contained in more stable high-voltage power supplies. Hence the overall temporal resolution of compact FED instruments was improved over the years. The increase in temporal resolution lines up chronologically with the listed sources (except for Ischenko et al. (1983)). The requirements of the laser source in the photogeneration of the electron pulse is not considered in this comparison, as the femtosecond laser technology has been readily available commercially for some time. The further

Parameters of prior state-of-the-art DC electron diffraction setups.				
Reference	E [keV]	Type	t_e [fs]	location
Mourou and Williamson (1982)	20	DC	$1 \cdot 10^5$	URochester
Ischenko et al. (1983)	40 (100)	DC	$1 \cdot 10^8$	RAS
Williamson et al. (1984)	25	DC	$2 \cdot 10^4$	URochester
Schelev et al. (1998)	30	DC	$5 \cdot 10^3$	RAS
Ihee et al. (2001)	30	DC	$2 \cdot 10^3$	Caltech
Dudek and Weber (2001)	30	DC	$1 \cdot 10^3$	Brown Univ.
Cao et al. (2003)	60	DC	$7 \cdot 10^2$	FSU
Nie et al. (2006)	60	DC	$4 \cdot 10^2$	FSU
Siwick et al. (2003)	30	DC	$5 \cdot 10^2$	UToronto
Sciaini et al. (2009)	55	DC	$35 \cdot 10^1$	UToronto
Aidelsburger et al. (2010)	30	DC	$35 \cdot 10^1$	MPQ
and Lahme et al. (2014)				
Waldecker et al. (2015)	100	DC	$1 \cdot 10^2$	FHI Berlin

Table 8: Prior state-of-the-art DC electron diffraction instruments. t_e denotes the instrument response time with respect to time resolution of the electron source. This table of electron sources is completed by table 14 of chapter 7, which summarizes the parameters of the developed sources of this PhD work.

advances have to be made in the electron accelerating section and source material to approach the fundamental limit of DC FED sources. State of the art design and machining have to be applied to guarantee the best conditions in compact DC FED sources. The alternative accelerating techniques to DC acceleration for femtosecond electron pulse generation reduce to rf-cavities and a combination with RF and/or DC fields with the eventual use of magnetic compressors, of which the present state-of-the-art for such sources are now presented in the following subsection.

2.3.2 RF AND HYBRID ACCELERATORS

An alternative to DC fields for the purpose of rapid acceleration of charged particles to highly relativistic energies is the application of rf-fields in cavities (see table 7 for keV to MeV range-related parameters). Normal- and superconducting rf-cavities are commonly used for the acceleration of charged particles to energies ranging up to the GeV and TeV range; substantial experience is present in the high energy physics community. The acceleration in rf-cavities happens within very short periods of time by the application of high electric field gradients, which are resultant of the collection of rf-waves in the

geometrically constraint spaces of the metallic cavities. The speed of propagation of the rf-waves within these constrained dimensions leads to the fast alternating character of the fields, with frequencies typically ranging in the MHz to GHz range. Due to the short durations of the peak intensities it is possible to maintain high field gradients without an occurrence of electric breakdowns. Rf-cavities are of special interest for femtosecond electron pulse generation. In the context of FED the impact of Coulomb repulsion and subsequent pulse broadening is significantly reduced, once highly relativistic energies are reached. Consequently, one of the other big advantages of rf-cavity acceleration over conventional DC acceleration gaps is the prospect of higher electron numbers in the bunches whilst maintaining a comparable longitudinal pulse length. Within the past decade there was special interest in the design and construction of MeV electron accelerators specially dedicated to FED experiments. The designs include TEM-like top-to-bottom machines and table top horizontal accelerator arrangements. A further approach to obtain femtosecond electron bunches is the combination of DC and RF fields. In this context, rf-cavities are used to re-compress the pre-accelerated electron bunches during a further drift of the pulse to the specimen [see Fill et al. (2006) or chapter 3].

Attempts have been made to build few-femtosecond electron-pulse-sources which utilize magnetic deflections to force a spatial realignment of the electrons of a pulse, which are due to the space-charge interaction propagating with different velocities. Sent through magnetic fields they experience a deflection which depends on the momentum of the electron, leading to different path lengths distinct to each electron. These magnetic deflecting arrangements are known as temporal lenses. Yang et al. (2011a) present a MeV electron setup with a prospective pulse duration on the order of 100 - 200 fs. This setup comprises an alpha-magnet structure used to re-compress the electron bunch and to narrow the energy spectrum of the pulse, which favors an improvement of the emittance (see following section 2.4 for further discussion of the emittance and pulse duration). A similar approach reported by Tokita et al. (2010) led to an electron pulse duration of 500 fs in a setup of 350 kV electrons. Settakorn et al. (1998) achieved 118 fs rms at the MeV SUNSHINE facility at SLAC (50 fs rms reported in Kung et al. (1994)), which is or was operating at 2.6 MeV with a combination of an rf-cavity with thermionic cathode and an alpha-magnet structure. The best time resolution of the present MeV electron bunches accelerated by rf- and hybrid techniques is located at the edge of 100 fs FWHM. When the overall pulse length cannot be reduced any further, a modulation of the electron bunch itself would result in micro-pulse-lengths within the attosecond regime [Zholents et al. (2001)]. According to the description of this last reference, a distinct manipulation within further deflecting field arrangements is possible to micro-bunch the electrons, if the energy of the intra-bunch electrons is slightly altered by an overlay with optical light pulses. These attosecond pulses are highly comparable with the thousands of micro-photon-pulses contained in a single XFEL macro-pulse (in particular comparable

to the XFEL parameters, which were summarized in table 4). Table 9 summarizes the prior state-of-the-art electron sources which utilize RF and hybrid technologies for the generation of electron bunches aiming at a 100-fs pulse-duration. The first part of the table lists those sources which exclusively utilize rf-cavities. The second part lists the sources which are using a combination of both DC and RF techniques. The latter instruments operate in the keV energy range, due to their initial acceleration by DC electric fields, again in contrast to the MeV (rf-) FED systems. More discussions of hybrid DC-AC simulations and setups are given by Fill et al. (2006) and Veisz et al. (2007). The sources discussed above which utilize magnetic temporal lenses are not incorporated due to the experimental character of the machines. These techniques are not commonly utilized and generate less spatial coherence due to the sensitive nature of these compression schemes.

Parameters of prior state-of-the-art RF electron diffraction setups.				
Reference	E [MeV]	Type	t_e [fs]	location
Hastings et al. (2006)	4.5	RF	$56 \cdot 10^1$	SLAC
Rudakov et al. (2006)	4.5	RF	$31 \cdot 10^1$	SLAC
Musumeci et. al.	3.75	RF	$\leq 1 \cdot 10^2$	UCLA
2008 and 2010				
Li et. al.	2.7	RF	$\approx 1 \cdot 10^2$	Tsinghua
2009 and 2010c				University
Yang et al. (2009)	1.5 - 4.0	RF	$\leq 1 \cdot 10^2$	Osaka Univ.
and Murooka et al. (2011)	3.0	RF	$\approx 1 \cdot 10^2$	Osaka Univ.
Yang et al. (2011b)	$1.0 - 3.0$	RF	$1\text{-}2 \cdot 10^2$	Osaka Univ.
Zhu et al. (2013)	2.8	RF	$\approx 1 \cdot 10^2$	Shangh.J.T.U.
Parameters of prior state-of-the-art hybrid electron diffraction setups.				
Reference	E [keV]	Type	t_e [fs]	location
van Oudheusden et al.	95	DC+RF	$\leq 1 \cdot 10^2$	TUE
(2007 and 2010)				
Chatelain et al. (2012b)	80 - 100	DC+RF	$\approx 3.5 \cdot 10^2$	McGill Univ.
Mancini et al. (2012)	30	DC+RF	$\approx 3.0 \cdot 10^2$	EPFL Switzl.
Gao et al. (2012)	95	DC+RF	$\approx 1.8 \cdot 10^2$	UToronto

Table 9: Prior state-of-the-art RF and hybrid electron diffraction instruments. This table of electron sources is completed by table 14 of chapter 7, which summarizes the parameters of the developed sources of this PhD work.

The best pulse durations of each RF and hybrid machines prior art are comparable. The potentially best hybrid source of van Oudheusden et al. reaches sub-100 fs, which lines up with multiple sources exclusively utilizing RF cavities. The differences between those two approaches are found in the electron energy and potentially in the overall bunch charge. Dependent on the application, the one or the other source might be favorable. It is however possible to further reduce the pulse length, when other parameters of the electron bunch are considered and altered. The quantities of coherence (i) and emittance (ii) are of special interest in this regard, which confine the limits of achievable pulse lengths. They are defined by the bunch distribution and correlated to the bunch density. They are discussed in moderate detail in the following section.

2.4 DYNAMICS AND REQUIREMENTS OF ELECTRON BEAMS

Temporal focusing of electron beams is one element in the chase of ultrafast structural phenomena. But there are other aspects which are equally important. One of them is the spatial resolution of the apparatus, of the light or electron pulse. The characteristics of an electron pulse have to meet optimal conditions at the point of interaction between the pulse and specimen of interest. The specimen itself has to meet certain requirements, as will also be outlined in the context of the penetration of electrons [section 2.4.3]. With the advent of new sources more electrons per pulse are available, while the pulse duration is still decreased compared to previous sources. Finally the detection efficiency is pushed to the single electron detection limit, which promotes full structural resolution in dynamic transmission experiments with single electron pulses.

2.4.1 COHERENCE AND EMITTANCE

(i) Apart from time-resolution, the spatial resolution of the electron source needs to be considered. The spatial resolution is determined by, among other factors, the de-Broglie wavelength, which was introduced earlier (see section 2.3 and table 7). The de-Broglie wavelength is one factor which determines the capability of the electrons to coherently scatter in the diffraction mode. The resolution in this mode is limited by variations in the electron energies and different propagation directions of the electrons within a spatial extent, which leads to smearing artifacts of the observed diffraction spots. Temperature-dependent lattice vibrations add another factor of smear, which also leads to the attenuation of the intensity of diffraction spots (described by the Debye-Waller-factor). To a greater degree the spatial resolution is limited by pulse-intrinsic relationships, namely the spatial distribution of the particles. This becomes clearly observable in the real space imaging mode. If the different properties of the electrons are plotted against each other, for example the current position in relation to a design position of the whole pulse versus the angular deviation in relation to the propagation direction, a part of

the phase space is plotted. The configuration of the whole electron pulse at a given point can be characterized, using the relations of the particles' energies, their momentum respectively, in reference to a nominal energy or momentum, the current angular direction of motion in relation to the design orbit, and the current position in relation to the particle-center of the electron-bunch.

The first quantity of interest herein, which can be derived from the phase space distribution, is the coherence. This property labels the ability of constructive interference of the electrons of the pulse with each other. Coherence can be specified temporally and spatially and is especially important in real-space imaging. In order to contribute to the creation of a useful diffraction pattern on the detector, the particles must retain a common phase-relationship relative to each other. Simplified, the smaller the area occupied in the phase-space, the more the electrons are condensed in the real-space and in their profile of properties. The more their properties are aligned, the more they scatter within the same amplitudes and directions, with preservation of their phase-relationships to each other, to result in an optimized spatial resolution. The conditions that contribute to the phase-space distribution at the very beginning of the electron pulse can be improved. The ideal condition is the compaction of all electrons in a certain restricted area, all traveling with the same momentum and in the same direction. Unfortunately the Coulomb repulsion successfully sabotages this ideal scenario. Rapid acceleration to the final energetic electron energy prevents a distinct increase of the occupied phase space area in the longitudinal-spatial direction. The compactification of the particles remains restricted. The other direction of alignment is the concentration of the energetic spectrum. We have learned (in section 2.3.1) that the initial energy spread has a significant impact on subsequent pulse broadening, especially in DC accelerating fields (since rf-cavities can be used to re-compress the pulse longitudinally). The development of suited nano-emitters [Hommelhoff et al. (2006), Barwick et al. (2007), Chang et al. (2009), Müller et al. (2014)] and photo-cathode materials needs to be considered. The earlier used two- or more-photon excitation processes lead to an excess in excitation energies, which convert into different initial kinetic energies and hence cause a significant initial energy spread [Agostini et al. (1979), Aeschlimann et al. (1995)]. The use of GaAs photo-cathodes [see for example Cultrera (2011) and Cultrera et al. (2012)] and materials with defined excitation energies required to set the electrons free from the Fermi-level into the continuum has a very beneficial influence on the quantum efficiency and initial energy spread. This significantly reduces the pulse-duration broadening-factor (equation 2.5). At the same time, the spatial resolution is improved.

(ii) A second quantity of interest is the total phase-space area occupied by all the particles of a pulse; this is the definition of emittance. It is impossible to reduce the emittance during the propagation of the electron-pulse through the accelerator struc-

ture and its optics, as long as all particles of a pulse are retained. The emittance is a physical quantity that keeps its size or expands due to anisotropic field distributions of either electric or magnetic nature (Liouville's theorem, Steffen (1965), Banford (1966)). Consequently, it is only possible to reduce the emittance through the diminution of the number of particles. It is possible to spatially filter those electrons that leave the design orbit and/or design energy by spatial apertures in bending sections of the beamline. The number of particles in the pulse will be reduced, but the overall pulse properties might be enhanced. For example, the developed dark current collimators for the *Relativistic Electron Gun for Atomic Exploration* (REGAE) [section 3.2.4] operate by spatially filtering electrons. This approach can be brought to the extreme state, where only single particles are used for diffraction experiments at a very high repetition rate, as discussed by Veisz et al. (2007), Baum and Zewail (2008) and Baum (2013), Aidelsburger et al. (2010) and Gliserin et al. (2012), amongst others. The temporal resolution was not yet that impressive due to restrictions included in their setup designs. However, the basic limitation is simple. Repititive sampling requires fully reversible conditions, which are generally two mutually exclusive conditions in the study of structural changes.

The physical interpretation of the pulse broadening induced by a growing emittance is the variation in the traveled distances of individual particles in a pulse, a variation which is induced by the different transverse positions of the particles within the optics of the accelerator. Throughout their propagation the single particles will experience anisotropic guiding fields, which ultimately influences the phase-space distribution of the pulse. At the point of interaction with the specimen, the distribution should be formed such that the spatial position of the electrons is longitudinally aligned to ensure the highest temporal resolution along the axis of motion of the pulse. Ideally the beam is non-divergent, collimated, without omni-directional Coulomb repulsion enforced by over-critical charge densities.

The special desired phase space configuration is displayed, amongst others, in Kan et al. (2007) and van Oudheusden et al. (2007). The alignment of particles in one axis is typically achieved by sacrificing a second coordinate of the distribution, namely the momentum or angular spread, as the overall occupied phase-space-area remains non compressible. The normalized emittance of a pulse in one direction can be written as [Luiten et al. (2004)]

$$\epsilon_{n,x} = \frac{1}{m\ c}\ \sigma_x\ \sigma_{p_x}. \tag{2.7}$$

Analogously along the other coordinates. σ_x denotes the rms extension in x and σ_{p_x} the momentum distribution in x respectively. With the emittance, the coherence can be expressed by [van Oudheusden et al. (2007)]

$$L_{n,x} = \frac{\hbar\ \sigma_x}{m_0\ c\ \epsilon_{n,x}}. \tag{2.8}$$

This formula points out, that the coherence and the emittance are entangled quantities. For a maximized spatially coherent resolution, the emittance has to be minimized. Due to a generally larger beam-size in the transverse directions, the Coulomb-force-induced pulse-broadening is less distinct. The space-charge induced broadening predominantly degenerates the longitudinal electron bunch properties.

2.4.2 BRIGHTNESS

As for photon sources, we can define a brightness for electron beams accordingly, which describes the electron current per unit cross sectional area per unit solid angle per unit energy spread [van der Geer et al. (2006)]:

$$B = \frac{N\ e\ c}{(2\ \pi)^3\ \epsilon_{n_x}\ \epsilon_{n_y}\ \epsilon_{n_z}}. \tag{2.9}$$

A question which needs to be addressed is how many electrons are actually required to resolve a structure by a single or very few shots. This depends of course on the object to be resolved and the level of detail needed. The higher the number of electrons per probe pulse, the fewer laser-induced excitation events of the specimen are needed to trigger and to image the structural change of interest. Further, less quantity of the specimen is required. Since structural changes are generally irreversible, each laser excitation damages the sample. Occasionally, there is only a very limited sample area to allow sufficient time points to stitch together an atomically resolved movie. The critical nature of the specimen to this class of experiments must be fully considered in the design of the electron source and sufficient electrons per pulse for single-shot structure determination are ideally available. To answer this question we review a few of the time-resolved studies, which were conducted with electrons within the Miller group.

Siwick et al. (2003) averaged 150 electron pulses with 600 $\pm$ 100 fs pulse duration and 6000 $\pm$ 500 electrons per pulse. This results in $9 \cdot 10^5 \pm 8$ % electrons per time-point, considering, that the detector was not operated at a 100 % efficiency. In Siwick et al. (2004), specifically the dependency of the visibility of structures on the number of pulses was investigated. They concluded, that even 50 electron pulses with the same number of electrons per pulse can resolve the structure of polycrystalline aluminum films, meaning, that $3 \cdot 10^5$ electrons were sufficient at an overall detection efficiency of 10 % (10^4 electrons). More pulses and therefore more electrons were used for the sake of noise reduction. This revealed additional information on the structure, as more rings, especially those of weak intensity, became visible.

Sciaini et al. (2009) investigated the laser-induced melting of bismuth. Their 55 keV electron pulses with a pulse duration of 350 fs contained 10^4 electrons each. For the image formation they averaged over 20 pulses, yielding $2 \cdot 10^5$ electrons. The limiting factors

of the resolution in this early electron diffraction setup were the MCP coupled detector and the beam dynamics, that is associated with electrons of this energy. In particular this is the de-Broglie wavelength and the resulting distribution of the electrons within the pulse, which determine the emittance and coherence length. However, the structural dynamics of melting of bismuth were clearly resolved, again with approximately 10^4 electrons for small (< 5 nm) unit cells. Figure 9 shows diffraction patterns of these prior discussed studies.

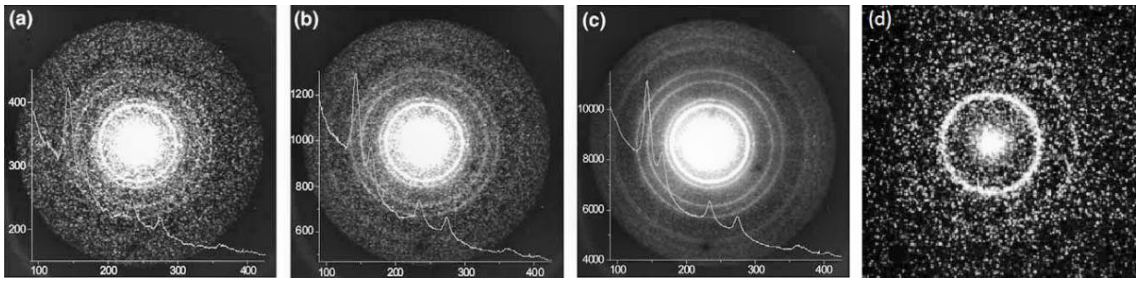

Figure 9: Early diffraction patterns: a) to c) adapted from Siwick et al. (2004). 50 to 150 averaged electron pulses of 30 keV form these images of thin aluminum films. Copyright 2003 Elsevier B.V, all rights reserved. Reprinted with permission from Elsevier. d) adapted from Sciaini et al. (2009). Electron numbers, as stated in the text above, image single-crystalline bismuth films. Reprinted by permission from Macmillan Publishers Ltd. Nature, vol. 458, 5 March 2009. Copyright 2009.

With the advent of new electron sources, more electrons per pulse can be used, while the electron pulse duration still decreases compared to the earlier sources.

2.4.3 PENETRATION AND SPECIMEN THICKNESS

The further characteristic features of electrons to consider are the penetration depth and the mean free path, which have to be matched with the thickness of the specimen. Both features are dependent on the electron energy, with energetic MeV electron beams having the advantage of an increased penetration depth. A minimum energy of electrons is required, at least 120 to 150 keV, to penetrate more sophisticated specimen holders such as nano- or liquid-cells [Mueller et al. (2013)]. These containers are especially attractive for the study of dynamic processes in their natural, liquid environment, if applicable. This concerns plain events in water [Cowan et al. (2005), Kraemer et al. (2008)] and more intriguingly biologically relevant proteins and their intra-cellular involvements. The availability of such special encapsulations alleviates the problematic circumstance that only a minority of specimen systems of interest can be crystallized. Thus the range of application for both x-ray and electron diffraction studies is widened.

For crystallizable systems it remains challenging to microtome crystals into thin slices with thicknesses on the 100 nm range, especially without the creation of deformations to crystallographic planes, such that diffraction patterns become deteriorated or completely vanish. This slices are also potentially required to allow electron transmission for the highest possible time-resolution and to avoid surface charging artifacts in the study of bulk specimen in reflection. Figure 10 shows the essential parts of a microtome with magnified view on a specimen (one that was prepared for the original PhD work).

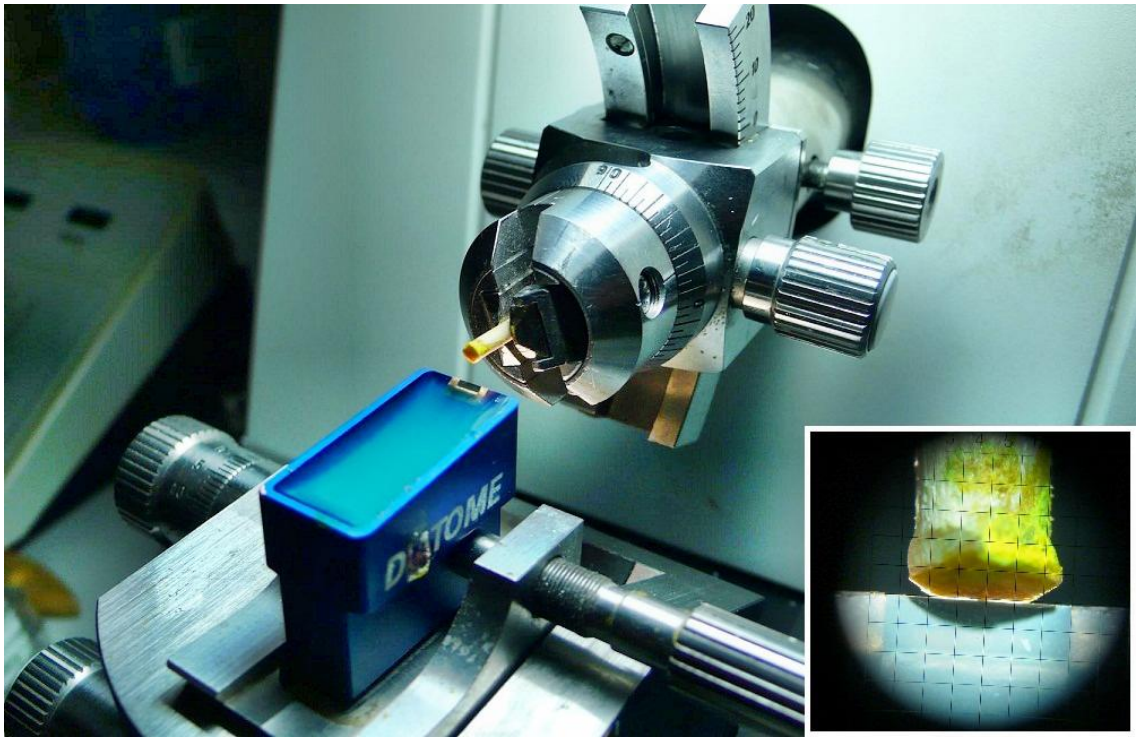

Figure 10: The essentials of a microtome. A boat with a diamond knife and motorized holder, which guides the specimen to the knife cutting edge in adjustable nanometer-sized steps. View through the magnifiers is shown in the insert with reflection of the specimen on the liquid in the boat.

For many specimen of interest this procedure of preparation remains to be one of the greatest difficulties, which potentially hinders the studies by electron diffraction, despite of improvement of the preparation techniques during recent years [Moriena et al. (2012), Eichberger et al. (2013)]. A higher electron energy can alleviate the requirements on the specimen, as thicker slices that can be more easily prepared are still penetrated by electrons with higher energy. Less energetic electron would completely lose their kinetic energy and be absorbed. Higher electron energies allow the observation of diffraction spots from slices as thick as 1 μm, without the loss of crucial information on the structure while there is capacity in the signal-to-noise ratio [see thickness-dependent scattering of MeV electron beams by aluminum slices (Manz et al. (2015))].

Despite the increase of penetration depth of highly relativistic electron beams the thickness of specimen is ideally matched to the avoidance of multiple scattering within the transmitted slice and to significant loss of kinetic energy due to inelastic scattering events. The preservation of single elastic scattering with mono-energetic electrons should be targeted to maintain distinct diffraction spots for maximized spatial resolution, as can be yield by the electron beam inherent parameters. The deterioration of diffraction peaks is mostly due to multiple elastic scattering during the transmission process and energetic smearing, which in turn can be caused by space-charge effects at lower energies [Chatelain et al. (2012a)]. The smearing is either given as prerequisite, implanted into the spectrum of the pulse by external influences or a consequence of the scattering processes.

Electrons scatter wildly and interact with the electrostatic potential of every atomic core in close proximity to their pathway. Any interaction changes the direction of propagation and potentially leads to a loss of kinetic energy, either through momentum transfer, which typically leads to ionization, or by radiation losses. These concern especially electrons with MeV kinetic energy, which predominantly lose kinetic energy through bremsstrahlung radiation. Whenever the assignment to a diffraction center is completely lost, the background noise in the diffraction images is increased and equally, when energy-induced broadening of diffraction projections is experienced.

A quantity of interest in this context is the mean free path. It specifies the path-length which is statistically traveled before another scattering event occurs. The mean free path is ideally matched with the thickness of the specimen such that only one single scattering event statistically occurs. This limit would result in the most accurate structural information. The mean free path depends on the density of atoms within the target material and on the according cross-section, as well as on the energy of the incident particle. The cross-section is a measure for the material-specific occupied area within a transmitted area, that can be integrated to give an effective diffraction volume. Within a fixed target with solid volume, the mean free path Λ_e is approximated by

$$\Lambda_e = \frac{A}{N\,\sigma_{el}\,\rho}, \tag{2.10}$$

where A denotes the mass number, N the number of atoms in the scattering volume, σ_{el} the scattering cross section of electrons and ρ the density of atoms. The cross-section for elastic scattering events herein can be approximated by [Reimer and Kohl (2010)]

$$\sigma_{el} = \frac{c^2\,h^2\,Z^{\frac{3}{4}}}{\pi\,E_0\,\beta}, \tag{2.11}$$

with c again denoting the speed of light in vacuum, h Planck's constant, Z the atomic number, $E_0 = m_0c^2$ the rest energy of the incident electron and $\beta = v/c$.

The interaction of electrons with matter can be further described by means of the mass stopping power (i), which accounts for all inelastic scattering processes, and the mass scattering power (ii), which handles elastic scattering processes that do not involve any losses of energy.

(i) The mass stopping power can be used to calculate the total path length which electrons travel in a given material during various interactions. In the context of transmission studies, the approximate calculation returns a valuable reference. The stopping power is defined as energy loss per path-length within a given material-density [ICRU (1980)]:

$$\frac{1}{\rho}\left(\frac{dE}{dl}\right)_{tot} = \left(\frac{S}{\rho}\right)_{tot} = \left(\frac{S}{\rho}\right)_{col} + \left(\frac{S}{\rho}\right)_{rad}. \tag{2.12}$$

The terms of equation 2.12 are outlined in the appended section A.1. The indexes denote the total; the collision, and the radiative mass stopping power, respectively. The mass stopping power accounts for all losses of energy, which are due to excitations and the creation of bremsstrahlung that is involved in processes of inelastic scattering. This term also includes particle collisions in which secondary electrons continue with energy from kinetic energy losses of incident primary electrons.

If the distance between the incident electron and the nucleus is comparably large, the collision is characterized as soft. The result is the excitation of an atom, which eventually releases an electron to dispel the excess energy from excitation. This collision has a high probability. If the distance between the incident electron and the core nucleus is rather small, a hard collision can occur. A secondary electron that is released by the atom from this process has itself sufficient energy for the cause of further ionization. Since an inner shell electron might be missing, bremsstrahlung with characteristic energies may occur, caused by the transfer of an electron into the vacant state with emission of stored potential energy as radiation. The energy transfer from soft and hard collisions that is accounted for by the first term of the stopping power, is comparable. The second addend of the stopping power deals with the creation of bremsstrahlung that is emitted as a consequence of the interaction of the incident electron with the nucleus. In the case of bremsstrahlung creation, the electron loses a significant portion of its energy. The mass scattering power increases with Z^2 and decreases with the inverse square root of the incident particle mass, important dependencies to remember.

Given the stopping power of a material, the total path-length r_0 of the electron can be calculated by

$$r_0 = \int_0^{E_0} \left(\frac{S(E)}{\rho}\right)^{-1}_{tot} dE. \tag{2.13}$$

This is known as the *continuous slowing down approximation* (CSDA) [ICRU (1980)]. It is important to note, that this expression does not return the penetration depth of an

electron. Instead, this formula allows the estimation of a practical range [Tufan et al. (2013)]. Experimentally, the scattering by thin slices of light materials was extensively studied. A review that is applicable to the energy range up to 600 keV, including an estimation formula concerning the penetration depth of electrons, was given by Gledhill (1973).

The stopping power of the target material is not only important for diffraction, but also for the considerations of radiation shielding. This is an important consideration of every electron diffraction apparatus and accelerator which exceeds energies of a few ten keV; was hence an important aspect of the development of the compact DC-operated installations of this work. The achievement of high voltages and electron energies is one aspect, the radiation protection of the users of the machine not of minor importance, the contrary is the case. No machine must be operated, when a user is exposed to unsubstantiated stray x-ray radiation. The REGAE, which will be outlined in the following chapter, is contained in a radiation safe building. The accelerator room can not be accessed without the interruption of an interlock for radiation safety. This makes additional shielding of the REGAE mostly irrelevant. Regulations only dictate a beam block at the very end of the accelerator and some electronic installations at the accelerator are covered by lead blocks to account for radiation during operation. Throughout the development of the compact electron gun designs, full consideration of radiation safety was required and obeyed.

(ii) The last of interaction of electrons with matter to consider in the context of electron diffraction is the amplitude of scattering, which can be obtained by considering the values of the mass scattering power. This quantity deals with scattering events that occur during the transmission of electrons through matter. For targeted studies, single-scattering events, ideally elastic, are favorable. The nature of electron scattering appears to be different though. Despite having a big advantage of better scattering power with fewer inelastic scattering events compared to photons [Henderson (1995)], energy is still deposited into the material of investigation by the electrons. Further, multiple scattering events occur and secondary electrons are generated. Because of the definition of the scattering power in the context of MeV electron beams and generally thicker targets, it may be inaccurate for thin absorbers. In thin absorbers, large angle scattering events have a relevant contribution and deform the cones and Gaussian distributions of scattered electrons, within which they leave the center of scattering. The mass scattering power is equally listed in the appended section A.2. Additional theories of scattering must eventually be considered.

3 DEVELOPMENT OF THE RELATIVISTIC ELECTRON GUN FOR ATOMIC EXPLORATION (REGAE)

We have learned that the investigation of ultrafast phenomena requires tools with sufficient time and spatial resolution. Using the previously outlined advantages of electrons and to close the gap to competing rf electron sources (as listed in table 9), a relativistic electron accelerator operated by two separate rf-cavities was designed and built. A special focus in design was laid on achieving an outstanding temporal resolution, while maintaining a sufficiently large transverse coherence length for the spatial resolution of complex biological structures. Within this work 2 and 1/2 years were spent on the design, manufacturing and installation of large sections of the *Relativistic Electron Gun for Atomic Exploration* (REGAE) [DESY (2014d)]. In this chapter I will outline the design of the accelerator and describe the efforts connected to this PhD work that brought this machine into its first state of operation.

3.1 INTRODUCTION

REGAE was designed for femtosecond electron diffraction experiments with relativistic electron pulses in the few MeV range. The pulses should contain a sufficient number of electrons (10^5 - 10^8) for recording single shot diffraction patterns while having electron pulse durations as short as 25 fs (fwhm). The accelerating section of REGAE measures approximately 2.5 meters in length and includes the two rf-cavities. The design of this part of the accelerator including had already been accomplished prior to the start of this work by DESY physicists and engineers. This prior work also included initially fairly primitive diagnostic means and a cathode exchange system, which further followed the design of the FLASH accelerator. Ultra-high vacuum components were equally provided by DESY. The first accelerator components were installed in the radiation safe building 23 of the former *linac 1* towards the end of 2010. The rest of this accelerator was neither designed nor anywhere under development at that point. Major tasks were then processed within this PhD work.

One of the first projects was a beam manipulating sub system for the REGAE - a set of dark current collimators. They are designed for blocking dark current electrons that are unintentionally generated within the rf-cavities, due to the application of intense electric fields for the acceleration of electrons. The handling of dark current and associated concomitants falls below the first sections of this chapter. Dark current electrons can obscure the signals that arise from experiments and potentially make those signals

non differentiable from the background. The intended benefit of the collimators is an enhanced separation of the valuable diffraction signals from the noise of background electrons. They can further be used to properly shape and clean up the electron beams, when a decent shape is not directly obtained. Another application of beam collimators is to avoid machine damage caused by energetic ionizing particles, that are accelerated to same final energies but travel off-axis in respect to the design trajectory. Energetic dark current electrons can damage components, as witnessed in highly relativistic electron accelerators of several hundred MeV to GeV, such as in accelerators of free electron lasers. This is however not an issue in REGAE, due to the restricted electron energy of a few MeV.

Downwards of the accelerating section of REGAE stands the core element for the interaction of electrons with the specimen systems of interest - a specimen chamber that can house all experimental installations anticipated at the time of design. This concerned the all-in-vacuum ponderomotive scattering experiment as well as installations of cryogenic and liquid cell diffraction holders. The first interaction chamber for the REGAE accelerator with all experimental requirements was in fact the first major engineering task for the REGAE and is described in section 3.2.2. This chamber proved to be a good educational entry point to engineering and UHV requirements.

The specimen chamber is embedded into the experimental section of the REGAE (as marked in figure 6). Initially, my responsibilities were the core elements in the experimental section of the machine. However the design and installation of the remaining beamline including first optical components for diffraction and their extensions were then also handled within this work to the state which is illustrated in the above mentioned figure.

To properly describe REGAE development to the present time and beyond the obligations of this work, the chapter starts with outlining the physical components of the REGAE accelerator (section 3.2), which are accompanied by studies of the electron pulse behavior in respect to its capabilities of temporal and spatial resolution (section 3.4). These simulations are based on input files for the ASTRA code [Flöttmann (2014)]. The dark current and associated problems are treated in section 3.3. First diffraction experiments and measurements on the electron pulse duration are now available and conclude this chapter, next to a summary of the current machine performance and envisaged extensions.

3.1.1 SCIENTIFIC CASE FOR REGAE

The development of the REGAE is fully embedded into the context of electron diffraction with its prospects and limitations. A long standing problem of electron diffraction is the requirement of thin slices of crystals or generally specimen for transmission studies

with electrons (as described in section 2.4.3). Otherwise insufficient numbers of electrons are transmitted and no diffraction image is obtained. Preparation of thin films remains challenging, and most systems of interest, especially those in the field of biology, will hardly ever be crystallized into macro-crystals at all. For thicker specimens as well as for vacuum-tight encapsulations, which allow the investigations of liquids, solution chemistry and protein crystallography using proteins contained in their natural environment, relativistic electrons overcome the restriction of penetration depth. Just considering the energy of REGAE, it allows the investigation of a broader range of dynamic structural processes in various systems, which are surrounded by holders and liquids which had further prevented the transmission by electrons up to this point. The energy of REGAE can be adjusted within a certain range to optimize the ratio of inelastic to multiple scattering. Due to the pulsed character of the electron beam, excessive heating as observed in classical TEM operation is avoided, which is known as radiation damage in the field of electron microscopy. While REGAE is an overall bright electron source, it can theoretically capture images of the structure before any deterioration manifests.

The second major key point of REGAE is the attention that was directed towards the generation of electron pulses with small transverse emittance. The emittance directly determines the coherence and therefore the spatial resolution (as treated in section 2.4.1). With consistently aligned electrons, the resolution of larger structures, with structural units as large as 30 nm (fwhm) in the transverse direction to the beam, is achievable, according to the simulations of the REGAE beam dynamics (section 3.4.1). Specifically this is achieved by carefully balancing charge densities, accelerator optics, cathode-materials and the driving laser pulses [Hauri et al. (2010), Li et al. (2012)]. This again widens the range of applications beyond lattice formations with simple unit cell structures, up to the scale of complex proteins, which are the main subjects of structural biology. With the introduction of nanofluidic liquid cells studies of structural biology can be conducted that are otherwise pursued at synchrotron sources and FELs.

The third major scientific aspect of the REGAE is the potential capability for the resolution of the fastest processes in chemistry on the order of few tens of femtoseconds with electron pulses as short as the physical limits of rf-acceleration and re-compression. When the simulated temporal resolution of 25 femtoseconds (fwhm) or less is obtained, REGAE will be on par with fourth generation light sources. In case that limitations from electronic timing jitter do not interfere with the machine operation, which is on the other hand common at all large FEL facilities, REGAE currently has the potential to even outperform the fourth generation of light sources. In this setting the sample-preserving advantages of electrons can be further exploited with one of the leading time-resolved electron accelerators.

The last design goal of REGAE was the development of a detector system that is capable of single electron detection [Li et al. (2011)]. This would add another gain factor to the effective brightness when comparing this electron source to conventional x-ray detectors in FELs. The quantum efficiency for detecting every photon, aside from a reduced scattering cross-section for photons, is limited. With the requirements of only 10^5 electrons per pulse (see section 2.4.2) with every electron detection, single-shot electron diffraction experiments are in reach. This feature was a critical aspect of design, especially for instances of non-reversible structural changes and few available specimen crystals. Single-shot structural determination is the only way to go, which could also be pursued with REGAE.

3.2 REGAE ACCELERATOR LAYOUT

REGAE, like many other rf-electron accelerators, utilizes standardized 3 GHz (s-Band) radio-waves to accelerate and generate femtosecond electron pulses in a normal-conducting rf-cell arrangement consisting of two cavities. A final electron energy of 2 - 7 MeV is obtained with the electro-magnetic power generated by a klystron and amplifier with 24 MW maximum power, which can be operated up to 50 Hz. This energy range and its application to femtosecond electron diffraction experiments is the initial design frame for which REGAE was drafted, following the design goals as specified in the scientific case above.

The first 1.5 cell cavity contains a photo-cathode plug [as illustrated in Hirano et al. (2004), with materials and methods as described in Sertore et al. (2006), Sertore et al. (2007) and Lederer et al. (2008)]. Receiving 75 % of the rf-power it carries out the major part of the acceleration. This distribution is important to avoid extensive space-charge broadening of the pulses in the low energy regime at the very beginning of electron pulse generation. The rf is further guided to the second 4 cell cavity, which is generally not used for further acceleration of the electrons from the first cavity, but primarily for the bunching of the electron pulses through a further drift [as described and investigated in Fill et al. (2006)]. The bunching effect is achieved by the diverging arrival time of the electrons at different electric field gradients. This is leading to a deceleration of the leading edge of the electron pulse in relation to an enhanced acceleration of the trailing edge of the pulse. With this induced velocity chirp the electrons are longitudinally realigned at a certain distance from the buncher-cavity while traveling with different energies. This compression by a drift section is the key working principle of the REGAE accelerator, as well as of the hybrid sources of table 9. With this trick REGAE presents a new class of electron accelerators, which is capable of producing ultra-short pulse-durations with rf-cavities at relativistic energies.

A further requirement for the generation of short pulses is the initial reduction of space-charge in the longitudinal direction, which is achieved by initiating long electron pulses on the photo-cathode lasting a few hundred femtoseconds. This mitigates the space-charge density problem close to the photo-cathode. Reaching the 4 cell buncher-cavity, the initially long electron pulse is longitudinally compressed during its further propagation through the beamline, subsequent to this second cavity. To support both cavities with the rf-power for the acceleration and bunching, the rf-waves are divided and tuned by a reflecting rf-guide arrangement in between the cavities. With the tuning of the resonance sections, which are also referred to as phase shifters [further illustrated in Hoffmann et al. (2013)], it is possible to influence the arrival time and the division of the rf-fields between the two cavities, in combination with the total rf-power control of the energy and temporal-spatial beam dynamics. This section decouples the cavities, which would otherwise have a fixed rf-wave distribution with respect to each other, being connected to the same source. This could prove problematic, since ideal timing settings could be out of reach. A more independent control of the rf-fields within the two cavities could be achieved with a second klystron. This feature will be added in the near future.

Further crucial elements are solenoids along the beam axis, of which three first solenoids are installed as a single and double solenoid arrangement within the accelerating section. This division of solenoids is beneficial for minimizing disturbing rotational and non-harmonic effects. In combination with the longitudinal position of the shortest electron pulse length, the solenoids determine the position of the specimen chamber. In the current REGAE layout, the center of this chamber is placed 5.5 meters from the photo-cathode. The specimen chamber contains all necessary ports for the execution of various experiments. Its size was adjusted to fit the largest experiment planned at that time. When a second scientific group moved into the project, which engages in laser wake-field based acceleration of prior-accelerated relativistic electron beams for compact FEL developments [Grüner et al. (2007), Maier et al. (2012), Grebenyuk et al. (2012)], the requirements exceeded the capacities of this first chamber, which was drafted for femtosecond electron diffraction experiments only. Therefore a second specimen chamber, which strongly adapted the design of this first chamber, is under development. Various vacuum shutters are installed in between the two cavities. The shutters are important to maintain the UHV condition within the cavities and generally in the first section of the accelerator. The shutters especially help with the installation and maintenance of the vacuum system and enable the specific maintenance of single units of the accelerator. To avoid electric breakdown whilst electric fields of 100 MV/m and more are applied in the cavities for short amounts of time, neither numerous rest gas particles nor contaminants should be present within or close to the cavities. The highest standards of vacuum maintenance are applied to REGAE.

To correct the beam orbit and to account for the offset of solenoids and lens errors, the beam can be deflected by steering-coils [Flöttmann (2010)], of which a few are installed along the beamline. This adds more flexibility to the parameter space of the machine, and the transmission of the electron beam from the photo-cathode to the detector at the very end can be assured. For example, deflections by the earth's magnetic field can to a certain extend be compensated. The measurement of the position and the beam shape along the accelerator is not of minor importance to evaluate the effects of lenses and steering elements and to provide the necessary and valuable feedback. Diagnostic screens are built into the two diagnostic crosses within the accelerator and into the specimen chamber to monitor the beam appearance at the various points of the acceleration and bunching process, before and behind specific solenoids, and at the specimen position [Bayesteh et al. (2013)]. The first diagnostic screens were especially helpful in the process of the first conditioning of the machine and for setting optimal machine parameters. In daily operation, they return valuable information on the beam shape and particle distribution. A mirror within one diagnostic cross is used for the alignment of the laser beam on the photo-cathode, and can be used to check the photo-cathode condition. The diagnostic screens aid in the aligning the position of the dark current collimators (which are described in section 3.2.4). Energetic analysis is accomplished using a dispersive arm. The deflection by a dipole magnet and optical recording returns information on the mean pulse energy and the energy spread. With this analysis, the beam energy can be precisely tuned. In combination with the diagnostic screens, this returns all vital information of the generated electron pulses.

In most measurements of the pulse properties, such as the spatial or energetic distribution, the electron pulses themselves get lost or deteriorated. Therefore measurement techniques, which do not affect the electron pulses, are ideally employed. The measurement of the charge of the pulses at REGAE is conducted in two ways. A Faraday-cup at the end of the accelerator, beside the detector station, measures the total incoming charge at the end of the beamline, which correlates to the optically measured signals of diffraction patterns observed by the detector. The precision of the cup is 10 fC [Delsim-Hashemi et al. (2013)]. The electrons are absorbed, converted into electric signals, and therefore lost. Close to the buncher-cavity of the machine, within the accelerator section of REGAE, a charge monitor measures the charge of transmitted electron pulses totally non-destructively. The charge is measured via a resonating cavity, which returns a signal that is proportional to the charge transmitting the cavity [Lipka et al. (2013)]. With this cavity, not only the charge of the pulses can be investigated with a few femto-Coulomb resolution, but the dark current (section 3.3) originating in the cavities can be equally monitored. Such monitors are used at FLASH and will be present at the European XFEL [Lipka et al. (2011)]. REGAE generally benefits from new devices for pulse manipulation and measurement as well as electronic synchronization, being one test bed

for the XFEL. An overview of the REGAE facility was given by figures 5 and 6. The beamline-components of the accelerating section of the REGAE are now presented in the following figure 11. For transparency, only the beamline elements are illustrated.

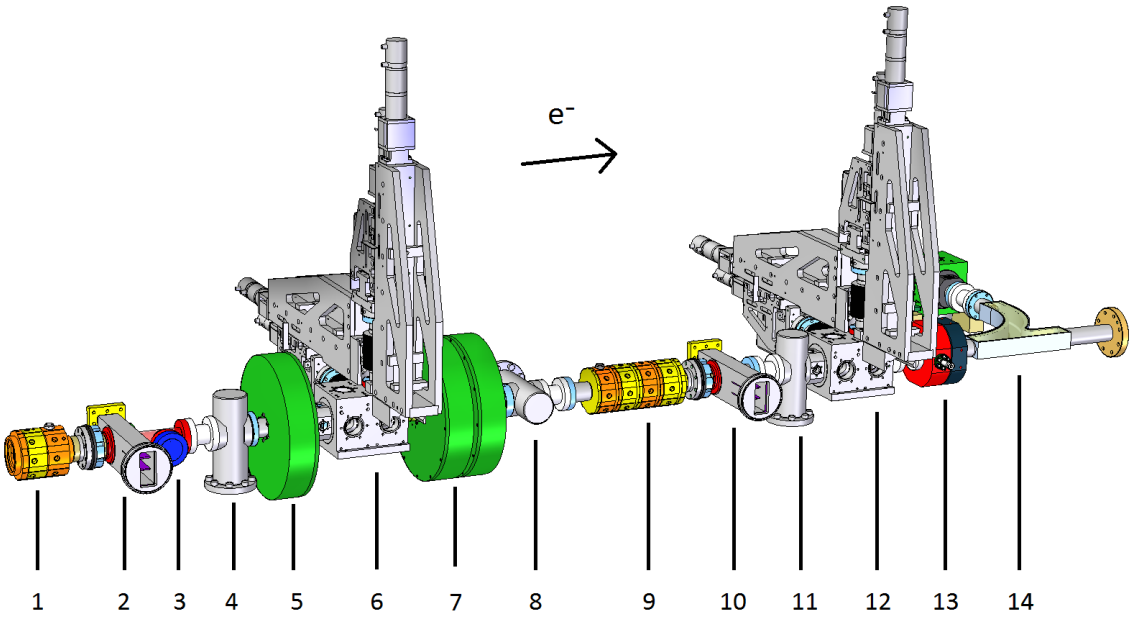

Figure 11: CAD depiction of the REGAE accelerator section - 1 gun cavity, $2+10$ rf coupler, 3 mirror chamber, $4+8+11$ vacuum shutter, $5+7$ single and double solenoid, $6+12$ diagnostic cross with dark current collimators and diagnostic screens (not shown), 9 buncher-cavity, 13 charge monitor, 14 dispersive arm.

The dark current collimators, which are contained in this section and illustrated in these graphics, present another sub-project for the REGAE, which was handled by this PhD work. Simulations on requirements for shielding of MeV electron beams and material studies were conducted. The dark current is treated in section 3.3 separately. The collimators are presented in section 3.2.4.

3.2.1 REGAE DESIGN WORK PART I - EXPERIMENTAL SECTION

The section which is attached to the accelerator is referred to as the experimental section, within its center the specimen chamber and at its end a detector station. This section to the extent shown in the following figure 12 was entirely designed and its construction organized and supervised within this PhD work. The efforts linked to this section of REGAE completed this project to a very crucial extent and helped the accelerator achieve its first full operation.

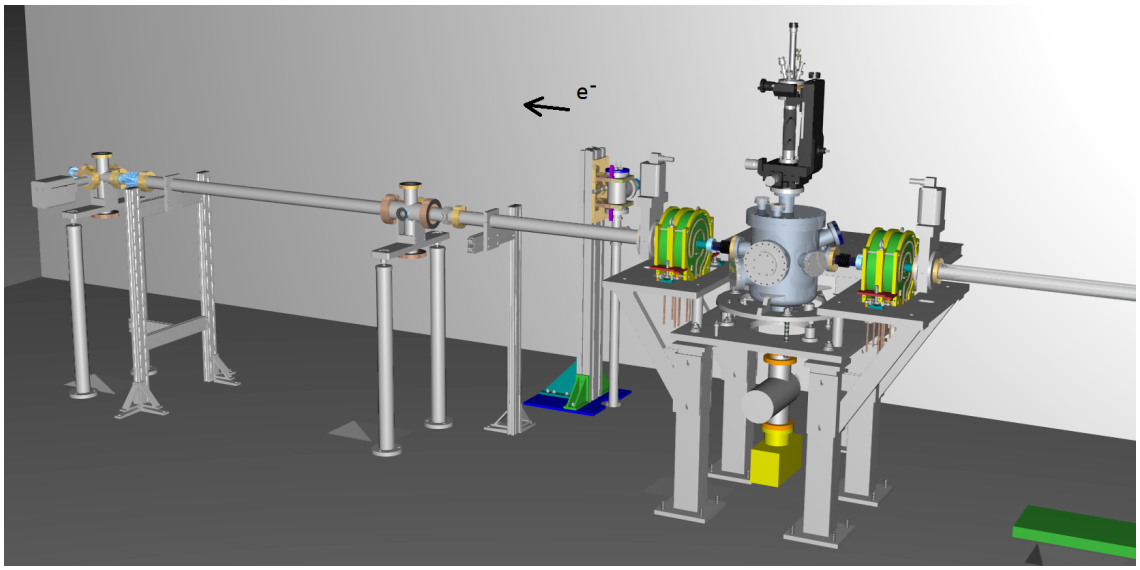

Figure 12: REGAE experimental section, showing everything that was designed and built within this PhD work. The specimen or target chamber is located in the center of this section, surrounded by solenoids and a breadboard for the optics of the pump beam. A manipulator with He-cryostat for investigations at low specimen temperatures is attached to the top of this chamber. The remaining work concerned the design and construction of the missing beamline, from the accelerator to the end of REGAE, as well as participation in the transfer of optical beams to the REGAE.

The specimen chamber herein (outlined in the following section 3.2.2) was the first engineering task solely treated by the author, the first of countless engineering projects, which followed the acquisition of urgently required CAD skills for these jobs. The position of the specimen chamber was determined in cooperation with REGEA beam simulations conducted by DESY physicist Klaus Flöttmann. The best spatial and temporal focus was determined to be at 5.5 meters in the beamline, and this is where the center of the specimen chamber was installed. The chamber, being the core element of this section, is surrounded by table extensions for solenoids, which at that point are used for the focusing of the electron beam at the sample and on the detector. Next to the laser beam port entry is a large breadboard, which houses the optical setup for the conversion of laser wavelength and is also containing the translation stage for time-resolved experiments. The remaining beam tube comprises further vacuum crosses, which are located at the potential positions for a detector station. The different positions within the beamline would allow a different magnification of the electron patterns. The first installation of the detector station, with technical details of the detector itself treated by DESY physicists Hossein Delsim-Hashemi and Shima Bayesteh, was placed at the very end of the beamline, just immediately in front of the Faraday-cup. It has not changed ever since, as this position was found to deliver a decent overall image of the diffraction patterns in combination with the fourth and fifth solenoid. The experimental section was further equipped with frames for diagnostics, lead shielding and equipment by our

former engineer Santosh Jangam. These additions are not shown in this illustration, but can be observed in the concluding photograph of REGAE at the end of this chapter. The installation of all beamline components as shown in this figure was completed by November 2011. For most of these beamline elements this means, that only little time had passed from the appointment of these jobs to the author to the final installation in the accelerator hall. The first electron beam was generated only shortly after the completion of the beamline, but the propagation of the beam to the detector at the very end of the beamline required another few months, as can be seen in the timelines of figure 8. An overview of the position of all important beamline elements of REGAE is provided in Delsim-Hashemi et al. (2013).

3.2.2 REGAE DESIGN WORK PART II - SPECIMEN CHAMBER

The specimen chamber, also referred to as the target-chamber, is an essential element in this machine. The requirements of the chamber were discussed and settled with group member Gustavo Moriena (based in Toronto) in November 2010. Once the first draft for the chamber was completed, the design was optimized with respect to REGAEs' UHV requirements, which involved guidance by DESYs leading vacuum engineering group MVS. By December 2010, the ordering of materials and preparation of manufacturing had started. Only two months later, the chamber was ready for final surface treatment and vacuum tests, before it found its way into the REGAE-bunker during early summer 2011. The size of the chamber was adjusted to fit the largest experiment planned at that time, namely the ponderomotive measurement of electron pulse durations. This measurement required a small breadboard with some mirrors and lenses, which are placed close to the electron beam inside the vacuum chamber. The crossing of the focused optical with the electron beam of a similar size causes electron scattering by the optical-electric field modulation, which can be observed as intensity change on the detector. With a controlled delay of optical and electron pulses, this can be used to visualize the pulse lengths in respect to each other [Siwick et al. (2005); Hebeisen et al. (2006, 2008)]. The optical layout of this experiment is shown within the cross-section through the vacuum chamber including the electron and laser beam paths. This chamber-cut further illustrates the purpose of the flange connections within the daily and envisaged use [figure 14]. The remaining experiments of interest, solid and liquid studies, would not require a chamber of this size, which would minimize the chamber surfaces and thus could improve the vacuum condition.

It is important to maintain the best vacuum conditions in the cavities. Any contamination originating from the specimen chamber can easily propagate through the common vacuum system to the accelerating section and must therefore be avoided at all times. Fast shutters and cryogenic traps were discussed to prevent damages to the rf-cavities

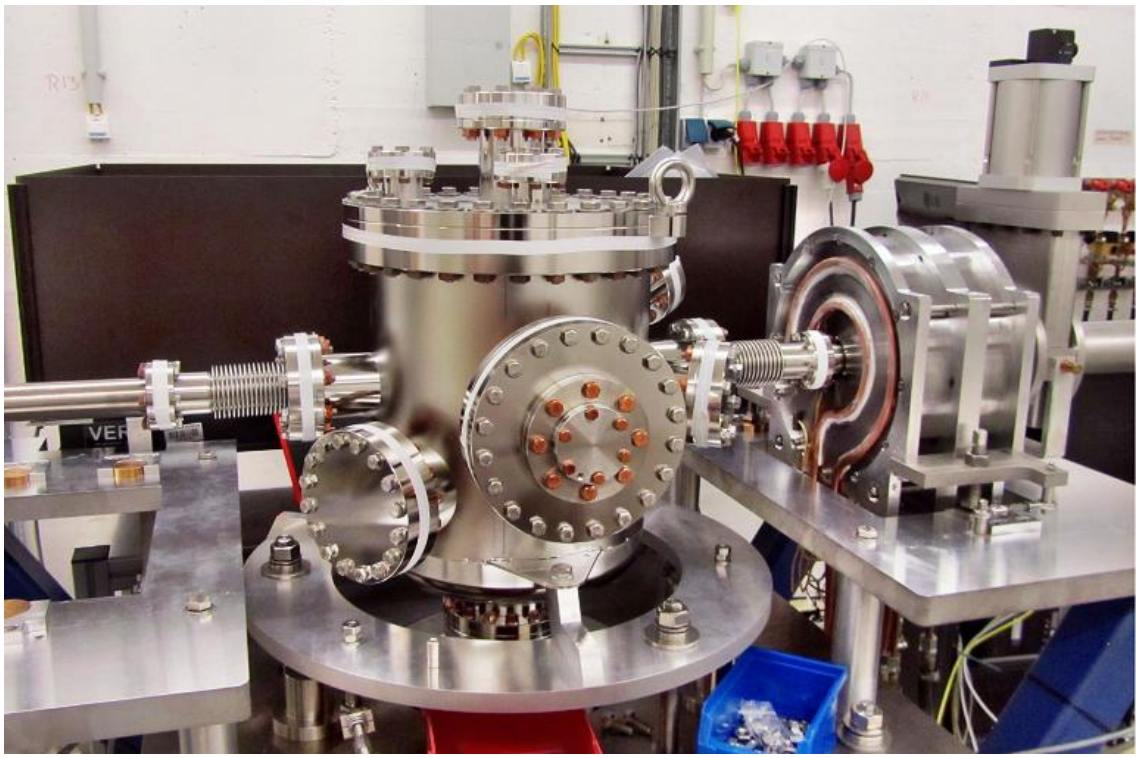

Figure 13: REGAE specimen chamber, freshly connected with the neighboring beam tubes and acceleration section of the REGAE. The ring of solid aluminum is the chamber base, which allows horizontal, vertical, rotational and tilting alignment by fine-pitch threads within the mounts.

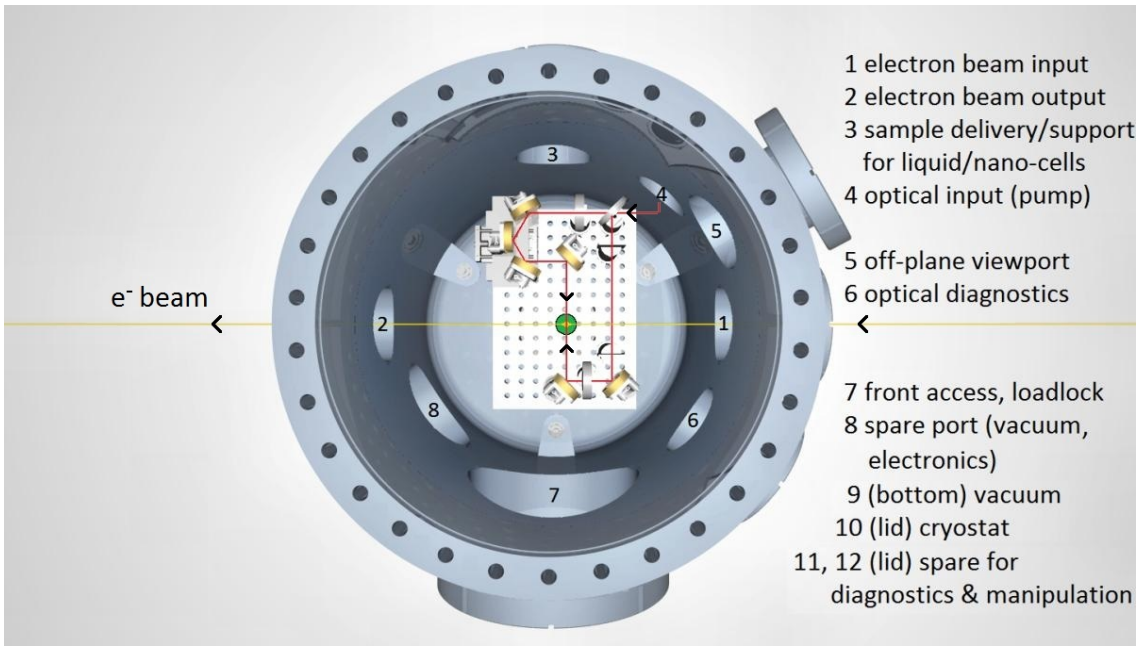

Figure 14: Cross section view into the REGAE specimen chamber with the installation for the ponderomotive experiment. The red line illustrates the beam path of the laser, the exaggerated fainted yellow line indicates the electron beam. Only one of the two intersections of the two beams denotes the position where a temporal overlap of both pulses is achieved, marked with the green spot.

in case of failures that could be related to bursting liquid cell encapsulations, but never realized. Not only biologic specimens would quickly deteriorate the fine vacuum systems. This still is one of the biggest fears that concerns the vacuum system and accelerator functionality, though up to today such an incident has not occurred in our studies.

3.2.3 REGAE DESIGN WORK PART III - LASER BEAM TRANSFER

Most of the optical installation for the REGAE, especially the laser system, is located below the accelerator (the laser system is described in section 4.1.1 of the following chapter 4). With this design feature continuous access to the laser system is granted, even when REGAEs' scattering electrons generate x-rays within the accelerator tunnel. On the other hand, due to restricted space in the accelerator hall and the desired proximity to the other compact electron sources in the same building (see figure 6 and chapter 4, respectively), there was no other choice. To connect the laser system to the REGAE accelerator, two holes were drilled into the sub-ceiling, which is made of 1.5 meter thick hardened concrete. Two laser beam transfer systems were installed to guide the photo-excitation and specimen-pump laser-pulses into the accelerator room.

Figure 15: Laser beam transfer systems, which guide the optical beams to the accelerator. Left: upper part of the pump-beam-transfer. This image shows when the laser beam was transmitted to the upper floor for the very first time. Middle: lower part of the pump-beam-transfer. Right: Lower part of the probe-beam-transfer.

The design and implementation of this system was organized within the efforts of this PhD work. In this case, initial drafts for the transfer system were developed in cooperation with the former engineer of the University of Hamburg, Benno Frensche and his assistant Jutta Pelz. This task was later transferred to former DESY engineer Josef Gonschior, who drafted a modified transfer system in collaboration with Otto Peters that

has a major benefit when compared to the former version. The traveling distance from the lower floor to the floor above measures several meters. Every laser beam experience divergence due to the scattering in air. For this reason the optical transfer system was designed such that all tubes can be evacuated using *Kleinflansch* (KF) elements. In total two similar transfer systems were installed. One in the front, close to the photo-cathode of REGAE, and another one close to the specimen chamber. The transfer system was illustrated within the figures 6, 12 and now in figure 15. The figure shows the top part of the pump-beam transfer close to the specimen chamber, with the first laser beam that was shot into the accelerator hall on a plastic cover. The other two pictures illustrate the bottom parts for both laser beams.

3.2.4 REGAE DESIGN WORK PART IV - DARK CURRENT COLLIMATORS

The PhD work also involved the design of the core elements of the dark current collimators, the collimating leafs, with their various apertures of different sizes. Additionally, the organization and supervision of the construction and installation of the collimators in their first functional condition was the author's responsibility. The manipulation system for the collimators, as illustrated in figure 4 and figure 17, was designed by DESY engineer Martin Lemke.

In the first planning phase, various designs and shapes were considered to estimate the best shape of the absorbers in respect to the useful electron pulses and the disturbing fractions of electrons, that would equally propagate through the beam-tubes of the accelerator. The incorporated design is a simple arrangement of holes of various sizes in heavy metal bars made of tungsten. These collimators are by means of a motorization of the manipulators inserted and moved within the diagnostic crosses of REGAE. Figure 16 illustrates, how the collimators are operated within the diagnostic cubes and illustrates, how the cross-section of the beam-aperture of the diagnostic cross is mostly covered by the tungsten bars. Only the little apertures allow the penetration of the electron pulses. The envisaged thickness of a single bar of 12 mm was reduced to 8 mm, to maintain a comfortable collision-free operation within the diagnostic crosses. The demanded thickness, which determines an attenuation of beam energy to a value of 0.001 %, can be obtained and exceeded by the overlap of two bars within the direction of the electron beam. The spatial masking of the cross-section of the beam-tube amounts to more than 60 % of the aperture, which was another design criterion. In total, four bars are present within the two diagnostic stations of the accelerator. Since the collimators are installed within the accelerating section of REGAE, electron pulses can be early separated from dark current and shaped, while they are guided to the experimental section.

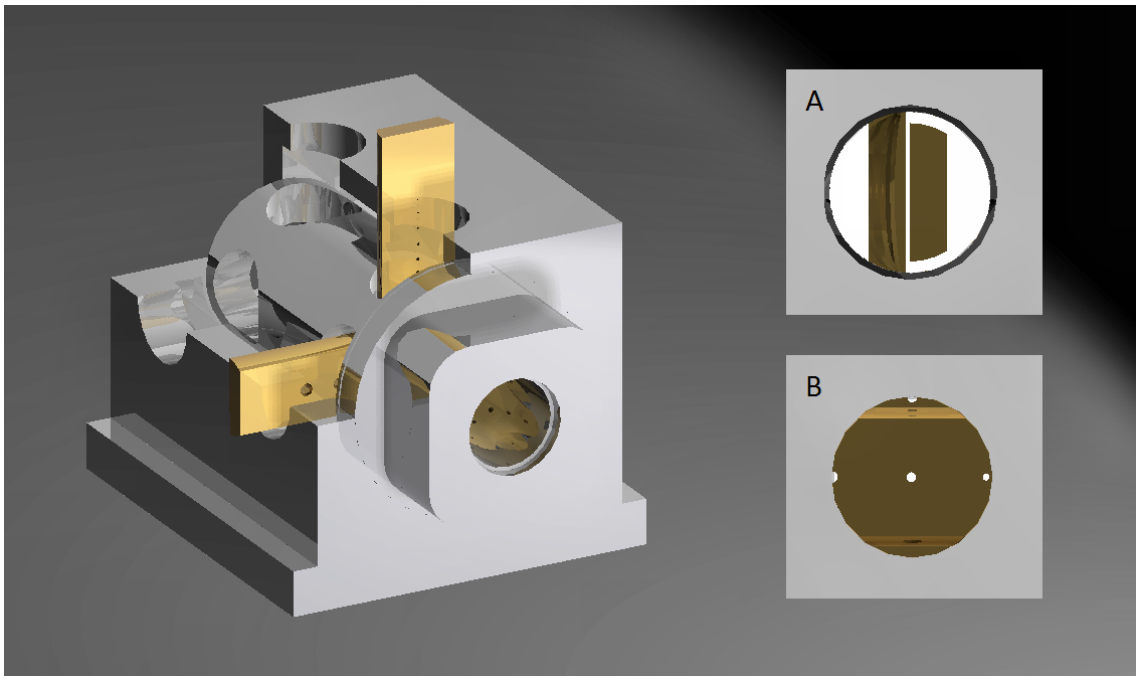

Figure 16: Illustration of the dark current collimators in a diagnostic cross. Each cross contains two bars, one in the horizontal, one in the vertical orientation. A and B show close ups of side and front views into the cross, respectively. The occupied area can be clearly observed. Bars are not precisely to scale and shape.

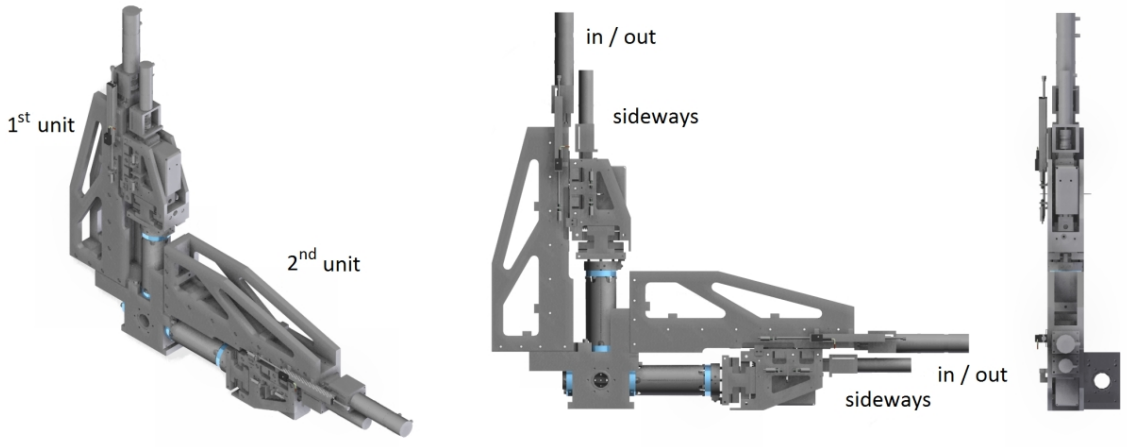

Figure 17: This illustration shows the mechanical installation for the manipulation of the dark current collimators. Two units are located at each diagnostic cross in the accelerator. Each unit is holding one collimating tungsten bar. The installation position at the diagnostic stations is extremely limited sideways, requiring a compact design of the manipulators in this direction with an inventive mechanism for the sideways movement. This is the 2011 design of DESY engineer Martin Lemke.

With the help of diagnostic screens in these sections, the effect of the collimators on the electron beam can be imaged instantaneously. The hole diameters in the collimators range from 0.3 mm to 6.0 mm to cover a wide range of apertures and beam sizes. The holes are equally distributed over each pair of bars. An off-set of the beam position can be accommodated with the capability to move sideways by $\pm$ 5 mm. With the previously mentioned steering coils [Flöttmann (2010)] along the accelerator and the flexibility of the collimators, the optimal beam position within the accelerator optics can be maintained, while the beneficial beam-clearing effect of the collimators is used. The golden color of the collimators in the illustration is used for better visibility, but it points out the value for obtaining a suitable electron beam shape for diffraction and real space imaging.

The collimators are operated by manipulators, which offer a high precision in the adjustment of the leafs. The requirement was 10% of the smallest aperture, i.e. within the few micrometer range at minimum, to allow a precise position of the smallest apertures. Further a high mechanical stability, which is not affected by environmental changes, was required. One of the bigger challenges in this design was the constrained installation space at the diagnostic crosses due to other diagnostic tools being in very close proximity. Figure 17 shows impressions of the complex mechanical appearance of the highly stable and precise collimator-manipulators.

3.3 DARK CURRENT

The generation of femtosecond electron pulses is accompanied by undesired dark current electrons. Especially within the cavities, dark current is created by the sheer presence of electric field gradients [Fowler and Nordheim (1928)]. The generation of secondary electrons in any part of the accelerator is furthermore possible (as outlined in section 2.4.3). Undesired electrons, which do not contribute to time-resolved measurements, should be separated from the usable electron pulses. These electron can either be erased, right after their generation, to prevent their arrival at the specimen and detector, or filtered from the design energy, requiring an energy filtering technique within the detection system. This latter technique is difficult to realize, since detectors so far only measure the presence or absence of electrons in a bin or pixel, not their energy.

As outlined above, spatial filters are used in REGAE to shield dark current from useful fractions of electron pulses. As long as the dark current electrons do not line up with the design orbit of the electron beam, they can be spatially filtered by these collimators. The remaining dark current electrons that align with the electron pulses for diffraction, can only be separated by temporal filtering on the detector, for example by external gating, to constrain the influence of the dark current electrons, which otherwise contribute to the background in the measurements. For low electron pulse charges, which are beneficial for

longitudinally short and laterally confined pulses, this background is a serious problem. Signals from diffraction can become totally indiscernible from the noise of the dark current background and the electronic noise of the detector itself. In electron diffraction experiments, the amount of dark current may well compete with the electron numbers that are used for diffraction experiments. With several pico-Coulombs they may even overwhelm the useful charge. Being distributed over most fractions of the rf-pulse within the cavities [investigated in Delsim-Hashemi and Flöttmann (2014)], the integration of dark current electrons with the detector is highly deleterious to signal detection, where the integration time exceeds the duration of the arrival of a single scattered electron pulse.

3.3.1 SOURCES AND SUPPRESSION OF DARK CURRENT

A free electron is generated when the binding energy of the material, or the work function, respectively, is overcome. Optical laser pulses for photo-excitation are not the only source that deliver the required energy for this process of liberation. In this context it is the acceleration of charged particles by rf-fields that provides the required counterpart to the binding energy. Electric field gradients inside the rf-cavities of REGAE, which range up to 120 MV/m, cause field emission. The barrier to the continuum, which is in this case the vacuum environment, can be significantly lowered, when electric field gradients are further increased by deviations of ideally flat surfaces (this is equally important to consider in the design and manufacturing of high voltage electrodes, as described in section 5.4 and section 5.4.2, as well as for the development of a high-voltage feedthrough, as described in section 5.5 of chapter 5). Instead of a gain of the average electric power, local deformations of the otherwise electrically flat surfaces lead to field enhancements, which free the contained electrons from the given metallic conductor.

The first problematic source in this sense is a given surface roughness, which is determined by the machining processes. If manual polishing is applied, it is the grain size that determines the average surface roughness. In electric polishing the enhancement of electric currents, caused by geometrical spikes, reduce these features and flatten the surface, which subsequently lowers the local electric field strength. The other factors that lead to field enhancements (besides cavity dimensions and shapes) are inclusions of and contamination by alien particles, impurities in alloys, which can lead to surface irregularities, dents and sharp edges. All of these sources lead to the emission of electrons due to a local enhancement of the electric field gradient. The dark current itself is accelerated, mostly in a non-predictable way towards grounded components, or along the accelerator. Multipacting can quickly damage and degenerate the performance of the photo-cathode [Han (2005)]. The energy of dark current electrons can be higher than the average beam energy, when dark current electrons enter cavities at different phases than the usable

electron pulses. As previously mentioned, components of the accelerator at any position suffer from radiation induced damage caused by off-axis electrons that originate from dark current. An extensive study of the generation and the dynamics of dark current electrons at the PITZ accelerator is given in the above reference and in Han et al. (2005). Further, effects and precautions for dark current in the XFEL were investigated [Han and Flöttmann (2006)].

Field emitters cause problems in the daily operation of accelerators in two different ways. First of all, they can lead to the emission of dark current, which can worsen the contrast and signal to noise ratio of the experiments. Furthermore, they can lead to electric breakdown and limit the overall applicable field strength [van Oostrom and Augustus (1982), Wang and Loew (1997), Norem et al. (2003)], which is otherwise only influenced by the condition of vacuum. Most emitters are produced or included within the manufacturing processes. Great care was taken in regard of the removal of alien particles in the production of rf-cavities and critical beamline elements. Besides pure glow- or rf-conditioning [Hossein2014], the application of current or rf-energy to cavities for a longer period of time removes field emitters by evaporation and subsequent evacuation. Techniques such as ultra-pure water rinsing [Kneisel and Lewis (1995)] or dry ice cleaning [Dangwal et al. (2007), Brinkmann et al. (2008)] can be employed. These treatments significantly improve the condition of cavities and protect surfaces, that are exposed to strong electric field gradients, from damages.

3.3.2 ELECTRON BEAM SHIELDING SIMULATIONS

For the development of the dark current collimators, Monte Carlo simulations with the EGS5 package were performed to determine the penetration depth of MeV electrons through heavy metals of choice, to estimate an appropriate thickness of applicable materials for the shielding of dark current. A 5 MeV electron pulse consisting of 10^4 to 10^5 electrons, which reflects the average energy and number of electrons used in REGAE, was in these simulations perpendicular incident on a bar of a heavy metal. The transmission, absorption, and reflection of electrons and their fraction of energies was determined in dependence of the simulated material. Studies were executed for the two heavy metals of choice, tantalum and tungsten, and compared to lighter materials, such as aluminum and copper. These materials are commonly used in several accelerator structures. A few data points of all results are listed in the following table 10. Since the collimators were designed for use in a vacuum environment, the only other heavy material, lead, could not be used, due to the problem of out-gassing.

	Aluminum (Z=13)			Copper (Z=29)		
thickness [mm]	R [%]	A [%]	T [%]	R [%]	A [%]	T [%]
1,0	1,053	95,901	3,046	4,570	91,501	3,929
2,0	1,106	96,394	2,499	4,607	92,869	2,523
4,0	1,166	96,890	1,944	4,639	94,253	1,108
6,0	1,146	97,348	1,506	4,514	94,924	0,561
8,0	1,190	97,641	1,169	4,630	95,108	0,262
10,0	1,217	97,864	0,918	4,547	95,327	0,126
	Tantalum (Z=73)			Tungsten (Z=74)		
thickness [mm]	R [%]	A [%]	T [%]	R [%]	A [%]	T [%]
1,0	12,875	83,462	3,663	12,920	83,936	3,144
2,0	12,849	85,569	1,582	12,837	85,921	1,242
4,0	12,776	86,863	0,361	12,952	86,825	0,223
6,0	12,762	87,152	0,087	12,877	87,082	0,041
8,0	12,795	87,187	0,019	12,903	87,090	0,007
10,0	12,792	87,204	0,004	12,902	87,096	0,002

Table 10: Values for the reflection (R), absorption (A) and transmission (T) of the energy of 5 MeV electron pulses in bars of Al, Co, Ta and W with varying thickness, obtained with EGS5.

With logarithmic scaling on the ordinate, this yields a mostly linear dependence with increasing thickness, as can be expected by the exponential attenuation factor for ionizing radiation [Vogt and Schultz (2011)]:

$$I = I_0 \cdot e^{-\mu \rho t}, \tag{3.1}$$

where I denotes the remaining intensity, I_0 the initial intensity, μ the attenuation coefficient $[cm^2/g]$, ρ the density of the absorber and t its thickness in cm. The following graph 18 illustrates all data points, which were obtained by the EGS5 simulations for the transmission of initial beam energy on a semi-logarithmic scale. The intensities and attenuation factors for these materials, as shown within the insert of the graph, were obtained by exponential fits to this simulated data (straight lines).

It can be observed from this graph and the values of table 10, that for thin sheets of absorbing material (< 1.5 mm) less energy is transmitted through aluminum than through any of the other, heavier materials. Instead, aluminum absorbs most of the energy and causes little reflection of around 1 % and little transmission of energy at this incident mean energy. This is not intuitive, since heavier materials are expected to

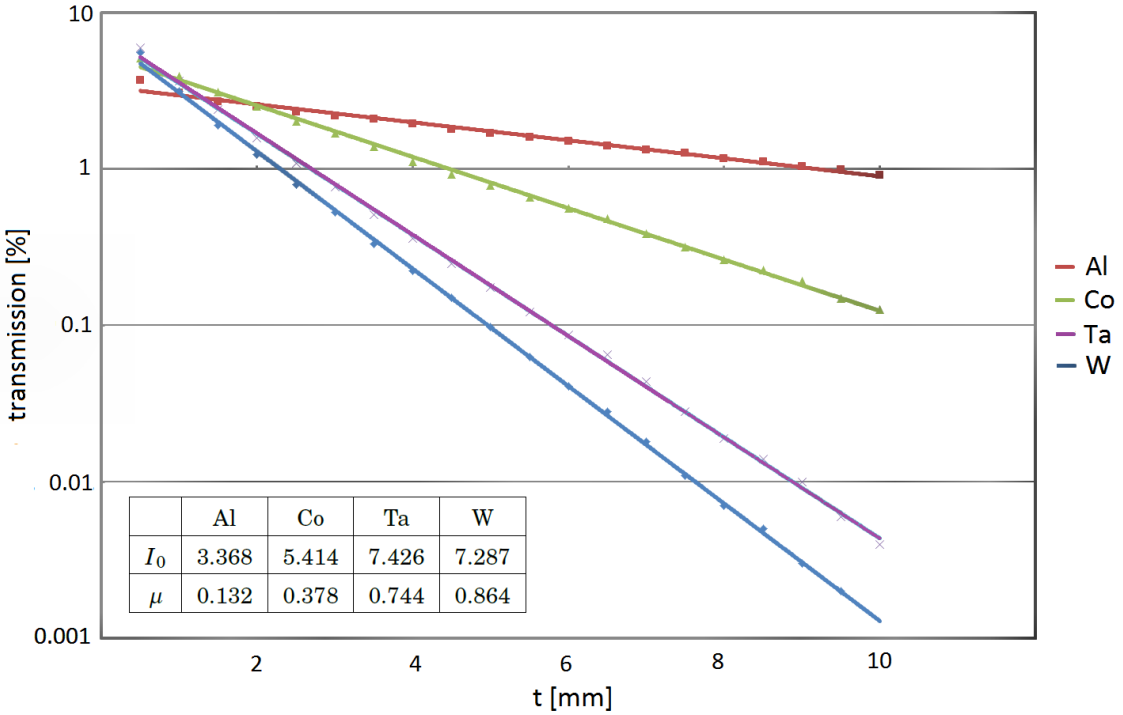

	Al	Co	Ta	W
I_0	3.368	5.414	7.426	7.287
μ	0.132	0.378	0.744	0.864

Figure 18: These curves show the dependency of the transmission of energy as dependent upon the material type and thickness.

shield radiation better, but can be explained. The loss of energy, mostly by radiation losses (as described in section 2.4.3), increases with the atomic number of the target material (proportional to Z^2). This energy loss correlates to increased attenuation factors, which are obtained from the fits and equally provided in this graph. Concurrently, a larger amount of bremsstrahlung that is produced in the heavier materials exits the rear surface of the bars. A generation and emission of secondary particles is also observed. In light materials energy is lost by proportionally more scattering events, in which energy is transmitted by collisions, not by a production of bremsstrahlung radiation. A light absorbing material, such as aluminum, is used as surface coating within many applications of radiation shielding for this reason. Aluminum is also used in the design of x-ray shields of the FED-CAMM experiment (described in section 5.7).

Considering the results of these simulations, tungsten seems to be the preferred material for dark current collimators due to the high attenuation factor and availability of the material. An attenuation of the energy of dark current electrons and the absorption of secondary particles and bremsstrahlungs-photons by a few orders of magnitude is desirable in time-resolved experiments with little charge per pulse. The remaining energy of dark current electrons that are leaving the rear side of the collimators is negligible. Further, the scattering within the absorbers leads to a deflection of the incoming electrons over wide angles. The dark current electrons will thus leave the trajectory of usable

electron pulses and will not contribute to diffraction signals from specimens.

The thickness of the collimators was selected such, that of initially 10^5 electrons, which produce secondary electrons and bremsstrahlungs-photons during their interaction and energy loss in the collimator, statistically less than one bremsstrahlungs-photon is transmitted through the collimator. For this threshold, the simulations return a material thickness of 12 mm. As previously described, each collimator has two bars with a thickness of 8 mm, due to the restricted space inside the diagnostic crosses of REGAE, and due to challenges in manufacturing the desired apertures. Both tantalum and tungsten are quite tough materials, making it difficult to prepare apertures of the smallest diameters. The required thickness of 12 mm is exceeded by the use of two collimators per diagnostic slot, even amounts to 16 mm. The total attenuation of the collimators will be less than 10^{-5} of the initially incident pulse energy with statistically no secondary electrons or x-ray photons, translating to a few ppm of transmitted energy only. This clearly helps with the visualization of the usable electrons from electron pulses on the detector and keep them separate from the dark current background.

The statistics of these simulations can be improved by using more electrons per simulation. The main conclusion of these simulations won't change though, only be refined in marginal ways. The other values of this table provide reflected and absorbed fractions of pulse energy. Another interesting aspect of heavy materials becomes visible. Numerous electrons get back-reflected towards solenoids and, if they pass, back into the accelerating cavities. Most likely, due to their wide range of scattering angles, not many of these back-scattered electrons will survive long, but get lost in the accelerator geometry. The values of reflection and absorption stay more or less constant throughout the increment of the collimator thickness, since most of these processes happen within the first few micrometers in proximity to the collimator surface. A treatment of scattering of electrons by both Monte Carlo simulations and analytical fits can be found in Hirscht (2009).

3.4 REGAE SIMULATIONS AND PERFORMANCE

3.4.1 ASTRA SIMULATIONS

REGAEs' capabilities were estimated by simulations executed with the ASTRA code [Flöttmann (1997)] and formed the basis for the design concept. The simulation parameters used herein are summarized in table 15 in appendix B, which provides in combination with Delsim-Hashemi et al. (2013) all of REGAEs' most important machine parameters. The results of emittance, coherence, beam-size and electron pulse duration for 10^5 electrons per pulse are presented in the following graphs.

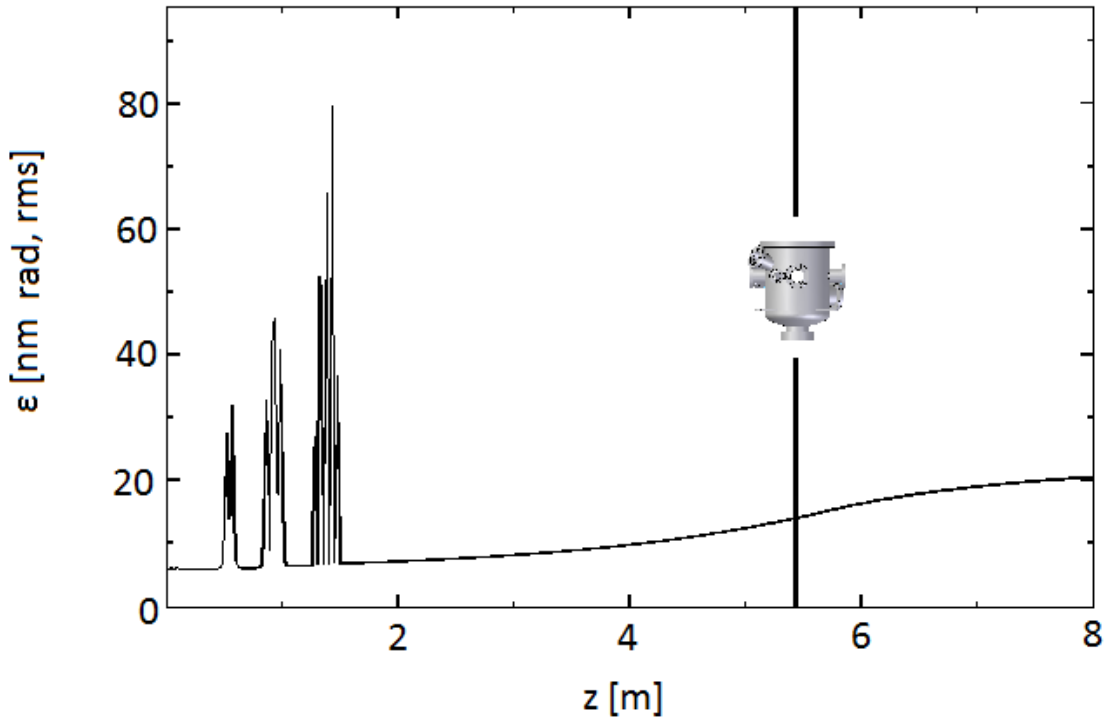

Figure 19: ASTRA simulation of the transverse emittance of REGAE.

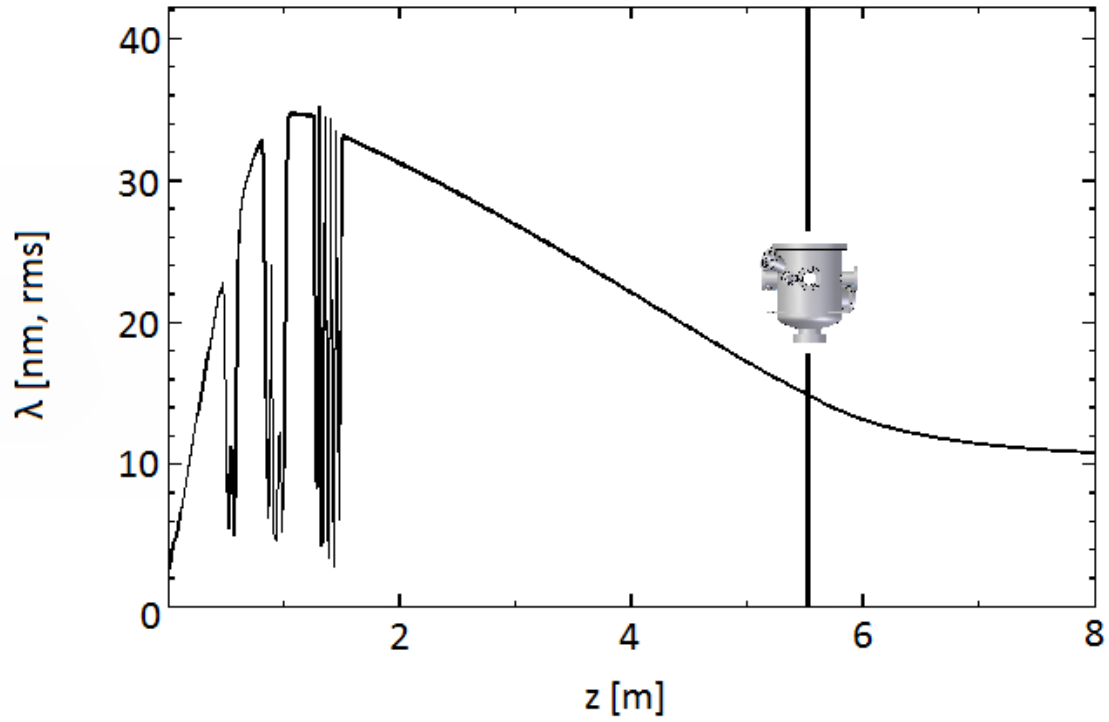

Figure 20: ASTRA simulation of the transverse coherence length.

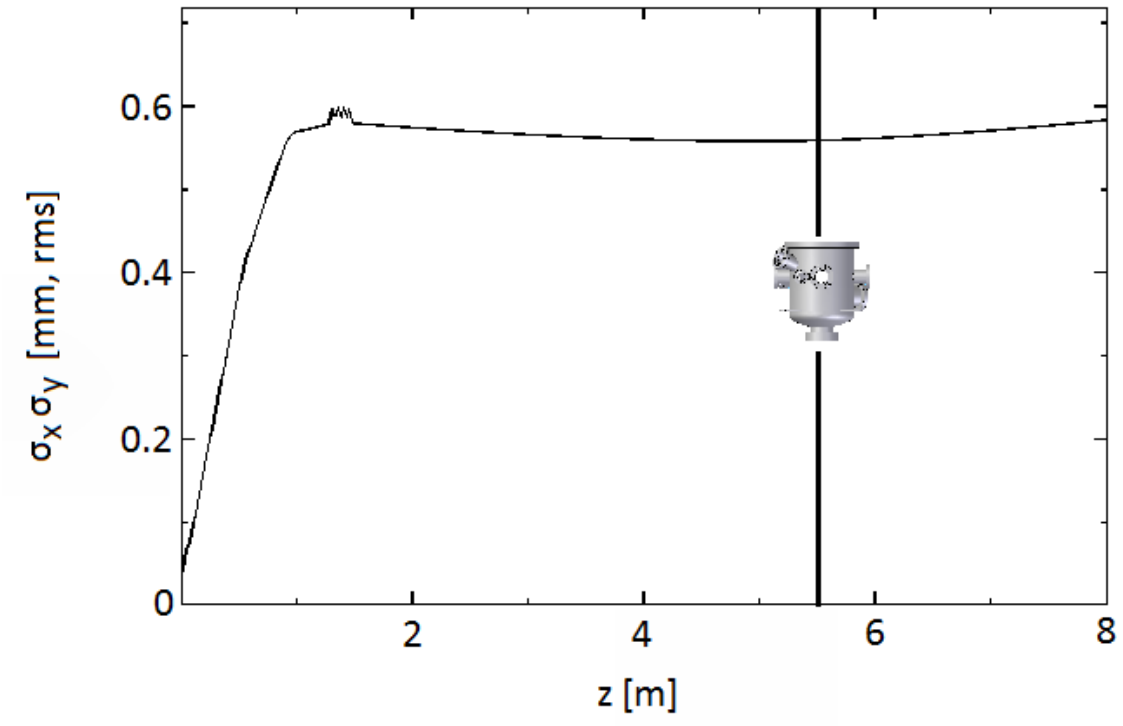

Figure 21: ASTRA simulation of the transverse beamsize of REGAE.

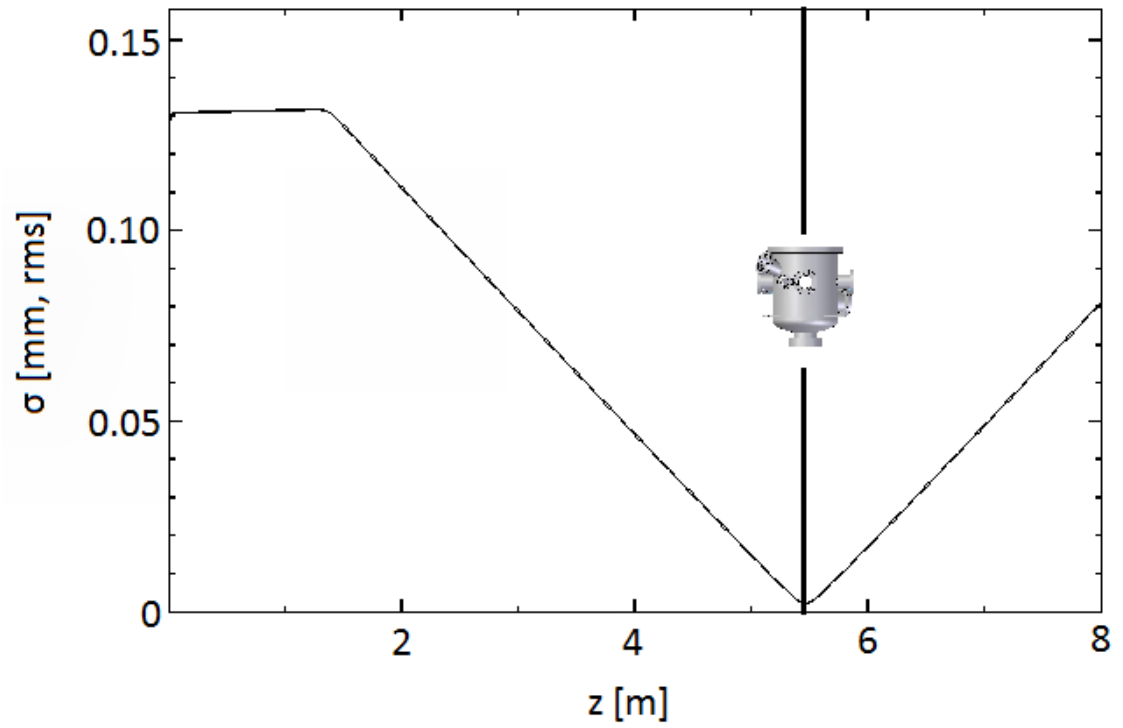

Figure 22: ASTRA simulation of the longitudinal pulse length.

The entanglement of emittance and coherence is clearly observable from the fluctuations of these attributes, which correlate with the positions of the solenoids and the buncher-cavity. The spikes are due to sharp cut-offs of simulated field distributions in the cavities and solenoids [Hachmann (2012)]; they have no physical meaning or relevance. The position of the specimen chamber is marked in the figures.

These simulations show the best case performance of the REGAE. Imperfections in field distributions in rf-cavities and solenoids, as well as imperfect shaped laser pulses for the generation of the electron pulses, are not at all considered. Currently, it is difficult to obtain small laser spots on the photo-cathode. This is due to the large distance between the photo-cathode and the last focusing lens, which is positioned next to the mirror chamber outside of the beamline (as shown in figure 11). Furthermore, the quantum efficiency and energy spread from the employed photo-cathodes is not as good as simulated. Also, sources of timing jitter (explained in section 3.4.4) significantly limit the machine performance and are not considered.

In these simulated best case scenarios, the shortest electron pulse length is 2 μm (corresponding to 7 fs rms) at the position of the specimen chamber. In theory, one can drive the minimum pulse length to even lower values [1.65 fs fwhm, Flöttmann (2014)]. The correlated coherence length of 30 nm (fwhm) at the specimen position is promising for imaging more complex structures with spatial extensions up to several nanometers. Currently, the electron beam diameter measures a few millimeters and is yet too large for distinct measurements of fine structures. The diameter of the electron beam can be extracted from the central maximum in the following diffraction patterns. The electron beam diameter definitely has to be decreased in size for both diffraction and real space imaging, to improve the spatial resolution. The reduction in size can be forced by the additional lenses that are installed next to the specimen chamber and along the beamline. To get an indication for the physical limits and capabilities it is necessary to determine the realistic capabilities of such a source by the measurement of important machine parameters. Improvements of single aspects of the operational parameters can then lead to a better approximation of a simulated machine performance. A few measurements of certain beam aspects have been conducted up to date and are presented in the following section.

3.4.2 PERFORMANCE MEASUREMENT OF REGAE

One of the most fundamental beam quantities is the emittance. Measurements of the emittance at REGAE were conducted via a solenoid scan [Hachmann (2012)] and via signals from diffraction by a copper mesh, which give clues on the divergence and thus emittance [Bayesteh et al. (2014)]. Through the first method, the emittance was

estimated to range within 3 to 7 mm mrad. This is significantly larger than simulated, and the deviations to theory are most likely due to the imperfect conditions of laser-beams and rf-field in the cavities at that time, in addition to influences by the earth's magnetic field. In the meantime, improvements on the machine were conducted, which included replacement of cavities and the installation of compensation coils around the accelerator. Thus, it is expected that repeated measurements would lead to better results. The measurement via divergence of the beam behind a copper mesh in the specimen chamber is less dependent on field errors in the solenoids and within the rf-cavities. These measurements reveal transverse emittances below 100 nm rad for charges as high as 245 fC (corresponding to at least two million electrons) at a very similar energy as the measurements via solenoid scans. For lower pulse charges, these results agree with the simulations within the uncertainties of the measurement. This is an important result, which supports the hypothesis that the emittance and coherence properties of REGAEs' electron beam will be sufficient to investigate nanometer-scaled structures.

The temporal resolution was recently determined with the laser-induced plasma formation in copper meshes [Gao et al. (2012)]. In Manz et al. (2015), these results are presented. Currently, the time resolution of REGAE is constrained to a few hundred femtoseconds. Rf-timing jitter and field errors in the cavities are the main reasons for this limitation, but improvements on the electronics, photo-cathodes, the laser system and the field distribution between the cavities will greatly improve the temporal resolution. The main problem at this point is missing electronics, which can improve the feed-back within the rf-system and improve REGAEs' overall stability. This problem is common to all, world-wide, accelerators using rf-technologies and is of great interest for the European XFEL.

3.4.3 PROOF OF CONCEPT DIFFRACTION

First results of static and dynamic diffraction experiments are summarized in the previous reference. The obtained diffraction patterns clearly show the typical pattern of polycrystalline gold, especially when multiple electron pulses are integrated. Single crystalline molybdenum sulfide and silicon are equally resolved by few electron pulses. The large beam diameter results in a broad zero order diffraction peak, especially observable in the gold and molybdenum specimens.

The first studies also focused on the thickness dependence of diffraction, in this case by aluminum slices with 50 to 800 nm thickness. Here, the advantage of relativistic electron beams becomes observable. The maximum specimen thickness must not exceed 50 to 200 nm with electron sources and TEMs, that use energies between 50 and 180 keV. With the 5 MeV electron pulses of REGAE, distinct diffraction peaks can be observed

at 400 nm thickness, and the most distinct reflections of 800 nm thick aluminum films are still visible. The penetration depth of electrons surely depends on the density of the material, as outlined earlier, but the benefit from MeV electron beams can also be observed in specimens with higher densities. In the first measurements conducted with REGAE, the background and smearing due to multiple scattering events in the measurements is significant, which reduces the signal to noise ratio and thus worsens the spatial resolution. The dependency of ring width on the specimen thickness is also presented in this reference. The results for scattering by aluminum films can be directly compared with Li et al. (2010b). For a beam energy of 2.8 MeV with a pulse charge of 800 fC, they investigated scattering on 200 nm thick aluminum films. The peaks of diffraction show up clearly in the azimuthal integration plot, one could say more details are observable in the present work. A quantitative comparison would require the raw source data from Li et al. (2010b), which is not available. Thus, the scattering obtained using these two sources is at least comparable, just from the data presented in these references.

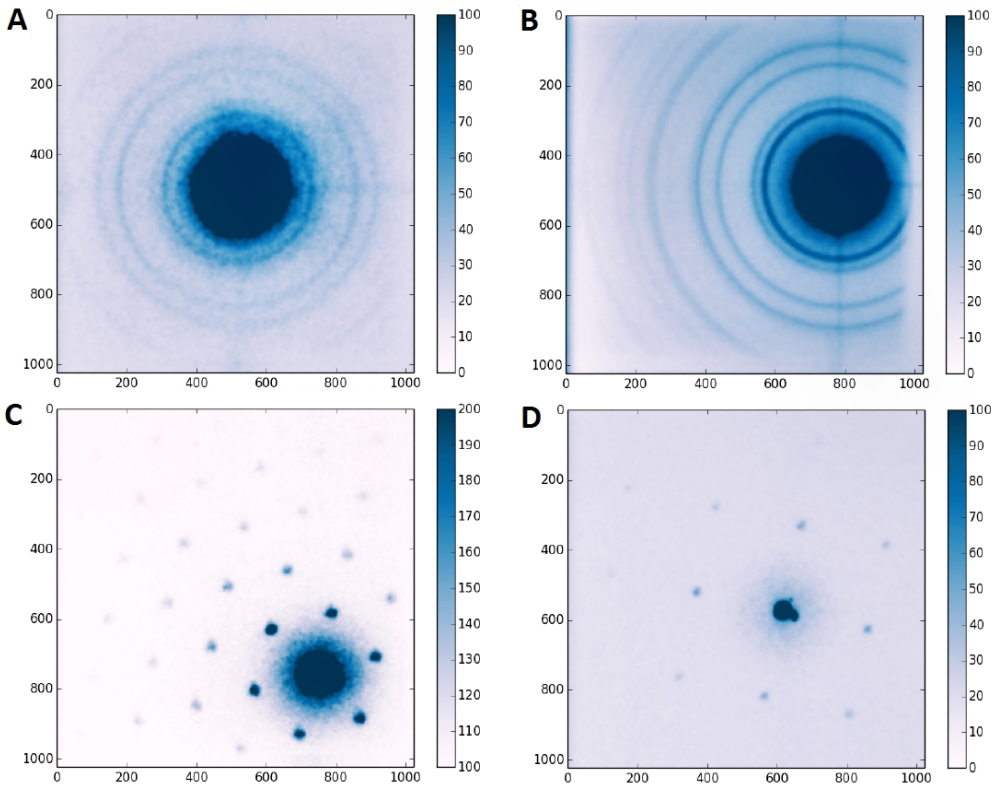

Figure 23: Early diffraction patterns of REGAE, adapted from Manz et al. (2015). A and B show polycrystalline gold, C: MoS_2, D: Si.

3.4.4 MACHINE STATUS AND FUTURE DEVELOPMENTS

REGAE is now in daily operation, running at 12.5 Hz. Although the klystron can deliver up to 50 Hz rf-pulses, the influence of the neighboring DESY-II storage ring is limiting the maximum applicable repetition rate. AC magnet currents from the storage ring, which is located on the same floor level, are propagating through the tunnel walls that are made of several meters of hardened concrete, and interfere with the fine electron pulses of the REGAE, causing periodic deflections. To circumvent this disturbing influence, the machine is operated with the trigger of this external 12.5 Hz frequency, the repetition rate of the AC magnet cycle. By triggering the repetition rate of the klystron, the pulse position along the accelerator appears to be static. This problem is known from other electron installations [Beard et al. (2011)], but was only accidentally identified within a maintenance period of the DESY-II ring. In addition to this, electric coils as bulky as the entire accelerator installation, are spanned around the machine to compensate the earths magnetic field, which interfered with the early emittance measurement by the solenoid scan. Both approaches of field compensation work well.

A complex time-resolved apparatus such as the REGAE and comparable installations require a synchronization of the laser system and the rf-system, with a precision that amounts to a small fraction of the targeted temporal resolution. In the REGAE, timing jitter of less than 10 fs rms is desirable, close to the fundamental noise limit of certain electronic readout speeds. Otherwise the instrument response time could not be reduced to the targeted 25 fs (fwhm). The required field stability is 10 ppm in amplitude and 0.01 deg in phase, respectively [Felber et al. (2012), Hada et al. (2013)]. The complex synchronization scheme of REGEA is described in Mayet (2012), Hoffmann et al. (2013), Hoffmann et al. (2014) and more clearly outlined in Rutkowski et al. (2013). The current electronic timing jitter was evaluated with 55 fs rms in phase (0.06 degree) and another 33 fs between the rf and the laser synchronization [Hoffmann et al. (2013)]. Further jitter problems, which lead to the reduced temporal resolution of REGAE as described above, are caused by the less precise control of the coupled rf-cavity system and field errors. Ongoing developments of timing electronics are continually improving the situation.

The dark current collimators are used on a daily basis to cut out the dark current originating in the rf-cavities and eventually to decrease the current beam size, as well as for clearing the beam up from deteriorating effects induced by inhomogeneities of the solenoid and cavity fields. The collimators significantly improve the signal to noise ratios and minimize the background, which is observed with the detector at the end of the beamline. The measurements of temporal resolution and in this context the improvement of beam dynamics, including work on the laser system, is ongoing. Future developments of REGAE include the extension of the machine with additional magnetic lenses, to

realize relativistic TEM capabilities in REGAE [Manz et al. (2015)] and laser-induced wake-field based acceleration of REGAEs' relativistic MeV electron pulses to GeV energies [Grebenyuk et al. (2012), Zeitler et al. (2013)]. This development is only possible with the ultra-short and pre-accelerated relativistic electron pulses of a source such as the REGAE. With further improvements on crucial accelerator components, the design goal of ultra-short electron pulses can eventually be obtained by this setup, at least amount to less than 100 fs (fwhm). The machine, as it presented itself in 2012, is shown in the following, concluding image of this chapter.

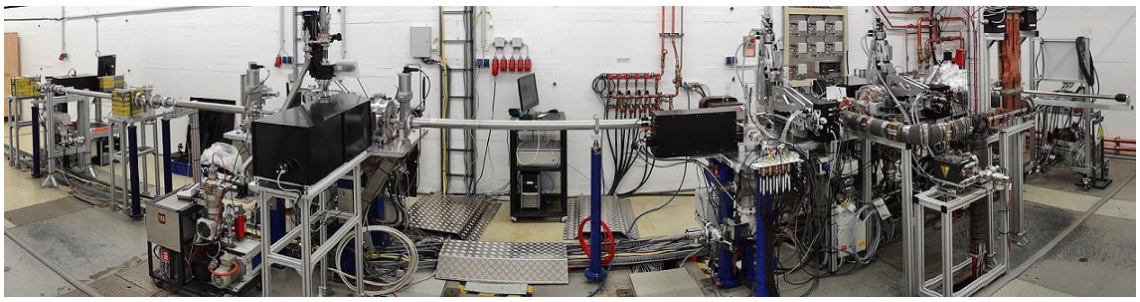

Figure 24: REGAE in the accelerator hall in building 23. Accelerator section on the right, sample chamber on the mid-left, and detector station at the very left with boxes for diagnostic equipment along the accelerator and supports for lead shields. Most of the design work on the experimental section, which followed the author's work, was conducted in collaboration with our former group engineer Santosh Jangam. Former DESY engineer Marcus Barenscheer was primarily in charge of the design and construction of the accelerating section. Further contributors are mentioned in the text at the according places. Picture source and additional information is hosted at: `http://regae.desy.de/`

4 E-GUN 300 - A COMPACT 120 KEV SOURCE FOR FEMTOSECOND ELECTRON DIFFRACTION

Compact electron diffraction instruments are a promising alternative to rf-driven highly relativistic electron accelerators such as the REGAE. Without sources of timing jitter, DC-operated electron guns offer an excellent spatial and temporal resolution. An entire setup, including a femtosecond laser source and detector, only occupies a very small area of lab space, while being less expensive than extended relativistic setups. The number of components can be reduced to a minimum and eventually be highly reliable. In the end, the reliability will mainly depend on the proper application of a stable high voltage.

The differences in the de-Broglie wavelengths, compared to relativistic electrons, are not that severe (as listed in table 7). The generated signals from diffraction and real-space imaging are equally strong, due to the large scattering cross-section of electrons. The absolute spread in the energetic spectrum of the pulses is overall smaller. The artificial reduction of a pulse by a drift, as targeted by the REGAE, requires an energetic chirp, which in turn influences the diffraction angles in the scattering off the specimen. This energetic chirp is by default less distinct in compact setups, as long as they reach a certain electric extraction field gradient and exceed a critical energy. This partially leads to more confined diffraction peaks on the detector and is connected to a reasonable temporal resolution of a few hundred femtoseconds, as was summarized in table 8.

A design for a new electron diffraction instrument had been drafted, based on the 95 keV DC-RF design [Gao et al. (2012)] of the group. Components of the gun section and the specimen chamber are obviously similar to this previous setup. An rf-cavity was not included in the new design, to reduce the complexity of the system and to enable a quicker start of operation. First drafts of the UHV chambers and electron gun were completed before the beginning of this work, but most parts of the new setups were built within the efforts of this PhD work. The optical laser installations were fully treated by other group members (most of the optical installations of REGAE and the compact setup are presented in Zhang (2013)). The anticipated energy of the new generation of compact setups was 300 kV. The applied high voltage would have been tripled compared to the previous 95 keV generation. The reasons for pursuing higher energy electrons were simply an increase in the electron penetration depth (as for REGAE), while the electron bunch length and thus temporal resolution are further improved. This latter hypothesis will be extensively investigated in the following chapter 5.

The first tests of the new setups two years after the beginning of the construction and installation revealed, that the envisaged electric potentials are accompanied by a range of new, unanticipated, high-voltage related problems, which had hindered the first attempts to realize the higher electron energies. It is especially unfortunate, that we were not allowed to test the new compact machines at all for an entire year, prior to the strict implementation of local radiation safety regulations.

The problems which occurred can be divided into two categories. First of all, machine functionality related problems, caused by high electric field gradients accompanying the applied voltages, leading to subsequent malfunctions of the electric components. This includes the commercial design of high voltage feedthroughs. Secondly, radiation safety becomes a major issue at electron energies exceeding 100 keV, even 50 keV. These problems form the subject of this chapter, once an introduction into the general setup layout and details on the apparatus functionality are given. The occurred problems were treated by the engineering of another setup, the FED-CAMM, which is the subject of the subsequent chapter 5.

4.1 INTRODUCTION

The generation of femtosecond electron pulses in compact evacuated instruments is achieved with femtosecond laser pulses in combination with static electric fields. The laser pulses target metal-coated photo-cathodes, typically excite electrons by mid-green (two-photon absorption) or UV laser-wavelengths (single photon absorption). Thus, one of the two main components of a compact diffraction apparatus is a femtosecond laser-source, of which a second beam with a controlled delay is used for the excitation of the specimen of interest, to trigger the response of interest (as explained in section 1.1.5). The laser system of the E-Gun 300 is briefly described in the following section 4.1.1, together with the overall layout of the compact setup

The other major component is the vacuum chamber, which houses the electron beam, the specimen including its mounts with heating and cooling capabilities, diagnostics for the electron pulses and a detector for the recording of diffraction signals. In DC accelerators, the energy is transferred to the electrons by ideally intense static electric fields. These are concentrated in a gap between the photo-cathode and a close-by and typically grounded anode. These components build the core of the entire femtosecond diffraction system. A highly stable power supply for the generation of static electric fields and the detector define most of the parameters that are characterizing such a compact setup. The following figure 25 illustrates the essential functionality of the electron diffraction setup. Additional beamline components for diagnostics of the electron beam are not shown in this schematic, to promote the important aspects of electrodes, the

application of high voltage, pump laser and probe laser and electron pulses, respectively, and the overall target of compact design, which is especially important for setups that utilize electron energies below 60 keV.

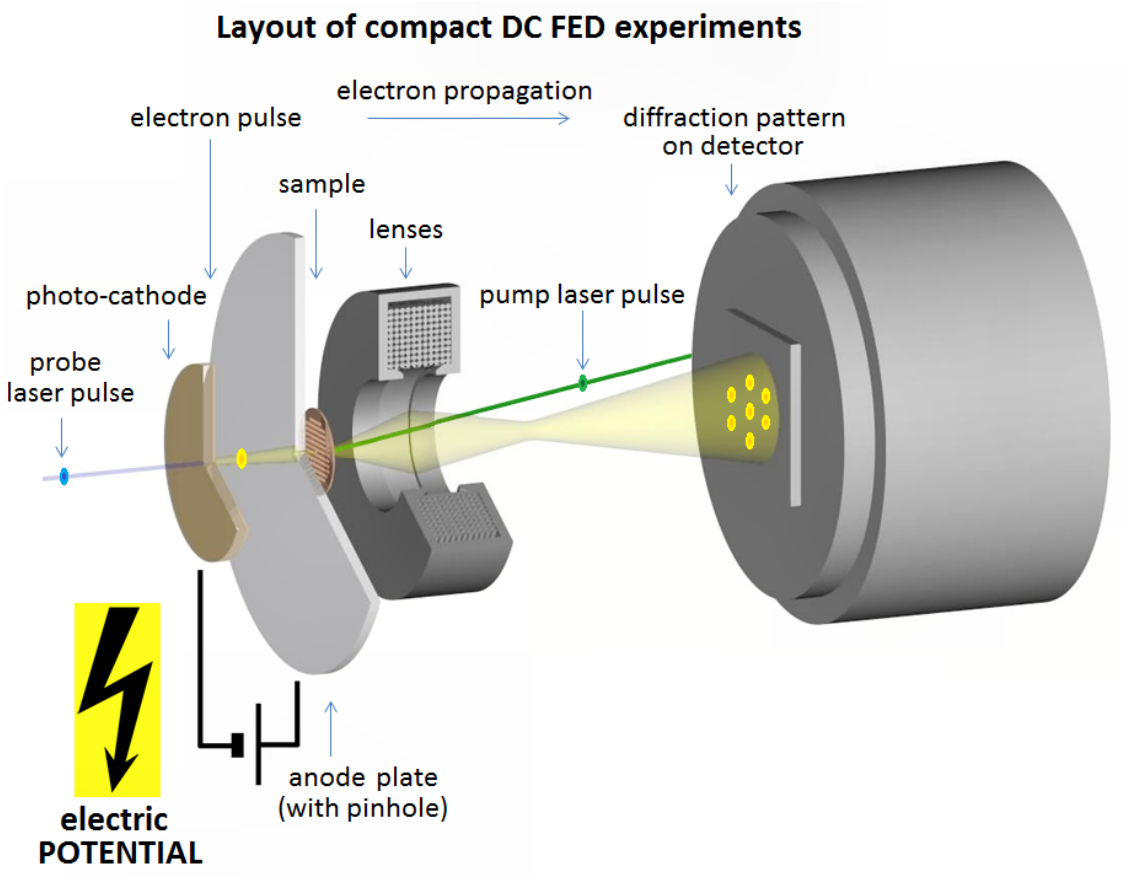

Figure 25: Schematic of a compact DC powered electron diffraction setup. This rendered illustration shows the actual arrangement within the E-Gun 300. From left to right: a metal-coated photo-cathode, photo-excited with a femtosecond laser-pulse, followed by an anode with a pinhole aperture. A TEM grid holds thin slices of the specimen. At least one magnetic lens focuses the electron diffraction pattern onto a detector. A second optical pulse is focused onto the sample to trigger the reaction of interest, followed by another probe pulse with precise delay.

The advantage of this layout, which is equally incorporated into the design of the FED-CAMM apparatus, in comparison to the earlier layouts (30 keV: Siwick et al. (2004), 55 keV: Harb et al. (2008) and Ernstorfer et al. (2009)), is the avoidance of longitudinal pulse broadening prior the sample in favor of advanced temporal resolution. When an aperture size of a few hundred micrometers is used in the anode plate or grid, a spatial focusing of the beam prior its interaction with the sample is mandatory to obtain a sufficient density of electrons within a small area of the specimen or brightness, respectively. With this layout, more electrons can be conserved in a single electron pulse of a less

energetic electron source, but only for the impairment of temporal resolution. In terms of spatial resolution, this might have the other disadvantage, that the incoming electrons of the pulse are not perfectly parallel when incident on the specimen, depending on the focal strength and distance between the solenoid and the specimen.

When the electron pulse is used shortly after its generation, without any re-compression prior to interaction with the sample, the temporal resolution is mainly dependent upon the incoming laser pulse length, the initial electron energy spread, the applied accelerating electric field gradient, the gap size and high voltage, respectively. The last two parameters define the duration of the acceleration, a critical aspect, as will be outlined later in this PhD work (see section 4.2 of this chapter and section 5.3 of the following chapter for detailed studies of time resolution by numerical simulations, using the GPT code). Coulomb repulsion among electrons in the pulse is significant. It scales with the number of electrons, is dependent on the initial electron density as controlled by laser pulse intensity and duration and the electron energy. As outlined earlier, the space charge effect decreases with increased energy. For this reason, electron numbers in a single pulse can be higher in highly relativistic electron beams with MeV electron energy for a given pulse length.

One of the prerequisites for femtosecond electron diffraction - femtosecond laser systems - was developed in the 1980*s*. Today, a variety of compact femtosecond laser systems are commercially available from different vendors for a third or less of the cost of a standard TEM. Opposed to compact time-resolved electron sources, TEMs do not provide any temporal resolution, except for *Dynamic Transmission Electron Microscopes* (DTEM, see section 2.3.1). Compact electron guns are less sophisticated in their technical details, especially in the lensing system, thus can be more easily designed and built. Up to the energy of 100 keV, this is not a challenge. With smart optimization of all components, the resulting instrument response time only depends on the optimal matching of the duration of the incoming laser pulse, its intensity and the use of optimized electric field gradients. With the time resolution of the machines, as introduced in table 8, a large number of interesting structural transitions and chemistry can be indirectly observed. The remaining is the installation of equipment, such as the controlled delayed of pump and probe pulses at the sample and synchronization of laser pulses with camera triggers.

The choice of a highly stable DC power supply plays a vital role in the regime of very short electron pulses, as otherwise timing-jitter is induced into the setup by the field dependent changes in electron pulse arrival at the specimen position. A closed-rack system, which is immune to humidity and temperature variations that occur in a laboratory, is the best choice for compact and highly time-resolved electron sources. The required stability for few tens of femtoseconds long pulses has to be as good as

10 ppm, which is the same requirement as within rf-cavities. The power supply was not the most crucial unit in the former setups with energies as high as 95 keV. There, the rf-system is a major source of timing jitter, which limits the temporal resolution, as there is a drift of rf-phases during the execution of time-resolved experiments [Gao et al. (2012)]. In other known setups, it is mostly the limit of the electric field gradient to values of 10 MV/m or less that leads to a restricted temporal resolution of these instruments.

Generally, the choice of the maximum electron energy is limited by commercially available stable power supplies. The only other limitation arises from the layout of the high voltage carrying components. With increased potentials, especially those exceeding 100 keV, the physical insulating properties of materials tend to show unreliable and unstable behavior, requiring special attention to layouts and requiring novel designs. The development of the FED-CAMM and the successful operation is based on uncommon designs, which prove to be physically and electrically stable and also perform excellent with respect to ultra-short electron pulses.

The current generation of compact time-resolved electron sources, to which the E-Gun 300 belongs, is based on prior experience with compact DC accelerated and RF re-compressed electron beams, not exceeding electron energies of more than 95 keV. The energies of the former DC setups were 30 [Siwick et al. (2003)] to 55 keV [Sciaini et al. (2009), both incorporated into table 8]. The only other former setup, which is still operational and based on DC acceleration with RF re-compression, is working at 95 keV [Gao et al. (2012)]. This latter setup is one of the best hybrid setups providing electron pulses with a duration of less than 100 fs, but the effective instrument response time amounts to 200 fs (fwhm). The 55 keV setup delivers electron pulses nearly twice as long (less than 400 fs fwhm). The electron energy was raised with each successor of the previous electron source for diffraction. For reasons of improved temporal resolution and increased penetration depth, besides the need of new sources for the newly founded group in Hamburg in 2010, it was pertinent to again raise the electron energy into the regime of a few hundred keV, more specifically to 300keV. This would halve the de-Broglie wavelength and therefore increase the spatial resolution, improve the sharpness of diffraction images, respectively. The energy spread is decreased and a more parallel direction of flight [Janzen et al. (2007)] achieved. Furthermore, an improved time resolution was targeted. Unfortunately, the high potential of 300 kV could not be obtained in this setup, the obtained results are still outstanding. The instrument has a response time of less than 300 fs (fwhm). The problems discovered in the E-Gun 300 ultimately led to the development of the FED-CAMM, to be discussed in chapter 5.

4.1.1 THE FEMTOSECOND LASER SYSTEM AND SETUP LAYOUT

The femtosecond laser is a commercial system, which is shared between the REGAE (chapter 3) and the compact E-Gun 300 diffraction system via the laser transfer system (section 3.2.3). The laser system consists of a diode pump laser, an oscillator and regenerative amplifier. The default wavelength of the system at the amplifier output is 800 nm, with a maximum energy of 8 mJ per pulse. The pulses have a duration of 35 to 40 fs, the maximum repetition rate of this system is 1 kHz. A simultaneous operation of both diffraction machines using the same laser source has to date not been feasible, due to different requirements on the repetition rate and the beam intensities.

The default wavelength is converted into the UV regime via third harmonic generation by two BBO crystals to generate the excitation pulse for the illumination of the photo-cathode. The excitation pulse approaches the photo-cathode from its back-side, the emission of electrons is directed in the contrary direction towards the grounded anode. A greater fraction of the laser power is separated via a harmonic beam splitter and converted to 400 nm by second harmonic generation in a single BBO crystal. This pump beamline comprises a translation stage, to insert the controlled delay in between the arrival times of the pump and the probe beam. The pump beam is directed towards the specimen through a flange on the side of the specimen chamber. The high voltage is guided into the system via a commercial high voltage feedthrough, which was designed for 300 kV, but is operable with 150 kV at most, due to occurring damages on the insulator due to high voltage breakdowns at higher field gradients around the central wire. A self made magnetic lens and a commercial CCD detector complete the setup. Electron beam analysis is conducted in terms of charge measurement via a Faraday cup in combination with a sensitive electrometer. These components, however, are not shown in figure 26, which shows the schematic of the entire setup.

4.2 ELECTRON BEAM SIMULATIONS

The temporal resolution of the E-Gun 300 is simulated by means of the *General Particle Tracer* (GPT) code. The parameters used for these simulations are based on the actual and most common settings in this setup. The maximum electron energy for stable conditions of operation is limited to 120 keV. This is due to high voltage breakdown problems, which will be discussed in section 4.3.1. The distance from the photo-cathode to the anode is fixed at 15 mm. For three different electron energies and two different numbers of electrons per pulse, the temporal evolution of the electron pulses is simulated along the direction of propagation.

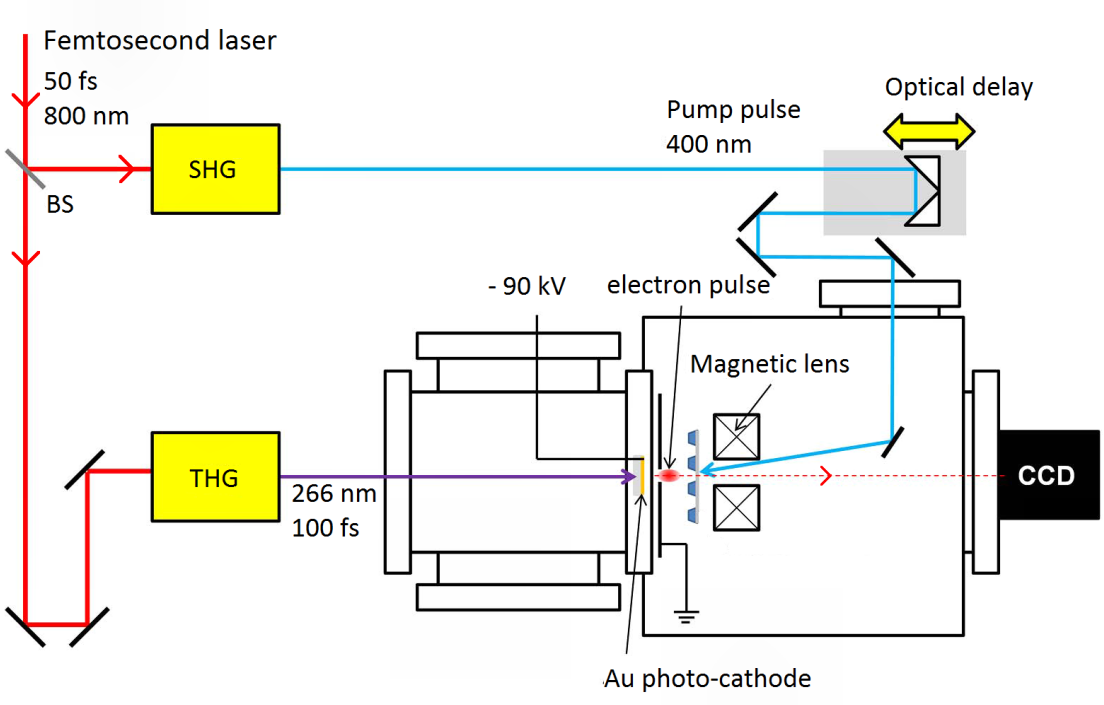

Figure 26: Layout of the E-Gun 300 setup. Illustration adapted from Hada et al. (2014).

Simulations with the GPT-code return a good estimate for achievable electron pulse durations, although a few phenomena are not considered, such as dark current electrons (as outlined in section 3.3). These can interfere with the intentionally photo-generated electrons. The assumptions within these simulations are plain and ideal, not considering any deviation from ideal gun geometries. This includes variations of the electric field distribution, caused by surface irregularities or wrong electrode shaping (see section 5.4), influences of laser pulse variations such as intensity, spatial or spectral inhomogeneities, unequal distribution of active photo-cathode material and sources of timing jitter, which impair the actual capabilities of the machine. However, the deviations between simulations and physical machine performance are not as large here as between the ASTRA simulations of REGAE and REGAEs' current performance. Table 11 summarizes the simulation parameters, which were used in these simulations of the E-Gun 300.

The simulated pulse durations are shown in figure 27. Other important characteristics to consider in simulations are the beam diameter and number of particles therein. Qualitatively, the dependency of the beam waist and focal spot on the electron energy and electrons per pulse can be observed in figure 28. The lens current was kept constant, although in reality it has to be adjusted to the electron energy to obtain focused diffraction spots on the detector. However, this is mostly irrelevant for the simulations of temporal resolution.

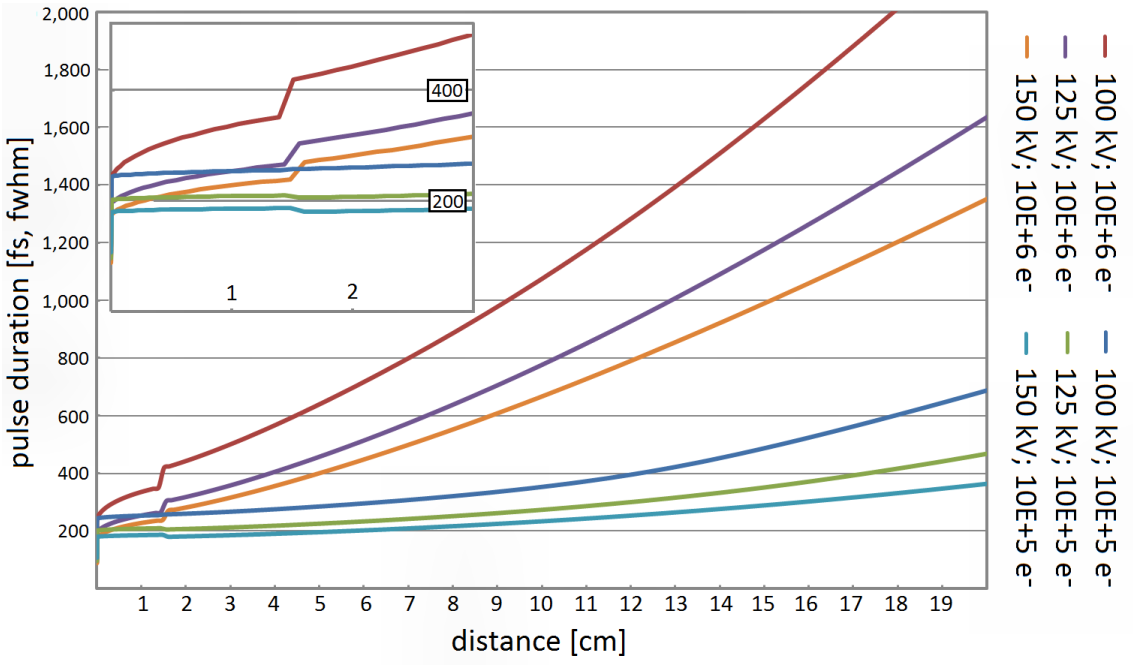

Figure 27: Simulated temporal resolution of E-Gun 300 with $\Delta E = 0.2$ eV and 10^5 as well as 10^6 electrons per pulse. The inset shows the development within the extraction region, between the photo-cathode and anode with pinhole aperture. The specimen is located 20 mm from the photo-cathode.

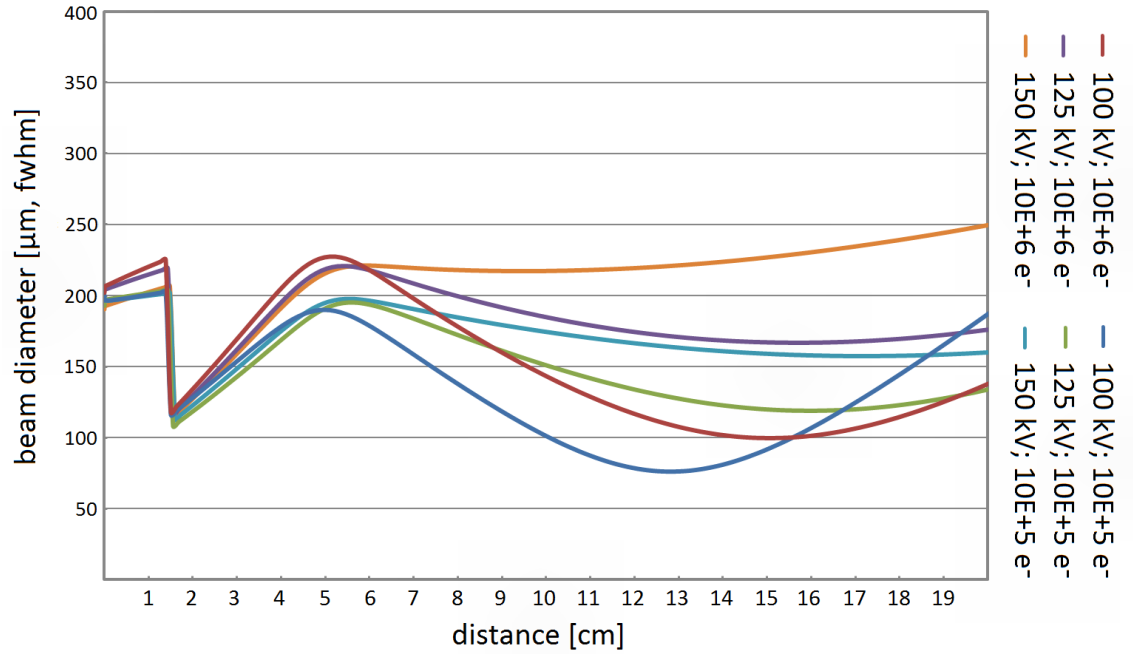

Figure 28: Beam diameter along the beam-path for the set of simulations. The pinhole in the anode and the effect of one solenoid is clearly visible, as well as the influence of the electron beam energy.

E-Gun 300 simulation parameters		
Cathode-anode-distance	15	mm
Anode-pinhole	200	μm
Laser pulse duration	100	fs
Laser spot size	200 x 200	μm
Electrons per pulse	10^5, 10^6	
Electric potential	100, 125 and 150	kV
Initial electron energy spread	0.2	eV
Photo-cathode position	0	mm
Anode position	15	mm
Sepcimen position	20	mm
Lens position	50	mm
Lens current	1500	mA
Lens winding	$\approx$ 1400	loops
Lens aperture	$\approx$ 30	mm

Table 11: Parameter used for simulation of time resolution.

These simulations show that for 125 kV and 150 kV, respectively, and with 10^5 electrons per pulse, a pulse duration of 200 fs fwhm can be obtained at the specimen position close to the anode, but also throughout a further drift within the setup. The pulse duration does not significantly broaden during the first five centimeters after the anode, for 125 and 150 keV, respectively. A requirement for such a short pulse duration is a photo-active material with low initial energy spread. If less electrons per pulse are simulated, the electron pulse duration shortens accordingly, leading to a compromised brightness of the source.

The effect of increased energy spread, which is inherent to standard photo-cathode materials, was also simulated for the otherwise same set of parameters. The initial energy spread was changed to 0.6 eV instead of using the previously simulated 0.2 eV. Figure 29 reveals, that the most obvious changes are located within the accelerating gap. Though the additional 0.4 eV in the energy spread make only a small fraction of the final electron energy, the effect on the electron pulse duration is distressing. The curves relating to 10^6 electrons per pulse (red, purple and orange) all have an offset in respect to the former propagation lines (dark grey). The differences in pulse duration and the offset at the beginning of propagation are more significant for the lower electron energies. The offset of the curves relating to 125 and 150 keV from each other is much smaller for the previously lower energy spread. The larger energy spread of 0.6 eV increases the offset

between these two energies. Partially, it seems that the initial pulse duration, due to a broadening in the acceleration gap, simply doubled or tripled, which agrees with the relationship as given by equation 2.5. Offsets in the temporal resolution as in the 10^6 electron case are seen for 10^5 electrons per pulse; otherwise no special occurrences.

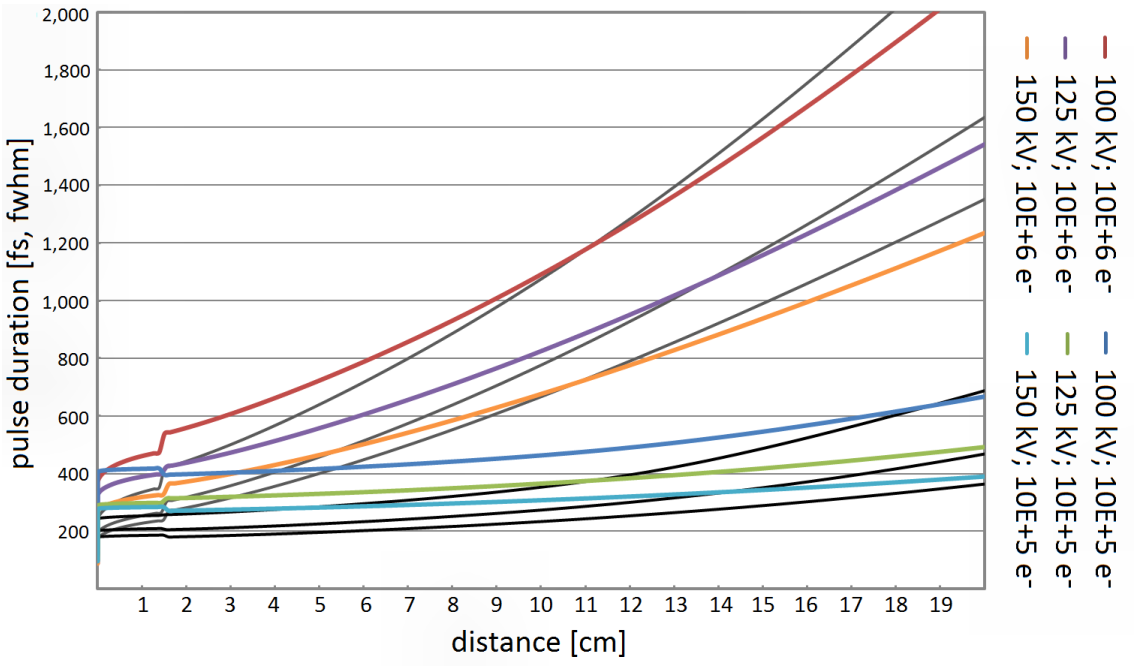

Figure 29: Simulated temporal resolution of E-Gun 300 with an initial energy spread of 0.6 eV. The former propagation lines are colored in dark gray and black and not additionally labeled. The labeling refers to the new curves with increased energy spread. The specimen is still located 20 mm from the photo-cathode.

Differences in the further propagation after the anode plate are obvious for all curves, when comparing the new results to the previous simulations with lower energy spread. Most likely a decreased electron density, after the initial acceleration of the pulse in the gap, leads to a delayed pulse broadening during the further drift of the pulse, compared to the simulations with less initial energy spread. Evidently, there is a crossing of all new curves with the former curves. The crossing occurs between 11 to approximately 22 cm, measured from the photo-cathode. The electrons start with a longer pulse length due to the increased energy spread, the pulse length still appears to be shorter at the end of the propagation in the beamline due to the decrease in broadening of the lengthened pulse. A more complete analysis of the beam dynamics requires the analysis of the particle numbers and beam sizes, as well as coherence and emittance. This treatment however is outside the scope of this section. Instead we note, that the emittance and coherence are primarily defined by the pinhole size in the anode plate, or additional aperture right before the specimen. A parameter that can be changed, depending on the requirements of brightness and beam quality. The particle numbers per pulse are approximately halved

by the pinhole in the anode plate in the current configuration and simulations.

The presence of a lens in the path of the pulse does not obviously influence the pulse duration, at least it is not observable from these traces. The elongated availability of short electron pulses over a range of various centimeters can thus be further deployed. It is possible to spatially focus the electron pulse prior the interaction with the specimen, at these energies at least. For less energetic electron pulses, this would be problematic, since the distance from the source to the specimen has to be minimized for highest temporal resolution.

If higher electron densities within a certain area are required, and the overall time resolution of 200 fs is acceptable, a magnetic lens can be positioned between the anode and the specimen. Temporal distortions in femtosecond electron bunches by magnetic lenses were investigated by Weninger and Baum (2012). They show that, depending on the focusing strength of the solenoid, only a minor temporal distortion is introduced into the pulse. By choosing an optimized focal point, the spatial focus can be aligned with the temporal focus, resulting in no error. In electron pulses as long as 200 femtoseconds, the influence of magnetic lenses in relation to the overall pulse length remains negligible. The use of a magnetic lens prior or post the specimen is therefore not significantly influencing the pulse duration. The dependency of the focusing strength of the solenoid on the electron beam energy and electron densities is evident. For the sake of completeness, the focusing parameter of the solenoid can be described by [Kumar (2009)]

$$f_{sol} = \frac{4\ m^2\ v_z^2}{e^2 \int B_z^2\ dz}. \tag{4.1}$$

As previously mentioned, the pinhole of the anode strips off up to 50 % of the electron pulses in these simulations. This amount is changed with the ratio of the initial laser spot-size on the photo-cathode, the transverse spreading within the acceleration gap and the first and additionally used pinhole apertures. The default pinhole size of the E-Gun 300, which is machined into a section of the anode, can be reduced with further insets down to 50 μm. Although influencing the brightness of the source, this loss of electrons might have a beneficial impact on the emittance and transverse coherence length.

The results of these simulations demonstrate the capability of these compact setups for delivering 200 fs (fwhm) short electron pulses. With less electrons per pulse, even shorter pulse durations can be obtained in setups like the E-Gun 300, which do only imply electric field gradients of less than 10 MV/m. This is still sufficient for the resolution of fast physical, chemical and certainly biological processes. For higher electron bunch densities at the same pulse lengths, the re-compression by an rf-cavity might be indispensable, but of no use, if timing jitter related to rf-components sabotages the overall performance. As will be shown in the simulations of the FED-CAMM (chapter 5), a higher extraction

field strength can even further shorten the electron pulse duration, and provide electron pulses of a duration that would otherwise only be achievable with rf-compression. These results from simulation and first experiments, as simple as they might be illustrated, retrospectively justified the time spent and hassles involved in the construction of these setups. Especially the failure of the E-Gun 300 led to the development of the FED-CAMM instrument, which solves all occurred high-voltage related problems, and provides electron pulse durations as short as 70 fs (fwhm).

4.3 MACHINE FAILURE AND ENCOUNTERED PROBLEMS

The headline of this section must not be misunderstood. The overall performance of the E-Gun 300 is outstanding in itself, as was previously shown by simulations, and as is meanwhile proved by experiments, which are presented elsewhere. Comparing the results of simulations and early measurements, the performance of 200 fs pulse duration of the E-Gun 300 pushes this machine onto the best rank of all compact DC operated electron diffraction setups that are known from publications and listed in table 8. It should be noted that no high temporal resolution has in fact been achieved by other concepts that would validate the additional complexity over the compact electron source design.

The final result in terms of applicable electron energy was not as good as anticipated and therefore generates a bit of a disappointment. Together with the obstructive radiation safety concerns, this is what we can understand as machine failure and occurred problems. Since the electron driving section of the machine remains unchanged until today, the highest possible voltage of electrons still amounts to 120 kV in stable conditions of operation. At that voltage level, the radiation safety concerns are reduced, but still had to be dealt with in advance of the prospective high energies of the E-Gun 300. With modest modifications of the electron gun section, the higher energies are still realizable. This complex of themes guides the rest of this chapter.

4.3.1 HIGH VOLTAGE BREAKDOWN

The designs of earlier setups from the group and elsewhere, have salient similarities in their individual components. The basic concepts that had worked fine below the anticipated high voltages exceeding 100 keV literally break down at higher potentials. This concerns specifically (i) the photo-cathode mounting, (ii) high voltage electrode design including inappropriate materials, (iii) the applied high voltages and subsequent electric field strength and (iv) the employed commercial feedthrough. To present details of the problems and to provide the fundamentals for the new developments within the

FED-CAMM apparatus, the specific components of the E-Gun 300 are discussed bit by bit.

(i) The photo-cathodes are based on polished sapphire disks, which are coated with either aluminum or gold films on top of stabilizing substrates. Both metals absorb laser pulses that comprise a UV spectrum, among other frequency ranges. The photo-cathodes were mounted in either a steel or ceramic encapsulation in previous electron diffraction setups. The encapsulations have a small window, through which a fraction of the metallic site is exposed to the electric field, which points towards a grounded anode structure. According to the previous designs, the photo-cathode in the previously drafted design plans of the E-Gun 300 is encapsulated in an insulating macor [Corning-Inc. (1851)] holder. The holder positions the photo-cathode with respect to the anode and further covers the edges of the photo-cathode. It was believed that breakdowns along the front rim of the photo-cathode are suppressed by a rim of macor around the edge of the photo-cathode. It was also believed, that an in-plane mount of the photo-cathode in respect to the surrounding electrode could not be achieved (conclusion in previous PhD theses).

During the operation of the E-Gun 300 at voltages exceeding 120 keV, the ceramic holders were severely damaged. Figure 30 shows one of the damaged ceramic photo-cathode holders, which comprises large cracks and was left missing material on the left side of the photo-cathode opening.

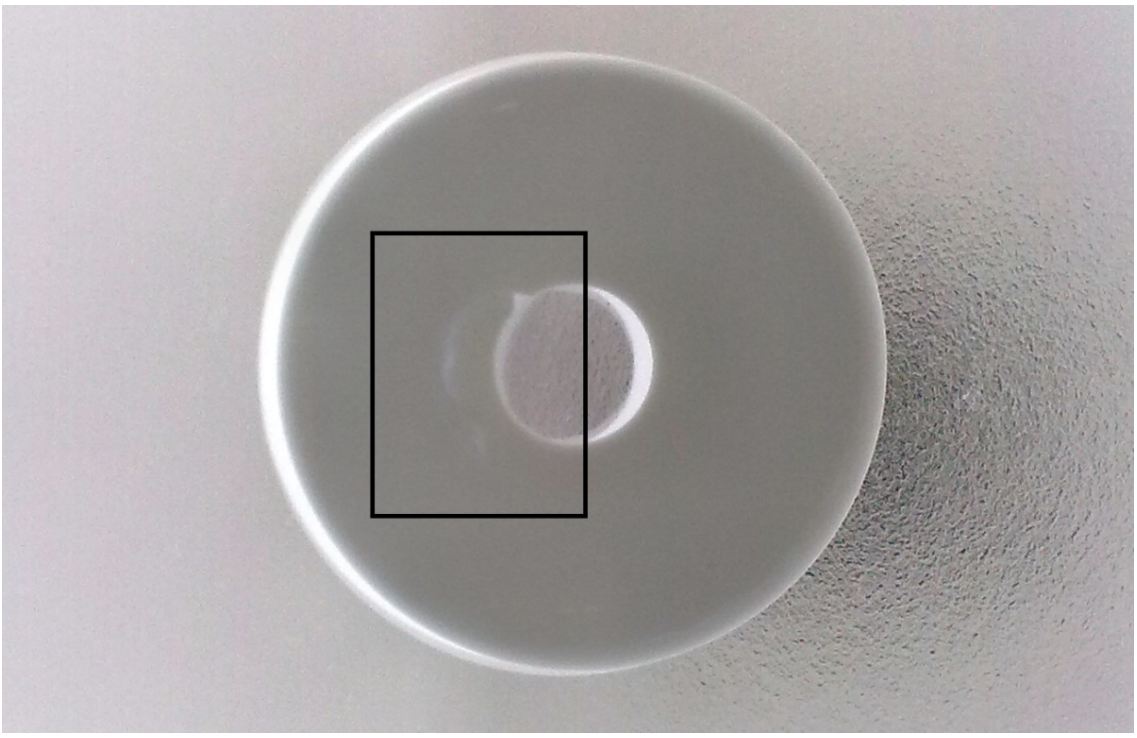

Figure 30: A damaged ceramic photo-cathode encapsulation, after first tests of the E-Gun 300.

The damages were caused by the amount of electric energy, or current, and electric stress that correlates with the applied electric potentials and used geometries. Though no big capacitors were present in the instrument setup, except for the high voltage cascade inside the connected power supply, the stored energy of the circuit was sufficient to crack and break the macor holders into separate pieces. Single electric flash-overs in proximity to the edges of the photo-cathode sufficed and certainly occurred.

The distances to grounded components on the rear side of the photo-cathode holder, this is the creeping distances across the remaining ceramic mounts, were not sufficiently long. Electrons are loosely bound along the surfaces of insulators and can potentially contribute to the conduction of electrons [as mentioned in Küchler (2009)]. Despite the good dielectric strength and breakdown voltage of macor, straight surfaces and short distances to ground are another limiting factor in sustaining high voltages.

(ii) In previous photo-cathode holders, an extra consideration of electric field shaping was not incorporated. This especially concerns the ceramic mounts in the most recent generations that run at 55 and 95 keV. Generally, the occurrence of electric breakdowns from spots of increased electric field gradients is eased if not considered in the design of setup components. In the previous setups as well as in the E-Gun 300, electric flashovers are predominantly caused by electric charges that gather on the surfaces of ceramic holders. These trigger the breakdown once critical field gradients and charge densities are reached. Electrically charged photo-cathodes inside electrically insulating ceramic holders are still accompanied by infinitely large electric field gradients around the rims. This is leading to the previously shown damage of the ceramics. The electric gradients exceed the dielectric field strength of the insulator. To remove this limitation, the photo-cathode should rather be incorporated into a conducting enclosure of a geometric conductive shape, of sufficient size and appropriately formed to avoid increased electric stress along curvatures. Extra insulation to ground separates general concerns of electrode shaping from the mount of a photo-cathode, or high voltage electrode, respectively, and simplifies the engineering.

(iii) Increased electric field gradients along curvatures become a predominant problem at higher voltages. The electric field scales with the applied voltage and is at least proportional to the inverse logarithm of the radius, up to its inverse square. This dependency is of course further determined by the electric geometry. The distribution of high voltages to the accelerating gap was formerly achieved through thin, polished metallic rods and sleeves, which both had diameters measuring only a few millimeters. The application of higher voltages requires larger radii and smoother surfaces. This decreases the electric field gradients and prevents the emission of dark current electrons from the surfaces of electrically charged components. Neither the larger diameters nor smooth surfaces

are present in the commercial feedthrough design. This directs the attention to the last problem that is involved in the electric malfunctions of the E-Gun 300 and the similar setups.

(iv) This topic is outlined in greated detail in section 5.5, especially in sections 5.5.1 and 5.5.2. Commercial UHV feedthrough usually employ a central conducting rod, which is transmitting the surface of a vacuum chamber and encapsulated in a ceramic. On the side of vacuum a gap to surrounding elements prevents a direct conductive contact, to also prevent electric charges from creeping along insulating surfaces. The availability of feedthrough for UHV conditions is strongly limited to voltages not significantly exceeding 100 kV. For the E-Gun 300 two custom made commercial products were ordered for the design electron energy of 300 keV. The design of these feedthrough is identical to the standard layout of feedthrough for lower voltages, although in this case the applied electric potentials are significantly increased. Consequently, it turned out that both of these commercial units suffer malfunctions at voltages above 150 kV. Physical damages occur on the insulators, which surround the central conducting wire inside the vacuum. This problem is equally discussed in detail in section 5.5.2. To avoid the occurred problems of the E-Gun 300 and similar setups, an innovative high-voltage feedthrough with special features for optimized time-resolved experiments and voltages of a few hundred keV was designed and recently successfully tested.

The conclusion of this section is, that it is not possible to simply scale parts in their dimension to account for higher electron energies and potentials. Partially this does work, but not for all aspects. An electron source is always as reliable and outstanding as its weakest component. New designs and concepts have to be implemented to operate with high electric potentials in a electron diffraction apparatus. To set this back into the content of structure-function relationship, the structure of the high-voltage feed-through requires significant changes for a proper functionality at higher voltages. Of course, this was only realized during the first part of this PhD work. Nobody, neither within this group nor within the broader community of scientists who engage in femtosecond electron diffraction, had gained experience with voltages exceeding 100 keV, prior to these developments. In this setting valuable lessons were learned from which all successors can extract important and crucial information.

4.3.2 RADIATION SAFETY CONCERNS AND MEASURES

The energy of electrons in combination with the maximum current of the high voltage power supply generated radiation safety concerns about critical amounts of stray x-ray radiation around the instrument. Besides electrons, which are purposely generated for the experimental investigations, stray emitted electrons from any charged component

occur within the presence of intense electric fields. Collisions of dark current electrons and the usable pulses, respectively, with components of the setup, potentially generate bremsstrahlung radiation. The maximum x-ray energy matches the maximum of the kinetic electron energy. The presence of x-rays is neither anticipated nor desired, but occurs as a side-product of the acceleration of electrons and the operation of a electron source. German and European laws regulate the necessary precautions for such stray-radiation devices, which have to be satisfied. The operation of electron sources as these built within this PhD work requires official permits from radiation authorities for operation.

When the utilized electrons possess energies between 5 keV and 1 MeV, the protecting rules of the X-ray Ordinance have to be applied [see Peinsipp et al. (2012), this version contains explanatory remarks]. For electron energies above 1 MeV, the German Radiation Protection Ordinance [BM f. U. (1976)] has to be followed. Both ordinances enforce the regulations of the European Atomic Energy Community [Euratom (1957)]. According to these regulations, any work that involves the exposure of humans or the environment to radiation and implements a potential impairment of health, has to be justified in regard to the economic, social and otherwise benefit. More importantly, maximum applicable dose values are specified that must not be exceeded throughout the operation of the device. Generally, the exposure to x-rays must be avoided, when a justification is not given. Otherwise, a minimization of radiation must be pursued, as for instance by the appropriate radiation shielding with state-of-the-art technologies.

When physical shields and precautions are installed, the maximum allowances confine the occurring dose per hour for a maximum number of hours of operation per year. These are calculated with 50 calendar weeks and 40 hours per week, leading to 2000 hours per year. The operation of a x-ray generating device requires official approval, when the electron energy exceeds 30 keV. The official approval might not be required, when the electron energy is lower than 30 keV and the dose rates at accessible surfaces do not exceed 1 μSv per hour and 10 cm from the accessible surfaces within normal operation. In these cases a clearly visible mark should be present that indicates the generation of x-rays. Other rules further apply.

The dose rates outside of the device determine the type of area, which is surrounding the instrument. For areas, in which persons can receive more than 1 mSv of radiation per year (with additional dose limits for other organs), the area is classified as *supervised area* . This area does not require specific labeling. In the case that the maximum potential dose exceeds 6 mSv within a calendar year, the area is classified as *control area* , which enforces restricted access, even no access during operation. The access to the source is controlled in such a way, that personal injury can not occur under compliance of all safety measures. The dose rates are limited to 0.5 μSv per hour for a supervised area

and 3 μSv for controlled areas for the given maximum doses.

The estimation of dose rates and subsequent doses around the E-Gun 300 setup were conducted with Monte Carlo simulations by the FLUKA code [Ferrari et al. (2005), Böhlen et al. (2014)]. These were initially executed by the DESY radiation safety group. Further, analytical formulas were applied. The following formula returns an approximate estimate of the dose-rate $\dot{H}$ of an electron accelerator or x-ray tube in close proximity of the usable beam [Vogt and Schultz (2011)]:

$$\dot{H} = \Gamma_X \cdot \frac{i}{r^2}, \tag{4.2}$$

in which i denominates the current of the source and r the distance to the source. The dose rate constant Γ_X depends on the electron energy and the construction of the source. For a source energy of 300 keV and a filtering by 1 mm aluminum Γ_X amounts to 4.5 $[Sv\ m^2\ mA^{-1}\ h^{-1}]$ in a distance of 1 m from the source [Vogt and Schultz (2011), p.439 tab. 15.20]. The maximum current of the connected power supplies is limited to 20 μA. In stable operation, creeping currents and dark current emission are not anticipated. Charges of femto-Coulombs per pulse with repitition rates of less than 1 kHz leave the remaining electron current in the setup at a minimum. The maximum available current has to be considered for worst case calculations, which can not be excluded from the considerations of radiation safety. With these given numbers, the dose rate according to equation 4.2 is 9 $[\frac{Sv}{h}]$.

The required shield thickness is determined by the attenuation factor of the used material. For supervised areas, an attenuation of $5.5 \cdot 10^{-8}$ is required, and for controlled areas an attenuation factor of $3.3 \cdot 10^{-7}$ is adequate. Considering lead as the radiation shield, a thickness of 3 cm is sufficient for the supervised and controlled area [Vogt and Schultz (2011), p.473 tab. 15.29].

In this simple calculation, two things are not considered, from which the realistic condition of the setup benefits. The factor for the conversion of energy into bremsstrahlung is significantly different to that specified for Γ_X, since the creation of bremsstrahlung also depends on the target material. In x-ray tubes, this is usually copper and carbon for reasons of a large yield of bremsstrahlung and heat dissipation. Therefore this calculation is expected to overestimate the overall occurring dose in the E-Gun 300.

Further, the chamber walls measure 6 mm in thickness and the material is made of 1.4404 (316L) stainless steel, which does itself not have the largest yield for bremsstrahlung creation (no characteristic absorption and according intense peaks). This material does itself absorb a small fraction of the total dose. Further, if we assume that dark current is the source for bremsstrahlung, the current of 20 μA is distributed over large angles in

all directions, originating from all conducting parts, that are operated with high electric potentials. These conditions significantly decrease the dose rate per solid angle. A person standing in proximity to the setup would never see an almost non-filtered directed pencil beam of x-rays. The photo-excited electron pulses with little charge at low repetition rates (in experiments) are scattered by the specimen and beam surrounding components, and partially absorbed within the chambers. The remaining electrons can be easily blocked by the detector flange and the radiation stop within the detector. In the case that the detector has no internal radiation stop, the beam can be easily stopped by an extra shield behind the detector and the end of the electron beamline.

The vacuum chambers of the setup were initially covered with 1 cm of lead, excluding the flanges and ports of the specimen chamber. In consideration of the above mentioned facts, this thickness is sufficient to guarantee a safe operation within a supervised area, with hermetically sealing of the enclosure. This however proves difficult or requires a large shields when the equipment that is directly attached to the chambers has to be included. Uncertainties and concerns about the expectable radiation from the E-Gun 300 could not be ruled out. The radiation safety requirements then foresaw an extra lead hutch that is surrounding the entire experiment and even sections of the optical tables. The framework of the hutch is sealed by aluminum-lead sandwich plates, with a 8 mm thick lead core being encapsulated by 1.5 mm thick layers of aluminum. The construction of the lead hutch with a interlock system required additional time and resources. Even worse, we were not allowed to test the E-Gun 300, not even at lower voltages, before the work on the hutch was completed. This caused a huge delay to both the first operation of the compact E-Gun 300 setup and this PhD work.

4.4 MACHINE STATUS AND OUTLOOK

The E-Gun 300 can be operated at 120 keV and is fully functional in terms of time-resolved electron diffraction. The lead hutch serves as outer shield and protects users of the source from potentially occurring stray radiation, regardless of the condition of the machine and the precautions taken directly at the machine. Most of the equipment is remote-controlled, since access to the machine during operation is not possible. In terms of radiation safety ordinances, the machine is filed with officials and supervised by the DESY radiation safety officers.

The temporal resolution of less than 300 fs (fwhm) has been experimentally confirmed. The source is further used to investigate the stability and reliability of novel liquid cell encapsulations for the investigation of solution phase dynamics. These encapsulations can afterwards be used within the REGAE specimen chamber and the fine vacuum conditions of the REGAE accelerator. The first publication related to the E-Gun 300 setup

is Hada et al. (2014). Further experiments are being regularly conducted now.

An upgrade of the maximum electron energy requires modifications of the electron source. The commercial feedthrough design remains inappropriate and must not be used for voltages exceeding 130 keV. The use of an improved feedthrough design would grant a safe operation without stray x-ray radiation along the feedthrough and further enhance the applications of this source.

The E-Gun 300 setup and a similar installation for gas phase experiments provided valuable experience regarding electric breakdown, which led to the development of an additional, outstanding setup, the FED-CAMM. The E-Gun 300 setup itself is a valuable development for the group and already suited for a wide range of investigations that concern ultrafast structural dynamics using electron energies up to 120 keV. The E-Gun 300 is also the first compact source of this type, which aimed at voltages exceeding 100 keV and thus revealed a range of unforeseen complications.

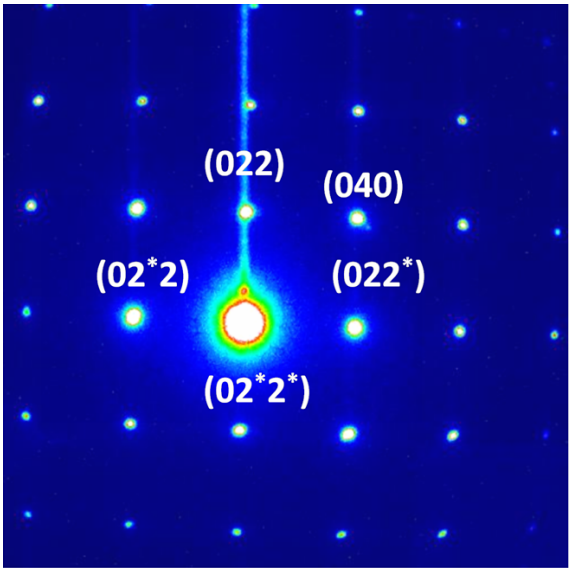

Figure 31: One exemplary diffraction pattern: single crystalline silicon, obtained with the E-Gun 300. The vertical traces are the result of the saturation single CCD pixel. Adapted from Zhang (2013).

5 THE FEMTOSECOND ELECTRON DIFFRACTION CAMERA FOR MOLECULAR MOVIES (FED-CAMM)

5.1 INTRODUCTION

The most important developments of this PhD work had started by the end of 2012 as a direct consequence of the problems experienced with the previously developed sources for femtosecond electron diffraction - the REGAE (chapter 3), the E-Gun 300 (chapter 4) and a clone of the E-Gun 300 with modified sample chamber for gas-phase diffraction studies. The REGAE still had years of commissioning work ahead. The overall progress in the machine conditioning and debugging was quite slow-going. The beam size, shape and stability was far from the requirements for diffraction and the synchronization of electron and laser pulses was not set up. The synchronization and first electron pulse length characterization by mesh ionization was ongoing throughout 2013 and 2014, the contemporary results were previously presented. The compact E-Gun 300-type installations were not working at the anticipated high voltages with the associated conflict of goals with respect to the specimen penetration and temporal resolution. Additionally, as attempts to prepare a specimen remained unsuccessful, I judged the overall advances at that time as insufficient, being disappointed by the overall outcome at that intermediate time-point. It was nothing other than an attempt to rescue the efforts, which had occupied the first years of my work, but did not specifically deal with the revelation of dynamic structural transformations of a targeted specimen system, but necessary preparations for such studies.

I started from scratch with the design and construction of a new compact (meaning man-sized) electron source for FED studies, once the installation of these previous machines had been concluded and they entered into operation, falling significantly short of their design values. The new source development was targeted at the fundamental limits to the achievable temporal resolution of a compact DC-operated electron diffraction setup. This was one of the declared primary goals of this development. The setup design was driven by the requirements of higher electric potentials, higher electron energies, respectively. The ultimately short pulse-duration is achieved by an external highly stable DC power supply and physically sustainable intense electric fields, in which dark current is minimized or not discernible, respectively, and the lifetime of photo-cathodes maximized. Together with ultra-short laser pulses and photo-cathode materials with low energy spread and high quantum yield, the new source can deliver electron pulses shorter than 100 fs (fwhm), even shorter than 80 fs (fwhm), with at least 10^4 electrons

per pulse, at the higher energies even 10^5 electrons. This temporal resolution with such bright electron pulses could only be beaten by installations incorporating a rf-cavity, which exhibits no timing jitter and no field errors. With such a short pulse duration and overall instrument response time, this compact electron source directly competes with the fourth generation light sources that were introduced earlier in section 2.2.

The compact installations of the type of E-Gun 300 are limited by the available commercial electric feedthroughs and the overall electron gun designs. The specific development of a high voltage feedthrough addresses one of the long existing limiting boundary conditions, since electric feedthroughs are not commercially available for high voltages and UHV environments. By addressing the high voltage feedthrough and limitations connected to individual components of the setup, the maximum energy of the new source, the *Femtosecond Electron Diffraction CAmera for Molecular Movies* (FED-CAMM), is only constrained by the capabilities of the external DC power supply and the electric breakdown conditions between the photo-cathode and the counter-electrode, in the gap for the electron acceleration, respectively. The FED-CAMM is operational up to the maximum energy of the external source. In other words, the machine functionality and time resolution of the FED-CAMM is not limited by any of its components, but rather by the laws of physics in terms of vacuum breakdown, field emission and the conditions that form the dynamics of femtosecond electron pulses.

The available high energies have significant beneficial impacts on the electron beam properties and the range of applications. The higher field gradients maintain shorter electron pulse lengths while more electrons per pulse can be used. For 30 keV as well as for 300 keV a pulse duration of 110 fs is obtainable, when the number of electrons per pulse is scaled from 10^4 at the lower to 10^5 at the higher energies. The prerequisite is that there must be flexibility in adjustment of the gap size. The gap size has to be minimized for the lower energies, and widened for the higher energies. This requirement is obvious but generally a predetermined extraction field for fixed conditions is involved. Any changes in machine parameters equates to an operation at sub-optimal extraction fields. The present work solves this problem through and adjustable gap - even in the presence of very high potential drops (> 100 kV). The mechanic flexibility is given as a novel feature within this instrument by the high voltage feedthrough assembly.

A small electron beam-size is given by an aperture measuring 75 μm in diameter that is part of the anode (the setup schematic is identical to what is shown in figure 25). This aperture size, in combination with parallel beam dynamics prior and immediately after the collimation by the anode-pinhole, automatically provides a low emittance and a transverse coherence length of several nanometers. With the higher electron energy, thicker specimens and specimen holders can be examined by this machine. To my knowledge,

there is to date no compact FED installation existing in this world, which could operate with electron energies and pulse brightness comparable to what is can be obtained with the FED-CAMM apparatus. There are compact DC injectors for synchrotron sources and small pulsed and compact electron accelerators used for x-ray generation and food processing, going up to 400 kV [Pirozhenko et al. (2001), Korolyov et al. (2001), Beard et al. (2011), Auditore et al. (2005), Korenev (2003)]. The pulsed character of the electric fields in these devices allows statistically higher field gradients for shorter amounts of time, similar to the advantage of rf-waves in cavities and the resultant field gradients over very short time. But the resulting energy spread in those devices needs to be considered. Further, DC sources for synchrotron accelerators use relaxed electric field gradients, to avoid the risk of electric flashovers and to extend the lifetime of the photo-cathodes. They enable a stable operation of continuous electron beams with currents in the mA regime [Rimmer (2005), Todd (2006), Sinclair (2006)]. None of these electron sources are aiming at, or used for, time-resolved studies in the sub-100 fs (fwhm) regime, which are pursued by this work. Thus, a high voltage and time-resolved setup such as the FED-CAMM is to the present date not known.

DC sources in synchrotron sources always use in-house high voltage feedthroughs and serve as a testament for the feasibility of the construction of a compact electron source, which has electron energies of a few-hundred keV and be used for highly time-resolved diffraction studies. In this respect, higher electron energy as previously utilized in the group and elsewhere seemed desirable to further enhance the temporal resolution as well as electron beam inherent properties (coherence and emittance), the penetration depth and scattering behavior (single scattering in thicker specimens). The new design was based around the requirements of highest potential carrying and electrically charged machine parts and the generation of ultra-short electron bunches for time-resolved electron diffraction experiments.

While exclusively working in the context of accelerator development and compact electron gun installations, I started to find the name electron gun generally misleading that is commonly used to name the whole apparatus used for FED experiments. While technically an electron gun does merely refer to the high voltage, electron generating and accelerating part of the FED setup, I decided to rename the new apparatus into its current name, focusing on its imaging capabilities. This nomenclature focuses on the real use of the electron pulses, namely their usage within a camera-like time-resolved electron diffraction apparatus that is capable of recording the data to render subsequent molecular movies. The content of this chapter is structured as follows. The engineering and design criteria are described, which are ultimately binding for the development of a (sub-) 100 fs (fwhm) electron source and to which there is no obvious alternative. It is similarly important, that required geometries in terms of electrode dimensions and

spacing in combination with applied potentials are outlined that lead to a corresponding temporal resolution or electron pulse length, respectively. In this case, it is the (sub-) 100 fs (fwhm) or a temporal resolution, which is closer to singularly defining the fundamental limit of obtainable electron pulse durations in DC-operated setups. Only those electron numbers per pulse within this pulse duration are considered, which return a sufficient signal to noise ratio to potentially resolve a structure in a single shot (minimum electron numbers per pulse were considered in section 2.4.2). The capabilities of the FED-CAMM are simulated, but the dimensions used in these simulations were at first evaluated by measurements of electric field gradients, which were already obtained with the instrument. Finally, the most crucial components are discussed in further detail, but the elements, which do not represent the fundamentals of such a setup, but meet the demands of experiments and user criteria and would vary with the experimental installation and its application, are neglected.

5.2 ENGINEERING AND DESIGN CRITERIA OF A (SUB-) 100 FS FED SETUP

One aspect of the FED-CAMM is the combination of the simplicity of a compact DC apparatus with the favorable short temporal resolution of relativistic electron accelerators, or generally setups that comprise of rf-operated cavities for the acceleration and re-compression of electron bunches (as discussed in section 2.3.2 and listed in table 9). Comparable to REGAE and other sources for FED experiments, a pulse length of sub 100 fs (fwhm) can be achieved in a compact DC setup. This statement is supported by the following simulations, which themselves are based on the experimental evaluation of applicable electric field gradients in the setup. It is also assumed, that a suitable femtosecond laser source with a laser pulse duration below 40 fs is available [e.g. Piel et al. (2006)]. The major emphasis was on the creation of electron gun part geometries, which maximize the static electrical field between the electrodes. The generated and accelerated electrons should see an electrical field that is kept uniform and stable with respect to amplitude fluctuations, which could induce timing jitter into the system. These two aspects alone bring a series of shape and dimension requirements to the core electron-pulse-generating elements and determine the basic layout (a repeated reference to figure 25 must be made).

The femtosecond DC electron source, which does not require a re-compression of the pulses before the interaction with the specimen, has to be optimized around two main aspects:

(i) A suited electrode shape generates uniform electrical fields in the center region of the photo-cathode. With an optimal shape, an ultrafast acceleration of electrons in a uniform electrical field over minimized gap sizes and in highest electrical field gradients is possible. Uniform electrical fields and a moderate electron density within the electron

pulse, which possesses a small initial dispersion, are important for the beam inherent characteristics. Among these are the energy spread, emittance and transverse coherence length. For the development of an appropriate electrode geometry, one must minimize the field enhancements that are induced by the curving of electrodes. By doing this, the nominal electrical fields in the critical region can be increased to intensities at which electric breakdown phenomena in UHV environments occur and can not longer be avoided.

A further necessity, which is connected to the optimal electrode development, is the appropriate follow-up treatment of the prior machining processes. The right materials have to be selected and the surface electrically optimized (typically manually and electrically polished), to reduce microscopic field enhancements caused by derivations from ideal electrode surfaces. Any roughness, ripples, scratches, particulates or contaminants embedded in the surface will corrupt the local electric field properties and lead to electric field peaks, which trigger electron emission and promote electric discharges at higher voltages (see the outline of dark current and its sources in section 3.3).

(ii) The electron pulse has to be used for the experiment as close as possible to its generation and acceleration; hence as close as possible to the primary anode. The effect of pulse-broadening is not as severe behind the anode at higher energies (> 120 keV). However, as the electron pulse broadens continuously along the beam path, every measure of extra travel distance contributes to the pulse-broadening and should be avoided. As was seen in the first simulations concerning the E-Gun 300 setup, the pulse broadening after the anode plate strongly depends on the electron beam dynamics. In some cases, the broadening effect is not as severe, and further optics can be used before the interaction of the electron pulse with the specimen [see figures 27 and 29].

Exceeding these fundamental requirements of maximized acceleration fields by optimized high voltage electrodes, a minimized acceleration gap and a minimum travel distance to the specimen, the following design criteria precede the development of each individual component of the new, the FED-CAMM setup:

(iii) The electron energy should be adjustable to meet the requirements of the experiment. Depending on the type of specimen and preparation different requirements on the electron energy and pulse duration are imposed. The upcoming simulations show, that for different energies with corresponding electron densities and gap sizes a pulse duration of 100 fs (fwhm) can be obtained. The electron numbers range from 10^4 electrons per pulse at the lowest energy to 10^5 electrons per pulse at 300 keV. The energy should exceed a threshold energy, below which the electron numbers per pulse do not allow the resolution of a structure by a single or very few probe electron pulses and

below which a significant short time resolution at the specimen of 100 fs can no longer be obtained at reasonable electron numbers and densities, source brightness respectively. An adjustable energy optimizes transmission properties in respect to penetration depth, the rate of scattering events, and the damage that is induced by inelastic scattering events. In a time-resolved setup, the flexibility of the energy requires an adjustable gap size. With the assumption that the electric field strength in ideal geometries is constant, the variation of energy scales linearly with the gap size. Similarly, the electron density scales linearly with the energy and the gap size for a constant pulse duration.

(iv) The maximum applied potential should reach a few hundred kV and should be limited only by the external power supply, not by electric breakdown in the apparatus. The electron energy of the electron source should be variable. The apparatus should adjust readily to the applied potential. Under this condition, the apparatus dimensions are not fixed to pre-determined specifications nor are they limiting the instrument properties to a previously determined temporal resolution corresponding to the component dimensions. On the contrary, the time resolution is not limited by the apparatus itself, but by other external and physical conditions. Explicitly this means, that for each electron energy, or electrode potential respectively, the distance between the cathode and anode can be adjusted to an optimum value to achieve the highest maintainable electric field strength at minimized acceleration gaps, next to a stable and reliable operation, which means an operation free of electric discharges, high voltage instabilities, and without timing jitter. A uniform electric field is ensured by an optimized electrode geometry as mentioned earlier. In the previous E-Gun 300 setup, the electron gun geometries, utilized materials and the high voltage feedthrough were each limiting the machine performance and achievable temporal resolution.

Beyond these previous specifications, the following good-to-have features should be included in the setup design:

(v) A collimation aperture positioned close to the specimen, which leaves sufficient electrons of the main beam, but potentially improves the spatial resolution and emittance properties. A first aperture is currently implemented into the anode plate.

(vi) The setup comprises a multiple-lens system with least three incorporated lenses. The layout of lenses is comparable to conventional transmission electron microscopes, in particular the imaging system herein, and technically allows the back-projection of diffraction patterns into real space image formation and magnification of both real- and reciprocal-space images with nanometer spatial resolution and femtosecond temporal resolution.

(vii) As mentioned in section 4.3.2, European safety regulations for x-ray sources and stray radiation emitters apply for energies ranging from 5 keV up to 1 MeV. While staying within this energetic confinement, one potentially faces less regulations affecting the design of the machine inherent and surrounding installations, which concern the radiation safety measures. Therefore, the maximum applicable energy of the electron source should not exceed 1 MeV, though individual components might be suited for higher potentials, or can be scaled accordingly. The design of the high-voltage feedthrough for example is suited for much higher voltages than are currently applied. Suited and conventionally used electron energies for diffraction and transmission range in the few hundred keV regime (between 100 and 400 keV). Within this range lies the trade-off between a satisfactory spatial resolution connected with a adequate penetration depth and reduced specimen damage.

All of these design criteria frame a world-leading and outstanding (sub-) 100 fs electron diffraction apparatus. The remaining hurdle is the engineering. The physical requirements are accessible. When all of these design and engineering criteria are implemented, incorporating the necessities of the theoretical estimations from the simulations of the beam dynamics, the distances between the photo-cathode, anode, and the sample grid have to be minimized at lower energies (< 100 keV), since every millimeter of path length measurably elongates the pulse duration and thus degenerates the temporal resolution. The distance to and positions of the magnetic lenses and the detector has to be optimized for the best spatial resolution.

5.3 ELECTRON BEAM SIMULATIONS

The simulations of the REGAE reveal that any time-resolution can be generated with a computer simulation that makes assumptions about ideal machine conditions. In the ASTRA simulations of the REGAE, the instrument response time could be as short as 25 fs (fwhm). These simulations include an accelerator arrangement with conditions which somewhat relate to the overall machine design and energy range. In reality, the electron pulses of the currently used REGAE layout are measured to 900 fs (fwhm). They are more than two orders of magnitude longer in duration than simulated. The simulated conditions for the 25 fs case do not match the real conditions. The main problems are the assumed initial energy spread and optimized phase of the buncher cavity. Differences in details, such as laser spot sizes, pulse shapes, electric and magnetic field inhomogeneities, field derivations and so forth, also contribute to the pulse broadening and are not considered in the simulated results of REGAE. The calculations give the achievable results that ultimately will be realized. However, REGAE is a complex machine that is not nearly as robust in performance as the simple compact DC source concept considered here.

Computer simulations with the GPT code, which were previously applied to the E-Gun 300 (section 4.2), allow the specification of any electric field strength in the acceleration gap, which leads to the expected result. In the current case, a temporal resolution of 100 fs (fwhm) or below is desirable. The gap size and the applied electric potential are the most important parameters in this scenario, which determine the resulting temporal resolution. Whether the simulated values are physically reasonable or not obviously needs to be considered.

The GPT simulations of the E-Gun 300 only include the parameters of electric field gradients and beam sizes, as well as electron numbers per pulse, which are actually found within the real experimental conditions. The only variable in these previous simulations is the energy spread, which is primarily dependent upon the utilized photo-cathode materials. Since research in this matter is ongoing, this parameter remains uncertain and will probably be improved. The energy spread of the gold photo-cathodes are larger than 0.2 eV and less than 0.6 eV. The realistic, including best and worst case scenarios are thus covered by the previous GPT simulations of the E-Gun 300. Unlike in REGAE, these simulated results are representative of the actual machine performance.

In the FED-CAMM, higher electron energies and more intense electric field gradients can be used, as is now explained. The highest electric potential is no longer limited by the high voltage feedthrough and can thus be raised to 300 keV, the current limit of the available power supply. The gap size between cathode and anode can be adjusted to any value from 0 to 60 mm, which in combination with the applied potential determines the electric field gradient in this region. This range of gap sizes satisfies both the lowest and highest energies, when constant electric field gradients are set (see table 12 and table 13, as well as figure 32 and figure 33). Besides these first two parameters, the gap size and electric potential, which combine to determine the electric field gradient, there is a third variable, namely the numbers of electrons per pulse. This parameter is directly controlled by the intensity of the incoming laser pulse, which strikes the photo-cathode. Furthermore, the laser pulse has an adjustable duration. In the environment of low electric field gradients, a longer initial laser pulse can lead to a shorter electron pulse at the specimen. The reason for this is the increased electron density at the photo-cathode caused by short excitation pulses, and the consequent stronger Coulomb repulsion, which has the greatest impact in proximity to the photo-cathode. The space charge dramatically elongates the electron pulse in its axis of propagation. For this reason a 100 fs (fwhm) laser pulse is used in the E-Gun 300, instead of a shorter pulse such as of 40 fs (fwhm) duration. In the E-Gun 300, the gap size is fixed to 15 mm at voltages that lead to electric field gradients of less than 10 MV/m. The elongated laser pulse leads to a decreased electron density in the pulse and less space-charge induced broadening. Thus, there is

an optimum laser pulse duration for each electron density and accelerating field.

Fixed geometries and limited potentials are no longer present in the FED-CAMM. To the contrary, the instrument is highly flexible in multiple aspects. Consequently there is more variability in the choice and the combination of the physical and simulated machine variables. A smart merge of ideal simulation parameters leads to the desired (sub-) 100 fs (fwhm) electron pulse duration, and to longer pulses with higher electron numbers, where those are needed. Theoretically, we have at least four main parameters to tweak, namely the energy, gap size, laser pulse length, and laser pulse intensity. These four variables span a four-dimensional parameter-space with an associated temporal resolution at each point in this space. This parameter-space has to be constrained to reasonable dimensions and to ranges, which relate to natural (physical) and instrument limitations. The latter point includes the devices connected to the electron source. The parameters are already known in some cases, such as for the laser or the high voltage power supply. The missing parameters relate to the maintainable electric field gradients and were evaluated experimentally. Table 12 summarizes the parameter space, which is reasonable for consideration in the upcoming GPT simulations.

FED-CAMM parameter space		
Default laser pulse duration	140 - 190	fs
Minimized laser pulse duration	25	fs
Laser pulse intensities	0 - 1	mJ
Laser spot sizes on the photo-cathode	50 - 200	μm
Repitition rate	1 - 2 $\cdot$ 10^5	Hz
Applicable electric potential	1 - 300	kV
Gap size	0 - 60	mm
Max. field gradient	28.0	MV/m
Field gradients without dark current	9.5 - 18.0	MV/m
Initial energy spread	0.2 - 0.6	eV

Table 12: Parameter space available for simulations of the FED-CAMM apparatus.

5.3.1 DETERMINATION OF SIMULATION PARAMETERS

The laser pulse duration is currently defined by the laser source itself. A further compression of the UV pulses for the photo-cathode requires additional optic elements, which are not set up yet. The shortest laser pulse duration of 25 fs (fwhm) is entirely realistic. Laser pulses of 40 fs (fwhm) are commonly provided by commercial and home-built systems,

but shorter laser pulse durations can be obtained with corresponding optical setups. For each energy and gap setting of the simulation, the optimum laser pulse duration and spot size on the photo-cathode is evaluated by the comparison of various simulated parameters. The final electron pulse durations are presented with the declaration of the used laser pulse duration and laser spot size that led to the optimal result for each assumed initial energy spread. The intensities of the laser pulses are incorporated by simulating different numbers of electrons per electron pulse. The lowest electron number per pulse of interest amounts to 10^4 electrons and ideally 10^5 electrons per pulse at the higher energies. The repetition rate is not relevant for the estimation of the electron pulse duration. From the available electric potentials, a range between 30 and 300 kV is selected. The earlier presented FED sources, which exhibit the smallest energies, do not fall below the lower end of this energy range or would otherwise not be useful for FED experiments. Higher energies up to 400 keV are obtainable and would allow higher electron numbers per pulse at a constant electron pulse duration, but dramatically increase the cost of the apparatus. The complexity of the setup is not affected by such a potential upgrade and remains at an easy to manage level, as no aspect of the layout needs to be changed. But at this point, it is questionable whether this additional increase in energy is of any advantage considering the additional cost and electron induced increased specimen damage.

The gap sizes are determined by the development of the maximum obtainable electric field gradients and dark currents. The previously highest field gradient, which was obtained in a series of experiments using the actual layout of the FED-CAMM, as it is described within the further parts of this chapter, amounts to 26.7 MV/m. This value was obtained with 40 kV applied to a gap size of 1.5 mm. In this scenario, the dark current was significant (several μA), but could be decreased to a non-measurable current (< 0.5 μA) by an increase of the gap size to 2.5 mm. This corresponds to 16 MV/m at this voltage. The neighboring voltages yielded similar electric field gradients at corresponding gap sizes. The electric field gradient of 16 MV/m led to practically zero (since not measurable) dark currents at a range of potentials up to 80 kV. Higher voltages were accompanied by lower field gradients, since a recently installed high voltage electrode was not yet sufficiently conditioned, and the diameter potentially too small, as will be explained shortly. During the course of conditioning, the same electric gradient was reached for a continually increasing energy. From single available data points at higher energies, it is reasonable to conclude that 15 to 16 MV/m can be ordinarily obtained for voltages up to 200 kV without the occurrence of any appreciable dark current in the current setup, using a well conditioned electrode and suitable photo-cathode.

The constrained size of the electrodes used in the first experiments became visible. The central flat region along the front side of the electrode measures 3 cm in diameter. At small gap sizes, the ratio of the plane area to the gap size is rather large, but decreases

with larger gaps. Practically this manifests in reduced electric field gradients, down to the conventionally used 9.5 MV/m at very high voltages and large gaps, which are those measuring more than 2 cm. This current limitation will be removed by the utilization of larger chambers (with e.g. ISO-K) and increased electrode diameters (such as 25 to 35 cm). Voltages of 350 kV were elsewhere obtained with electrode shapes similar to the developed shapes of this work, but had a diameter twice as large as the currently used 14 cm [Naidu and Kamaraju (1996) and Bruce (1947)]. The ISO-K technology will be sufficient for this setting, since vacuum pressures of more than 10^{-5} mbar, even more than 10^{-3} mbar are sufficient for the operation of high voltages. This was experimentally confirmed. Based on these first experimental findings, the electric field gradient was fixed to 15 MV/m for all energy ranges. We will see shortly, that this is a threshold field gradient for the anticipated (sub-) 100 fs (fwhm) electron pulse duration and 10^4, or 10^5 electrons per pulse, respectively. The applied electric potential U thus scales with the gap size as follows:

$$U\ [\mathrm{MV}] = d\ [\mathrm{m}] \cdot 15\ [\mathrm{MV/m}], \tag{5.1}$$

with d denoting the gap size. The other fixed variable is the position of the specimen and the distance to the photo-cathode, at which the electron pulse duration is determined. If we consider thicker specimen encapsulations, such as liquid cells, the position of the specimen is at most 10 mm away from the anode. Neglecting the thickness of the anode in these simulations, the pulse duration is measured at

$$s\ [\mathrm{mm}] = d + 10\ [\mathrm{mm}], \tag{5.2}$$

For comparison purposes, the pulse duration right after the anode, this is 1 mm from the side facing the photo-cathode, is also given. The pinhole in the anode plate is fixed to 100 μm. As previously mentioned, a slightly smaller aperture is incorporated into the anode of the actual setup. This is expected to lead to more confined diffraction spots, which are more easily differentiated from the main beam. A smaller pinhole aperture reduces the number of transmitted electrons, which also influences the electron pulse duration. When fewer electrons of the initial distribution are transmitted through the anode, the statistical value of the pulse length automatically changes due to the modified distribution of electrons in the pulse. One of the remaining variable parameters in the simulations is the initial number of electrons per pulse, including their initial energy spread.

The results of these simulations characterize the nominal operational range of a compact DC-operated electron source. More extreme conditions can be reached in such a setup, a few cases are simulated and included in this discourse. The parameter space, which is covered by the simulations for the previously discussed variables, is summarized in the following table 13.

Summary of FED-CAMM simulation parameters		
Gap sizes	2 - 20	mm
Gap size increment	2	mm
Volt	30 - 300	keV
Volt increment	30	keV
Electric field gradient	15	MV/m
Spot sizes	50 - 200	μm^2
Spot increment	50	μm^2
Laser pulse durations	35 - 55	fs
Laser pulse durations increment	5	fs
Electrons per pulse	10^4 and 10^5	
Initial energy spread	0.2 and 0.6	eV
Positions of pulse duration from the anode	1 and 10	mm
Pinhole aperture	100	μm

Table 13: Summary of the simulated parameters for the FED-CAMM instrument. Further parameters are specified in the above text.

5.3.2 FED-CAMM SIMULATION RESULTS

The numerical results of the simulations, which were used for the creation of the following graphs, are listed in appendix C. Due to the occurrence of statistical errors within the first 320 datasets, the dependency upon the number of simulated macro-particles was investigated. These errors are purely statistical in nature, since randomized variables within certain ranges build the foundation for these simulations. In the final simulations, which concern 10^4 electrons per pulse, each electron was simulated rather than using macro-particles. The same amount of macro-particles was used for 10^5 electrons, which reduced the total number of electrons by a factor of ten in favor of a reduced simulation time. It was found that with 10^4 macro-particles in each simulation, the statistical spread reduced to 2 fs (fwhm) for 10^4 electrons. The spread for 10^3 macro-particles, which was previously used for the simulations, amounted to 25 fs (fwhm), which significantly smears the significance of the simulated results. For the simulations, which concern 10^5 electrons, the spread amounted to less than 10 fs (fwhm). A single laser spot-size and laser pulse-duration is presented for each of the settings of the previous table, which present the optimum within the simulated parameter range.

One of the fundamental questions which had to be answered by these simulations was, whether an increase of energy directly improves the pulse duration or whether

the pulse duration is also dependent on other factors. As previously mentioned, the compact sources that were developed over the past decades (table 8) showed a continuous improvement in pulse duration with ever shorter electron pulses. Most of those sources utilize electric fields at gradients of 10 MV/m or less. This appeared as one constant factor within all those setups with electron energies up to 100 keV. As will be outlined here, the electric field gradient is one of the most determining factors in a compact source. The following figure 32 shows the development of the simulated pulse durations at 1 and 10 mm from the front-side of the anode. The upper two lines represent the pulse duration, which belong to electron pulses with initial 0.6 eV energy spread.

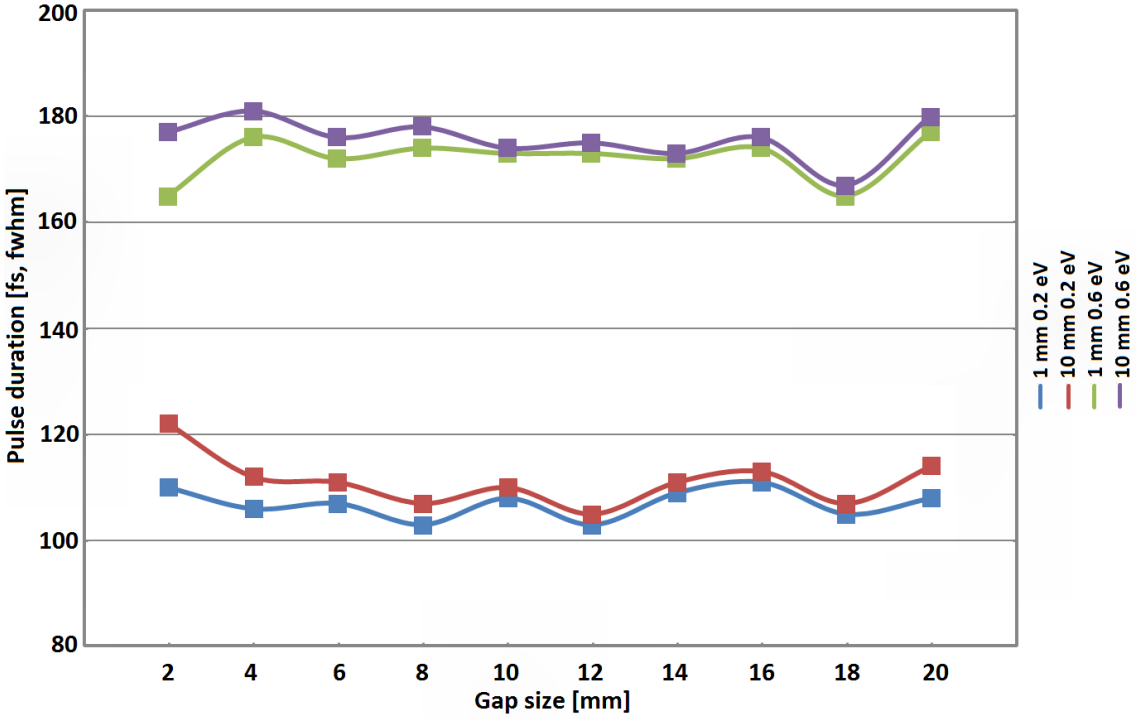

Figure 32: Simulation results for 10^4 electrons per pulse, 15 MV/m in the cathode-anode gap and the according potentials. Pulse durations at 1 and 10 mm from the anode-front are given for energy spreads of 0.2 and 0.6 eV. Numerical values are listed in table 16 of appendix C.

Surprisingly, the pulse duration for an electron spread of 0.2 eV appears to be almost constant over all simulated gap sizes at both 1 and 10 mm from the front-side of the anode. The fluctuations of the data points around a mean value of 109 fs may be resultant of beam dynamics, which do not have an obvious explanation, but might be related to specific inherent simulation parameters. The oscillations are more distinct for the higher energy spread of 0.6 eV, and in some regions correlate with the simulations of the lower energy spread. As these are independent simulations, a correlation suggests a systematic mechanism as cause. The offset of the curves of 1 mm to 10 mm of the same energy

spread is generally smaller for larger gaps. For lower gap sizes and corresponding smaller energies, the differences in pulse duration indicate how important it is to constrain the spatial extent between the anode and the specimen. For energies higher than 150 keV this is of lesser importance.

It is obvious, that the electron pulse durations including the curvatures of the data points stay within a window of less than 20 fs (fwhm) spread over all gap sizes. The width of the window is mainly determined by the fluctuations of the simulations, which are not caused by insufficient statistics, as discussed above. For the lower energy spread, the mean pulse duration centers at around 109 $\pm$ 4 fs (fwhm). An offset of 65 $\pm$ 5 fs is present to the data points, which correlate with the larger energy spread. Those pulse durations are centered around 174 $\pm$ 4 fs (fwhm).

The next set of simulations was conducted with 10^5 electrons per pulse for each energy spread. The results are shown in the same manner as for 10^4 electrons in the following figure 33.

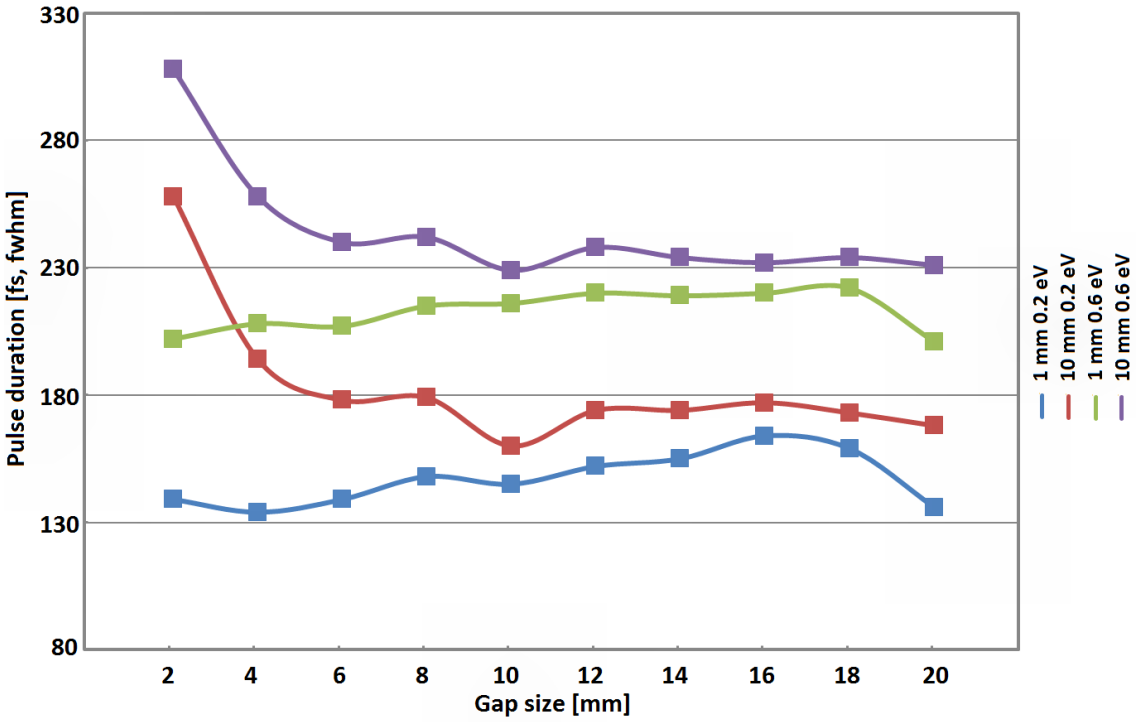

Figure 33: Simulation results for 10^5 electrons per pulse, 15 MV/m in the gap and the according potentials. Pulse durations at 1 and 10 mm from the anode-front are given for energy spreads of 0.2 and 0.6 eV. Numerical values are listed in table 16 of appendix C.

The development of the pulse duration with an increasing gap size is comparable to the previous 10^4 cases utilizing 10^4 electrons, for those points which refer to the simulated pulse durations at 1 mm from the anode-plane (blue and green curve, 0.2 and

0.6 eV respectively). The development is rather linear within a certain width, as seen previously. The offset between these two curves, which center around 144 $\pm$ 10 fs (fwhm, blue line) and 213 $\pm$ 7 fs (fwhm, green line), is fairly constant over all gap sizes and measures 66 $\pm$ 5 fs (fwhm), comparable to the previous simulations for 10^4 electrons.

However, there is a distinct difference to the previous case for the simulated pulse durations at 10 mm. A large increase is seen in the pulse durations from 139 to 258 fs (fwhm, blue and red curve at 2 mm and 30 keV respectively) and 202 to 308 fs (fwhm, green and purple curve at 2 mm). This indicates a much larger increase in the growth of the pulse durations with each increment of the propagated distance of the pulse and a significant larger linear energy chirp or energy spread, respectively. Practically, this means that the electrons have a significantly larger energy spread for electron sources with electron energies up to 90 keV. Spatial care needs to be taken in making the experimental setups more compact in this energy range. At energies above 120 keV, this energy spread is less distinct and one can afford to further propagate the pulses before they interact with the specimen. This is another important result of this first extensive set of simulations.

A comment has to be made about the number of electrons, which actually reach the rear-side of the anode and form the electron pulse with its subsequent pulse duration. The simulations start with 10^4 and 10^5 electrons respectively at the photo-cathode, but not all electrons leave the acceleration gap. They are instead absorbed by the anode if their axis of propagation is not aligned with the pinhole. A transverse spreading perpendicular to the axis of propagation within the gap is surely present, though not as distinct as in the longitudinal direction, as discussed earlier. Spot sizes of 200 μm^2, which were ideal for the simulation results, but are actually larger than the simulated pinhole. The larger spot size correlates to a decreased electron density and thus yields the better results in terms of pulse duration compared to 50 to 150 μm. The differences in the pulse durations of pulses with a 200 μm spot size to 150 μm spot size are overall small and quite often even insignificant (1 - 2 fs). The larger spot-sizes automatically reduce the numbers of surviving electrons, due to the ratio to the diameter of the pinhole and initial electron beam size. The important point is how many electrons actually reach the specimen.

The first dependency of the spot size to the decrease of transmitted electrons appears to be inversely proportional for all simulated cases. About 15 % of all electrons survive the 100 μm aperture when a laser spot size of 200 μm is simulated, and twice as many electrons survive for 100 μm spot sizes and so forth. The size of the pinhole aperture however is dependent upon the preferences of the experimental setup. Commonly larger apertures are used in diffraction experiments to maintain a higher number of electrons.

Larger pinholes allow most of the electrons, this is around 80 to 90 %, to pass the anode.

It would be interesting to find a relation between the number of surviving electrons and the pulse duration after the anode, to quantify a potential impact of the pinhole upon the electron pulse duration. If the statistical value of the pulse duration is increased after the pulse has transmitted the pinhole it means, that the electron pulse has a smaller transverse extent than before and more electrons of the longitudinal direction dominate the statistical value of the pulse duration. The electrons of the pulse that propagate far from the center of the beam and the pinhole, respectively, get stripped from the pulse, which then appears to be elongated. Simply said, the ratio of longitudinal to transverse expansion is changed due to the transmission. It was found that for most of the simulated cases the change in pulse duration directly before and after the pinhole position was insignificant. This correlates to similar electron densities along the main axis of propagation and a conserved ratio of spatial pulse extensions. The amount of electrons in the pulses, which have intrinsic Gaussian distributions within the FWHM range, is only slightly changed and thus has no large effect on the remaining pulse duration.

The next question seeks for other factors, which majorly influence the electron pulse duration, besides the initial energy spread. Since the sheer increase of the electron energy does not lead to the anticipated result, a quicker acceleration to the same end energy within a shorter gap must be a key parameter. To investigate this dependency, the gap sizes were varied at three different energies. Simulations were carried out for 100, 200 and 300 keV, starting below the commonly employed 10 MV/m to the remarkable and experimentally obtained electric field strength of more than 26 MV/m for 10^4 and 10^5 electrons per pulse. Dark current electrons, which play a role at the higher field gradients, are neglected for the moment.

Figure 34 and 35 illustrate the dependency of the pulse duration on the extraction field. The extent of initial pulse broadening is, as suggested by equation 2.6, directly proportional to the inverse of the square root of the electric field. The three different energies lead to highly comparable pulse durations at the same field gradients. The variations in pulse durations at each electric field gradient range from 1 to 10 fs (fwhm) for 10^4 electrons and from 1.6 to 27 fs (fwhm) for 10^5 electrons from the highest to the lowest electric field gradients. The differences, which are seen between the different energies at each simulated electric field gradient, are partially due to the remaining statistical fluctuations of the simulations and partially depend on the pulse dynamics, which are associated with the extension of the acceleration gap and especially with the simulated pinhole aperture.

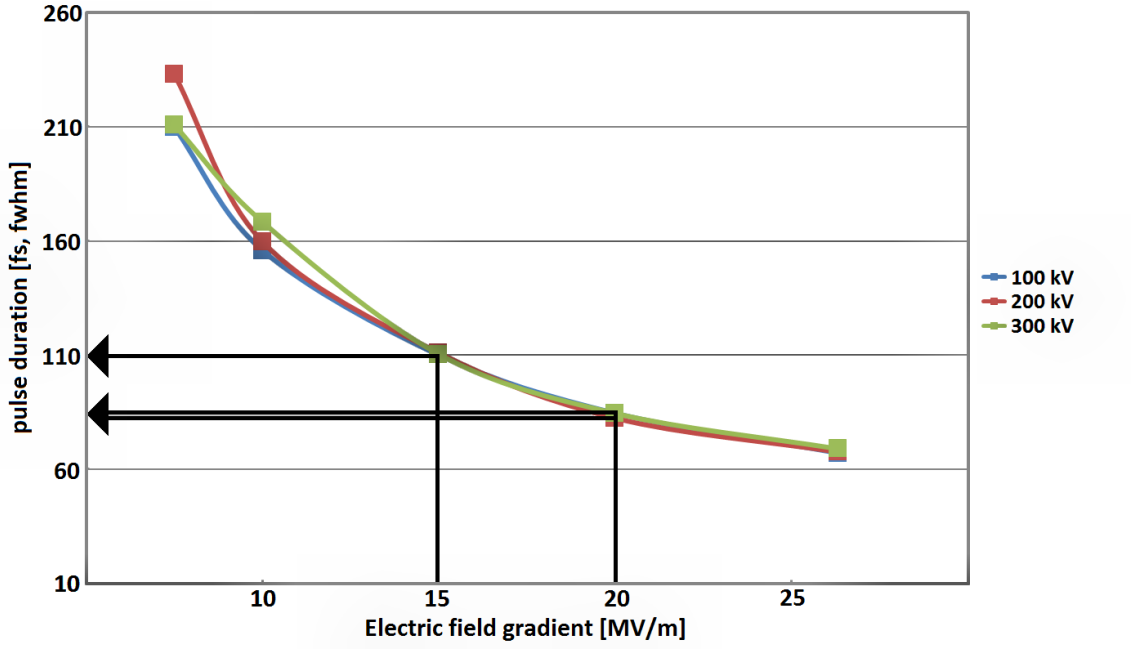

Figure 34: Dependency of the pulse duration at the three given energies for 10^4 electrons, extracted around 1 mm from the front side of the anode plane. Numerical values are listed in table 17 of appendix C.

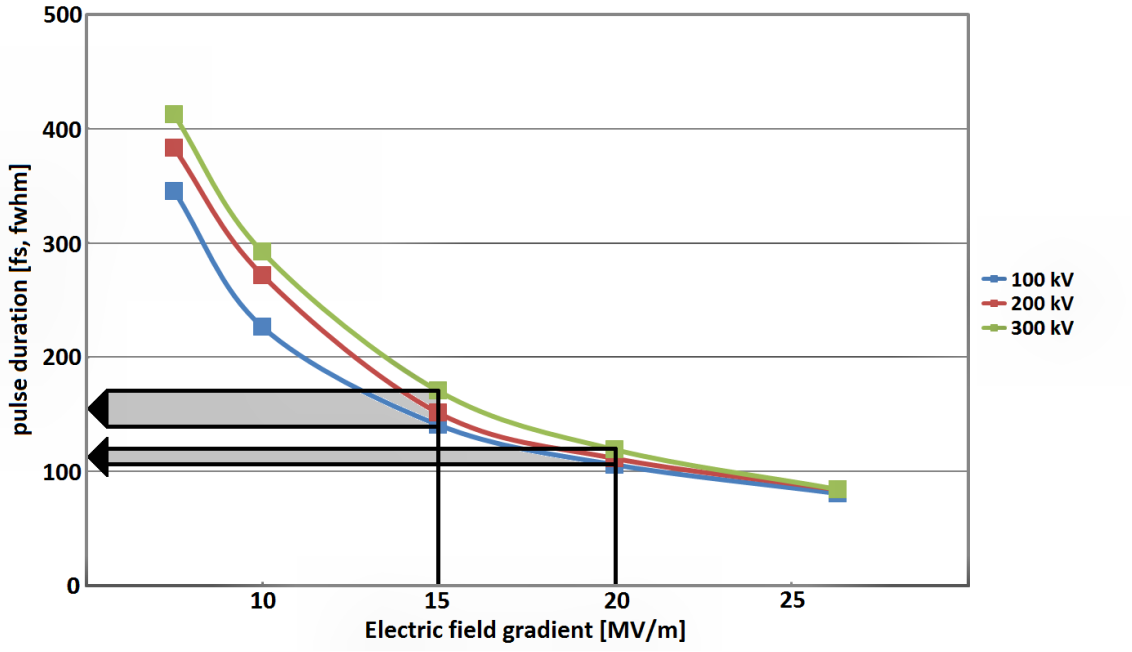

Figure 35: Dependency of the pulse duration at the three given energies for 10^5 electrons, extracted around 1 mm from the front side of the anode plane. Numerical values are listed in table 17 of appendix C.

For 10^5 electrons, the pulse durations are significantly longer for the higher energies at the lowest field gradients than for the lowest energy at the lowest electric field gradients. This relates to the much larger gap sizes, which are required for 200 and 300 kV to achieve the same electric field gradient as for 100 kV. At the lower field gradients the pulses with smaller electron energies perform better than the pulses with higher energies, at least within these simulated settings with 10^5 initial electrons per pulse.

The data points, which were extracted at 10 mm, are not shown. This is because the performance of the pulse duration is identical to the extracted pulse duration at 1 mm. An extra increase in the pulse duration is not quantifiable and falls within the statistical uncertainties of the simulations of a few femtoseconds. Physically this means, that the pitch of the electron broadening throughout the drift through the setup is small.

The simulations of this chapter help to characterize the development and dependencies of the pulse duration upon various parameters, which can be set and reached with the current prototype of the FED-CAMM apparatus. It is shown that electron pulses with a duration of less than 200 femtoseconds (fwhm) can be easily reached for a broad range of energies and bright electron pulses, when photo-cathodes with low energy spread are used. With average pulse durations of 109 femtoseconds (fwhm) at 15 MV/m, compact electron sources such as the FED-CAMM instrument with corresponding features outperform all presently existing compact hybrid setups listed in table 9, which were already producing more promising results than the currently existing DC sources of table 8. If we assume that an rf-cavity doubles the instrument cost and requires more sophisticated electronics, which are further prone to failure and which most likely introduce electronic timing jitter, it is not worth the investment. The best performance of a hybrid setup is seen at the 95 keV setup in Toronto. The instrument response time is slightly shorter than 200 femtoseconds.

When the electric field gradient is increased beyond 15 MV/m, even shorter electron pulses can be obtained, as marked in figure 34. Electron pulse durations below 100 fs can be reached, although higher electric field gradients might be accompanied by dark current electrons, which might impair the stability of the electric field, electron numbers per pulse and signal to noise ratios. However, electron pulses with remarkable short durations are feasible and can serve as the alternative or be complementary to FEL-based time-resolved structural investigations with the only difference, that compact electron diffraction setups can be more widely built and disseminated to a larger user base.

The negative aspect of compact sources, which became clearer in development, is the potential loss of electrons, due to the strip off at the pinhole in the anode. This of course is only true, if very small apertures are used. In addition extraction meshes with little

spatial occupation can be used, as they were utilized in early FED sources [Siwick et al. (2002)]. Alternatively, besides of the utilization of more electron pulses per time point of the structural transition, the rf-cavity technology might conserve larger bunch densities, but improved electronics for optimal synchronization is a prerequisite requirement.

The electron pulse duration can be further reduced by the use of materials with even less energy spread. As discussed in chapter 2, GaAs photo-cathodes are a very promising candidate in this regard. But the requirements on the vacuum are exacting, which forces a great deal of care to be taken in the design of the vacuum system, the maintenance of the UHV conditions as well as special care in the actual execution of experiments, to not impair the vacuum and performance of the photo-cathodes. The alternative of higher electric field gradients seems to be less challenging, although this in itself requires certain optimized techniques within the production of the high-voltage electrodes, a necessary subject with is treated next.

5.4 DEVELOPMENT OF A HIGH VOLTAGE ELECTRODE

The electron pulse simulations reveal a higher electric field gradient in the gap to be the decisive parameter for shorter electron pulses. Further, this dependency is independent of the target electron energy. A high mean electric field requires the consideration of certain design and manufacturing aspects concerning the involved parts. The design, machining and following treatment procedures have to be optimized, the maximum electric field gradient will otherwise be constrained to lower values. The commonly assumed breakdown and maximum operation voltage of 10 MV/m that is specified in countless publications and to which all previous electron diffraction setups were limited, is most likely based on imperfections in the actual experimental installation. Since the electric field gradient is such an important parameter to consider, and since it can not be afforded to operate a DC accelerator for state of the art FED experiments with field gradients in the same regime as competitors did before, all necessary precautions for more intense and stable electric fields have to be taken.

The development should further conserve a reasonable lifetime of cathode materials and avoid the emission of electrons, when no external trigger (such as electric or optical fields) is present. This is the only valid approach in the development of a setup, which defines the current state of the art. A discourse of the definition of the electric field, a study of electric field distributions, and the derivation of ideal electrode geometries is given for this reason. The implementation of the previous design criteria and findings into a high voltage electrode are treated and concluded by aspects of manufacturing, experimentally determined and theoretically predicted breakdown thresholds, as well as

by the underlying mechanisms of electric breakdown. Electrode design is generally a subject of great experimental interest in many different fields and applications.

5.4.1 ELECTRIC FIELD DISTRIBUTIONS AND ELECTRODE DESIGN

The first key point in electrode development is the embedding of the photo-cathode into a metallic surrounding, facing a uniform electric field. The mixture of conducting and insulating materials in the sensitive region, which is exposed to maximized electric fields, should be avoided. It is obvious, that otherwise the electric field distribution will become inconsistent. Due to the unfortunate shaping of the electric field by abruptly changing conducting geometries within non-conducting elements, intense field gradients arise on the curvature of the metallic elements that had previously led to the limitations and malfunctioning of the E-Gun 300 and machines of that type. Further, the electric field distribution is no longer uniform, leading to an additional angular spread and enlarged emittance.

In a sideways non-constrained vacuum chamber that houses a high voltage electrode, the ideal arrangement of surfaces of different potentials facing each other would be flat, as in a parallel-plate capacitor. Within such a device, the electric field, neglecting effects along the corners of the plates, is defined as

$$E = \frac{U}{d} = \frac{Q}{\epsilon_0 \, \epsilon_r}. \tag{5.3}$$

In here, Q denotes the full electric charge, ϵ_0 denotes the electric constant and the relative permittivity ϵ_r equals to 1 in a vacuum, due to the absence of a material with polarizability. The trivial but important information is contained within the first part of this equation, which returns the value of the electric field gradient, the guiding parameter in highly time-resolved electron sources (sadly this information is neither declared in nor derivable from relevant publications, instead only pulse durations and final electron energies are described, without further crucial information).

The extend of vacuum chambers is in reality unfortunately constrained and not infinite, as could be in theory. Generally, the space within FED instruments is limited and compact instruments are more attractive than bulky evacuated barrels. It is also true, that extended electrode areas decrease the breakdown voltage [Mazurek and Cross (1987), Shioiri et al. (1994), Schümann and Kurrat (2002)], but this is just one of many factors, which influence the electrode performance and will be discussed.

The edges of the considered charged plates, which will form the surfaces of electrode and counter-electrode, have to be curved to make them fit into an evacuated chamber. This is a well-known electro-static problem, which had been dealt with by famous

physicists such as Maxwell and Kirchhoff in the 19th century, amongst others who followed. A practicable solution was provided by W. Rogowski [Rogowski (1923)], who worked out an analytical electrode geometry, which follows the equi-potential electric field lines around the charged plates of a capacitor. A similar electrode profile is known as "Borda-profile" and was developed in as early as 1766 [see for example Punekar et al. (2003) and Schümann et al. (2004)]. According to this approach, the surface of the electrode can be defined by

$$f(x) = \frac{d}{\pi}\left(\frac{\pi}{2} + e^{\frac{x\,\pi}{d}}\right) \tag{5.4}$$

The Rogowski profile is one of the most utilized electrode profiles used today that is especially suited for fixed electrode gaps. Voltages up to 600 kV were obtained. The Rogowski profile leads to perfect electric field distributions along the surface at constant gap sizes, with the highest electric field gradient located in the center of the electrode. For an electron source with a fixed gap size, no other approach needs to be considered. Unfortunately, adjustable gap sizes are targeted in this special instrument development and thus make the Rogowski profile, which provides a perfect solution for fixed gap sizes, completely inappropriate. As the electric field distribution changes with an adjustable distances between the cathode and the anode, a different electrode Rogowski profile is required for each gap spacing. The Rogowski profile alone is thus not sufficient to satisfy the requirements for the development of the FED-CAMM, generally setups with adjustable cathode-anode gaps, respectively. However, the Rogowski and other relevant designs are considered to relate the development of this work to the context and potentially ideal solutions.

The overall design goal in electrode shaping is the avoidance of an increase of the electric field strength in reference to the nominal field, which is obtained in the center of the capacitor, or electrode respectively, as defined by equation 5.3 and equally required by the design goals of the ultrafast electron source at the beginning of this chapter. This nominal field strength should not be exceeded at any other part of the high voltage electrode arrangement, since any increase above the nominal electric field will automatically decrease the maximum field in the center of the electrode, at the photo-cathode, respectively, where an intense electric field gradient is most important.

The curvature of an electrically charged surface in the presence of a charged counterpart is generally accompanied by the local enhancement of the electric field. This effect is due to the condensation of electric field lines, or electric flux respectively, at the curved surface. The flux is defined by

$$\Phi = \int_A \vec{E}\,\vec{n} \quad dA, \tag{5.5}$$

with A denoting the integrated surface area, E the electric field, and $\vec{n}$ accounts for the amount of field lines perpendicular to the surface, leading to a re-normalized value of Φ. For tiny curvatures in arrangements with opposite potentials, such as for nano-emitters facing a plain metallic surface, the integrated area dA shrinks accordingly with incremental small steps along the curved surface. A certain electric flux is still required within this incremental integration, which proportionally leads to theoretically infinite electric field gradients.

The first direct consequence of the dependency of the electric field on the electrode surface is the introduction of radii along the edges, to avoid an increase of the electric field at those geometric transitions. Intuitively, these radii should be as large as possible to avoid any field enhancement. However, the problem of field strength enhancements is not solved with the approach of a fixed radius alone, which was investigated by simulations of the electric field distribution around plain electrode geometries, using the CST studio suite.

The development of suited electrode profiles was guided by the possibilities and constraints of manufacturing of complex shapes. For this reason, easiest geometries were at first simulated with the target to develop the most simple but functional geometry, which is easy to manufacture. The plain geometries of the first simulations were improved step by step, but always kept within the possibilities of manufacturing, which were present in the direct environment of this work [as outlined in section 1.3.2 and in the following section 5.4.2].

A question which had to be answered is, to what extend the single approach of constant radii leads to a successful implementation of the desired uniform electric field distribution for ultrafast time-resolved electron sources on the axis of electron propagation.

Figure 36 illustrates the dependency of the electric field enhancement on the size of the radius around the edges of a simple, charged cylinder in a surrounding vacuum chamber. For the simulations, an insulating rod was used to "mount" the cylinder in a virtual test chamber, but also to test the distribution of electric fields around the insulating mount. Each simulation shows the field enhancement around the rounded edges of the electrode. The problem is reduced with larger radii, but not solved. The specification of absolute potentials and distances is irrelevant at this point, since these simple shapes are far from the sought solution, and the relative distribution is further not changed. However, it can be noted, that the most intense electric field gradients shrink significantly from A to C without changing the applied electric potential nor any other parameter in this simulation, except for the radius.

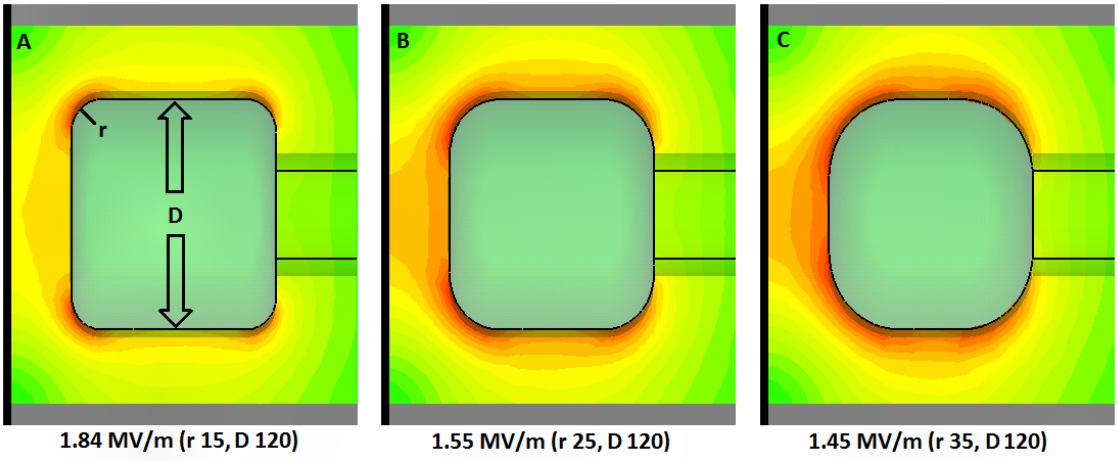

Figure 36: CST simulations of a simple cylindrical geometry with varying radii, visualizing the electric field enhancements around the edges. The color indicates the local field gradient, with red being most intense and green resulting in the absence of an electric potential.

The next features that were varied within further CST simulations were the diameter of the cylinder and the shape of the rear end. The diameter is important, as the geometric constraint of the housing vacuum chamber restricts the lateral size of the electrodes. The only promising configuration that was found in these simulations is a distribution of electric fields, in which the enhancements of opposite corners that face the anode merge into a uniform field enhancement that is centered around the central axis of the electrode (geometry similar to case C). For photo-excited electrons in proximity to this central axis that propagate on-axis towards the anode, within a small corridor around the central beam axis at least, the acceleration in a uniform electric field is obtained. If the ratio of diameter to the radius of the edge becomes too large, a highly non-uniform electric field in the center of the electrode is obtained (geometry similar to cases A and B). Otherwise, this is the only configuration, in which a simple radii alone is sufficient to generate a uniform electric field distribution on the axis of electron propagation.

Figure 37 shows an acceptable configuration of plain radii, which can be used within an appropriate distance to the anode. A disproportionation of the diameter to the radius, or unsuited gap spacing, leads to the previous results of figure 36. At a larger distance (B) the distribution of the electric field around the central beam axis deteriorates. Simulation (C) illustrates the very promising approach of elliptic surfaces, which guided the remaining electrode development. The elliptical shapes were already incorporated into the intermediate designs, which are shown in inserts (D) to (F). These simulated shapes relate to a further progressed development, that already relates to actually useful electrode geometries. For larger distances, the field gradients around the edges of profile of (D) to (F) still degenerate.

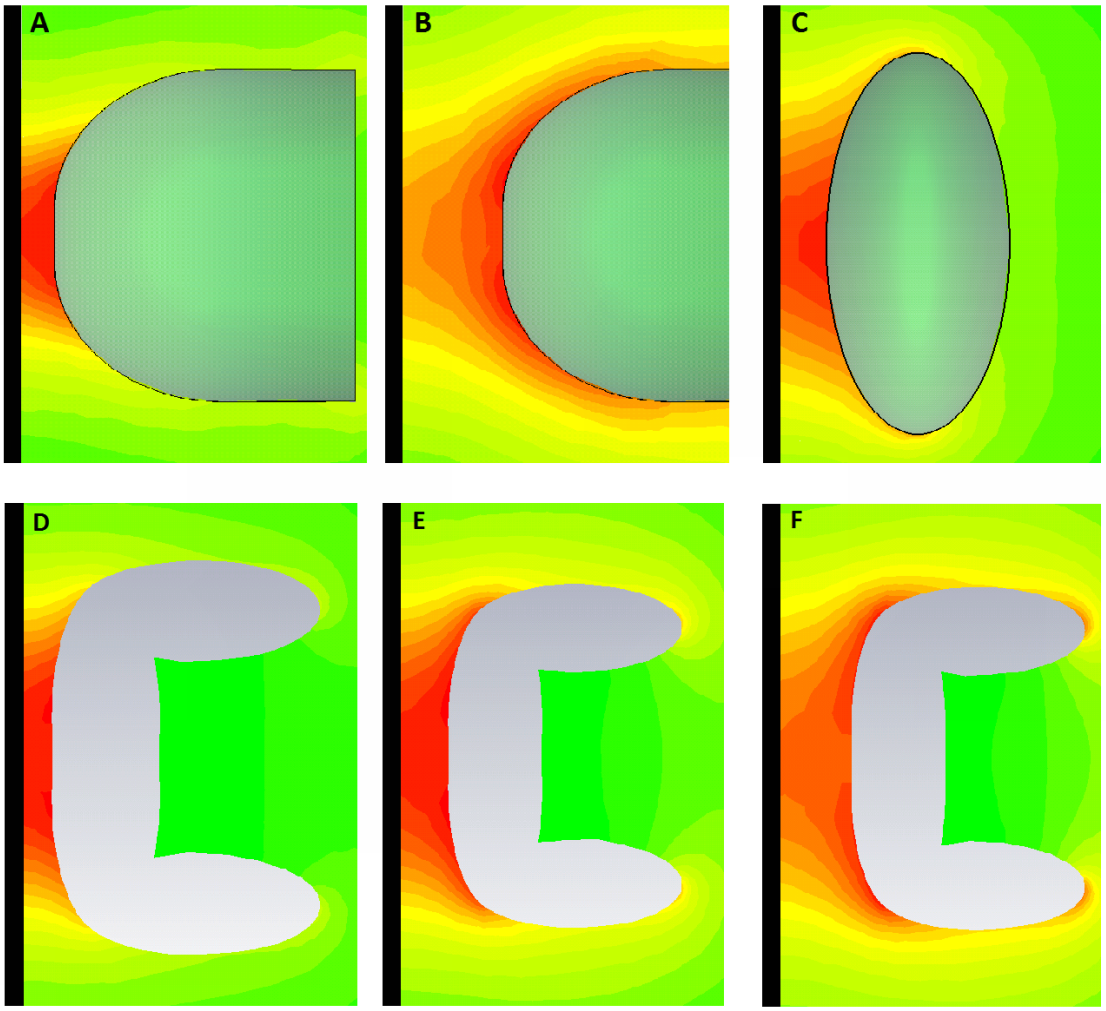

Figure 37: CST simulations of a acceptable ratio of corner radii to diameter at a given distance (A), visualizing the effect of increasing distance to the anode (B). Simulation and geometry (C) illustrates the promising approach of elliptical geometries, which in combination with further modifications will lead to satisfactory results. Geometries of simulations (D) to (F) incorporate such elliptical geometries and already performed well. These also provide a basis for the implementation of a photo-cathode into the center of the electrode.

Simulation (A) yields a maximum electric field gradient of 3.28 MV/m with 300 kV applied on a gap spacing of 10 mm, which relates to an increase of the maximum electric field by almost 10 %. Such an enhancement consequently relates to the reduction of the maximal applicable field in the center of the electrode or photo-cathode, respectively. The field enhancement only amounts to 2.7 % for simulation (D). This set also uses 300 kV applied on a 10 mm gap. The maximum of the resulting electric field gradient in proximity to the center amounts to 3.08 MV/m.

From plain radii as a starting point, ellipsoidal shapes were investigated more intensively. These simulations yielded very promising results with field enhancements of less than 2 % in respect to the central nominal electric field, even for large gap sizes and will be presented shortly. Especially when an ellipsoidal torus was generated, which resulted in a small indentation of a few tenth of a mm in the center, into which a photo-cathode could be inserted, no effect of the presence of such a photo-cathode was observed in simulations. It was further observed that even a shallow start of curvature at the end of the plain area leads to incremental field enhancements, which could only be reduced by increasing the radii, which belong to this first sinusoidal section of the ellipses. It was also stated in earlier studies [for example Harrison (1967)], that it is impossible to avoid field enhancements, when a central flat region is incorporated into the electrode. But this enhancement and any anisotropy of the electric field around the central axis can be avoided or at least reduced, when the electrode is operated at gap sizes, which measures a fraction of the maximum permissible gap size. This behavior could be confirmed and is illustrated in the upcoming simulations of the final electrode geometry.

The simulated elliptical shapes, which later on developed plain regions in the center that were generated by the transverse extraction of the elliptical geometry from the center, strongly correlate to the second relevant electrode profile, which is also known from the literature. F.M. Bruce [Bruce (1947)] developed a similar electrode profile, which is based on experimental observations. The investigated voltages, which were covered by his original work, range up to 315 kV. Subsequent work increased the maximum voltage applied to the Bruce profiles up to 420 kV with electrodes, which measure at least 26 cm in diameter [Craggs and Meek (1954)]. The electrodes of this PhD work measure only half of this size.

The basic geometric construction comprises a flat area in the center with a sinusoidal curve that merges into a fixed radius around the outer rim. The original electrode profile of Bruce was also included into the set of CST simulations. After several iterations it was found that for the current geometric restriction in the FED-CAMM, which require an overall smaller electrode diameter, slightly different geometries lead to better results over a wider range of gap spacings. In particular, the first segment of the sine-curve was stretched towards the outside rim of the electrode. The simulations of the incorporated final design is shown in figure 38. For the sake of reproduction and inspection of the results of this work, the measures of the geometry that was developed for the FED-CAMM is also given in this figure. This design is currently used in overall three front electrodes, of which each fulfilled a different purpose in first experimental tests.

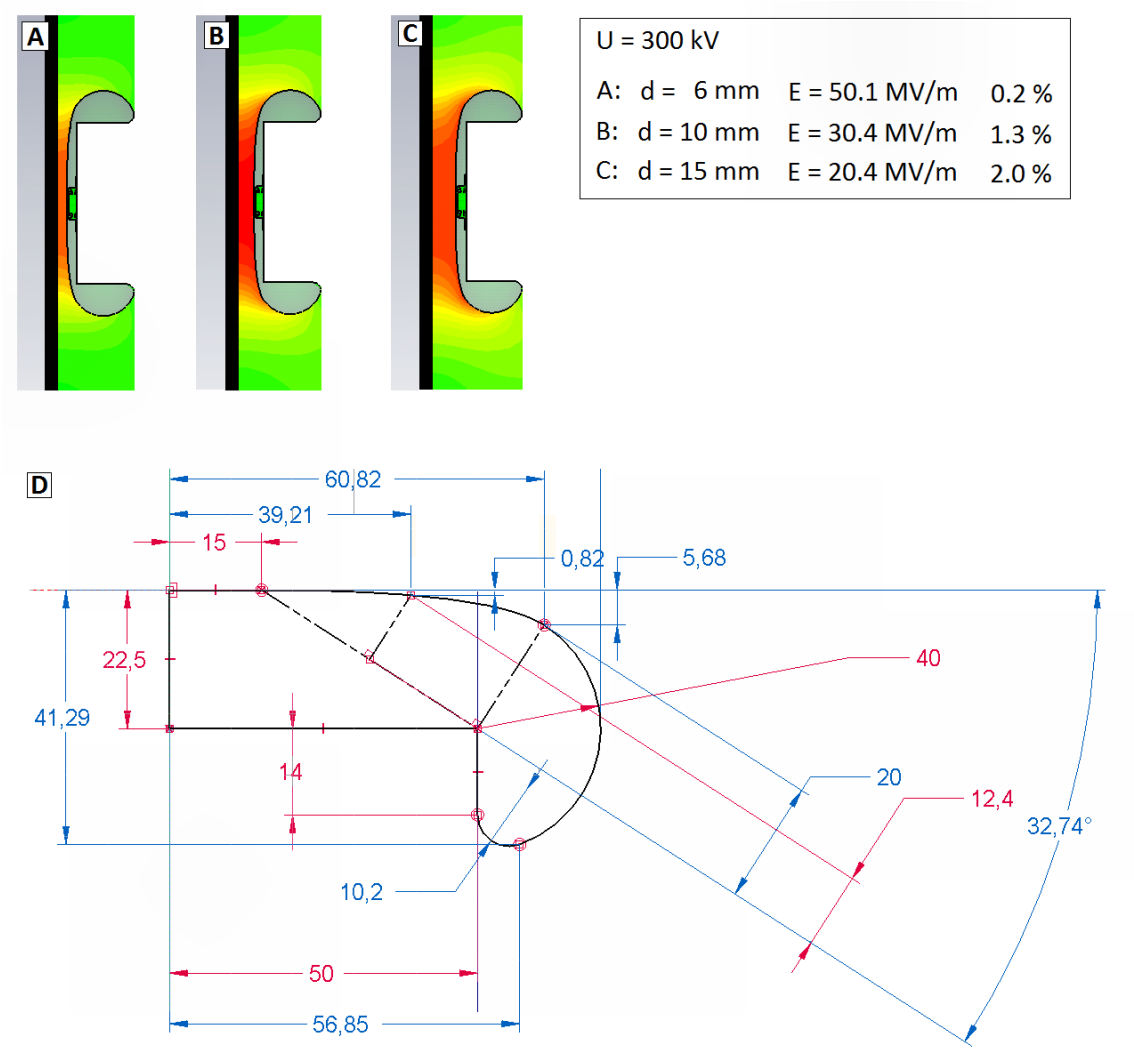

Figure 38: Geometry of the high voltage electrode, which was developed and produced for the FED-CAMM instrument. The upper images A to C show the final CST simulations, which reveal a uniform electric field distribution within the center of the electrode, between the photo-cathode and grounded anode. As can be observed no other region around the electrode possesses a higher electric field gradient than present in the gap. This is also true for those remaining electrode parts in the center and back (not shown). The applied electric potential and resultant electric field enhancements in relation to the nominal field values are specified in percent in the box that is placed on the right of these simulations. The red numbers in the drawing below indicate the crucial geometry-determining measures. This includes the connection points, which refer to tangential or centered alignment. The blue values were included as source of additional information.

It can be observed in these simulations that the field enhancement, which is caused by the curvature of the electrode geometry, amounts to less than 2 % for gap sizes as wide as 15 mm. The determination of this curvature was difficult. It can be considered a success, since the applied electric potential will only see an insignificant small decrease due to such a small field enhancement. The electric field gradient on the electron beam axis possesses the same electric field strength as regions that are centimeters away from the photo-cathode. This development provides the implementation of the required uniform electric field gradient, which is a crucial part of the development of the FED-CAMM apparatus.

Besides the front end, all remaining sides of the high voltage electrode that are facing the surrounding vacuum chamber require simultaneous attention. The electrode arrangement in the FED-CAMM instrument comprises a few but different elements, each element fulfills a dedicated purpose. Once the geometry of the front end was determined, the remaining sides of all electrodes were optimized.

The rear end, which is facing the opposite direction of the electron propagation, is not less important in these considerations than the front end, which is facing the anode. In some cases, the provision of the high voltage is established at this end. If insulators are used to mount a high voltage electrode, the radii on this side will reduced to smaller values. Any resulting sharp edge around the insulator requires itself a radius, as otherwise electrons will be emitted from this edge towards the insulator surface and gather there, only to promote electric flash-overs along the surface of the insulator and damage to the insulator. This is one of the sources of malfunctioning in the commercial high voltage feedthrough design, which is described in section 5.5. Generally, the design of the transition onto a potential ceramic holder and within proximity to the triple point (vacuum, metal, insulator) requires special design efforts to reduce the electric stress.

As stated by Rogowski, the outer diameter and further curvature is not captured by formulas or rules of the thumb. Outside of the central region, starting at electric field gradients that only measure a fraction of the most intense electric field, the curvature is instead continued in an appropriate manner by radii that account for neighboring geometries and generally requirements, which emerge from the surroundings. For this reason, the optimal design was related to the maximum outer diameter of the electrodes.

In a chamber of constrained size, the best suited electrode diameter can be easily determined. The electric field in a cylindrical geometry is given by [Roth (1959)]

$$E(r) = \frac{U}{r \cdot ln(\frac{R2}{R1})}. \tag{5.6}$$

The electric field at the surface is obtained at r = R1. The first derivation of this equation reaches a minimum value for

$$R1 = \frac{R2}{e}. \tag{5.7}$$

This ratio returns the ideal outer diameter of the high voltage electrode, once the diameter of the surrounding chamber is determined. The presence of an extra aluminum shield for radiation safety considerations [see section 5.7] is currently reducing the inner diameter and hence decreases the ideal electrode extension to less than 10 cm. The electric field gradients along the side of the electrodes are increased by 30 to 40 % to a maximum value of 4.2 MV/m at 300 kV. This field gradient is still below critical values. The following figure 39 shows the development of the electric field strength at the surface of the electrode as fuction of the electrode diameter, in the presence (higher field gradients) and the absence (lower field gradients) of the aluminum shield.

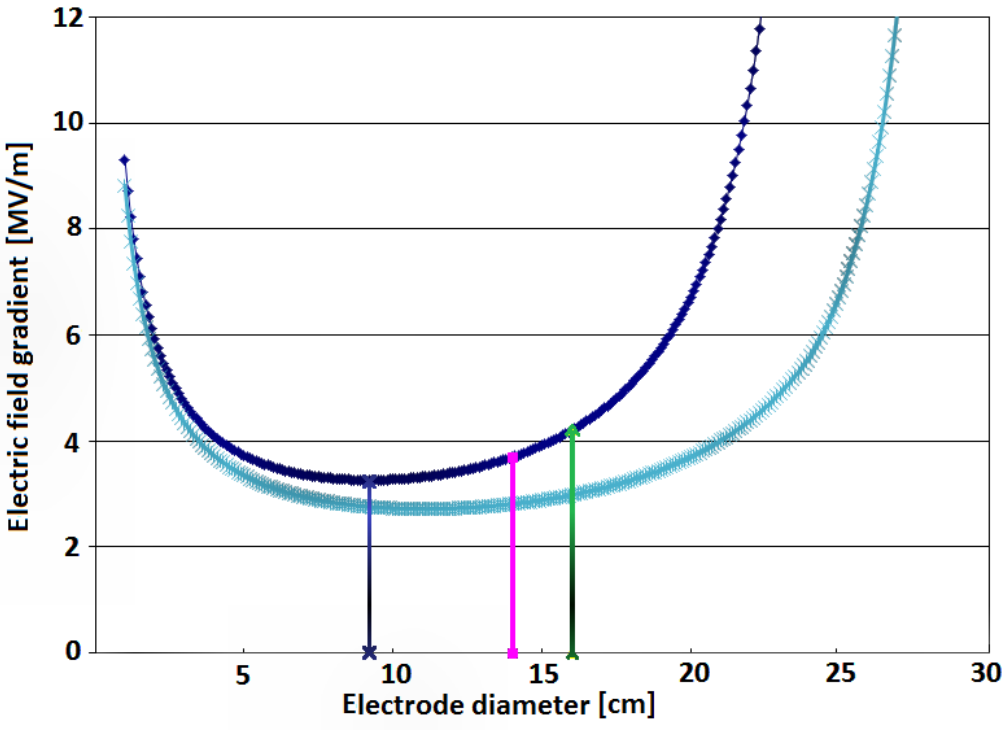

Figure 39: Electric field gradient at the radial surface of the high voltage electrode in dependence of the electrode diameter. The lower field values are obtained with the removal of the internal aluminum shield. The ideal diameter and two presently used electrode dimensions have vertical marks.

In the absence of the aluminum shield, the diameter of the electrodes insignificantly increases the electric field gradients on the electrode surfaces. In compact vacuum chambers that operate at higher voltages, this is becoming a major consideration though. A guiding parameter in the development of the FED-CAMM was a maximum chamber diameter, which in turn restricted the sizes of the electrodes. It should be duly noted

that the previous works, which involve the debated electrode geometries, were partially conducted in air and thus might require larger diameters, as opposed to the dimensions used in the FED-CAMM, which operates with a UHV environment.

This leads to another final point of the discourse on electrode development. A UHV environment is not necessarily required for the operation of high voltages. The operation is primarily determined by a mix of the pressure, the dielectric strength of the residual gases in the chamber and by the cathode-anode distance, always in combination with the present electric field gradient that is generated by the geometry. For various gases, the dependencies of dielectric strength upon partial pressure were experimentally determined by F. Paschen [Paschen (1889)]. In this work, it was experimentally confirmed, that high electric potentials can already be obtained at pressures, which are lower than 10^{-2} mbar. This was a critical pressure, below which the highest voltages could be applied to the electrodes of the FED-CAMM. The experimental findings align well with the predictions made by F. Paschen.

The most common pressures that are normally utilized within present compact instruments range down to 10^{-9} mbar. Since this criterion of the applied potential is not that strict, chambers sealed by ISO-K elements become reasonable. Pressures of 10^{-8} mbar can be reached therein, which is essentially less costly and allows the construction of much larger vacuum chambers that are still affordable. By this change of vacuum technology, the electrode dimensions could be expanded to further ideal values. Nanotips and GaAs photo-cathodes can unfortunately not be used in such conditions, due to a faster degradation of the tips and oxidization of the semiconductors. But for conventional photo-cathodes in ultrafast electron sources, this is no obstacle.

Summarizing, the electrode geometry that was developed for the FED-CAMM was optimized for a variable distance between photo-cathode and anode and fulfills the requirements, in contrast to the most commonly used Rogowski electrode profile. The Rogowski profile will have a significant field enhancing influence, once the gap size is changed. The simulations of electrode geometries, out of which only a few were presented in this section, and the iteration to optimal results were naturally leading to an implementation similar to what is already known as a Bruce profile. Especially within smaller gap sizes (up to 15 mm), the field enhancements induced by the curvature of the electrode surface, range below 2 %. With slight chances of the geometry these values can well be extended to a 20 mm gap spacing.

This finding of performance compares well to what was previously determined by other computer-guided studies [Harrison (1967) specifies 1 % for the Bruce profile]. With average electric field gradient of 15 MV/m, the anticipated high potential of 300 kV from

the external power supply can be maintained and safely operated with the high voltage electrodes of the FED-CAMM. The field distribution on axis is mostly uniform and even more intense electric field gradients than 15 MV/m on axis can be employed, which was experimentally determined [see section 5.6]. This results in even shorter electron pulse durations and overall improved electron beam dynamics. The resulting geometries can be machined on CNC lathes, which is another important aspect to consider and treated in the next subsection.

5.4.2 MACHINING HIGH VOLTAGE ELECTRODES AND FOLLOW-UP TREATMENT

Once the geometry of the metallic electrode was developed by means of CAD and CST, one of the first steps of manufacturing was done using a CNC lathe. A lathe with the plug-in for the direct translation of STEP files (*STandard for the Exchange of Product model data*) is required, as the digital geometries are generated by the CAD program. Only with this feature of the lathe it is possible to manufacture the advanced sine curves of the electrode geometry into a suited semi-manufactured metallic form. Within this work, this machining method turned out to be quick and efficient and otherwise would not have been realizable.

The application of high electric potentials requires overall smooth surfaces, which are also microscopically free of sharp edges. For this purpose, additional steps were investigated for the enhancement of the surface quality. Once the shapes of the electrodes were made, a special diamond tool [Baublies-AG (2007)] was used to flatten irregularities and to minimize the average roughness, which naturally occurs from the manufacturing of the raw-material and the processing by the lathe. This first step towards electrically suited electrode surfaces was equally conducted using the CNC lathe. The artificial spring-mounted diamond on the tip of an adjustable head and its holder is shown in figure 40.

It was important to determine the resultant surface roughness after this first processing of the surface. The diamond is supposed to smooth the surface, which optically appears to be flat. The remaining roughness and structure was determined using a perthometer, which comprises a micro-tip, equally made of diamond. Various regions of one of the manufactured electrodes were characterized in terms of average and total roughness. Among these regions were the central region around the photo-cathode, which appears to be flat, the closer proximity to this center and some areas on the outer rim.

Figure 40: Artificial diamond on a flexible holder, which was used to flatten the surfaces of the high voltage electrode parts. The tool was purchased from the Baublies AG [Baublies-AG (2007)]. The pictures shows the actual usage in one CNC machine on DESY ground.

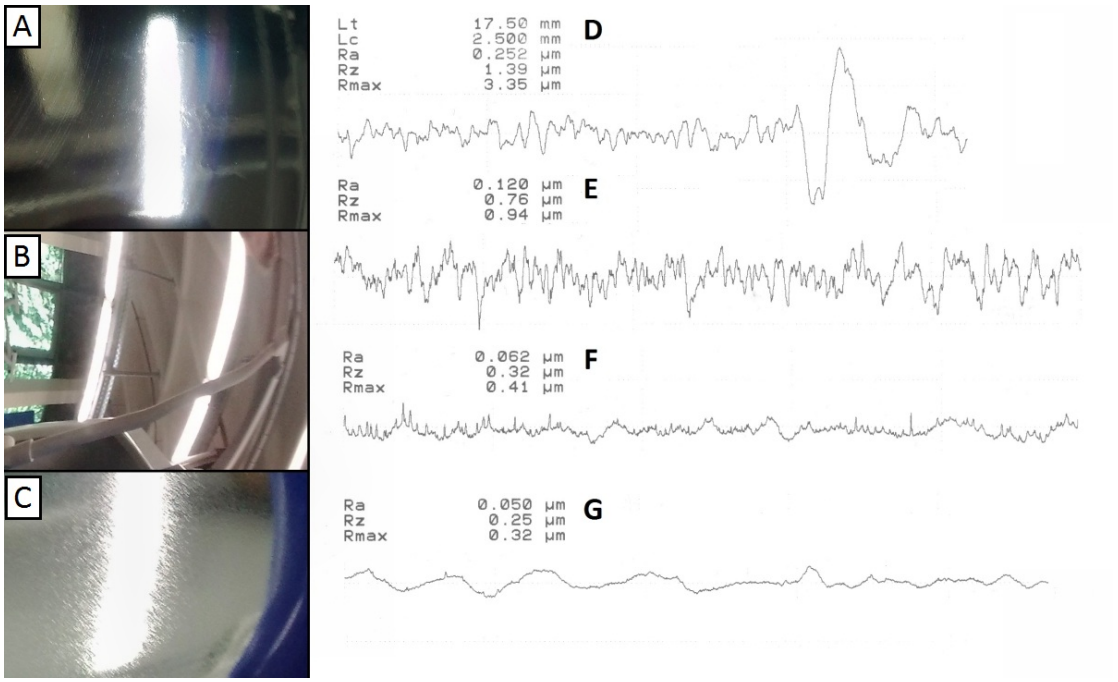

Figure 41: Left side: Optical appearance of the high voltage electrode after CNC machining (A), manual polishing (B) and electro-polishing (C). Right curves: Average and total surface roughness of one high voltage electrode at different positions and processing steps (D - G).

The images on the left of figure 41 illustrate the appearance of the surface of the same electrode, after CNC machining with the diamond tool (A), manual polishing, which leads to a visibly scratch-free surface (B), and after electro-poishing, which reveals material-instrinsic structures, but is electrically the best suited surface (C). The surface profiles on the right belong to one of the small bumps, which became visible after the CNC machining step with the diamond tool (D), shown in image (A). Different areas on the electrode reveal different surface structures (E - G). The smoothest surface profile (G) gives the profile of the surface, which was oriented almost parallel to the striae formation of the turning process, measured on the outer rim of the electrode. In all cases, a surface roughness in the micro- and sub-micrometer range is present (this covers the surface classes of average roughness N6 to N1, 0.8 to 0.025 μm , respectively). The electrodes were tested in the setup at different stages of manufacturing, to determine the best approach [section 5.6].

Generally, a surface roughness of R_a 60 nm or less can be achieved by elaborate machining and polishing methods, which are concluded by the lapping of surfaces. No other manual method can yield optically superior results compared to lapping. Unfortunately, this technique can only be applied to plain surfaces and thus does not apply to curved electrodes. The surface roughness of image (C) might appear to be somewhat porous, but electrically works best. No sharp edges, which are resulting from other manufacturing

steps, especially those which involve diamond particles in emulsions and pastes are left. In this regard, even lapping might be an inappropriate methode to upgrade surfaces. To the contrary, the surface yield with diamond particles, which appears to be optically perfect (see image (B), 1 μm diamond particles in suspension on a soft carrier were used), ultimately promotes field emission [Watanabe et al. (2001), Watanabe et al. (2003)], due to microscopically sharp edges along the cutting tracks of the diamond particles.

Besides the general geometry, the surface quality is the most crucial aspect of electrode manufacturing and not only determined by the further treatment, but also by the choice of a suitable material. Soft materials can be polished better, but quickly degrade upon breakdowns. Known from experience and guided by physical intuition, hard materials should be used. The work function of the electrode materials only plays a subordinate role in the electric performance (see equation 5.8 and according information in the surrounding text), but the tougher materials typically have larger work functions.

For reasons of availability, manufacturing, sustainability and conservation, stainless steel alloys were investigated. Out of the variety of available alloys, those materials were excluded that, for example, possess ferromagnetic properties, contain softening additions or toxic substances. In combination with high voltage breakdowns a toxic vapor can be produced that would leave the evacuated chamber through the vacuum generating system. Further, not all stainless steel alloys typically yield smooth surfaces, neither after manufacturing of the alloy, nor after further manual or electrical, even galvanic processes. It was found that stainless steel alloys that are commonly used for UHV engineering fulfill the requirements of electrode manufacturing and high voltage performance.

5.4.3 IMPLEMENTATION OF PHOTO-CATHODES

The extend of the previously used photo-cathodes measures 16 mm in diameter, which is of advantage for the alignment of the excitation laser pulses with the pinhole of the anode. To include the full extend of the photo-cathode, a whole was incorporated into the high voltage electrode in the center of the plane electrode region, which has the same extend as is required for the full visibility of the photo-cathode. As previously described, the first electrodes in the FED-CAMM possess a plain area that measures 3 cm in diameter. Reviewing this choice at the end of this work, a smaller aperture within the electrode might have been beneficial, next to an increased plain area in the electrode geometry. But a compromise between cost and size of the experiment was done at an early stage in the development, which directly influences the overall performance.

For the distribution of the electric field around the central-axis of the electrode it is ideal, when the photo-cathode is mounted in-plane with the front surface of the electrode,

to avoid changes of the electric field in and in close proximity to the photo-cathode. Typically, there is a very shallow curvature of the thin rim of the electrode, that surrounds the photo-cathode. The photo-cathode can be retracted from the front surface by the use of spacers within the mount of the photo-cathodes. The potential presence of sharp edges around the photo-cathode requires additional design efforts to avoid performance problems. Even the sheer presence of tiny curvatures of the cutout around the photo-cathode leads to microscopic electric field enhancements. This however, after a moderate occurrence of electric discharges along the rim of the high-voltage electrode during conditioning, was not affecting the electric performance of the electrodes any further. The discharge spots, which arose from the arcs during conditioning, can be spotted in part (B) of figure 42, where the room lighting was sufficient for the observation of these marks within the close proximity of the photo-cathode.

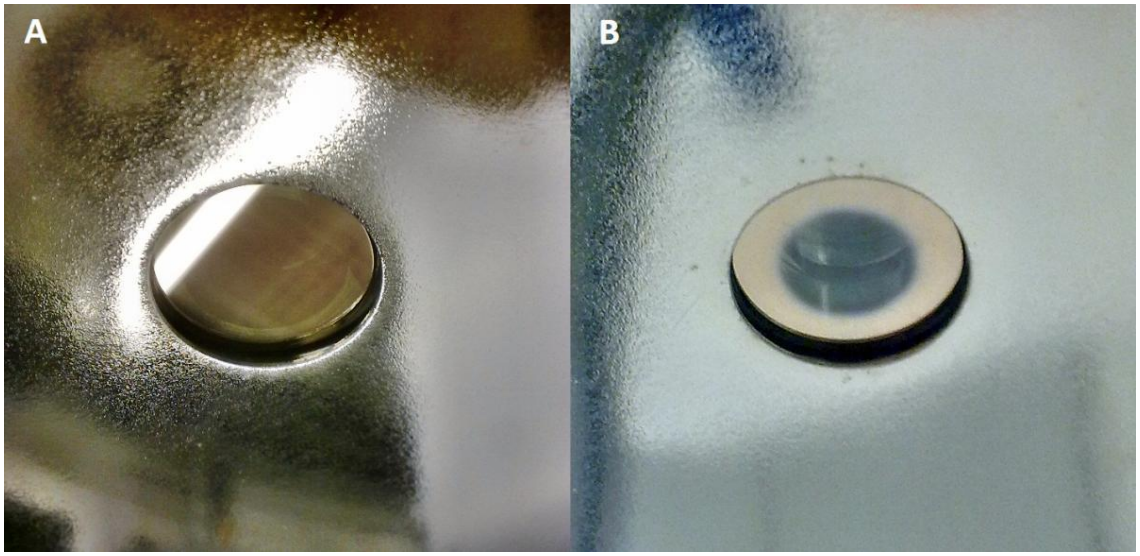

Figure 42: Photocathode, prior (A) and after (B) the application of electric potentials, which exceeded 195 kV on a 20 mm gap.

The conditioning was done prior the insertion of photo-cathodes. Partially, an old photo-cathode was used as dummy, to seal the hole of the electrode. The effect of removal of gold from the front surface of photo-cathodes, which is seen in the right half of figure 42, is not due to the conditioning of the surrounding high voltage electrode. Instead it is plausible that microscopic deviations in the coating of the photo-cathode lead to local field enhancements, which cause the removal of gold particles in the presence of high electric fields and microscopic, non measurable electron currents. The gold coating probably melted due to these currents and subsequently covered parts of the anode. Another source of such currents, such as ions within the residual gases of the vacuum, can equally not be excluded.

This observation of gold-removal led to the test of different photo-cathode materials. The tested substrates included protected metallic mirrors, where a removal of gold from the surface was not observed. Equally, a thicker coating on a photo-cathode did not suffer from more intense electric fields. This allows the conclusion that the bound strength of thin gold films to conventional substrates of chromium and silicon is rather weak and further not suited for high electric potentials, which can be achieved in the FED-CAMM apparatus. Alternatively, the radius of the central opening can be reduced and the photo-cathode slightly subtracted, such that the area that is exposed to the intense electric fields, is reduced, and the electric field strength limited. The subtraction of a photo-cathode was also tested, as shown in the previous figure, but did not avoid the removal of gold in the presence of such a large electrode apertures. At least the resulting uncovered area, within which the gold film was removed, is smaller, due to the decrease of the electric field strength at the outer regions of the photo-cathode, which is covered by the surrounding high voltage electrode. The use of single crystalline gold crystals, which also reduce the initial energy spread, will certainly enable higher field intensities and absolute potentials and potentially avoid this finding. The protected metallic films support this assumption.

5.5 DEVELOPMENT OF A HIGH VOLTAGE ELECTRICAL FEEDTHROUGH

The development of a high voltage electrode is one aspect of the FED-CAMM. The supply with high electric potentials is a different aspect. For the delivery of additional kinetic energy to the previously photo-excited electrons in a vacuum environment, an electric high-voltage feedthrough is mandatory. The plain purpose of the feedthrough is the transmission of electric power, either voltage or current, to the conducting machine parts, which are operated at high potentials. The development of the FED-CAMM required the design of a high-voltage feedthrough, which does not under any circumstance constrain the applied external voltage. The high voltage feedthrough must instead deliver any available electric power to the electrode geometries within the instrument. The development also has to meet the above discussed engineering and design criteria, which are partially incorporated into the overall feedthrough design.

5.5.1 BACKGROUND: PROBLEM STATEMENT

The fundamental problem, which triggered this development, was the absence of commercial products that could deliver high electric potentials measuring a few hundred kV into UHV environments. Except for a few products, standard commercial feedthrough are typically limited to 100 to 125 kV. Some products can deliver currents as high as 1,000 Ampere (see inset in figure 43). Exceptions concern the application of feedthrough in oil-filled transformers, in which the oil is insulating the electric contacts at the exit of

the high potential. These devices are for example used for high voltage power supply lines. As previously described, we had bad experiences with the ordering and purchasing of two custom-made commercial units. They were rated for our design voltage of 300 keV, but the design was unfortunately merely an inflation of the layout, which is commonly used and standard for the lower potentials. This standard design does not account for the physical limitations, which arise when the applied electric potential leads to critical electric field strength along the conducting surfaces. The limitations are predominantly induced by the appearance of electron emission from the surface of the central conductor and subsequent electric breakdowns, which lead to physical damages of the high voltage insulating elements. The standard design consequently can not provide a stable operation in the high voltage range.

The conventional commercial design and its limitations are described in the following section 5.5.2. On top of the development of the robust design of a high voltage feedthrough for UHV environments, the development of a device of this type that can be manipulated within the UHV environment and directly influence and optimize the working conditions of the ultrafast electron source, is a further very important development of this PhD work. The manipulation of the position of the feedthrough and the mounted high voltage electrodes lead to the adjustment of the working parameters of the instrument, namely by changing the distance in between the cathode and the anode. This feature is an important design consideration. The manipulation of the gap size in this geometry directly influences the extraction field strength, time of flight of the electron pulse within the accelerating gap, and resulting electron pulse length, as was previously outlined. By the manipulation of electrode positions, the time resolution of the apparatus is thus directly affected. The applied potential has to be maximized and the gap size minimized for the shortest electron pulses. This generates the maximize electric extraction fields at the photo-cathode and in the acceleration gap. The propagation distance of the electron pulse, from its generation at the photo-cathode to the position of the specimen, is reduced, and the electron pulse duration at the specimen minimized. For lower requirements on the electron pulse length, the electric potential can be reduced and the distances increased, which reduces the electric field stress at the photo-cathode. Besides a reduction of potentially occurring dark current, this lower extraction field can avoid the occurrence of electric breakdowns and conserve a reasonable lifetime of photo-cathodes. Additionally, specific specimen systems might survive longer periods of electron transmission at lower electron energies, while other specimens and embodiments require higher electron energies or are less affected by electron induced damage. The variability of the high applied potential in combination with the variability of the electron pulse durations are essential points of the FED-CAMM, which also make this development unique.

Conventionally, the distance between the cathode and anode in time-resolved electron diffraction experiments is fixed, unless the instrument is vented, opened and single mounting parts are exchanged, as in previous installations. The design of the mounts for the parts at high potentials was additionally limiting the maximal applicable electric potential in a manner that the capacities of the power supply were never fully exploited. To my knowledge, there is currently no compact DC-operated electron diffraction setup present in the world, which exceeds the energy levels of the devices listed in table 9 and the voltage of at most 140 kV of the compact E-Gun 300 installations (with 140 kV being unstable). There is especially no DC-FED apparatus existing in the world that can maintain or exceed 300 keV as achieved with the FED-CAMM.

This maximum potential can be upgraded to 400 kV by using another model of power supply from the same supplier [Heinzinger-GmbH (2012)]. This is the highest known voltage that is commercially available in a closed-rack design. As previously mentioned, the closed-rack design of a high voltage supply is required for the precise performance of the ultrafast electron diffraction setup, in which timing jitter, induced by variations of the applied potential, has to be avoided. The open-rack and open-stack solutions, which can yield higher electric potentials, generally suffer from high voltage instabilities and require advanced electrical engineering, which includes the installation of an extra electrical service room, which does not grant open access during operation.

Prior to this development, the maximum applicable potential was limited by the design of the feedthrough and by the electron gun components. In the current design of the FED-CAMM and its components, these previously existing limitations are removed. The highest potentials can be guided to the electrodes of the diffraction system without a risk of electric flash-overs. This is related to the feedthrough design itself. In addition to the breakdown-free feedthrough design, the distance in between the charged and grounded electrode can be adjusted. With optimized electrode geometries (which were treated in the previous section 5.4), it is possible to increase the electric field strength to new breakdown limits of vacuum, higher than any electric field gradients that were ever obtained before in DC acceleration.

For every applied voltage that can be adjusted up to the maximum potential of the power supply by arbitrary increments, the distance of the electrodes can be set such that a breakdown-free and stable operational condition is reached. Even for the smallest gap sizes and most intense electric field gradients, a stable operation is obtained by using a well conditioned and suited electrode. The entire process of optimization can be automated by using the feed-back of the dark current, that is generated by the presence of intense electric potentials. The closed-loop control of the motorization of the new design including the feed-back of its current position does the rest.

5.5.2 CONVENTIONAL DESIGN

Feedthroughs are available for the delivery of materials as well as electric energy. A mechanical component of a system is labeled to be a feedthrough, when it is involved in the transmission of materials, such as liquids or granulates, or electric energy through the walls of a building, a room, a confined sealed chamber and generally a surface, to ensure the supply for the required good. Electric feedthroughs are widely used in many areas, ranging from micro- to macro-scale applications in private and public as well as industrial and commercial applications. This is also true for scientific applications, where often either voltage or current has to be transmitted into chambers or instruments, which comprise UHV environments.

Commercial electrical feedthrough that are suited for high and ultra-high vacuum pressures, typically comprise a central wire or metal rod, which is the conductor or charge carrier. In vacuum-tight enclosures, this conductor is typically hard brazed with insulating ceramics of appropriate composition and dimensions. The extend of both the charge carrier and the insulating ceramics depend on the applied voltage and current and within a certain range scale accordingly. No rule of thumb is present and margins of safety vary with the manufacturer. Simulations of the dielectric strength and electric stress help to develop optimal geometries. Generally, the higher the current, the thicker the diameter of the central conductor typically is and in some cases liquid cooling is directly applied to the metallic rod. Figure 43 illustrates the typical layout of a commercial electric feedthrough. Ripples on the outer side of the insulator are not always present. In particular in cases where the applied potential ranges below 10 keV, simple straight ceramic rods are commonly used.

The feedthrough requires electric insulation to ground on both ends. This affects the end, which is typically exposed to air, or generally the exterior, and the other end, which enters into the vacuum environment. The exterior is obviously connected via a power cord adapter to the power supply. The transition from the conductor to the high voltage cable requires additional electric shielding to ground when higher potentials are used. The insulation to ground is given without further means, when a sufficient distance to ground is present and air is sufficient as the sole insulator to ground (1 kV/mm is the normed reference, but the dielectric strength is decreased along surfaces and triple points and also depends on further environmental conditions). Pressurized gas tanks are otherwise used at high voltages and intense field gradients, especially for static MV accelerators. SF6 has been used in recent decades, which leads to reactive products upon electric discharges and environmental concerns. Today, alternatives are known and more commonly used [see for example Christophorou et al. (1997)].

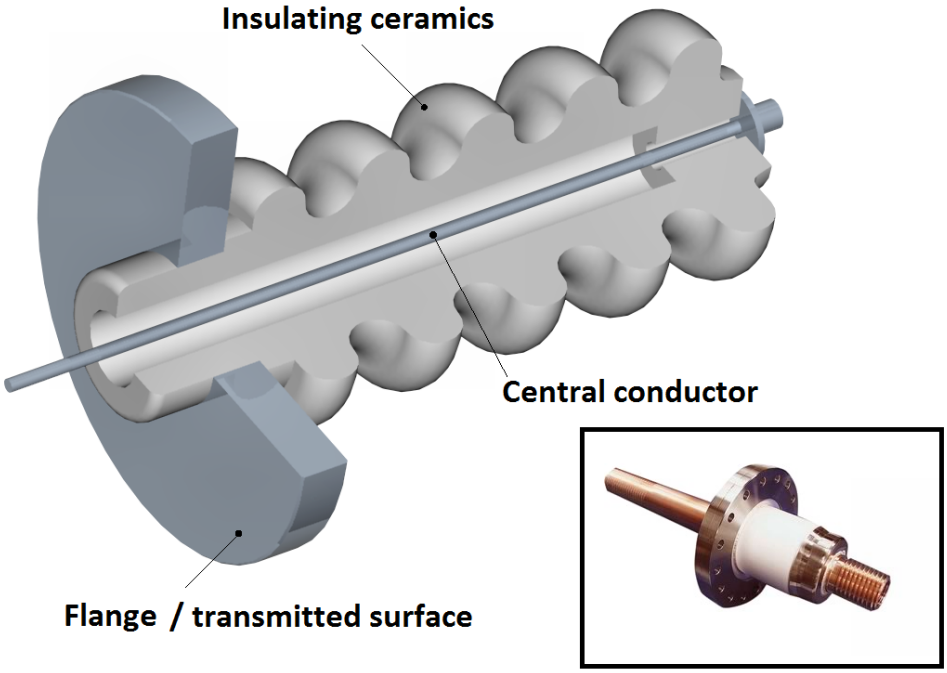

Figure 43: Commercial UHV feedthrough design (not to scale). A hard brazed central conducting rod is used for the transfer of electric energy through the surface of, for example, a vacuum chamber. The inset shows a high power feedthrough [CeramTec (2012)].

Dielectric oil and equivalent liquids are available to insulate the external connection [for example fluorocarbon-based liquids, http://www.3m.com/], especially where space is limited. To keep dimensions compact, engineering plastics, gels and epoxies are further candidates, which are used in various industries on a regular basis, for example to insulate electric connections within power supplies. Dielectric liquids are commonly used to shield and cool electric panels, which include integrated circuits and microchips. Finally, corona-rings around connection points on the exterior reduce the electric stress by reshaping the electric field distribution. These are commonly found at insulators, which are exposed to air.

The electric insulation in vacuum is commonly implemented by an appropriate creeping distance to ground in the conventional design, vacuum remains to be an excellent electrical insulator. The creeping path ideally includes surface orientations that are perpendicular to the electric field lines. This can hinder the electric field to drive electrons along the surface to ground, an occurrence, which can require extensive amounts of time and is involved in the process of insulator aging. However, this mechanism leads to avalanches of electrons along the insulator, subsequently leading to electric flash-over, which damages the insulator as well as connected electrically sensitive equipment of the apparatus. Commercial feedthroughs of the above type have a few weak points, which previously hindered the successful application of very high voltages.

(i) The conducting wire is not guided inside the vacuum and especially flexible, when long and thin metallic rods are used. A contact to the insulating ceramics should be avoided to prevent a change of the electric field distribution, which partially creates increased electric stress in nonuniform distributions. A direct contact with the ceramics at the lower end in the vacuum section has to be avoided, to prevent the direct transfer of electric charge onto the ceramic body. In the lower section on the vacuum side, the transfer of charge is the first step towards physical damage and electric avalanches across ceramic surfaces. In case of mechanical contact, the creeping distance to ground is significantly reduced. In this possible case, the performance of the feedthrough is corrupted. Electric breakdowns towards neighboring grounded instrument components are promoted and expected to appear quickly, which was the case in the E-Gun 300 type installations.

(ii) The conducting wire is guided through a vacuum flange, which forms the transmitted surface. The distance to the surface of the vacuum chamber that is most likely at ground potential (exceptions are present), reaches a minimum at the transition point and the electric field gradient consequently reaches a maximum in that region. The required dielectric material strength in the transition point is typically estimated by combining the dielectric strength of vacuum and of the ceramic layer, which separates the wire from the penetrated, typically metallic surface. However, this estimation alone does not guarantee an error-free operation. Additional physical processes, which are involved at the surface of the conductor (next point), are not considered.

(iii) The second false assumption in this context that leads to further problems, is that dimensions of electric parts can be simply scaled up and down in size, according to an increase of the applied electric potential. The scale factor is linear in the worst case scenario.

(iv) The radially symmetric geometry allows an easy description of the electric field distribution. It is identical to the field within a cylindrical capacitor and was already used to determine the ideal outer extension of the high voltage electrodes [equation 5.6]. The electric field strength at the surface of the inner layer, or the wire of the feedthrough respectively, is inversely proportional to the square of the radius. High electric field gradients can be reached even at very small applied potentials, if the radius of the inner conductor as well as the distance to the surrounding metallic surface is small. For electric feedthroughs, which operate below 50 or 100 kV, this is not necessarily leading to any problem, even if no special care is taken for the surface quality of the central conductor. However, this design causes major problems and forms a primary source of malfunctioning at high potentials.

The electrical field gradient on the surface of the wire reaches extreme values at higher potentials such that a critical field strength is easily reached, beyond which electrons are emitted from the surface of the wire. It was calculated that the resultant electric field gradient at the surface of the wire exceeds 30 MV/m at 300 kV in the transition of the surrounding metallic surface in the present commercial design. The threshold potential for fiel emission can be calculated using the work function of the material. A theoretical estimation of the required electric field strength for electron emission from ideal metallic surfaces is given by [Imhof (1957)]

$$E_c \text{ [kV/cm]} = \frac{U_a^2}{9 \cdot 10^{14} \, q_e}, \tag{5.8}$$

in which U_a denotes the work function of the material and q_e the charge of an electron. The practically relevant field strength for the emission of electrons from imperfect surfaces ranges a few orders of magnitude below the theoretical value. A poor surface significantly decreases the electric field strength that is required for the emission of electrons. Microscopic substructures lead to field enhancements, which reduce the local work function and ease the emission of electrons. Practically, E_c reduces to 5 to 10 ppm of its original value. Still, the corrected values relate to field strengths between 30 to 150 MV/m for materials, which can be used for both high voltage feedthroughs and high voltage electrodes.

The wire surfaces of the purchased commercial feedthroughs were rather rough. No special treatment was evidently applied to the wires, before or after they were hard-brazed into the ceramic bodies. The small wire diameter that measured only a few millimeters, certainly promotes the emission of electrons at the targeted potentials of this work. The calculated electric field gradient of 30 MV/m is locally dramatically increased and easily exceeds theoretical sustainable potentials.

Emitted electrons gather on the neighboring ceramic surfaces. Because of the absence of conduction bands in the insulator, electrons can not be removed by conduction and remain on the surface, until a critical electric charge is reached. Eventually, a creeping along micro-channels in the direction of grounded components develops with time. Partially, electric discharges and permanent damage to the insulating materials of the feedthrough occurs, which decreases the dielectric strength. This processes is known as aging of insulators and was previously mentioned. The increased occurrence of electric breakdowns more quickly degenerates the feedthrough, until the feedthrough can not sustain the applied potential any further and has to be replaced. Electric discharges and damage in the direct neighborhood were inevitable with the commercial units in the first two compact sources of the type E-Gun 300. The malfunctioning consequently prevented successful operation at the original design criteria.

(v) The emission of electrons is leading to the final problem of the standard feedthrough design, which most certainly occurs at high potentials. Next to the accumulation of charge on surrounding insulating components, the standard design involves the generation of x-rays. Emitted electrons are accelerated towards metallic surfaces at lower potentials, and x-rays are produced wherever the electrons impact. For this reason, measures of radiation safety have to be applied to the standard electric feedthrough design that is operated at higher voltages. The measurable emergence of stray x-ray radiation outside of the vacuum chamber manifests at electron energies that exceed 25 to 30 keV.

Summarizing, the conventional feedthrough design expedites the appearance of breakdowns due to the layout of metallic and ceramic surfaces in vacuum. The design is not suited for high electric potentials and x-ray stray radiation is a accompanying side product that requires consideration. Unless a dramatic modification of the standard layout is made, the electric performances of the feedthrough and electron source overall remains limited to potentials that range below the targets of this work.

5.5.3 IMPROVED DESIGN

All of the above mentioned problems were solved by the development of a novel design. The central wire was replaced by an insulated high voltage cable, which is surrounded by a further dielectric medium. A free standing wire, which transmits a grounded surface and which is surrounded by vacuum, is no longer required. A critical, minimized distance of the transition of the electric potential to the grounded surface is equally removed. The point of transition of the potential and current into the vacuum environment is shifted towards the photo-cathode. In the present design, both the generation of x-rays and generally the emission of electrons is avoided at any applied electric potential. Consequently, the novel feed-through design can be operated at much higher potentials than targeted in this work. The limitations that may occur, are due to the insulation properties of the utilized materials, which still generally allow extreme conditions. Alumina-oxide ceramics, also known as ultra-porcelain, are ideal candidates for electric installations due to chemical and thermal resistivity and a generally vacuum compatibility.

Electronic avalanches along the surfaces of the utilized insulators can not occur in the developed design for two reasons. Firstly, there is no source of electrons close by, which can cause a collection of charge on the surface of the insulator. Secondly, a modified orientation of the surface to the electric field distribution hinders the electric field in pushing electrons towards grounded components, which over time otherwise leads to the occurrence of increased creeping currents. Another important feature of the new design is the general manipulability, which is required to set different gap sizes between

the photo-cathode and the anode, to optimize the operation condition of the FED-CAMM.

Unlike the former conventional designs, the new design can be scaled with the applied electric potential. The appropriate scaling factor is mostly linear to the maximum electric potential. It is impossible that a field-gradient induced malfunctioning can occur. Further, the components that form the new feedthrough, are low cost, widely available and the required manufacturing processes established and reproducible. These factors make the new high voltage feedthrough a candidate for mass production. Consequently, this will lead to a widespread utilization and use of high voltage feedthrough of this type in other fields, far beyond the scope of instruments for time-resolved electron diffraction. However, for the community of time-resolved electron diffraction, this development has a significant and great impact, especially if these devices become commercially available, eventually in combination with a further developed compact FED-CAMM.

5.6 CONDITIONING AND HIGH VOLTAGE TEST RUNS

All electrodes were conditioned and tested after each of the previously described steps of manufacturing. Within the first attempts the capability of the high-voltage feed-through also had to be evaluated, since such a design was not tested before. This made it initially difficult to differentiate the influences of the high voltage feed-through from the performance of the high voltage electrodes. When more tests with different configurations were made, the effects that are related to the single components could be more clearly differentiated and assigned to the individual components.

To fulfill the promises that were justifying the construction of the FED-CAMM, both the upper limit of the high voltage power supply as well as most intense electric fields in the accelerating gap had to be established. The construction and execution of first experiments was especially challenging and thrilling, since for most components of the setup no spare or replacement part was available. This is especially true for the first prototype of the new high-voltage feedthrough design, which actually suffered from electric perforation after a major electric breakdown. This perforation was due to the presence of blowholes in the first ceramic element, that was used. The electric insulation was locally strongly degenerated with gas, that was trapped within small cavities in the insulator. Local inhomogeneities of the dielectric strength serve as weak points and were unfortunately incorporated during the manufacturing of the first batch. These insulators could subsequently not stand the applied electric potential. The irreversible damage led to the death of the first feedthrough prototype at a potential which measured more than 160 kV.

This first malfunctioning was supported by the back then not electro-polished electrodes. The first tests of the high voltage feedthrough were conducted with manually polished electrodes. This led to the increased emission of dark current that potentially promoted the electric perforation of the insulator. This condition improved once all electrodes were electro-polished. The performance during conditioning and the sustainability of very high potentials was subsequently strongly improved; while the emission of dark current strongly decreased.

For the further tests, especially those involving measurements of the electric field strength between a front-electrode and the anode plate, arc conditioning guided the process. Glow conditioning rarely occurred, but intermediately dominated the conditioning processes. The purpose of these tests was still the determination of the electrically best suited manufacturing procedures, which overall was a very time consuming process. The manual polishing of all electrodes alone, including the acquisition of required techniques, and testing of various methods, required more than five month inside the workshops. Once the effect of surface treatment was determined, the specific influence of the presence of photo-cathodes and various materials for this purpose was investigated. One of the earliest good results was obtained with the conventional gold-coated photo-cathodes, which led to 190 kV applied on a gap of 20 mm. At that time, the front electrode was not conditioned yet to that high voltage. This leads to the assumption, that a repetition of this test yields even higher potentials, and more importantly, more intense electric field gradients with the standard photo-cathodes.

An interesting experimental test was conducted with a blind electrode. This is a dummy electrode, which does not comprise a hole in the center. This test series serves as the reference for the maximal obtainable electric potentials. As the previous discourse of high voltage electrode development already concluded, the noted performance of the electrodes is especially outstanding at small gap sizes, due to the restricted diameter of electrodes and chambers. The highest electric field gradient that was obtained at small gap spacings, ranged up to 26.8 MV/m at 40 kV. This is almost three times as much as what is conventionally used in FED experiments, and ranges at the lower theoretical limit of field emission. As previously mentioned, it is not stated in any publication of the reference setups, which include all known installations, that a field gradient of 10 MV/m is exceeded.

The feedthrough itself had to be tested up to the limit of the connected high voltage power supply. Because of the large area of the electrode assembly that is required for FED experiments, the performance at high field gradients was partially limited. Without a blind electrode, the feedthrough can not be operated. Hard brazed seals require an appropriate shielding to account for the otherwise occurring electric stress. To achieve the

highest voltages, a special electrode assembly was designed. This assembly reduces the effective area of the electrode arrangement, but still sufficiently removes the electric stress from the crucial end of the high voltage feedthrough. Only with this special development it was possible to test the high voltage feedthrough to the maximum potential of the connected power supply.

An alternative to DC electric fields are pulsed AC fields. For shorter periods in time even higher electric field gradients can be obtained, even in the same electrode arrangement and setup layout of the FED-CAMM. Working with the same physical limitations as rf-cavities conventionally do, the field gradients could easily exceed 40 MV/m and still yield uniform electric fields within the gap between the high voltage electrode and grounded anode. The references for high voltage devices for food-processing are generally operated using this scheme. However, it has to be excluded, that dark current is generated while the electric fields build up and vanish. Potentially, a trigger of electron pulse generation at the peak of the electric field, separates electron pulses from dark current background. The operation of high voltages in combination with static DC fields is more challenging. Thus, the implementation of high voltages and intense electric fields in the FED-CAMM is a remarkable success.

5.7 RADIATION SAFETY AND SHIELDING CONSIDERATIONS

A more extended background of regulations and precautions of the subject of radiation safety was provided in section 4.3.2. The FED-CAMM potentially produces x-rays whenever it is operated, or more specifically whenever a high electric potential is applied to its core electronic components. These x-rays are neither of any use nor desired. Because of the FED-CAMMs energy range of more than 5 keV and less than 1 MeV, it falls within the classification of stray-radiation device. The final implementation of radiation protection at the E-Gun 300 is such that an external radiation shield in form of a lead hutch was needed. This hutch is surrounding the entire experiment and large sections of the attached optical table [yellow box in figure 6]. Unfortunately the hutch of the E-Gun 300 prevents a direct access to the instrument. A live-adjustment of equipment that is connected to the vacuum chamber, is impossible during operation. For this reason, most of the elements in and around the chamber are motorized and remote-controlled, which solves some of the associated problems. This requirement still makes operations very cumbersome and greatly slows down experimental progress.

A similar installation of an extensive radiation shield is avoided at the FED-CAMM instrument for the following reason. The implementation of a radiation shield is partially incorporated into the design of the setup and part of interior components. The upper chamber section, which contains the high voltage electrodes, produces most of the stray

x-ray radiation. Due to the applied electric potential, electrons are emitted from principally any fragment of all conducting surfaces into all directions.

A tubular insertion made of aluminum is a new element in the radiation shielding concepts of this instrument. The aluminum is the first layer of the x-ray shield, on which electrons, which leave the electrode arrangement sideways in respect to the central beam axis, will impact. As previously mentioned, the creation of bremsstrahlung that scales with the atomic weight of the target material [Bethe (1930), Bethe (1932)], is minimized. The penetration depth of electrons of 300 keV only measures a few micrometer. Hence, they are fully stopped and absorbed by the aluminum shield. The resulting bremsstrahlung proceeds much further and requires a heavy and dense material. Here it is important to note that the guaranteed x-rays are lower energy than would occur using other materials than aluminum. This feature greatly reduces the amount of additional shielding needed. In all cases lead is the most commonly used material for the shielding of x-rays outside of vacuum environments. Lead does not impair a high health risk, but serves well as a radiation shield. To prevent the leakage of x-ray radiation, this section of the vacuum chamber is surrounded by a 3 cm thick lead shield, of which the thickness was determined by equation 4.2 in the same manner, which is described in that according section and below.

With the aluminum inside the chamber, the dose rate constant Γ_X is reduced compared to the calculation for the E-Gun 300. The dose rate is still significantly overestimating the actual situation that is found in the setup. No real copper target inside the chamber and no x-ray pencil beam is present, for which Γ_X is specified. However, the scenario of an intense x-ray pencil beam that is colliding with various instrument components, is used for the calculations of radiation safety. The thickest layer of aluminum, for which Γ_X is specified, is 4 mm. For this thickness, the dose rate constant is specified with 3.5 $[Sv\ m^2\ mA^{-1}\ h^{-1}]$ [Vogt and Schultz (2011), p.439 tab. 15.20]. The distance from the inner layer of the aluminum tube to the outer reachable surface is increased by at least 40 mm. The required attenuation factors for the controlled and supervised area amount to 4.3 $\cdot\ 10^{-7}$ and 7.1 $\cdot\ 10^{-8}$ in close proximity to the surface of the vacuum chamber. A lead thickness of 3 cm is required [Vogt and Schultz (2011), p.473 tab. 15.29] to reach the legal regulations.

Towards the detector end of the setup, separating the chamber section with the electrodes, is a thick anode made of heavy metal serving as radiation shield. All electrons that are extracted into this direction, are stopped by 10 mm of solid tungsten, except for those electrons and electron pulses that are aligned with a small aperture in the center of this plate. The attenuation factor amounts to at least $7 \cdot 10^{-3}$ for 300 keV photon-energy and to less than $1 \cdot 10^{-6}$ for 200 keV and less energetic electrons [Vogt and Schultz (2011),

p.454 tab. 15.27]. Beyond this anode plate, the electron beam is enclosed by heavy metal plates, which form a box around the usable electron beam. This box is continued through all magnetic lenses and ranges to the detector, which itself is at its rear end enclosed by a lead plate. This design is a compactification and incorporation of most of the necessary precautions for radiation shielding measures. Figure 44 summarizes the single elements of this design.

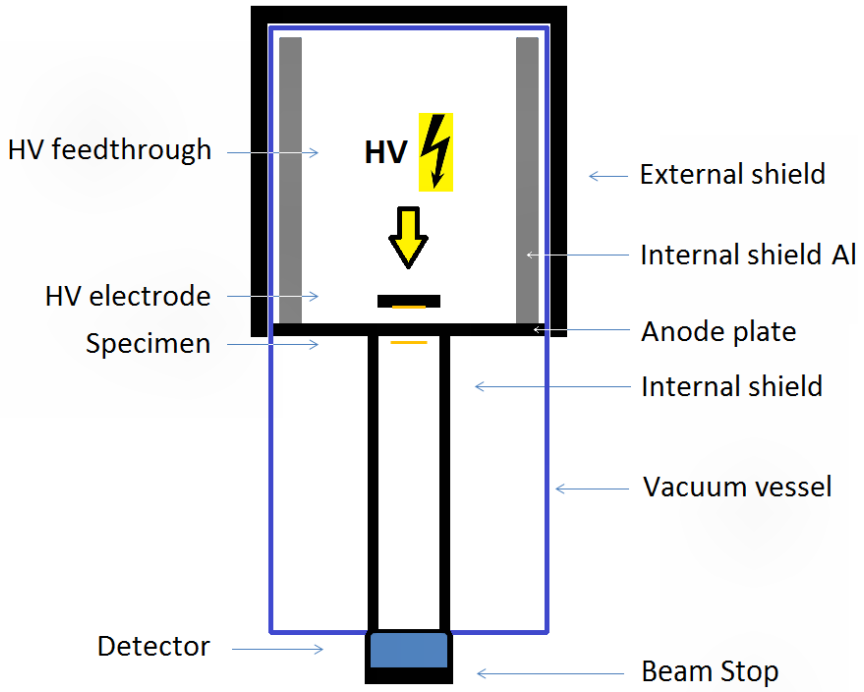

Figure 44: Radiation shielding concepts developed for the FED-CAMM. Single elements were incorporated into the instrument to restrict the size of an outer x-ray shield. The beam direction is, as indicated in this figure, from top to bottom. Dimensions are not to scale.

Another beneficial aspect of this setup is the orientation of the electron beam axis in regard to the room, in which this setup is built. The instrument is vertically mounted and the pulsed electron beam is directed towards the floor of the laboratory, below which no further floor or cellar is present. This eliminates the need of extra thick x-ray shields at the end of the beamline, if it was oriented horizontally. Further, all electrons and x-rays are predominantly directed towards the floor, instead of sideways, as in all earlier setups. A thick lead plate is incorporated into the detector section. If necessary, another lead plate can be easily arranged below the setup. For additional safety, a sliding lead door arrangement, involving eight removable doors, is set up around the FED-CAMM. Since this first apparatus remains a prototypical development with higher electron energies than ever used before in a compact DC electron diffraction setup, which further serves to validate several new concepts and approaches, it remains a test installation, in which

modifications to the current arrangements of setup components can not be excluded. The external lead enclosure allows an easier access to the instrument than the lead hutch around the E-Gun 300, but by construction ensures full compliance with currently applicable radiation safety regulations. Users of this installation will be sufficiently protected from potentially occurring x-ray radiation, which will remain an important consideration for all electron diffraction experiments.

5.8 PARAMETER SPACE AND CURRENT OPERATION CONDITIONS

The maximum voltage, which is endured by the high voltage feedthrough alone, is the current maximum of the connected 300 kV high voltage power supply. A special end cap was used for this test. The possible potential of the current feedthrough is located at higher values, but a more powerful power supply to test a scenario above 300 kV currently not available. With the installation of electrodes with photo-cathodes and other components, the maximum voltage is currently limited to values around 200 kV, partially to avoid damages to conventional photo-cathodes. This limitation is also due to insufficient conditioning of the high voltage electrodes. The large electrode area, aside from the region around the photo-cathode and the most intense electric field, requires more current or time, respectively. This is needed to electrically prepare the electrodes for the higher potentials. A larger vacuum chamber and electrode diameters can improve the distribution of field gradients. At least a further test without the internal aluminum shield could be conducted.

The most intense potentials, to which the electrodes were already conditioned, range up to 100 kV. Within these potentials, more intense electric field gradients than usually employed can be set, up to the previously mentioned 26.8 MV/m. The intermediate field gradients of 15 MV/m do not lead to a measurable emission of dark current and return electron pulse durations around 109 femtoseconds (fwhm, simulated). The simulated average can be further reduced by the sheer increase of the electric field gradient, which is accessible without doubt and already experimentally confirmed. Partially, there was no dark current at higher field gradients observed. The intensity of the laser pulse for the excitation of the photo-cathode can be reduced to limit the number of photo-excited electrons per pulse. This can lead to even shorter electron pulses, which approximate the minimum possible pulse duration at the accessible electric field gradients. The shortest electron pulses will surely undercut the pulse durations that were determined as the minimum of electron pulse duration by Aidelsburger et al. (2010) at field gradients of 10 MV/m. Simulations of pulse durations at higher field gradients (this is above 15 MV/m) and with less electrons per pulse, were not yet covered by the simulations of this work and remain to be conducted. The simulations will reveal even shorter pulse durations at relaxed electric field gradients. The first simulated estimates of pulse durations with 10^4

electrons lead to electron pulse durations between 60 and 100 fs (fwhm).

As will be presented shortly, laser generated electron pulses were recently used, while the development of the setup is still ongoing. The number of photo-excited electrons is too small to create a plasma that could induce an electric breakdown between the photo-cathode and anode. Otherwise, the electric condition of the instrument is performing absolutely stable, which is not the case in any of the other known setups.

The time required to reach the maximum potential is only determined by the maximum used current that charges the cascade of the power supply and the high voltage electrodes. It takes a few seconds to reach potentials above 200 kV with higher currents. The currents disappear, once the target potential is reached. The high-voltage feedthrough is not obviously affected in any way by the pace of the increase of voltage, only by the vacuum pressure and residual gases, which work on the surfaces of the insulator.

5.9 MACHINE STATUS AND UPCOMING DEVELOPMENTS

The prototype of the FED-CAMM was recently completed for first static and subsequent dynamic electron diffraction experiments. The highest available potential of the connected power supply was successfully tested with the partial removal of the high voltage electrodes. Additional conditioning will further advance the obtainable electron pulse durations while reliable photo-cathodes are used, which would by now already be outstanding and range around 100 fs (fwhm) with the needed upgrade of the laser system. The generated electron pulses will be even shorter with less electrons per pulse and certainly with higher electric field gradients. On the other hand, lower electric field gradients can be exploited and help to optimize the life-time of photo-cathodes or more optimally match requirements of the specimen.

Further advances in respect of suitable photo-cathodes have to be made, to avoid the observed degeneration of gold-coated photo-cathodes. First tests of alternative materials provide leads to suitable materials. Promising candidates are single crystalline layers of gold in combination with front-side photo-excitation, to reduce the initial energy spread. The vacuum requirements are not as strict as for GaAs photo-cathodes, but the operation will be stable during the use of intense electric fields and higher electron currents. Further, semi-conducting and crystalline photo-cathodes would decrease the energy spread, compared to vapor deposited or epitaxial grown metallic layers on photo-cathodes. Also, changes to the current photo-cathode cutout in the high voltage electrode are a potential adjustable parameter, which can potentially improve the overall performance.

Software, which can operate the apparatus and conduction of the experiment, is currently in preparation. But this development including the remaining wiring of additional components of the setup do not affect the full success of the range of developments, which were pursued in the development of the FED-CAMM prototype and within the second half of this PhD work, but rather require additional time and manpower. Not all details are fully exploited at the end of this work, but a promising start into a novel direction for FED research is made.

The current laser source for the FED-CAMM has by default pulse durations of 140 femtoseconds. Optical setups, which further compress these laser pulses, will be set up, characterized and subsequently used to generate shorter laser pulses in the coming development phase. It is then possible to experimentally generate the shortest electron pulses at various electron energies between 30 and 300 keV. A load-lock system for the quick exchange of specimens is envisaged to speed up the exchange of specimen in the FED-CAMM, although currently it does not require much time to exchange sample holders (< 15 minutes). From the initiation of vacuum pumps to the operation of high voltages, 10 mins are at least required, until the pressure justifies the initiation of high voltage and generation of electron pulses.

Finally, the FED-CAMM is the currently best suited highly time-resolved electron source for specimens that are contained in liquid cell environments. Other than transmission electron microscopes at higher electron energies, the investigations with the FED-CAMM include this aspect for time-resolved dynamics. With the current configuration of an additional nanosecond laser-source next to the FED-CAMM, nanosecond electron pulses and pseudo-continuous electron beams can be generated to imitate the operation of common TEMs. The multiple-lens system within the FED-CAMM allows a comparable flexibility, as is commonly employed in TEMs.

5.10 SINGLE-SHOT DIFFRACTION PATTERNS

Only recently, laser pulses were used for the excitation of short electron pulses to generate first diffraction patterns. As discussed above, the laser system is not yet fully built. For this reason, the used laser pulses had a duration of 140 fs (fwhm). The compression to shorter pulse durations that meet the optimum for shortest electron pulses will follow. The quantification of electrons per pulse requires electron diagnostics, which was equally not present during the production of these first images. Since the number of electrons per pulse determine the electron pulse duration at the specimen, the pulse duration can only be estimated within certain boundaries, primarily depending upon the number of electrons per pulse. The intensity of laser pulses was reduced to a minimum, but could equally not be measured yet. Based on the intensities of diffraction, the electron number

was estimated to range in between 10^4 and 10^5 electrons per pulse, certainly not more than 10^6 electrons. These first experiments that were using a real photo-cathode, were conducted at reduced electric field gradients (< 6.7 MV/m) to avoid potential damages to the photo-cathode (as illustrated in figure42). The applied potential was intentionally limited to 90 keV for the same reason. The electron beam diameter could be measured using a TEM mesh that was positioned in the sample plane as the other specimens, which were used for the first diffraction. The diameter of the electron beam measured less than 44 μm, which is significantly smaller than the currently present pinhole of the anode. The laser was tightly focused on the photo-cathode, which explains such the small electron beam diameter. Stretched laser pulses of 140 fs (fwhm) pulse duration artificially reduce the electron density in the pulse and avoid space-charge induced broadening, in both longitudinal and lateral direction. The resulting electron pulse duration should have a minimum of 180 fs (fwhm), but not exceed 600 fs (fwhm). No further pinhole or other image-improving component was used for these first shots.

Standard specimen systems were used for the first tests of diffraction such as gold, aluminum, and compounds with molybdenum and indium. These systems of known structure help to characterize the instrument. Out of all diffraction patterns, which were without exception single-shot measurements, a few are presented in the following images.

Figure 45 shows the focussed electron beam on the detector. Without laser pulses that photo-excite electron pulses, no dark current electrons were detected. Instead, the image converts into electronic noise from the detector, when no electrons are produced by laser pulses. Figure 46 shows diffraction by a 50 nm thin layer of InSe, equally captured by a single shot at 90 keV. The central spot in this pattern correlates well to the original beam diameter. One could say that multiple scattering is mostly avoided in these thin films of InSe. Figure 47 shows diffraction by poly-crystalline gold. This image is one of many and illustrates that a complete structural resolution with single electron pulses is already possible. This images compares also very well to the diffraction that was obtained by REGAE (previously shown). The difference in between the images of the REGAE and the FED-CAMM is that the electron beam of the FED-CAMM is smaller compared to the REGAE, which equally can be observed in the diffraction patterns. Figure 48 finally demonstrates, how the electron beam diameter was estimated. Each bar of the TEM grid is 6 μm thick, with windows of 19 by 19 μm size, resulting in less than 44 μm beam diameter.

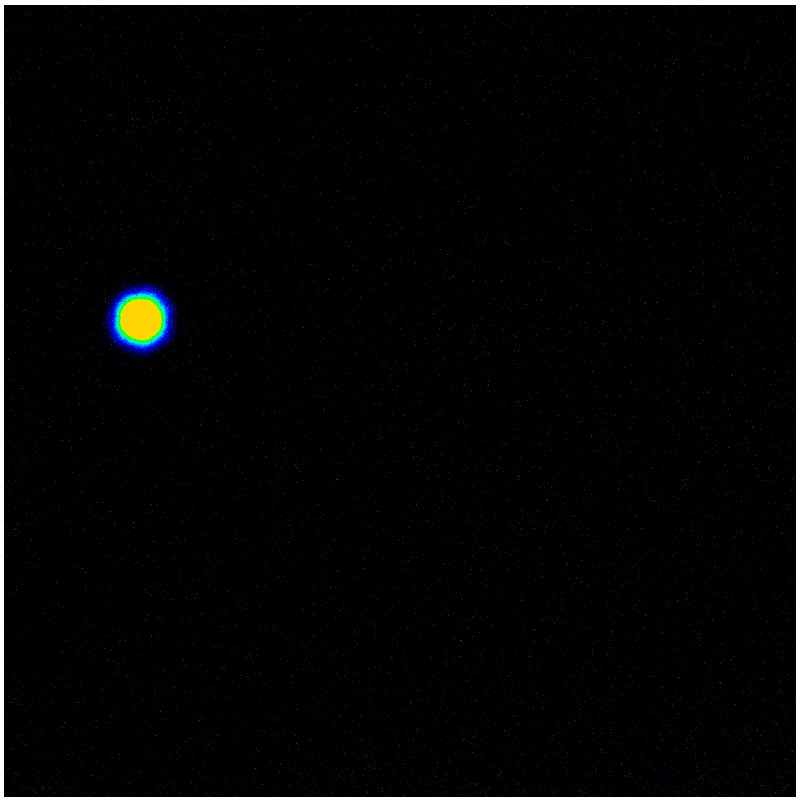

Figure 45: Focussed electron beam. Image showing a single electron pulse with 90 keV.

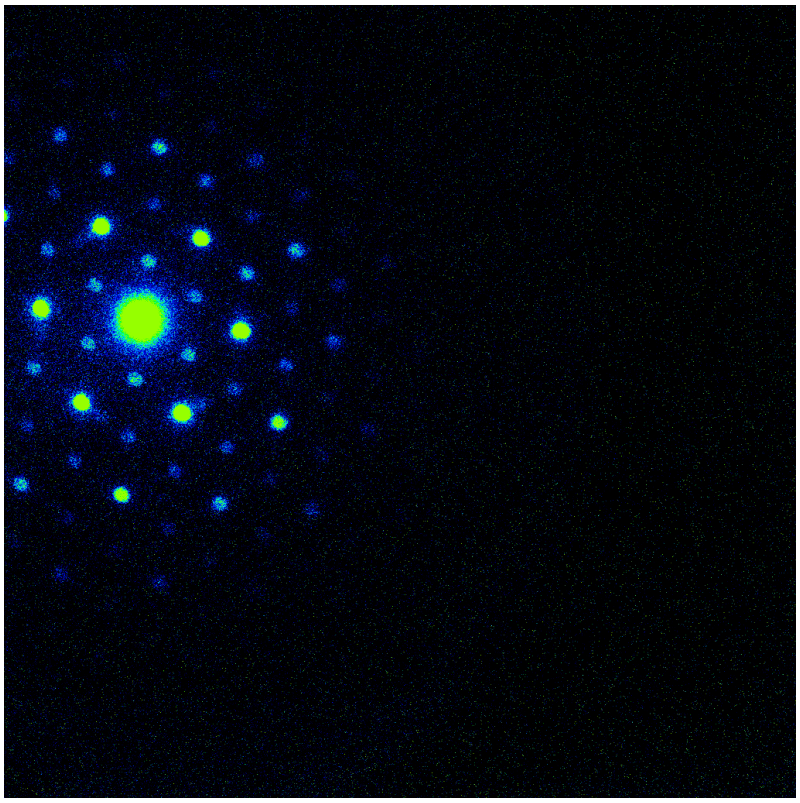

Figure 46: Diffraction from 50 nm InSe, single shot illumination, 90 keV.

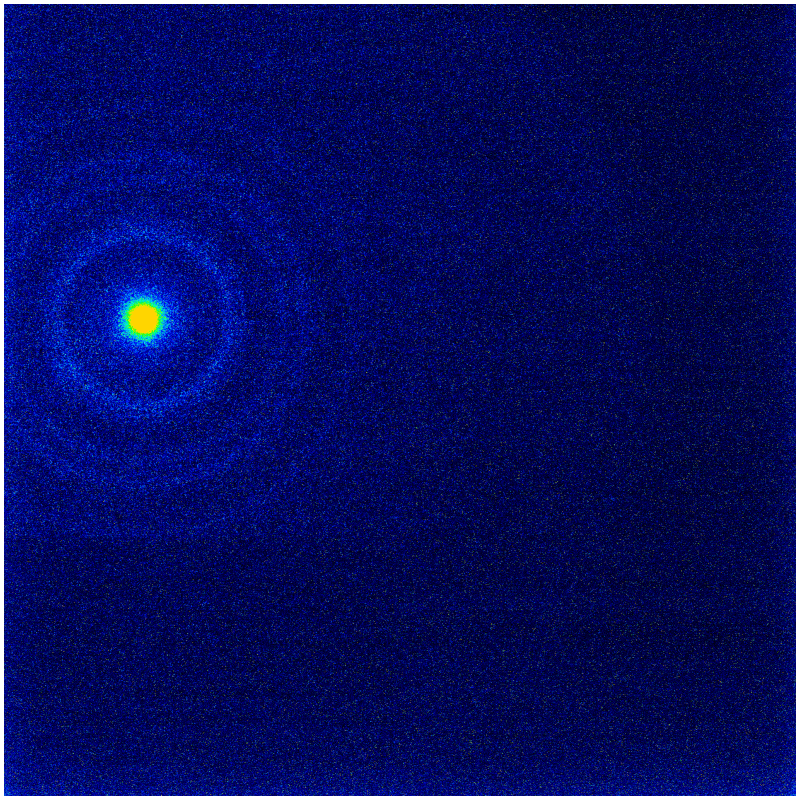

Figure 47: Diffraction from 100 nm Au, single shot illumination, 90 keV.

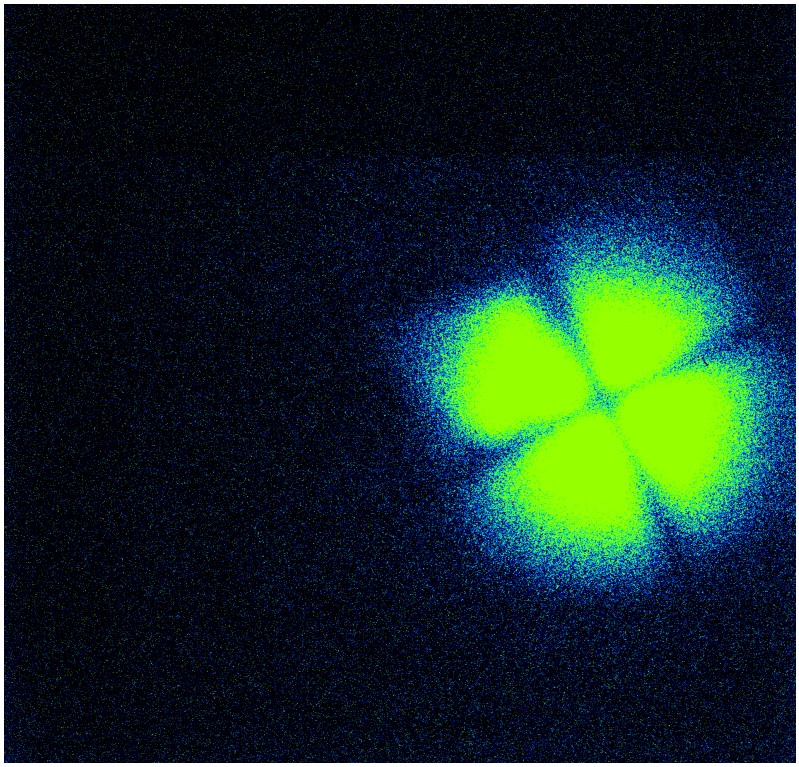

Figure 48: Estimation of beam diameter by imaging a TEM grid.

6 DISCUSSION

6.1 ACCELERATOR DEVELOPMENT

During this work three scientifically relevant setups for the application of femtosecond electron diffraction were developed. This work dealt with the design and installation of large sections of the REGAE accelerator as well as different sub-projects to that instrument. The organization of the manufacturing and the installation of the E-Gun 300 setup and a similar clone was processed. The FED-CAMM project included the complete machine design with all necessary developments and considerations, the preparation and supervision of manufacturing, the installation and testing with further development and improvements. The FED-CAMM is a progressed development, and a direct consequence of the experienced performance problems of the REGAE and the E-Gun 300.

The development of the REGAE beam line in the experimental section, which included the first specimen chamber and related developments, enabled further research. The dark current collimators significantly improve the electron beam of REGAE. The observation of diffraction patterns is currently difficult without the usage of the collimators, due to a large electron beam diameter, angular and energy spread. Further, the dark current produced by the rf-cavities decreases the signal of diffraction. This had been one of the major concerns in this project during the early development stage. Thus, great attention was laid on the detectors' capability of every electron detection, which has been achieved.

The time resolution of REGAE is still limited, although the concept of two separate cavities for the quick acceleration and re-bunching of initially long electron pulses remains promising. The ASTRA simulations support this prospect at least. Ongoing improvements of the rf-system and the femtosecond laser source will most likely improve REGAEs' performance. This machine may then not only compete with the other rf accelerators of table 9, of which quite a few already reach 100 fs pulses, but eventually beat them. The energy of REGAE (minimum 2 MeV, average 5 MeV, maximum 7 MeV) is comparable to the prior existing sources [table 9]. Due to a long time of comissioning, a time-resolved experiment subject to conduction with the REGAE was postponed.

The construction of the E-Gun 300 revealed crucial performance problems, which naturally occur at the high potentials that were targeted by this machine. While the overall performance of the E-Gun 300 was not as expected, it is in itself an outstanding apparatus. The highest electron energy, at which a compact time-resolved FED setup was

operated prior to this work, and this comparison includes the hybrid setups of table 9, amounts to 100 keV [Chatelain et al. (2012b)]. The E-Gun 300 can be operated with up to 140 keV, but will suffer electric instabilities at this higher potential. However, the machine operates in a stable way around 120 keV. Although this is only a small increment in energy compared to the sources, which were established prior to this work, the time resolution of the E-Gun 300 is at least better than 300 fs (fwhm). It thus operates in proximity to the hybrid setup, which is operated at 95 kV and equally belongs to our group [Gao et al. (2012)]. This source provides electron pulses of less than 200 fs (fwhm) duration, but includes timing jitter from the rf-cavity system.

Another beneficial aspect of the E-Gun 300 is the subsequent development of the FED-CAMM. The overall development of the FED-CAMM was also prompted by the non-availability of the REGAE for time-resolved experiments at the time. The development of a high voltage feedthrough for compact instruments that comprise UHV environment was a full success. No commercial high voltage feedthrough performs similar to the development for the FED-CAMM. By today, the situation of machine-availibility for time-resolved experiments has changed. Both the REGAE as well as the E-Gun 300 are set up for time-resolved measurements at currently 900 and 300 femtosecond temporal resolution, respectively. In addition, the FED-CAMM is now available and operating with pulse durations below 500, even below 200 fs. With the further compression of the laser pulses that drive the photo-cathode of the FED-CAMM, the simulated 70 fs will be accessible.

Besides the developed high voltage feedthrough, the FED-CAMM comprises additional, not less important novel technical features. These concern high voltage electrodes, a smart radiation shielding and design concepts which were incorporated into the first prototype, but are not explicitly mentioned. This is because these concern the conduction of experiments using this instrument, details which were not outlined in this thesis.

The simulated results concerning the electron pulse duration of the FED-CAMM are stunning. The acceleration within the required uniform electric field in the acceleration gap is given by the developed high-voltage electrode design. An intense electric field gradient can be set for all applied electric potentials to obtain the shortest achievable electron pulse duration that can be generated by a compact DC operated setup. Intense field gradients are maintained by the most appropriate manufacturing of high-voltage electrodes, which results in stable electrical operation. Without further re-compression by a rf-cavity, the obtained electron pulse durations is shorter in time than the magic threshold of 100 fs (fwhm). This includes timing jitter on the order of 10 fs, which may arise from the source of the applied electric field. Great care was taken to pick a stable

high voltage power supply, almost free of residual ripples on the generated high voltage.

Electric field gradients up to 18 MV/m can be set up to energies of 100 kV. Dark current electrons did not occur at this field strength, at least no measurable creeping current or illumination of the image detector was measured. Even at the obtained field gradients of 27 MV/m it may be possible to conduct time-resolved diffraction experiments with outstandingly short electron pulses of 70 fs in time. This will depend on the overall transmission of dark current electrons through the pinhole aperture of the electric anode. Most of the arising dark current of the high voltage electrodes will dispose itself in the anodic radiation shield. It yet has to be measured how clear signal from diffraction at high electric field gradients will show up on the image detector. I am certain that the situation is improved compared to the REGAE, since less intense electric field gradients are used in the FED-CAMM (compared to at most 120 MV/m in the cavities of REGAE). As long as collimation apertures for dark current are used prior to the interaction of the electron pulses with the specimen, the dark current will not degenerate parts of the diffraction images.

The feedthrough concept, which was one of the key developments for the FED-CAMM, can also be used in other fields of research, as well as in various industries. Commercial electric feedthrough ranging up to a few hundred keV are still not available, at least not for UHV applications and certainly not in a compact format. Once the availability is given, the increased need and applications will naturally emerge. Especially for the target of higher electron energies in compact electron accelerators, the availability of a high voltage feedthrough is of major interest.

Radiation safety is mostly already incorporated into the design of the FED-CAMM. This is another crucial necessity, which accompanies the operation of FED setups incorporating electron energies of more than 30 keV. The current construction of an extra surrounding lead shield with sliding doors still allows a less complicate access to the instrument than the radiation hutch, which is surrounding the E-Gun 300. A measure of radiation safety that was enforced to be built prior to operation.

The electron sources built and developed in this work are unique installations. Despite of many similarities of the E-Gun 300 and the previous 95 keV setup, which is standing and operated in Toronto, the electron gun sections of these two compact installations are each unique attempts to obtain the high potentials. The FED-CAMM instrument is an overall novel design, which has no similarities to any component of a previously built FED setup. The design is optimized for FED experiments. The REGAE is unique in the utilization of two separated rf-cavities for the acceleration and bunching of electrons.

The electron beam dynamics of each machine was simulated using either the ASTRA or GPT program. The ASTRA simulations of the REGAE are based on optimized simulation parameters, which yield the best-case results. There are deviations between the actual achievable machine parameters and the assumptions of the simulations. However, the REGAE is under constant development and experiences a continuing improvement of all of its components, such that the theoretical prediction of less than 25 fs (fwhm) pulse duration can be eventually reached within the coming years of development. Further improvement is also connected with enhanced reliability of the rf-system, which tends to break during to elaborate usage.

The compact installations E-Gun 300 and the FED-CAMM behave more stable, since the employed techniques and required components are overall less complicated. This also affects the cost of the instruments. Most of the components involve compact and robust electronics, which are reliable, depending on the model and supplier. In terms of the E-Gun 300, the high voltage related performance problems are only obtained above potentials relating to 120 keV are applied to the high voltage carrying parts. The FED-CAMM is less sensitive in this regard, with the photo-cathode being the only consumable. The behavior in conditioning the FED-CAMM is different to the E-Gun 300. Only metallic components were used in the mount of photo-cathodes oppose to insulating mounts, which were surrounding the photo-cathodes of the most of the earlier setups. Further, the gap size is adjustable even while the high voltage is applied. This crucial parameter with the most direct influence on the electron pulse duration was not accessible before during the operation of the instruments. The overall design considerations act beneficial on machine performance. The high voltage feed-through, which is used to mount high voltage electrodes, does not limit the applied electric potential, as opposed to the ceramic mounts in earlier setups.

The simulated pulse durations of the E-Gun 300 actually match the current machine performance. Since pulse duration mostly depends on the applied electric field gradient, the information on pulse duration obtained by GPT simulations becomes an excellent indicator of the realistically achievable result. Pulse durations around 109 fs (fwhm) with 10^4 electrons per pulse can be effortless reached in the FED-CAMM at field gradients of 15 MV/m. It is known from experiments with this instrument, that this field gradient is a few MV/m apart from the emission of dark current. At field gradients of 18 MV/m, no dark current was observed. Whether or not dark current will cause any conflicts within further diffraction by this setup remains to be investigated. It was at least no issue in the first single-shot images, which were recently recorded and which were free of dark current or electron-induced background. With further conditioning of the

high-voltage electrodes and eventual adjustment of electrode size, the upper limit of dark-current-free operation is shifted towards more intense electric fields and shorter electron pulse durations.

Two adjustable parameters are generally available for the further reduction of the electron pulse length. Aside from the enhancement of the electric field gradient, discussed above, the number of electrons used per pulse can be decreased. Both changes will lead to a shortening of the electron pulse. Provided that timing jitter of a few femtoseconds related to remaining fluctuations of the applied electric field remains an intrinsic property of such a setup, the pulse duration will in any case range around or below 100 fs (fwhm). This is remarkable and generally not easily obtained with rf-generated electron pulses due to the generally larger rf- and electronics-related sources of timing jitter. Being a great disadvantage for rf-operated FED setups, this condition is of big advantage for the typically more compact DC-operated setups to rule the field of dynamic-structural investigations. The development of the FED-CAMM is the first successful implementation of all requirements of a time-resolved electron diffraction instrument, which provides remarkably short electron pulse durations. The FED-CAMM is further a prototype with successful proof-of-principle validation of a few novel approaches.

The obtained pulse durations of the three instruments of this work can be directly compared to already established sources for FED, which are known from literature and listed in this thesis. The technical instrument-specifications which belong to each of the reference points in figure 49, were listed in table 8 and table 9. All currently known machines (as of 2014) are combined in this figure.

The comparison of worldwide and thesis-related sources is missing some accuracy due to the partially unavailable specification of rms or fwhm denotion of electron pulse duration in the referenced publications. In contrast to the references, the pulse duration of the developed instruments of this work is consistently specified in fwhm values. Some if not most of the reference machines, especially those which further range back in time, have to be shifted by the according scaling factor of 2.355 towards longer pulse duration. Still it can be seen, that the E-Gun 300 performs within the center of a bulk of comparable DC machines between 300 to 690 fs. The REGAE currently operates below 1 ps at a higher electron energy in close proximity of the other rf-operated pulsed electron sources in the few MeV range. The FED-CAMM operates around 100 to 120 fs (fwhm) at energies below 300 keV.

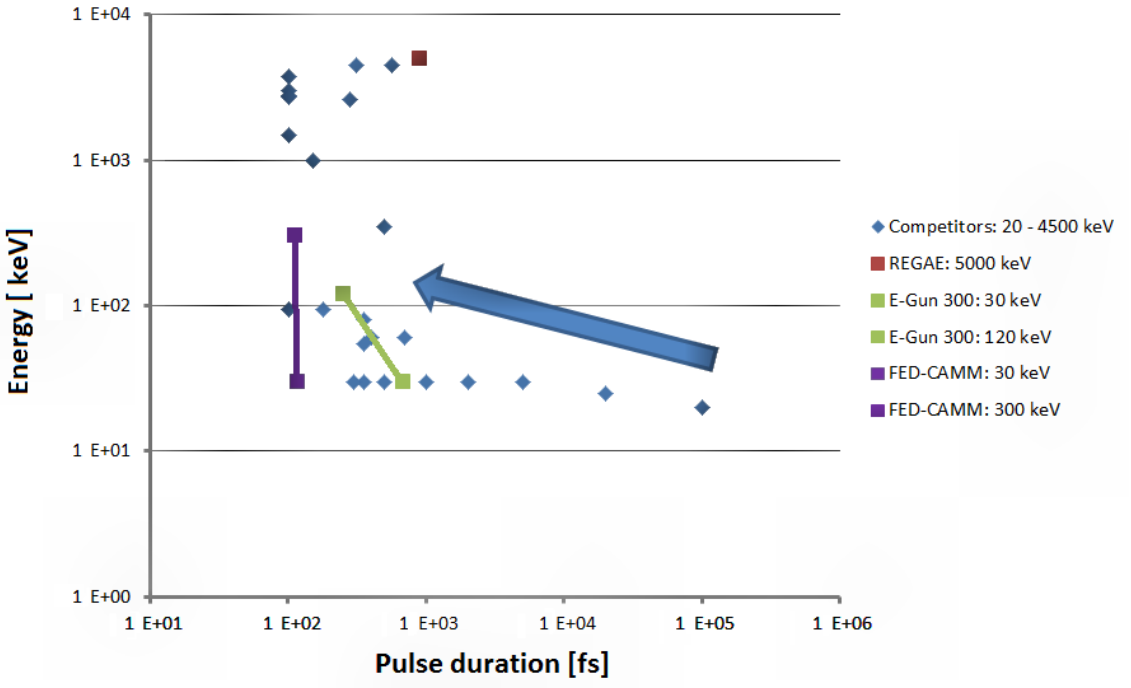

Figure 49: Comparison of worldwide FED setups with the instruments developed in this work. The big blue arrow indicates the former increase of time resolution with energy as one of the majorly changing parameters. The red dot denotes the REGAE with ≈ 5 MeV and 900 fs (fwhm) electron pulses. The green line marks the capability of the compact E-Gun 300, ranging from 690 to 250 fs (fwhm). The purple line marks the temporal resolution of the FED-CAMM instrument, ranging below 120 fs (fwhm), potentially below 70 fs (fwhm) for all applied potentials. The competitors inconsistently provide rms and fwhm specifications, mostly not specified at all. Thus many data points, especially those of a few MeV, have to be shifted by a factor of 2.355 towards longer electron pulse duration.

The overall trend over the last decades of setup development of compact setups with solely DC acceleration is a slight increase of applied electron energy. This partially led to the reduction of electron pulse duration, which is indicated by the arrow in the figure. It is observable from the simulations of the FED-CAMM instrument [especially figures 34 and 35] that not the increase of electron energy leads to shorter electron pulses. Instead, the applied electric field gradient determines the temporal resolution. A further increase of the applied electron energy seems irrelevant at energies above 60 keV [see figures 32 and 33]. The only other benefits at higher electron energies are affordable extended drift between anode and specimen and potentially larger mean free path or penetration depth, respectively.

Most of the extended rf-operated accelerators generate electron pulses of 100 fs pulse duration. They operate on par with the compact FED-CAMM apparatus. One of the major differences in respect of temporal resolution is the presence of rf-related timing jitter in rf-operated sources. This is generally not considered when only the electron pulse duration is specified for publication. In consideration of this aspect and the correction of the temporal resolution of the rms values, the gap between the FED-CAMM instrument at the 100 fs (fwhm) range and other setup widens in terms of temporal performance.

In terms of electron energy, both the E-Gun 300 and the FED-CAMM apparatus exceed the applied electric potentials of all previously existing compact DC and hybrid sources. The REGAE reaches 7 MeV at most, although this energy is currently not used for experiments. The mean energy of 5 MeV does not range far from competing rf-operated MeV sources. This is reasoned with the S-Band rf-technology, available average power of commercial clystrons and according electric field intensities in the cavities, which do not significantly vary.

Comparing the costs of the installations of this work the compact setups generally range at least one order below the REGAE project costs, which are six compared to seven figures. Since most of the commercial equipment determines the price of the compact installations, the development costs of both the E-Gun 300 and the FED-CAMM are comparable. The parts which concern the core of the FED-CAMM instrument remain relatively low-cost, which was another pursued design goal of the FED-CAMM. With optimization of manufacturing and equipment costs, the price of a compact highly time-resolved setup may be further reduced, especially with more in-house developments and industrial collaborations.

Preliminary results concern diffraction of various specimen systems, initially static followed by first time-resolved measurements. The specimens include standard systems for the calibration of the machines. The optimization of the spatial resolution of the REGAE is required prior its usage on unknown structures. The timing jitter and field errors in both rf-cavities and solenoids is so far limiting the temporal resolution to 900 fs (fwhm). The default electron beam diameter remains too large, which emphasizes the importance of the collimators, equally developed in this work. The collimators are currently used to reduce the electron beam diameter to extents which range between the sizes of the largest and smallest apertures of the collimator leafs. The apertures range from 6.5 down to 0.3 mm in size, with small incremental steps through a large variation of hole sizes. Once the size of the electron beam is corrected, the dark current collimators can be used for their intended purpose of the shielding of the most unwanted cavity electrons, which otherwise deteriorate diffraction signals.

Inhomogeneities in the fields in the rf-cavities and the various solenoids along the accelerator degenerate the electron beam dynamics of REGAE. A circumstance, which is worsened by REGAEs' large electron beam diameter. Urgent improvements of machine components are required. The diffraction patterns remain at this point similar to those of comparable rf-operated machines. It is too early for more distinct, quantitative statements about the spatial resolution, since various issues of the machine yet have to be investigated, which are included in the currently obtained diffraction patterns.

The compact E-Gun 300 can meanwhile be operated at 120 keV. This is sufficient for diffraction of most of the solid specimen systems. The energy is not yet sufficient to penetrate thicker specimen encapsulations, such as windows of liquid cells. Multiple scattering will be another issue. The time resolution measures less than 300 fs (fwhm) and is thus already suited for a wide range of time-resolved experiments. Without large modifications of the current installation the energy can be increased to 200 keV. This enables the study of specimen systems which are contained in liquid environments. The time resolution will however remain around 200 fs (fwhm) without further modifications of the remaining sections of that machine.

The FED-CAMM has results from conditioning, maximum achievable voltages, measurement of most intense electric fields which can be set for a wide range of gap sizes and has obtained first results from diffraction. As previously specified, the operation below 10 mm and 200 keV yields intense electric field gradients and results in electron pulse durations of less than 200 fs (fwhm) with 10^5 electrons per pulse. This is currently based on the set of GPT simulations of these various machine conditions. Shorter electron pulse

durations down to 70 fs (fwhm) are feasible. Less than 10^4 electrons per pulse could be used to obtain even shorter electron pulses. The use of single electron diffraction, for which references are given in the main text, emphasizes the general dependency of overall pulse duration on the number of electrons per pulse. The simulated set of initially 10^4 electrons already reaches down to 70 fs (fwhm) pulse durations within the most intense electric fields, which were experimentally obtained and stable. In contrast to single electron diffraction, the use of electron packages allows the resolution of full structures from few illuminations. The first diffraction patterns, which were recently obtained using the FED-CAMM, demonstrate the potential for full structural resolution by single electron pulses. This is very promising for time-resolved experiments on specimen with a scarce number of crystals.

The average field gradient of 15 MV/m leads to electron pulses around 109 fs (fwhm) using 10^4 electrons per pulse. No dark current was observed up to an electric field gradient of 18 MV/m after the initial conditioning of the high voltage electrodes. Since the electric field gradient is the most important parameter of such a machine which was experimentally evaluated, the simulations well indicate the actual performance of the FED-CAMM in respect of its temporal resolution. Through further conditioning and improvements on the photo-cathodes, the average electric fields can be further increased, which pushes the FED-CAMM apparatus close to the absolute limit of electron pulse durations, as it can be obtained by compact DC-operated setups. The remaining components of the system are already well known from earlier generations, matured and thus will simply serve during the first experiments, which involve static and dynamic investigations of different matter.

The diffraction patterns of various standard specimen systems compare very well to the images recorded by other machines. It should be emphasized, that the images shown in this thesis are the first images which were recorded with the FED-CAMM. The images were obtained after the conditioning of the high-voltage electrode using a new photo-cathode for a very first electron beam test. A fine-alignment of the electron optics, the insertion of a central beam block and further apertures may result in even better diffraction signals. Energy-dependent diffraction can now be investigated with electron energies ranging up to 300 keV. Solid-state, liquid- and gas-phase electron diffraction fall within the capabilities of the FED-CAMM. Any investigation can be performed with a temporal resolution that can well compete with other light sources, which are today used for time-resolved diffraction.

Photon and electron-sources remain complementary instruments for the structural investigation of matter. Especially the temporal duration of photon and electron pulses are now approaching each other. The development of the FED-CAMM of this work pushes the compact DC-operated sources on par with the rf-operated electron and photon machines. Light pulse durations on a few ten fs scale (fwhm) are obtainable using large free electron laser sources or medium to compact-sized electron sources. However, photons and electrons physically remain to interact differently with matter and thus provide different aspects of insights into the matter, besides leaving the investigated in a different condition after the interaction with the pulses. The 4^{th} generation photon sources are known for a devastating ionization of any specimen, which experiences a single pulse. This may be different at the 3^{rd} generation, which was also outlined within the previous text. Electrons generally conserve the condition of the specimen, due to very little inelastic scattering. A second precondition is, that the overall beam charge remains below the currents, which are commonly employed in electron microscopes. Consequently, each source technology has its intrinsic advantages and disadvantages for structural and dynamical structural investigations.

In the inverse diffraction mode electrons beat photons by two to three orders of magnitude, due to their much smaller de-Broglie wavelength. The overall resultant spatial resolution may not be as good as the de-Broglie wavelength would suggest, but remains in the sub-Angstrom range. This allows a refined determination of atomic positions within small scattering volumes. Due to a larger elastic scattering cross-section a packet of 10^5 electrons yields the same diffraction signal as can be obtained by 10^{11} photons in a single pulse. Additional factors of resolution are contributed by the detector technology. The capability of every electron detection adds at least a factor of 10 compared to detector arrays for x-rays. With a complementary 10^{12} photons per pulse, the standard compact electron diffraction setup already performs as well as the currently operated and upcoming photon light sources in terms of their brightness. The remaining difference to the higher peak intensities of the state-of-the-art photon sources is partially due to a microscopic bunching of electron pulses, which then in turn yields thousands to several ten thousand of photon pulses within a single shot. These strike the experimental stations in an ultrafast series, which in turn requires ultrafast readout rates at the detector stations, which yet have to be developed.

In contrast to the large facilities, which as previously mentioned comprise timing jitter and intensity fluctuations, compact DC sources such as the FED-CAMM have the other beneficial advantage of the absence of sources for such uncertainties. FELs require time and pulse stamping methods, which improves the resultant temporal resolution,

but does by far not solve all currently existing problems. Another major point that makes electrons a better suited choice for the investigation of matter is the more optimal matched penetration of electrons with optical excitation pulses. The optical pulses only reach through the first atomic layers of the specimen, before their absorption. Finally, the manufacturing costs of the compact DC sources, which were developed in this work, are constrained. The funds, which are typically required to design, construct, maintain and operate a kilometer long free electron laser, are known from newpaper articles and public tax reports. We compare a few hundred thousand Euro to several hundred million. This in turn would allow the wide-spread use of the compact sources, as opposed to the rarity of beam-time at the fourth generation light sources.

7 CONCLUSIONS AND OUTLOOK

As previously described, this work dealt with the design and construction of three instruments for time-resolved electron diffraction - the REGAE [chapter 3], the E-Gun 300 [chapter 4] and the FED-CAMM [chapter 5]. Their common goal is the conduction of time-resolved experiments to unveil atomic structural changes on the few ten femtosecond time-scale. Each machine was targeting the improvement of electron pulse dynamics, which includes pulse duration, emittance, coherence length and source brightness. Details on these instruments are provided in the according chapters. The background of molecular movies is provided by the chapter 1 of this thesis. Competing sources for the same purpose are described and listed in chapter 2 to globally benchmark the developments of this work.

The REGAE is the largest experiment in our group to date, was built and is operated in a collaboration with DESY and the University of Hamburg. Large sections of this accelerator were designed and built as tasks of this PhD work. The machine does currently not meet its simulated specifications, but experiences continuous improvements of single accelerator components.

The compact E-Gun 300 is the first time-resolved instrument world-wide that targeted an electron energy above 100 keV while being operated with static electric fields. Within this work felt the construction of this machine. The energy of the E-Gun 300 remains limited to 120 keV. This is in combination with a temporal resolution of less than 300 fs (fwhm) sufficient for various specimen and studies that concern time-resolved dynamics. The observed problems during operation in respect of the high voltage were solved by the development of the FED-CAMM.

The FED-CAMM is the state-of-the-art time-resolved electron diffraction apparatus that operates with electron energies up to 300 keV. This third instrument currently outperforms the REGAE and E-Gun 300 in terms of temporal resolution and exceeds the high voltages of all previously known compact electron diffraction setups. This compact source makes a direct competition to fourth generation light sources. Without sources of timing-jitter it can provide electron pulses shorter than 100 fs (fwhm). It was elucidated in the main text of this work, that the FED-CAMM can provide pulses, which are potentially shorter than 70 fs (fwhm). First diffraction patterns of known structures emphasize its capability and suitableness of structural solution by single electron pulses. In the following, specific conclusions concerning each instrument are drawn.

7.1 REGAE

The layout of the REGAE is most promising and yet the obtained pulse duration is limited due to rf-related field errors and timing jitter, the quantum efficiency of photo-cathodes and performance problems with the laser system. Continuing improvements will further enhance the time resolution and beam quality of this machine, which should eventually meet the initially simulated 25 fs (fwhm) and further specifications.

The REGAE was tested in terms of dark current and energy spread. The findings are found in the referenced publications of this work. The emission of dark current remains significant during the operation of REGAEs' normal conducting cavities, but the situation is greatly improved through the application of the dark current collimators, which were also developed in this work.

The development of all missing beamline and accelerator-components as part of this work enabled the commissioning of the REGAE and later on led to its first diffraction results. REGAEs' expanded capabilities enable it to perform like a highly relativistic TEM. The required lensing system is currently being installed. The highly relativistic electron pulses of this source will be used for laser-based electron acceleration into the GeV regime. With these extensions the original purpose of REGAE for time-resolved electron diffraction experiments was significantly extended throughout the past few years and leave the REGAE a prototype in various aspects.

REGAE serves as a test bed for new accelerator technology, that will be used at the European XFEL. This is not the only aspect in which REGAE and the XFEL are related to and benefit from each other. Experience gained in engineering large sections of the accelerator laid the foundations for the independent machine design of the FED-CAMM. The work related to the REGAE involved the consideration of UHV vacuum conditions and the implementation of general engineering standards, which are mandatory in the DESY environment.

7.2 E-GUN 300

Two major unexpected findings accompany the development of the E-Gun 300, which relate to the high electric potentials. Electric breakdown and the occurrence of x-ray radiation were observed. At the time that this setup was drafted, it was not fully understood what effect the increase in energy could have on the time resolution of electron pulses. It was generally believed that the higher electron energy automatically corresponds to shorter electron pulses. That this is not the case will be summarized shortly in the conclusions of the research as related to the FED-CAMM. The other aspect of the higher

targeted potential was the increased penetration depth of electrons, which had been another limiting factor of previous generation electron sources and a general drawback in electron microscopy. The first prototype however did not reach the anticipated high electron energy of 300 keV. The potential for x-ray emission from this setup was another major obstacle, which then luckily could be mitigated in later designs, operating at even higher electron energies (FED-CAMM). The fulfillment of radiation safety requirements was obtained prior to the first tests of the E-Gun 300.

The encapsulation of the photo-cathode in a ceramic mount decreases the achievable electric field gradients. The maximum applicable potential is further limited by the commercial high voltage feedthrough used. Now that these components that lower performance have been discovered, they can be changed to yield higher electron energies, more intense electric fields, and consequently shorter electron pulses, as obtained by the FED-CAMM apparatus.

The early diffraction patterns obtained by the E-Gun 300 compare well with the diffraction recorded using the REGAE. The single crystal diffraction patterns of silicon, in particular, demonstrate the feasibility of such experiments in compact sources like the E-Gun 300, as long as the pulse duration is sufficient for time-resolved studies. REGAEs' study of optimal specimen thickness or the diffraction signals correlating to different specimen thicknesses respectively, revealed that a range up to a few hundred nanometers is certainly ideal for both relativistic and highly-relativistic electron beams.

The E-Gun 300 setup is a further test vessel for the experiments at the neighboring REGAE. Novel specimen holders, such as liquid cells, can be tested here to avoid potential damage of REGAEs' ultra-high vacuum system.

Both the performance of the E-Gun 300 as well as the REGAE, which to date has remained below the design specifications, led to the development of an advanced prototype (FED-CAMM).

7.3 FED-CAMM

The reduction of pulse duration in compact sources in recent years [see tables 8 and 9 in section 2.3] is primarily due to an increase of the electric field gradient, in which the photo-excited electron pulses are accelerated, improvements of photo-cathodes and more remotely related to advances in laser sources. The pulse duration is not primarily dependent on the absolute value of the applied electric potential [see tables 34 and 35 in section 5.3]. Simulations of the FED-CAMM and similar sources reveal the electric field gradient and the initial energy spread as the two most important parameters in

electron beam dynamics, which determine the final temporal resolution of the apparatus [see tables 32 and 33 in the same section]. Next in order of importance is the overall density of electrons within the photo-excited pulses. The electric field gradient primarily influences the initial pulse broadening, which the electron pulse will experience in the gap between photo-cathode and anode, or between cathode and extraction mesh.

For lower electron energies and wider gap spacings, the shortest excitation laser pulse does not automatically result in the shortest electron pulse at the specimen position. A compression of the laser pulse under conservation of pulse intensity leads to an increase of the electron density in a shorter electron pulse. This in turn dramatically increases the Coulomb repulsion between the electrons and leads to fast pulse broadening. Below a critical electric field gradient, the shortening of the laser pulse has detrimental effects. There is an optimum for laser pulse length with constant pulse energy for each applied electric potential and gap spacing. These dependencies have to be investigated further by electron beam simulations and experiments.

For the FED-CAMM an electric field gradient of 15 MV/m was validated experimentally as a preliminary optimal working condition where no dark current occurs. This gradient relates to 150 % to 170 % of the commonly used electric field gradient of 9 MV/m to at most 10 MV/m. Further conditioning of the high voltage electrodes in a recent state of the setup led to even higher field gradients, at which no dark current was observed. The optimal laser pulse durations for 15 MV/m were determined and are listed with the general results in appendix C.

The maximum of the obtained electric field gradient of more than 27 MV/m exceeds the commonly employed maximum of 10 MV/m by approximately a factor of three. The achievement of such high electric field gradients in a static electric field is due to the optimized electrode arrangement, which was realized courtesy of research that accompanied the development of the FED-CAMM apparatus and optimized manufacturing procedures used. This enhancement is significant in respect to the generation of ultra-short electron pulses.

Uniform electric fields are required for the constant acceleration of electron pulses and the avoidance of lensing or other detrimental effects within the acceleration gap. An implementation in a compact FED setup with static electric fields requires appropriate electrode shapes, which were developed and incorporated into the FED-CAMM prototype. An electrode geometry which is a mix of a Bruce profile and elliptical shapes, both incorporating sinusoidal curves, yields the best electric field distribution in the given apparatus dimensions. The electric field enhancement ranges below 2 % for a wide range of gap spacings. Literature provides 1 % as the reference for the Bruce profile. The

widest gap spacing for which a uniform electric field can still be obtained, can be further increased by increasing the electrode dimensions. This can be accomplished easily in larger KF vacuum vessels, whose technology will lower the manufacturing costs of the setup. In instruments that incorporate lower electron energies, the size factor of the high voltage electrodes is more important than in setups with higher electron energies. An area effect correlated with increased electrode size will not compromise the operation, when the electrodes are properly conditioned.

Instruments with electron energies significantly below 60 keV, will have problems obtaining the shortest pulses. In those setups, the compaction of the setup geometry is much more important than at higher electron energies. At energies above 100 and 125 keV, the electron pulse can propagate further through the apparatus and remains compact at a distant specimen position. Hence, the higher electron energy allows for the inclusion of lenses or collimating and beam manipulating elements between the extraction pinhole of the anode plate and the specimen position.

It was shown, that a novel high voltage feedthrough assembly solves the problems of high voltage breakdown, insulator damages and high voltage instabilities. Overall, the prior limit of maximum energy imposed upon the electrons, is no longer a restriction in the design of the prototype for the FED instrument, in contrast to feedthrough in earlier setups. Generally, the maximum applicable potential ranges below the industrially specified sustainable potential, and this limitation applies from the lowest voltage to the highest voltage commercially available feedthrough. The development of this high voltage feedthrough will also be interesting for other industries and branches of science, especially those concerned with applications in UHV conditions, but not limited to these.

In combination with a general mechanic flexibility, the high voltage feedthrough assembly directly influences the most important feature of the compact femtosecond electron diffraction system, namely the electron pulse duration. By determining the electric field gradient, the emergence and disappearance of dark current electrons is controlled directly. The overall stability and performance of the electron diffraction system is significantly improved by this critical component.

In contrast to the conventional design the basic concept layout of the feedthrough can be scaled. The limitations of the conventional feedthrough were outlined in great detail in this work [see section 5.5 and the following subsections thereof]. It becomes clear that high electric field gradients can in generally not be maintained in the standard design, but a physics-related malfunction will certainly occur above critical electric field gradients. The novel feedthrough design of this work is completely impervious to the field gradients, which occur along the axis of transmission of the electric potential or

current. All of the previously occurring high-voltage feedthrough related damage was not observed in tests of the FED-CAMM instrument. The high voltage feedthrough is further no source of stray x-ray radiation.

The maximum applicable potential is currently limited by the connected high voltage power supply. The current 300 kV power supply can potentially get an upgrade to 400 kV by replacing the current power supply with a similar model from the same supplier. The ultimate energy in static electric fields can be obtained by arranging high potentials of opposite polarities against each other. With this approach, a maximum electron energy of 800 keV is within reach. The costs for the two required high voltage power supplies alone will range up to 340 k euro. If intermediate potentials are used around the core of the high potentials, mainly to decrease the emergence of stray radiation and further control of the stability, the costs will be increased further by 100 k euro. The use of a single high voltage power supply of 300 kV is a reasonable compromise and is scientifically more than sufficient currently.

The availibility of an increased range of electron energies provided by the FED-CAMM source correlates to increased penetration depth of electrons. This allows for the study of specimen systems which can be investigated in their natural, liquid environment using electron energies above 150 keV. Liquid cell encapsulations, previously developed as part of the ongoing research of the group, have now matured and are ready for testing conducted by static imaging in TEMs and certainly also by high energy time-resolved compact electron diffraction instruments, such as the FED-CAMM. The higher electron energy provides in combination with a stabilization of the high voltage a smaller energy spectrum, which leads to greater detail in diffraction.

The high electric field gradients highlighted a new phenomenon, which had not been observed before. The standard gold-coated photo-cathodes were partially uncoated by the intense electric fields. This requires us to develop tougher materials, potentially single crystalline gold disks. This will also reduce the initial energy spread of the electrons, which again acts beneficially on the electron pulse duration and spatial resolution.

Overall, this is a working proof-of-principle prototype which demonstrates, that sub 100 fs electron pulses (fwhm) can be obtained with simple DC acceleration. The short pulses are guaranteed through the connected femtosecond laser source. Although the acceleration to high energies itself in a static electric field is trivial, the implementation into a fully functional instrument requires appropriate component design, which was finally successfully developed within the second half of this PhD work. The demonstration of the functionality of the FED-CAMM prototype also replaces rf components that are usually used in the generation of short electron pulses.

The list of electron sources of chapter 2 [in particul table 8 and table 9], can now be extended by the following parameters, which belong to the instruments developed in this work.

Parameters of electron sources developed in this work.				
Reference	E [keV]	Type	t_e [fs (fwhm)] sim. (meas.)	present location
REGAE	2000 - 7000	RF + RF	25 (900)	MPSD / DESY Hamburg
E-Gun 300	30 - 120	DC	690 - 250 (< 300)	MPSD / DESY Hamburg
FED-CAMM	30 - 300	DC	80 - 180, (-)	MPSD / CFEL (DESY)

Table 14: Parameters of the REGAE, E-Gun 300 and the FED-CAMM. t_e denotes the instrument response time with respect to time resolution of the electron source.

The REGAE accelerator requires further optimization to reach the simulated short electron pulse duration of 25 fs (fwhm). The E-Gun 300 and the FED-CAMM exceed previously employed electron energies of DC and compact hybrid electron sources. All machines generated first single-shot diffraction patterns of various specimen that were used to calibrate the instruments.

The pulse duration of the E-Gun 300 is at least better than most of the other known DC machines. The only exception is the recently published work by Waldecker et al. (2015), who in turn only utilize at most $5 \cdot 10^3$ electrons per pulse to obtain electron pulse durations of less than 100 fs, opposed to 10^4 simulated and measured electrons per pulse in the E-Gun 300. With same electron numbers per pulse these machines will operate on par. The simulation of fewer electrons per pulse were discarded in this work, since single-shot structural resolution is preferred and not guaranteed with low brightness electron sources.

The pulse duration of the FED-CAMM, as obtained from simulations with 10^4 and 10^5 electrons per pulse and listed above, was not yet measured. As previously mentioned, the obtained simulation parameters using the GPT code typically yield excellent agreement with the measured response time of DC machines. This is not only proved by the agreement of simulations and measurements concerning the E-Gun 300 apparatus.

The FED-CAMM further exceeds the commonly employed electric field strength with electric gradients up to 28 MV/m, while it is operated with static electric fields at high voltages. The maintained electric fields during operation remain extremely stable at any voltage over long time. Well conditioned electrodes and photo-cathodes produce no

dark current, even at the higher electric field gradients and voltages. This significantly improves the SNR compared to RF operated sources and to those which only utilize very little charge.

The FED-CAMM defeats any of the currently existing compact DC and hybrid electron source in terms of instrument response time and operates especially close to free electron laser in respect of the pulse duration. In terms of response-time of the instrument, the FED-CAMM even outruns single fourth generation light sources. This is based on the absence of sources of major timing-jitter in DC instruments. Only residual 10 fs (fwhm) from the utilized power supply can be expected. With the much higher electric field gradients and intrinsic flexibility of the instruments parameter-space, the FED-CAMM re-creates the state-of-the-art of electron sources for femtosecond electron diffraction and sets new records with ultra-short high-brightness electron pulses.

7.5 GENERAL CONCLUSION

The availability of short electron pulses further questions the sole dependence on fourth generation light sources for time-resolved experiments, which simply demand ultra-short probe pulses of a few ten femtosecond duration. It is well known that electrons still possess a smaller wavelength than x-rays, though coherence over extended transverse areas may remain a limiting factor. When electron pulses with coherence lenghts in the few ten nanometer regime become available, in combination with a highly time-resolved character, the new electron instruments can become similarly interesting for the investigations of, for example, static and time-resolved structural biology and nano-crystallography. Basically any fast structural transformation from the fields of biology, chemistry and physics, except for direct probing of attosecond atomic electron fluctuations, may now be accessible with electrons.

Free electron laser sources, which are driven by rf-powered electron accelerators, yet have timing and intensity fluctuations. The operation of compact static DC-driven electron accelerators can be free of timing jitter, or be within an acceptable 10 fs (fwhm), at least. Once scientific communities recognize the potential of the availability of highly time-resolved electron sources, such as the FED-CAMM and further instruments, the technology can be distributed through standard commercial channels. Such a development will significantly enhance the outcome and amount of major scientific findings. With relatively inexpensive compact electron sources, individual research groups will be able to have their own time-resolved table-top electron source and investigate their preferred specimen system. Prospective findings, related to the dynamical structural changes that determine every aspect of living organisms and life in general will emerge from various users, simultaneously. Constraint available beam time at free electron laser sources and

synchrotron facilities will no longer be an issue. Applications for the investigation of specimens with priority and waiting lists will become dispensable. Furthermore, novel free-electron laser sources can then be dedicated to experiments, to which they are uniquely suited, such as investigations of electronic dynamics in molecules or condensed matter. The sheer investigation of atoms and molecules in space may be more accessible with electron sources, which directly probe the positions of the core nuclei.

Photon and electron sources continue to possess complementary features, although the state of the art of electron sources can now compete with or outperform the time resolution of fourth generation light sources, mainly due to the absence of timing jitter in compact DC electron sources. Together with further improvements of the coherence of ultra-short electron pulses, this indeed opens up an electron-bright future.

BIBLIOGRAPHY

Aeschlimann, M., Schmuttenmaer, C. A., Elsayed-Ali, H. E., Miller, R. J. D., Cao, J., Gao, Y., Mantell, D. A., 1995. Observation of surface enhanced multiphoton photoemission from metal surfaces in the short pulse limit. The Journal of Chemical Physics 102 (21), 8606–8613, doi: 10.1063/1.468962.
URL http://dx.doi.org/10.1063/1.468962

Agostini, P., Fabre, F., Mainfray, G., Petite, G., Rahman, N. K., Apr 1979. Free-free transitions following six-photon ionization of xenon atoms. Phys. Rev. Lett. 42, 1127–1130, doi: 10.1103/PhysRevLett.42.1127.
URL http://link.aps.org/doi/10.1103/PhysRevLett.42.1127

Aidelsburger, M., Kirchner, F. O., Krausz, F., Baum, P., 2010. Single-electron pulses for ultrafast diffraction. Proceedings of the National Academy of Sciences 107 (46), 19714–19719, doi: 10.1073/pnas.1010165107.
URL http://www.pnas.org/content/107/46/19714.abstract

Alpert, D., Lee, D., Lyman, E., Tomaschke, H., 11 1964. Initiation of electrical breakdown in ultrahigh vacuum. Journal of Vacuum Science and Technology 1 (2), 35–50, doi: 10.1116/1.1491722.

ALS, 2014. Advanced Light Source, 1 Cyclotron Road, Lawrence Berkeley National Laboratory, Berkeley, CA 94720-8229. Web. 18. Sep 2014.
URL http://www-als.lbl.gov/

Anderson, P., Aug 1959. Work function of gold. Phys. Rev. 115, 553554, doi: 10.1103/PhysRev.115.553.
URL http://link.aps.org/doi/10.1103/PhysRev.115.553

Armstrong, M. R., Boyden, K., Browning, N. D., Campbell, G. H., Colvin, J. D., DeHope, W. J., Frank, A. M., Gibson, D. J., Hartemann, F., Kim, J. S., King, W. E., LaGrange, T. B., Pyke, B. J., Reed, B. W., Shuttlesworth, R. M., Stuart, B. C., Torralva, B. R., 2007. Practical considerations for high spatial and temporal resolution dynamic transmission electron microscopy. Ultramicroscopy 107 (4-5), 356 – 367, doi: 10.1016/j.ultramic.2006.09.005.
URL http://dx.doi.org/10.1016/j.ultramic.2006.09.005

Armstrong, M. R., Ogilvie, J. P., Cowan, M. L., Nagy, A. M., Miller, R. J. D., 2003. Observation of the cascaded atomic-to-global length scales driving protein motion. Proceedings of the National Academy of Sciences 100 (9), 4990–4994, doi:10.1073/pnas.0936507100.
URL http://dx.doi.org/10.1073/pnas.0936507100

Arthur, J., Bergmann, U., Brunger, A., Bostedt, C., Boutet, S., Bozek, J., Cocco, D., Devereaux, T., Ding, Y., Dürr, H., Fritz, D., Gaffney, K., Galayda, J., Goldstein, J., Gührs, M., Hastings, J., Heimann, P., Hodgson, K., Huang, Z., Kelez, N., Montanez, P., Robert, A., Rowen, M., Schlotter, W., Seibert, M., Stöhr, J., Turner, J., White, W., Wu, J., Williams, G., Yachandra, V., Yano, J., 2012. Science driven instrumentation for lcls-ii - a white paper outlining science and scope of instrumentation. Tech. rep., LCLS.
URL https://portal.slac.stanford.edu/sites/lcls_public/Instrument_Document_Repository/LCLS-II_Instrumentation_Whitepaper_DOE.pdf

Auditore, L., Barna, R. C., De Pasquale, D., Interdonato, S., Italiano, A., Trifiro, A., Trimarchi, M., 2005. Compact 300kev electron gun for radiation processing. Review of Scientific Instruments 76 (12), –, doi: 10.1063/1.2140466.
URL http://dx.doi.org/10.1063/1.2140466

Australian-Synchrotron, 2014. Australian Synchrotron, 800 Blackburn Rd Clayton, VIC 3168. Web. 16. Aug 2014.
URL http://www.synchrotron.org.au/

Banford, A., 1966. The transport of charged particle beams. London: Spon Ltd.
URL http://trove.nla.gov.au/work/21970864

Barty, A., Küpper, J., Chapman, H., 2013. Molecular imaging using x-ray free-electron lasers. Annual Review of Physical Chemistry 64 (1), 415–435, doi: 10.1146/annurev-physchem-032511-143708, PMID: 23331310.
URL http://dx.doi.org/10.1146/annurev-physchem-032511-143708

Barwick, B., Corder, C., Strohaber, J., Chandler-Smith, N., Uiterwaal, C., Batelaan, H., 2007. Laser-induced ultrafast electron emission from a field emission tip. New Journal of Physics 9 (5), 142.
URL http://stacks.iop.org/1367-2630/9/i=5/a=142

Barwick, B., Park, H.-S., Kwon, O.-H., Baskin, J. S., Zewail, A. H., 2008. 4d imaging of transient structures and morphologies in ultrafast electron microscopy. Science 322 (5905), 1227–1231, doi: 10.1126/science.1164000.
URL http://www.sciencemag.org/content/322/5905/1227

Baublies-AG, 2007. Brunnenfeldstr. 42, D-71272 Renningen-Malmsheim.
URL http://www.baublies.de/

Baum, P., 2013. On the physics of ultrashort single-electron pulses for time-resolved microscopy and diffraction. Chemical Physics 423 (0), 55–61, doi: 10.1016/j.chemphys.2013.06.012.
URL http://dx.doi.org/10.1016/j.chemphys.2013.06.012

Baum, P., Zewail, A., 2008. Femtosecond diffraction with chirped electron pulses. Chemical Physics Letters 462 (1-3), 14 – 17, doi: 10.1016/j.cplett.2008.07.072.
URL http://dx.doi.org/10.1016/j.cplett.2008.07.072

Baum, P., Zewail, A. H., 2007. Attosecond electron pulses for 4d diffraction and microscopy. Proceedings of the National Academy of Sciences 104 (47), 18409–18414, doi: 10.1073/pnas.0709019104.
URL http://www.pnas.org/content/104/47/18409.abstract

Bayesteh, S., Delsim-Hashemi, H., Flöttmann, K., 2013. Beam profile monitors at regae. In: Proceedings of IBIC2013, Oxford, UK.
URL http://ibic2013.org/prepress/papers/mopf06.pdf

Bayesteh, S., Flöttmann, K., Delsim-Hashemi, H., 2014. Transverse emittance measurement at regae. In: Proceedings of IPAC2014, Dresden, Germany.
URL http://accelconf.web.cern.ch/AccelConf/IPAC2014/papers/thpme119.pdf

Beard, C., Ames, F., Austen, S., Baartman, R., Chao, Y.-C., Fong, K., Gong, C., Khan, N., Koscielniak, S., Laxdal, A., Laxdal, R., Levy, P., Louie, D., Lu, J., Merminga, L., Mitra, A., Rowbotham, D., Vincent, P., Yosifov, D., 2011. Conceptual design for the ariel 300 kev electron gun. In: Proceedings of 2011 Particle Accelerator Conference, New York, NY, USA.

Bender, H., Schwellenbach, D., Sturges, R. andTrainham, R., 2008. Variable energy 2-mev s-band linac for x-ray and other applications. In: Proceedings of EPAC08, Genoa, Italy.
URL http://accelconf.web.cern.ch/accelconf/e08/papers/tupp139.pdf

Bethe, H., 1930. Zur theorie des durchgangs schneller korpuskularstrahlen durch materie. Annalen der Physik 397 (3), 325–400, doi: 10.1002/andp.19303970303.
URL http://dx.doi.org/10.1002/andp.19303970303

Bethe, H., 1932. Bremsformel für elektronen relativistischer geschwindigkeit. Zeitschrift für Physik 76 (5-6), 293–299, doi: 10.1007/BF01342532.
URL http://dx.doi.org/10.1007/BF01342532

BM f. U., N.-u. R., f. G. f. V. B.-u. W., 1976. Verordnung über den Schutz vor Schäden durch ionisierende Strahlen, Strahlenschutzverordnung StrlSchV. BRD.

Böhlen, T., Cerutti, F., Chin, M., Fasso, A., Ferrari, A., Ortega, P., Mairani, A., Sala, P., Smirnov, G., Vlachoudis, V., 2014. The {FLUKA} code: Developments and challenges for high energy and medical applications. Nuclear Data Sheets 120 (0), 211 – 214, doi: 10.1016/j.nds.2014.07.049.
URL http://dx.doi.org/10.1016/j.nds.2014.07.049

Brinkmann, A., Reschke, D., Ziegler, J., 2008. Various applications of dry-ice cleaning in the field of accelerator components at desy. In: Proceedings of LINAC08, Victoria, BC,

Canada.
URL http://accelconf.web.cern.ch/accelconf/LINAC08/papers/thp013.pdf

Bruce, F., April 1947. Calibration of uniform-field spark-gaps for high-voltage measurement at power frequencies. Electrical Engineers - Part II: Power Engineering, Journal of the Institution of 94 (38), 138–149, doi: 10.1049/ji-2.1947.0052.
URL http://dx.doi.org/10.1049/ji-2.1947.0052

Bruzzese, R., Sasso, A., Solimeno, S., 1989. Multiphoton excitation and ionization of atoms and molecules. La Rivista del Nuovo Cimento 12 (7), 1–105, doi:10.1007/BF02743063.
URL http://dx.doi.org/10.1007/BF02743063

Cao, J., Hao, Z., Park, H., Tao, C., Kau, D., Blaszczyk, L., 2003. Femtosecond electron diffraction for direct measurement of ultrafast atomic motions. Applied Physics Letters 83 (5), 1044–1046, doi: 10.1063/1.1593831.
URL http://dx.doi.org/10.1063/1.1593831

CeramTec, 2012. North America Corp, One Technology Place, Laurens, SC 29360, USA. http://www.ceramtec.us/.

Chang, C.-C., Kuo, H.-S., Hwang, I.-S., Tsong, T. T., 2009. A fully coherent electron beam from a noble-metal covered w(111) single-atom emitter. Nanotechnology 20 (11), 115401.
URL http://stacks.iop.org/0957-4484/20/i=11/a=115401

Chapman, H., Fromme, P., Barty, A., White, T., Kirian, R., Aquila, A., Hunter, M., Schulz, J., DePonte, D., Weierstall, U., Doak, R., Maia, F., Martin, A., Schlichting, I., Lomb, L., Coppola, N., Shoeman, R., Epp, S., Hartmann, R., Rolles, D., Rudenko, A., Foucar, L., Kimmel, N., Weidenspointner, G., Holl, P., Liang, M., Barthelmess, M.and Caleman, C., Boutet, S., Bogan, M., Krzywinski, J., Bostedt, C., Bajt, S., Gumprecht, L., Rudek, B., Erk, B., Schmidt, C., Homke, A., Reich, C., Pietschner, D., Struder, L., Hauser, G., Gorke, H., Ullrich, J., Herrmann, S., Schaller, G., Schopper, F., Soltau, H., Kuhnel, K.-U., Messerschmidt, M., Bozek, J., Hau-Riege, S., Frank, M., Hampton, C., Sierra, R., Starodub, D., Williams, G., Hajdu, J., Timneanu, N., Seibert, M., Andreasson, J., Rocker, A., Jonsson, O., Svenda, M., Stern, S., Nass, K., Andritschke, R., Schroter, C.-D., Krasniqi, F., Bott, M., Schmidt, K., Wang, X., Grotjohann, I., Holton, J., Barends, T., Neutze, R., Marchesini, S., Fromme, R., Schorb, S., Rupp, D., Adolph, M., Gorkhover, T., Andersson, I., Hirsemann, H., Potdevin, G., Graafsma, H., Nilsson, B., Spence, J., Feb. 2011. Femtosecond x-ray protein nanocrystallography. Nature 470 (7332), 73–77, doi: 10.1038/nature09750.
URL http://dx.doi.org/10.1038/nature09750

Chatelain, R., Morrison, V., Godbout, C., van der Geer, B., de Loos, M., Siwick, B., 2012a. Space-charge effects in ultrafast electron diffraction patterns from single crystals.

Ultramicroscopy 116 (0), 86 – 94, doi: 10.1016/j.ultramic.2012.03.001.
URL http://dx.doi.org/10.1016/j.ultramic.2012.03.001

Chatelain, R. P., Morrison, V. R., Godbout, C., Siwick, B. J., 2012b. Ultrafast electron diffraction with radio-frequency compressed electron pulses. Applied Physics Letters 101 (8), –, doi: 10.1063/1.4747155.
URL http://dx.doi.org/10.1063/1.4747155

Christophorou, L., Olthoff, J., Green, D., 1997. Gases for electrical insulation and arc interruption: Possible present and future alternatives to pure sf6. NIST Technical Note 1425 -, –.
URL http://www.epa.gov/highgwp/electricpower-sf6/documents/new_report_final.pdf

CLS-Inc., 2014. Canadian Light Source Inc., 44 Innovation Boulevard, Saskatoon, SK, S7N 2V3, Canada. Web. 16. Aug 2014.
URL http://www.lightsource.ca/

Corning-Inc., 1851. Macor machinable glass ceramic.
URL http://www.corning.com/

Cosslett, V. E., 1978. Radiation damage in the high resolution electron microscopy of biological materials: A review. Journal of Microscopy 113 (2), 113–129, doi: 10.1111/j.1365-2818.1978.tb02454.x.
URL http://dx.doi.org/10.1111/j.1365-2818.1978.tb02454.x

Cowan, M., Bruner, B., Huse, N., Dwyer, J., Chugh, B., Nibbering, E., Elsaesser, T., Miller, R., 3 2005. Ultrafast memory loss and energy redistribution in the hydrogen bond network of liquid h_20. Nature 434, 199–202, doi:10.1038/nature03383.
URL http://dx.doi.org/10.1038/nature03383

Craggs, J., Meek, J., 1954. High voltage laboratory technique. Butterworths Scientific Publications.

CST, 2014. Computer simulation technoloty (cst).
URL http://www.cst.com

Cultrera, L., 2011. Cathodes for photoemission guns. In: Proceedings of 2011 Particle Accelerator Conference, New York, NY, USA.

Cultrera, L., Bazarov, I., Conway, J., Dunham, B., Hwang, Y., Li, Y., Liu, X., Moore, T., Merluzzi, R., Smolenski, K., Karkare, S., Maxson, J., Schaff, W., 2012. Photocathode r&d at cornell university. In: Proceedings of IPAC2012, New Orleans, Louisiana, USA.

Dangwal, A., Müller, G., Reschke, D., Flöttmann, K., Singer, X., 2007. Effective removal of field-emitting sites from metallic surfaces by dry ice cleaning. Journal of Applied

Physics 102 (4), –, doi: 10.1063/1.2772505.
URL http://dx.doi.org/10.1063/1.2772505

Daniel, T., Harris, F., 1970. The spatial growth of ionization currents in nitrogen at voltages up to 500 kv. Journal of Physics B: Atomic and Molecular Physics 3 (3), 363.
URL http://stacks.iop.org/0022-3700/3/i=3/a=007

De Loos, M. j., Van Der Geer, C. a. j., 2006. The general particle tracer (gpt) code. Gerontechnology.
URL http://www.pulsar.nl/gpt/

Delsim-Hashemi, H., Floettmann, K., Seebach, M., Bayesteh, S., 2013. Charge monitors at the relativistic electron gun for atomic exploration - regae. In: Proceedings of IBIC2013, Oxford, UK.
URL http://ibic2013.org/prepress/papers/wepf24.pdf

Delsim-Hashemi, H., Flöttmann, K., 2014. Dark current studies at relativistic electron gun for atomic exploration - regae. In: Proceedings of IPAC2014, Dresden, Germany.
URL http://accelconf.web.cern.ch/AccelConf/IPAC2014/papers/mopri027.pdf

DESY, 2014a. Deutsches Elektronen-Synchrotron DESY, Notkestraße 85, D-22607 Hamburg. Web. 18. Sep 2014.
URL http://petra3.desy.de/

DESY, 2014b. Flash 1 parameter. Deutsche Elektronen-Synchrotron DESY. Web. 28 July 2014.
URL http://photon-science.desy.de/facilities/flash/flash_parameters/index_eng.html

DESY, 2014c. Prospective xfel parameter. Deutsche Elektronen-Synchrotron DESY. Web. 28 July 2014.
URL http://xfel.desy.de/technical_information/

DESY, 2014d. Relativistic electron gun for atomic exploration. Deutsche Elektronen-Synchrotron DESY. Web. 28 July 2014.
URL http://regae.desy.de/

Diamond, 2014. Diamond Light Source Ltd, Diamond House, Harwell Science & Innovation Campus, Didcot, Oxfordshire, OX11 0DE. Web. 18. Sep 2014.
URL http://www.diamond.ac.uk/

Dudek, R. C., Weber, P. M., 2001. Ultrafast diffraction imaging of the electrocyclic ring-opening reaction of 1,3-cyclohexadiene. The Journal of Physical Chemistry A 105 (17), 4167–4171, doi: 10.1021/jp010122t.
URL http://dx.doi.org/10.1021/jp010122t

Dwyer, J., Hebeisen, C., Ernstorfer, R., Harb, M., Deyirmenjian, V., Jordan, R., Miller, R., 2006. Femtosecond electron diffraction: "making the molecular movie". Philosophical Transactions of the Royal Society of London A: Mathematical, Physical and Engineering Sciences 364 (1840), 741–778, doi: 10.1098/rsta.2005.1735.
URL http://www.doi.org/10.1098/rsta.2005.1735

Dwyer, J., Jordan, R., Hebeisen, C., Harb, M., Ernstorfer, R., Dartigalongue, T., Miller, R., 2007. Femtosecond electron diffraction: an atomic perspective of condensed phase dynamics. Journal of Modern Optics 54 (7), 905–922, doi: 10.1080/09500340601095348.
URL http://dx.doi.org/10.1080/09500340601095348

Eichberger, M., Krumova, M., Berger, H., Demsar, J., 2013. Sample preparation methods for femtosecond electron diffraction experiments. Ultramicroscopy 127 (0), 9–13, frontiers of Electron Microscopy in Materials Science, doi: 10.1016/j.ultramic.2012.07.005.
URL http://dx.doi.org/10.1016/j.ultramic.2012.07.005

Elizondo, J. M., Benze, J. W., Moeny, W. M., Small, J. G., Apr 1985. High performance electrode profile generation method. Review of Scientific Instruments 56 (4), 532–534, doi: 10.1063/1.1138281.
URL http://dx.doi.org/10.1063/1.1138281

Ernstorfer, R., Harb, M., Hebeisen, C., Sciaini, G., Dartigalongue, T., Miller, R., 2009. The formation of warm dense matter: Experimental evidence for electronic bond hardening in gold. Science 323 (5917), 1033–1037, doi: 10.1126/science.1162697.
URL http://www.sciencemag.org/content/323/5917/1033.abstract

Farish, O., Tedford, D., 1966. Cathode spots in the transient glow discharge in nitrogen. British Journal of Applied Physics 17 (7), 965.
URL http://stacks.iop.org/0508-3443/17/i=7/a=418

Farish, O., Tedford, D., 1969. Similarity in air and nitrogen i. breakdown voltages. Journal of Physics D: Applied Physics 2 (11), 1555.
URL http://stacks.iop.org/0022-3727/2/i=11/a=310

Farrall, G., Oct 1985. Electrical breakdown in vacuum. Electrical Insulation, IEEE Transactions on EI-20 (5), 815–841, doi: 10.1109/TEI.1985.348842.
URL http://dx.doi.org/10.1109/TEI.1985.348842

Felber, M., Hoffmann, M., Mavric, U., Schlarb, H., Schulz, S., Jalmuzna, W., 2012. Laser synchronization at regae using phase detection at an intermediate frequency. In: Proceedings of IPAC2012, New Orleans, Louisiana, USA.
URL http://accelconf.web.cern.ch/AccelConf/IPAC2012/papers/WEPPD048.PDF

Ferrari, A., Sala, P., Fasso, A., Ranft, J., 2005. FLUKA: a multi-particle transport code.
URL http://www.slac.stanford.edu/cgi-wrap/getdoc/slac-r-773.pdf

Fill, E., Veisz, L., Apolonski, A., Krausz, F., 2006. Sub-fs electron pulses for ultrafast electron diffraction. New Journal of Physics 8 (11), 272, doi: 10.1088/1367-2630/8/11/272.
URL http://iopscience.iop.org/1367-2630/8/11/272/

Fischer, H., 1894. Einfluß der konfiguration auf die wirkung der enzyme. Ber. Dtsch. Chem. Ges. 27, 2985–2993, doi:10.1002/cber.18940270364.
URL http://dx.doi.org/10.1002/cber.18940270364

Flöttmann, K., 1997. A space charge tracking algorithm.
URL http://www.desy.de/~mpyflo

Flöttmann, K., 2010. Design and performance of printed circuit steering magnets for the flash injector. In: Proceedings of IPAC'10, Kyoto, Japan.
URL https://accelconf.web.cern.ch/accelconf/IPAC10/papers/mopeb003.pdf

Flöttmann, K., 2014. Generation of sub-fs electron beams at few-mev energies. Nuclear Instruments and Methods in Physics Research Section A: Accelerators, Spectrometers, Detectors and Associated Equipment 740 (0), 34–38, proceedings of the first European Advanced Accelerator Concepts Workshop 2013, doi: 10.1016/j.nima.2013.12.031.
URL http://dx.doi.org/10.1016/j.nima.2013.12.031

Fowler, R. H., Nordheim, L., 5 1928. Electron emission in intense electric fields. Proceedings of the Royal Society of London 119 (781), 173 – 181.
URL http://www.jstor.org/discover/10.2307/95023?uid=3737864&uid=2&uid=4&sid=21105093301073

Gahlmann, A., Tae Park, S., Zewail, A. H., 2008. Ultrashort electron pulses for diffraction, crystallography and microscopy: theoretical and experimental resolutions. Phys. Chem. Chem. Phys. 10, 2894–2909, doi: 10.1039/B802136H.
URL http://dx.doi.org/10.1039/B802136H

Gao, M., Jean-Ruel, H., Cooney, R. R., Stampe, J., de Jong, M., Harb, M., Sciaini, G., Moriena, G., Miller, R. J. D., May 2012. Full characterization of rf compressed femtosecond electron pulses using ponderomotive scattering. Opt. Express 20 (11), 12048–12058, doi: 10.1364/OE.20.012048.
URL http://www.opticsexpress.org/abstract.cfm?URI=oe-20-11-12048

Gao, M., Lu, C., Jean-Ruel, H., Liu, L. C., Marx, A., Onda, K., Koshihara, S., Nakano, Y., Shao, X., Hiramatsu, T., Saito, G., Yamochi, H., Cooney, R. R., Moriena, G., Sciaini, G., Miller, R. J. D., 4 2013. Mapping molecular motions leading to charge delocalization with ultrabright electrons. Nature 7445 (496), 343–346, doi:10.1038/nature12044.
URL http://dx.doi.org/10.1038/nature12044

Genberg, L., Richard, L., McLendon, G., Miller, R., 1991. Direct observation of global protein motion in hemoglobin and myoglobin on picosecond time scales. Science

251 (4997), 1051–1054, doi: 10.1126/science.1998121.
URL http://www.sciencemag.org/content/251/4997/1051.abstract

Giere, S., Kurrat, M., Schumann, U., 2002. Hv dielectric strength of shielding electrodes in vacuum circuit-breakers. In: Discharges and Electrical Insulation in Vacuum, 2002. 20th International Symposium on. pp. 119–122, doi: 10.1109/ISDEIV.2002.1027323.
URL http://dx.doi.org/10.1109/ISDEIV.2002.1027323

Gledhill, J. A., 1973. The range-energy relation for 0.1-600 kev electrons. Journal of Physics A: Mathematical, Nuclear and General 6 (9), 1420.
URL http://stacks.iop.org/0301-0015/6/i=9/a=017

Gliserin, A., Apolonski, A., Krausz, F., Baum, P., 2012. Compression of single-electron pulses with a microwave cavity. New Journal of Physics 14 (7), 073055, doi: 10.1088/1367-2630/14/7/073055.
URL http://iopscience.iop.org/1367-2630/14/7/073055/

Goebel, D. M., Schneider, A., Aug 2005. High-voltage breakdown and conditioning of carbon and molybdenum electrodes. Plasma Science, IEEE Transactions on 33 (4), 1136–1148, doi: 10.1109/TPS.2005.852410.
URL http://dx.doi.org/10.1109/TPS.2005.852410

Goodson, B., Ruan, C.-Y., Lobastov, V., Srinivasan, R., Zewail, A., 2003. Ultrafast electron diffraction: complex landscapes of molecular structures in thermal and light-mediated reactions. Chemical Physics Letters 374 (5-6), 417 – 424, doi: 10.1016/S0009-2614(03)00803-0.
URL http://dx.doi.org/10.1016/S0009-2614(03)00803-0

Grebenyuk, J., Mehrling, T., Tsung, F., Floettman, K., Osterhoff, J., 2012. Simulations of laser-wakefield acceleration with external electron-bunch injection for regae experiments at desy. AIP Conference Proceedings 1507 (1), 688–692, doi: 10.1063/1.4773781.
URL http://dx.doi.org/10.1063/1.4773781

Grüner, F., Becker, S., Schramm, U., Eichner, T., Fuchs, M., Weingartner, R., Habs, D., Meyer-ter Vehn, J., Geissler, M., Ferrario, M., Serafini, L., van der Geer, B., Backe, H., Lauth, W., Reiche, S., 2007. Design considerations for table-top, laser-based vuv and x-ray free electron lasers. Applied Physics B 86 (3), 431–435, doi: 10.1007/s00340-006-2565-7.
URL http://dx.doi.org/10.1007/s00340-006-2565-7

Hachmann, M., 2012. Transverse emittance measurement at regae via a solenoid scan. diploma thesis. university of hamburg.

Hada, M., Hirscht, J., Zhang, D., Manz, S., Pichugin, K., Mazurenko, D., Bayesteh, S., Delsim-Hashemi, H., Floettmann, K., Huening, M., Lederer, S., Moriena, G.,

Mueller, C., Sciaini, G., Miller, R., 2012. Regae: New source for atomically resolved dynamics. In: Research in Optical Sciences. Optical Society of America, p. JT2A.47, doi:10.1364/HILAS.2012.JT2A.47.
URL http://dx.doi.org/10.1364/HILAS.2012.JT2A.47

Hada, M., Pichugin, K., Sciaini, G., 2013. Ultrafast structural dynamics with table top femtosecond hard x-ray and electron diffraction setups. The European Physical Journal Special Topics 222 (5), 1093–1123, doi: 10.1140/epjst/e2013-01909-9.
URL http://dx.doi.org/10.1140/epjst/e2013-01909-9

Hada, M., Zhang, D., Pichugin, K., Hirscht, J., Kochman, M., Hayes, S., Manz, S., Gengler, R., Wann, D. A., Seki, T., Moriena, G., Morrison, C., Matsuo, J., Sciaini, G., Miller, R., 3 2014. Cold ablation driven by localized forces in alkali halides. Nat Commun 5, –, doi:10.1038/ncomms4863.
URL http://dx.doi.org/10.1038/ncomms4863

Han, J.-H., 2005. Dynamics of electron beam and dark current in photocathode rf guns. Ph.D. thesis, Department of physics, University of Hamburg.
URL http://www.physnet.uni-hamburg.de/services/fachinfo/___Kurzfassungen/Jang-Hui___Han.htm

Han, J. H., Bahr, J., Grabosch, H.-J., Krasilnikov, M., Miltchev, V., Oppelt, A., Petrosyan, B., Riemann, S., Staykov, L., Stephan, F., Hartrott, M., Flöttmann, K., Schreiber, S., Ronsch, J., Michelato, P., Monaco, L., Sertore, D., 2005. Dark current and multipacting in the photocathode rf guns at pitz. In: Proceedings of 2005 Particle Accelerator Conference, Knoxville, Tennessee.
URL http://accelconf.web.cern.ch/accelconf/p05/PAPERS/WPAP004.PDF

Han, J.-H., Flöttmann, K., 2006. Dark current collimation and modified gun geometry for the european x-ray fel project. In: Proceedings of FEL 2006, BESSY, Berlin, Ge.
URL http://accelconf.web.cern.ch/Accelconf/f06/PAPERS/THPPH012.PDF

Harb, M., Ernstorfer, R., Hebeisen, C., Sciaini, G., Peng, W., Dartigalongue, T., Eriksson, M., Lagally, M. G., Kruglik, S., Miller, R., Apr 2008. Electronically driven structure changes of si captured by femtosecond electron diffraction. Phys. Rev. Lett. 100, 155504, doi: 10.1103/PhysRevLett.100.155504.
URL http://link.aps.org/doi/10.1103/PhysRevLett.100.155504

Harrison, J., 1967. A computer study of uniform-field electrodes. British Journal of Applied Physics 18 (11), 1617.
URL http://stacks.iop.org/0508-3443/18/i=11/a=316

Harrison, J., 1977. The electric field on the surface of bruce electrodes. Journal of Electrostatics 2 (4), 327–330, doi: 10.1016/0304-3886(77)90003-1.
URL http://dx.doi.org/10.1016/0304-3886(77)90003-1

Hassanvand, A., Illias, H., Mokhlis, H., Bakar, A., March 2014. Effects of corona ring dimensions on the electric field distribution on 132 kv glass insulator. In: Power Engineering and Optimization Conference (PEOCO), 2014 IEEE 8th International. pp. 248–251, doi: 10.1109/PEOCO.2014.6814434.

Hastings, J. B., Rudakov, F. M., Dowell, D. H., Schmerge, J. F., Cardoza, J. D., Castro, J. M., Gierman, S. M., Loos, H., Weber, P. M., 2006. Ultrafast time-resolved electron diffraction with megavolt electron beams. Applied Physics Letters 89 (18), –, doi: 10.1063/1.2372697.
URL http://dx.doi.org/10.1063/1.2372697

Hauri, C. P., Ganter, R., Le Pimpec, F., Trisorio, A., Ruchert, C., Braun, H. H., Jun 2010. Intrinsic emittance reduction of an electron beam from metal photocathodes. Phys. Rev. Lett. 104, 234802, doi: 10.1103/PhysRevLett.104.234802.
URL http://link.aps.org/doi/10.1103/PhysRevLett.104.234802

Hebeisen, C., Ernstorfer, R., Harb, M., Dartigalongue, T., Jordan, R., Miller, R., Dec 2006. Femtosecond electron pulse characterization using laser ponderomotive scattering. Opt. Lett. 31 (23), 3517–3519, doi: 10.1364/OL.31.003517.
URL http://ol.osa.org/abstract.cfm?URI=ol-31-23-3517

Hebeisen, C., Sciaini, G., Harb, M., Ernstorfer, R., Dartigalongue, T., Kruglik, S., Miller, R., Mar 2008. Grating enhanced ponderomotive scattering for visualization and full characterization of femtosecond electron pulses. Opt. Express 16 (5), 3334–3341, doi: 10.1364/OE.16.003334.
URL http://www.opticsexpress.org/abstract.cfm?URI=oe-16-5-3334

Heinzinger-GmbH, 2012. Heinzinger electronic GmbH, Anton-Jakob-Strasse 4, D - 83026 Rosenheim.
URL http://www.heinzinger.de

Helmholtz-Zentrum, 2014. Helmholtz-Zentrum Berlin für Materialien und Energie GmbH. Hahn-Meitner-Platz 1, D-14109 Berlin. Web. 16. Aug 2014.
URL http://www.helmholtz-berlin.de/quellen/bessy/

Henderson, R., 5 1995. The potential and limitations of neutrons, electrons and x-rays for atomic resolution microscopy of unstained biological molecules. Quarterly Reviews of Biophysics 28, 171–193, doi: 10.1017/S003358350000305X.
URL http://journals.cambridge.org/article_S003358350000305X

Hirano, K., Nomura, M., Fukuda, M., M., T., Yamazaki, Y., Muto, T., Araki, S., Terunuma, N., Kuriki, M., Akemoto, M., Hayano, H., Urakawa, J., 2004. Development of a multi-bunch photo-cathode rf gun system. In: Proceedings of EPAC 2004, Lucerne, Switzerland.
URL http://accelconf.web.cern.ch/AccelConf/e04/PAPERS/THPLT061.PDF

Hirscht, J., 10 2009. Development of an easy to comission electron beam model. diploma thesis. university of hamburg.

Hoffmann, M., Butkowski, L., Schmidt, C., Schlarb, H., Koehler, W., Piotrowski, A., Rutkowski, I., Rybaniec, R., 2014. High speed digitial llrf feedbacks for normal conducting cavity operation. In: Proceedings of IPAC2014, Dresden, Germany.
URL http://accelconf.web.cern.ch/AccelConf/IPAC2014/papers/wepme066.pdf

Hoffmann, M., Kay, H., Mavric, U., Schlarb, H., Schmidt, C., Jalmuzna, W., Kozak, T., Piotrowski, A., 2013. Precision llrf controls for the s-band accelerator regae. In: Proceedings of IPAC2013, Shanghai, China.
URL http://accelconf.web.cern.ch/accelconf/IPAC2013/papers/wepme008.pdf

Hommelhoff, P., Sortais, Y., Aghajani-Talesh, A., Kasevich, M. A., 2 2006. Field emission tip as a nanometer source of free electron femtosecond pulses. Phys. Rev. Lett. 96, 077401, doi: 10.1103/PhysRevLett.96.077401.
URL http://dx.doi.org/10.1103/PhysRevLett.96.077401

ICRU, 1980. Quantitative concepts and dosimetry in radiobiology. ICRU report 30, address: 7910 Woodmont Avenue, Suite 400, Bethesda, MD 20814-3095, USA.
URL http://www.icru.org/

ICRU, 1984. Radiation dosimetry: Electron beams with energies between 1 and 50 mev. ICRU report 35, address: 7910 Woodmont Avenue, Suite 400, Bethesda, MD 20814-3095, USA.
URL http://www.icru.org/

Ihee, H., Lobastov, V. A., Gomez, U. M., Goodson, B. M., Srinivasan, R., Ruan, C.-Y., Zewail, A. H., 2001. Direct imaging of transient molecular structures with ultrafast diffraction. Science 291 (5503), 458–462, doi: 10.1126/science.291.5503.458.
URL http://www.sciencemag.org/content/291/5503/458.abstract

Ilhan, S., Ozdemir, A., 11 2011. Effects of corona ring design upon impulse voltage withstand level of 380 kv v-strings. Dielectrics and Electrical Insulation, IEEE Transactions on 18 (5), 1638–1646, doi: 10.1109/TDEI.2011.6032834.

Imhof, A., 1957. Hochspannungs-Isolierstoffe. Verlag G. Braun - Karlsruhe.

Irie, M., 2010. Photochromism of diarylethene molecules and crystals. Proceedings of the Japan Academy, Series B 86 (5), 472–483, doi:10.2183/pjab.86.472.
URL http://dx.doi.org/10.2183/pjab.86.472

Ischenko, A., Golubkov, V., Spiridonov, V., Zgurskii, A., Akhmanov, A., Vabischevich, M., Bagratashvili, V., 1983. A stroboscopical gas-electron diffraction method for the investigation of short-lived molecular species. Applied Physics B 32 (3), 161–163, doi:

10.1007/BF00688823.
URL http://dx.doi.org/10.1007/BF00688823

Janzen, A., Krenzer, B., Heinz, O., Zhou, P., Thien, D., Hanisch, A., Meyer zu Heringdorf, F.-J., von der Linde, D., Horn von Hoegen, M., 2007. A pulsed electron gun for ultrafast electron diffraction at surfaces. Review of Scientific Instruments 78 (1), –, doi: 10.1063/1.2431088.
URL http://dx.doi.org/10.1063/1.2431088

Joy, T., 1990. Electrostatic accelerator tubes âĂŤ recent progress and future directions. Nuclear Instruments and Methods in Physics Research Section A: Accelerators, Spectrometers, Detectors and Associated Equipment 287 (1-2), 48–63, doi: 10.1016/0168-9002(90)91766-5.
URL http://dx.doi.org/10.1016/0168-9002(90)91766-5

Jüttner, B., Siemroth, P., 1981. über den gleichspannungsdurchschlag im ultrahochvakuum. Beiträge aus der Plasmaphysik 21 (4), 233–245, doi: 10.1002/ctpp.19810210402.
URL http://dx.doi.org/10.1002/ctpp.19810210402

Kan, K., Kondoh, T., Yang, J., Yoshida, Y., 2007. Simulation study on attosecond electron bunch generation. In: edings of PAC07, Albuquerque, New Mexico, USA.
URL http://accelconf.web.cern.ch/accelconf/p07/PAPERS/THPMN036.PDF

Katz, L., Penfold, A. S., Jan 1952. Range-energy relations for electrons and the determination of beta-ray end-point energies by absorption. Rev. Mod. Phys. 24, 28–44, doi: 10.1103/RevModPhys.24.28.
URL http://link.aps.org/doi/10.1103/RevModPhys.24.28

King, W. E., Campbell, G. H., Frank, A., Reed, B., Schmerge, J. F., Siwick, B. J., Stuart, B. C., Weber, P. M., 2005. Ultrafast electron microscopy in materials science, biology, and chemistry. J. Appl. Phys. 97 (11), –, doi:10.1063/1.1927699.
URL http://dx.doi.org/10.1063/1.1927699

Kneisel, P., Lewis, B., 1995. Advanced surface cleaning methods - three years of experience with high pressure ultrapure water rinsing of superconducting cavities. In: Proceedings of the 1995 Workshop on RF Superconductivity, Gif-sur-Yvette, France.
URL http://accelconf.web.cern.ch/accelconf/SRF95/papers/srf95l02.pdf

Korenev, S., 2003. The pulsed electron accelerator for radiation technologies. In: Proceedings of the 2003 Particle Accelerator Conference.
URL http://accelconf.web.cern.ch/accelconf/p03/PAPERS/TPPE031.PDF

Korolyov, A., Simonov, K., Pirozhenko, V., 2001. Design of compact system with wide electron beam for radiation technologies. In: Questions of nuclear science and

engineering 2001.
URL http://vant.kipt.kharkov.ua/ARTICLE/VANT_2001_3/article_2001_3_30.pdf

Kraemer, D., Cowan, M. L., Paarmann, A., Huse, N., Nibbering, E. T. J., Elsaesser, T., Miller, R. J. D., 2008. Temperature dependence of the two-dimensional infrared spectrum of liquid h2o. Proceedings of the National Academy of Sciences 105 (2), 437–442, doi:10.1073/pnas.0705792105.
URL http://dx.doi.org/10.1073/pnas.0705792105

Küchler, A., 2009. Hochspannungstechnik: Grundlagen - Technologie - Anwendungen. VDI-Buch. Springer.

Kumar, V., 2009. Understanding the focusing of charged particle beams in a solenoid magnetic field. American Journal of Physics 77 (8), 737–741, doi: 10.1119/1.3129242.
URL http://dx.doi.org/10.1119/1.3129242

Kung, P., Lihn, H.-C., Wiedemann, H., Bocek, D., Aug 1994. Generation and measurement of 50-fs (rms) electron pulses. Phys. Rev. Lett. 73, 967–970, doi: 10.1103/PhysRevLett.73.967.
URL http://link.aps.org/doi/10.1103/PhysRevLett.73.967

LaGrange, L., Reed, B. W., Santala, M. K., McKeown, J. T., Kulovits, A., Wiezorek, J. M. K., Nikolova, L., Rosei, F., Siwick, Campbell, G. H., 2012. Approaches for ultrafast imaging of transient materials processes in the transmission electron microscope. Micron 43 (11), 1108 – 1120, in situ {TEM}, doi: 10.1016/j.micron.2012.04.010.
URL http://dx.doi.org/10.1016/j.micron.2012.04.010

Lahme, S., Kealhofer, C., Krausz, F., Baum, P., 2014. Femtosecond single-electron diffraction. Structural Dynamics 1 (3), –, doi: 10.1063/1.4884937.
URL http://dx.doi.org/10.1063/1.4884937

Lederer, S., Schreiber, S., Michelato, P., Monaco, L., Pagani, C., Sertore, D., Han, J. H., 2008. Photocathode studies at flash. In: Proceedings of EPAC08, Genoa, Italy.
URL http://epaper.kek.jp/e08/papers/mopc072.pdf

Li, J., Liu, Z., Tan, C., Guo, X., Wand, L., Sancar, A., Zhong, D., 08 2010a. Dynamics and mechanism of repair of ultraviolet-induced (6-4) photoproduct by photolyase. Nature 466, 887–890, doi:10.1038/nature09192.
URL http://dx.doi.org/10.1038/nature09192

Li, R., Huang, W., Du, Y., Yan, L., Du, Q., Shi, J., Hua, J., Chen, H., Du, T., Xu, H., Lu, X., Tang, C., 2010b. Recent progress of mev ultrafast electron diffraction at tsinghua university. In: Proceedings of IPAC'10, Kyoto, Japan.

Li, R., Huang, W., Du, Y., Yan, L., Du, Q., Shi, J., Hua, J., Chen, H., Du, T., Xu, H., Tang, C., 2010c. Note: Single-shot continuously time-resolved mev ultrafast electron diffraction. Review of Scientific Instruments 81 (3), –, doi:10.1063/1.3361196.
URL http://dx.doi.org/10.1063/1.3361196

Li, R., Tang, C., Du, Y., Huang, W., Du, Q., Shi, J., Yan, L., Wang, X., 2009. Experimental demonstration of high quality mev ultrafast electron diffraction. Review of Scientific Instruments 80 (8), –, doi: 10.1063/1.3194047.
URL http://dx.doi.org/10.1063/1.3194047

Li, R. K., Musumeci, P., Bender, H. A., Wilcox, N. S., Wu, M., 2011. Imaging single electrons to enable the generation of ultrashort beams for single-shot femtosecond relativistic electron diffraction. Journal of Applied Physics 110 (7), –, doi: 10.1063/1.3646465.
URL http://dx.doi.org/10.1063/1.3646465

Li, R. K., Roberts, K. G., Scoby, C. M., To, H., Musumeci, P., Sep 2012. Nanometer emittance ultralow charge beams from rf photoinjectors. Phys. Rev. ST Accel. Beams 15, 090702, doi: 10.1103/PhysRevSTAB.15.090702.
URL http://link.aps.org/doi/10.1103/PhysRevSTAB.15.090702

Lipka, D., Kleen, W., Lund-Nielsen, J., Nölle, D., Vilcins, S., Vogel, V., 2011. Dark current monitor for the european xfel. In: Proceedings of DIPAC2011, Hamburg, Germany.
URL http://accelconf.web.cern.ch/accelconf/DIPAC2011/papers/weoc03.pdf

Lipka, D., Lund-Nielsen, J., Seebach, M., 2013. Resonator for charge measurement at regae. In: Proceedings of IBIC2013, Oxford, UK.
URL http://ibic2013.org/prepress/papers/wepf25.pdf

Lu, X., Huang, W., Du, Y., Qian, H., Tang, C., 2012. R&d of an ultrafast probe apparatus based on mev electron diffraction at tsinghua university. In: Proceedings of IPAC2012, New Orleans, Louisiana, USA.
URL http://accelconf.web.cern.ch/accelconf/IPAC2012/papers/tuppc024.pdf

Luiten, O. J., van der Geer, S. B., de Loos, M. J., Kiewiet, F. B., van der Wiel, M. J., Aug 2004. How to realize uniform three-dimensional ellipsoidal electron bunches. Phys. Rev. Lett. 93, 094802, doi: 10.1103/PhysRevLett.93.094802.
URL http://link.aps.org/doi/10.1103/PhysRevLett.93.094802

Maier, A. R., Meseck, A., Reiche, S., Schroeder, C. B., Seggebrock, T., Grüner, F., Sep 2012. Demonstration scheme for a laser-plasma-driven free-electron laser. Phys. Rev. X 2, 031019, doi: 10.1103/PhysRevX.2.031019.
URL http://link.aps.org/doi/10.1103/PhysRevX.2.031019

Maitland, A., Nov 1961. New derivation of the vacuum breakdown equation relating breakdown voltage and electrode separation. Journal of Applied Physics 32 (11), 2399–

2407, doi: 10.1063/1.1777081.
URL http://dx.doi.org/10.1063/1.1777081

Mancini, G. F., Mansart, B., Pagano, S., van der Geer, B., de Loos, M., Carbone, F., 2012. Design and implementation of a flexible beamline for fs electron diffraction experiments. Nuclear Instruments and Methods in Physics Research Section A: Accelerators, Spectrometers, Detectors and Associated Equipment 691 (0), 113–122, doi: 10.1016/j.nima.2012.06.057.
URL http://dx.doi.org/10.1016/j.nima.2012.06.057

Manz, S., Casandruc, A., Zhang, D., Zhong, Y.-P., Loch, R., Marx, A., Hasegawa, T., Chung, L., Bayesteh, S., Delsim-Hashemi, H., Hoffmann, M., Felber, M., Hachmann, M., Mayet, F., Hirscht, J., Keskin, S., Hada, M., Epp, S., Floettmann, K., Miller, R., 2015. Mapping atomic motions with ultrabright electrons: Towards fundamental limits in space-time resolution. Faraday Discuss. -, –, doi: 10.1039/C4FD00204K.
URL http://dx.doi.org/10.1039/C4FD00204K

Marchesini, S., He, H., Chapman, H. N., Hau-Riege, S. P., Noy, A., Howells, M. R., Weierstall, U., Spence, J. C. H., Oct 2003. X-ray image reconstruction from a diffraction pattern alone. Phys. Rev. B 68, 140101, doi: 10.1103/PhysRevB.68.140101.
URL http://link.aps.org/doi/10.1103/PhysRevB.68.140101

Mayet, F., 2012. Simulation and characterization of the rf system and global stability analysis at the regae linear electron accelerator. master thesis. university of hamburg.
URL http://bib-pubdb1.desy.de/record/141143/files/MasterThesisFrankMayet.pdf

Mazurek, B., Cross, J., June 1987. An energy explanation of the area effect in electrical breakdown in vacuum. Electrical Insulation, IEEE Transactions on EI-22 (3), 341–346, doi: 10.1109/TEI.1987.299000.
URL http://dx.doi.org/10.1109/TEI.1987.299000

Michalik, A. M., Sherman, E. Y., Sipe, J. E., 2008. Theory of ultrafast electron diffraction: The role of the electron bunch properties. Journal of Applied Physics 104 (5), –, doi: 10.1063/1.2973157.
URL http://dx.doi.org/10.1063/1.2973157

Michalik, A. M., Sipe, J. E., 2006. Analytic model of electron pulse propagation in ultrafast electron diffraction experiments. Journal of Applied Physics 99 (5), –, doi: 10.1063/1.2178855.
URL http://dx.doi.org/10.1063/1.2178855

Michalik, A. M., Sipe, J. E., 2009. Evolution of non-gaussian electron bunches in ultrafast electron diffraction experiments: Comparison to analytic model. Journal of Applied

Physics 105 (8), –, doi: 10.1063/1.3093899.
URL http://dx.doi.org/10.1063/1.3093899

Miller, R., 1994. Energetics and dynamics of deterministic protein motion. Accounts of Chemical Research 27 (5), 145–150, doi: 10.1021/ar00041a005.
URL http://dx.doi.org/10.1021/ar00041a005

Miller, R., 2014a. Mapping atomic motions with ultrabright electrons: The chemists' gedanken experiment enters the lab frame. Annual Review of Physical Chemistry 65 (1), 583–604, pMID: 24423377, doi: 10.1146/annurev-physchem-040412-110117.
URL http://dx.doi.org/10.1146/annurev-physchem-040412-110117

Miller, R., Ernstorfer, R., Harb, M., Gao, M., Hebeisen, C., Jean-Ruel, H., Lu, C., Moriena, G., Sciaini, G., Mar 2010. "making the molecular movie": first frames. Acta Crystallographica Section A 66 (2), 137–156, doi: 10.1107/S0108767309053926.
URL http://dx.doi.org/10.1107/S0108767309053926

Miller, R. J. D., 2014b. Femtosecond crystallography with ultrabright electrons and x-rays: Capturing chemistry in action. Science 343 (6175), 1108–1116, doi: 10.1126/science.1248488.
URL http://www.sciencemag.org/content/343/6175/1108.abstract

Moriena, G., Hada, M., Sciaini, G., Matsuo, J., Miller, R. J. D., 2012. Femtosecond electron diffraction: Preparation and characterization of (110)-oriented bismuth films. Journal of Applied Physics 111 (4), –, doi: 10.1063/1.3684975.
URL http://dx.doi.org/10.1063/1.3684975

Mourou, G., Williamson, S., 1982. Picosecond electron diffraction. Applied Physics Letters 41 (1), 44–45, doi: 10.1063/1.93316.
URL http://scitation.aip.org/content/aip/journal/apl/41/1/10.1063/1.93316

Mueller, C., Harb, M., Dwyer, J. R., Miller, R. J. D., 2013. Nanofluidic cells with controlled pathlength and liquid flow for rapid, high-resolution in situ imaging with electrons. The Journal of Physical Chemistry Letters 4 (14), 2339–2347, doi: 10.1021/jz401067k.
URL http://dx.doi.org/10.1021/jz401067k

Müller, M., Paarmann, A., Ernstorfer, R., 10 2014. Femtosecond electrons probing currents and atomic structure in nanomaterials. Nat Commun 5, –.
URL http://dx.doi.org/10.1038/ncomms6292

Murooka, Y., Naruse, N., Sakakihara, S., Ishimaru, M., Yang, J., Tanimura, K., 2011. Transmission-electron diffraction by mev electron pulses. Applied Physics Letters 98 (25), –, doi: 10.1063/1.3602314.
URL http://dx.doi.org/10.1063/1.3602314

Musumeci, P., Moody, J. T., Scoby, C. M., 2008. Relativistic electron diffraction at the ucla pegasus photoinjector laboratory. Ultramicroscopy 108 (11), 1450–1453, proceedings of the Eleventh Conference on Frontiers of Electron Microscopy in Materials Science, doi: 10.1016/j.ultramic.2008.03.011.
URL http://dx.doi.org/10.1016/j.ultramic.2008.03.011

Musumeci, P., Moody, J. T., Scoby, C. M., Gutierrez, M. S., Bender, H. A., Wilcox, N. S., 2010. High quality single shot diffraction patterns using ultrashort megaelectron volt electron beams from a radio frequency photoinjector. Review of Scientific Instruments 81 (1), –, doi: 10.1063/1.3292683.
URL http://dx.doi.org/10.1063/1.3292683

Muybridge, E., 1887. Animal Locomotion - An Electro-Photographic Investigation of Consecutive Phases of Animal Movements. J.B. Lippincott Company, Philadelphia, pub. under the auspices of the University of Pennsylvania.

Naidu, S., Kamaraju, V., 1996. High Voltage Engineering. McGraw-Hill special reprint edition. McGraw-Hill.
URL http://books.google.de/books?id=OeZSAAAAMAAJ

Nevrovskiy, V., 1983. Comments on the role of space charges in initiation of electrical breakdown of vacuum gaps. Journal of Physics D: Applied Physics 16 (9), 1701.
URL http://stacks.iop.org/0022-3727/16/i=9/a=015

Nevrovsky, V. A., Rakhovsky, V. I., Zhurbenko, V. G., 1983. Dc breakdown of ultra-high vacuum gaps. Beiträge aus der Plasmaphysik 23 (4), 433–458, doi: 10.1002/ctpp.19830230410.
URL http://dx.doi.org/10.1002/ctpp.19830230410

Nie, S., Wang, X., Park, H., Clinite, R., Cao, J., Jan 2006. Measurement of the electronic grüneisen constant using femtosecond electron diffraction. Phys. Rev. Lett. 96, 025901, doi: 10.1103/PhysRevLett.96.025901.
URL http://link.aps.org/doi/10.1103/PhysRevLett.96.025901

Nobel-Media, 1902. The nobel prize in physics 1902, fischer, h.e. Nobelprize.org. Nobel Media AB 2013. Web. 4 Feb 2014.
URL http://www.nobelprize.org/nobel_prizes/chemistry/laureates/1902/

Nobel-Media, 2009. The nobel prize in chemistry 2009, a.e. yonath and t.a. steitz and v. ramakrishnan. Nobelprize.org. Nobel Media AB 2013. Web. 4 Feb 2014.
URL http://www.nobelprize.org/nobel_prizes/chemistry/laureates/2009/

Nolan, T., Singh, N., McCurdy, C. R., 2010. Ligand macromolecule interactions: Theoretical principles of molecular recognition. In: Roque, A. C. A. (Ed.), Ligand-Macromolecular Interactions in Drug Discovery. Vol. 572 of Methods in Molecular

Biology. Humana Press, pp. 13–29.
URL http://dx.doi.org/10.1007/978-1-60761-244-5_2

Norem, J., Hassanein, A., Konkashbaev, I., 2003. Mechanisms limiting high gradient rf cavities. In: Proceedings of the 2003 Particle Accelerator Conference.
URL http://accelconf.web.cern.ch/accelconf/p03/PAPERS/TPAB002.PDF

Ota, A., Yamochi, H., Saito, G., 2002. A novel metal-insulator phase transition observed in (edo-ttf)$_2$pf$_6$. Journal of Materials Chemistry 12, 2600–2602, doi:10.1039/B206293C.
URL http://dx.doi.org/10.1039/B206293C

Pabst, S., 2013. Atomic and molecular dynamics triggered by ultrashort light pulses on the atto- to picosecond time scale. The European Physical Journal Special Topics 221 (1), 1–71, doi:10.1140/epjst/e2013-01819-x.
URL http://dx.doi.org/10.1140/epjst/e2013-01819-x

Palmer, C., Flöttmann, K., Grebenyuk, J., Hirscht, J., Kleinwaechter, T., Kuhn, M., Mehrling, T., Miller, R., Schaper, L., Schnepp, M., Schwinkendorf, J.-P., Zeitler, B., Gruener, F., Osterhoff, J., 12 2011. Exploring the physics of external electron-bunch injection into laser-driven plasma wakes at regae.
URL http://fla.desy.de/publications/2011/index_eng.html

Park, H., Hao, Z., Wang, X., Nie, S., Clinite, R., Cao, J., 2005a. Synchronization of femtosecond laser and electron pulses with subpicosecond precision. Review of Scientific Instruments 76 (8), –, doi: 10.1063/1.1994922.
URL http://dx.doi.org/10.1063/1.1994922

Park, H., Nie, S., Wang, X., Clinite, R., Cao, J., 2005b. Optical control of coherent lattice motions probed by femtosecond electron diffraction. The Journal of Physical Chemistry B 109 (29), 13854–13856, pMID: 16852738, doi: 10.1021/jp052857u.
URL http://dx.doi.org/10.1021/jp052857u

Paschen, F., 1889. Ueber die zum funkenübergang in luft, wasserstoff und kohlensäure bei verschiedenen drucken erforderliche potentialdifferenz. Annalen der Physik 273 (5), 69–96, doi: 10.1002/andp.18892730505.
URL http://dx.doi.org/10.1002/andp.18892730505

Pearson, J., Harrison, J., 1969. A uniform field electrode for use in a discharge chamber of restricted size: design and performance. Journal of Physics D: Applied Physics 2 (1), 77.
URL http://stacks.iop.org/0022-3727/2/i=1/a=312

Peinsipp, N., Roos, G., Weimer, G., 2012. Röntgenverordnung RöV, 6th Edition. ecomed Sicherheit, Verlagsgruppe Hüthig Jehle Rehm GmbH.

Pfeifer, T., Spielmann, C., Gerber, G., 2006. Femtosecond x-ray science. Reports on Progress in Physics 69 (2), 443, doi: 10.1088/0034-4885/69/2/R04.
URL http://dx.doi.org/10.1088/0034-4885/69/2/R04

Piel, J., Riedle, E., Gundlach, L., Ernstorfer, R., Eichberger, R., 5 2006. Sub-20 fs visible pulses with 750 nj energy from a 100 khz noncollinear optical parametric amplifier. Opt. Lett. 31 (9), 1289–1291, doi: 10.1364/OL.31.001289.
URL http://ol.osa.org/abstract.cfm?URI=ol-31-9-1289

Pirozhenko, V., Korolev, A., Simonov, K., 2001. Compact 200-kev electron beam systems. In: Proceedings of the 2001 Particle Accelerator Conference, Chicago.
URL http://accelconf.web.cern.ch/accelconf/p01/PAPERS/FOAA012.PDF

PLM, S., 2012. Solid edge st3.
URL http://www.plm.automation.siemens.com/de_de/products/solid-edge/index.shtml

Polanyi, J. C., Zewail, A. H., 1995. Direct observation of the transition state. Accounts of Chemical Research 28 (3), 119–132, doi:10.1021/ar00051a005.
URL http://dx.doi.org/10.1021/ar00051a005

Proskurovskii, D., Puchkarev, V., Chesnokov, S., 1974. Breakdown in ultrahigh vacuum. Soviet Physics Journal 17 (7), 1025–1026, doi: 10.1007/BF00891084.
URL http://dx.doi.org/10.1007/BF00891084

Punekar, G., Thejovathi, G., Kishor, N., Dec 2003. Simulation study of borda's profile parallel plane electrode to assess electric field uniformity. In: Electromagnetic Interference and Compatibility, 2003. INCEMIC 2003. 8th International Conference on. pp. 371–374, doi: 10.1109/ICEMIC.2003.1287875.
URL http://dx.doi.org/10.1109/ICEMIC.2003.1287875

Qian, B.-L., Elsayed-Ali, H. E., 2002. Electron pulse broadening due to space charge effects in a photoelectron gun for electron diffraction and streak camera systems. Journal of Applied Physics 91 (1), 462–468, doi: 10.1063/1.1419209.
URL http://dx.doi.org/10.1063/1.1419209

Reed, B. W., 2006. Femtosecond electron pulse propagation for ultrafast electron diffraction. Journal of Applied Physics 100 (3), –, doi: 10.1063/1.2227710.
URL http://dx.doi.org/10.1063/1.2227710

Reimer, L., Kohl, H., 2010. Transmission Electron Microscopy: Physics of Image Formation. Springer-Verlag.

RIKEN, 2014. RIKEN, 1-1-1, Kouto, Sayo-cho, Sayo-gun, Hyogo 679-5148 Japan. Web. 18. Sep 2014.
URL http://www.spring8.or.jp/

Rimmer, R., 2002. A high-gradient high-duty-factor rf photo-cathode electron gun. In: Proceedings of EPAC 2002, Paris, France.

Rimmer, R., 2005. A high-gradient cw rf photo-cathode electron gun for high current injectors. In: Proceedings of 2005 Particle Accelerator Conference, Knoxville, Tennessee.

Rogowski, W., 1923. Die elektrische festigkeit am rande des plattenkondensators. Archiv für Elektrotechnik 12 (1), 1–15, doi: 10.1007/BF01656573.
URL http://dx.doi.org/10.1007/BF01656573

Ropers, C., Solli, D. R., Schulz, C. P., Lienau, C., Elsaesser, T., Jan 2007. Localized multiphoton emission of femtosecond electron pulses from metal nanotips. Phys. Rev. Lett. 98, 043907, doi: 10.1103/PhysRevLett.98.043907.
URL http://link.aps.org/doi/10.1103/PhysRevLett.98.043907

Roth, A., 1959. Hochspannungstechnik. Springer-Verlag.

Rousse, A., Rischel, C., Gauthier, J.-C., Jan 2001. Femtosecond x-ray crystallography. Rev. Mod. Phys. 73, 17–31, doi:10.1103/RevModPhys.73.17.
URL http://dx.doi.org/10.1103/RevModPhys.73.17

Rudakov, F. M., Hastings, J. B., Dowell, D. H., Schmerge, J. F., Weber, P. M., 2006. Megavolt electron beams for ultrafast time-resolved electron diffraction. AIP Conference Proceedings 845 (1), 1287–1292, doi: 10.1063/1.2263560.
URL http://dx.doi.org/10.1063/1.2263560

Rutkowski, I., Butkowski, L., Hoffman, M., Schlarb, H., Schmidt, C., 2013. Regae llrf control system overview. In: Proceedings of IPAC2013, Shanghai, China.
URL http://accelconf.web.cern.ch/accelconf/IPAC2013/papers/thpea031.pdf

Sachtler, W., Dorgelo, G., Holscher, A., 1966. The work function of gold. Surface Science 5 (2), 221–229, doi: 10.1016/0039-6028(66)90083-5.
URL http://dx.doi.org/10.1016/0039-6028(66)90083-5

Saldin, E., Schneidmiller, E., Yurkov, M., 2008. Coherence properties of the radiation from x-ray free electron laser. Optics Communications 281 (5), 1179 – 1188, doi: 10.1016/j.optcom.2007.10.044.
URL http://dx.doi.org/10.1016/j.optcom.2007.10.044

Schelev, M. Y., Bryukhnevich, G. I., Lozovoi, V. I., Monastyrski, M. A., Prokhorov, A. M., Smirnov, A. V., Vorobiev, N. S., 1998. 500-fs photoelectron gun for time-resolved electron diffraction experiments. Optical Engineering 37 (8), 2249–2254, doi: 10.1117/1.601743.
URL http://dx.doi.org/10.1117/1.601743

Schlünzen, F., Zarivach, R., Harms, J., Bashan, A., Tocilj, A., Albrecht, R., Yonath, A., Franceschi, F., 10 2001. Structural basis for the interaction of antibiotics with the

peptidyl transferase centre in eubacteria. Nature 413, 814–821, doi:10.1038/35101544.
URL http://dx.doi.org/10.1038/35101544

Schoenlein, R. W., Chattopadhyay, S., Chong, H. H. W., Glover, T. E., Heimann, P. A., Shank, C. V., Zholents, A. A., Zolotorev, M. S., 2000. Generation of femtosecond pulses of synchrotron radiation. Science 287 (5461), 2237–2240, doi: 10.1126/science.287.5461.2237.
URL http://www.sciencemag.org/content/287/5461/2237

Schümann, U., Budde, M., Kurrat, M., 9 2004. Influence of shield capacity on the breakdown voltade of vacuum tubes. In: Discharges and Electrical Insulation in Vacuum, 2004. Proceedings. ISDEIV. XXIst International Symposium on. Vol. 2. pp. 618–621, doi: 10.1109/DEIV.2004.1422693.
URL http://dx.doi.org/10.1109/DEIV.2004.1422693

Schümann, U., Kurrat, M., 2002. Break down voltage of electrode arrangements in vacuum in consideration of surface area. In: Discharges and Electrical Insulation in Vacuum, 2002. 20th International Symposium on. pp. 459–462, doi: 10.1109/ISDEIV.2002.1027408.
URL http://www.doi.org/10.1109/ISDEIV.2002.1027408

Sciaini, G., Harb, M., Kruglik, S. G., Payer, T., Hebeisen, C. T., zu Heringdorf, F.-J. M., Yamaguchi, M., von Hoegen, M. H., Ernstorfer, R., Miller, R. J. D., Mar. 2009. Electronic acceleration of atomic motions and disordering in bismuth. Nature 458 (7234), 56–59, doi: 10.1038/nature07788.
URL http://dx.doi.org/10.1038/nature07788

Sciaini, G., Miller, R., 2011. Femtosecond electron diffraction: heralding the era of atomically resolved dynamics. Reports on Progress in Physics 74 (9), 096101.
URL http://stacks.iop.org/0034-4885/74/i=9/a=096101

Sertore, D., Michelato, P., Monaco, L., Pagani, C., Stephan, F., Schreiber, S., 2007. High quantum efficiency photocathodes for rf guns. In: APAC 2007, Raja Ramanna Centre for Advanced Technology(RRCAT), Indore, India.
URL https://accelconf.web.cern.ch/accelconf/a07/PAPERS/TUPMA083.PDF

Sertore, D., Monaco, L., Michelato, P., Pagani, C., Han, J. H., Schreiber, S., 2006. High qe photocathodes at flash. In: roceedings of EPAC 2006, Edinburgh, Scotland.
URL http://accelconf.web.cern.ch/AccelConf/e06/PAPERS/WEPLS052.PDF

Settakorn, C., Hernandez, M., Woods, K., Wiedemann, H., 1998. Femtosecond electron bunches. Conf.Proc. C9803233, 731.

Shioiri, T., Kamikawaji, T., Kaneko, E., Homma, M., Jul 1996. Influence of electrode shape and electron beam treatment on conditioning in vacuum gap breakdown. In: Discharges and Electrical Insulation in Vacuum, 1996. Proceedings. ISDEIV., XVIIth International Symposium on. Vol. 1. pp. 85–88 vol.1, doi: 10.1109/DEIV.1996.545327.

Shioiri, T., Kamikawaji, T., Kaneko, E., Homma, M., Ohshima, I., 1994. Influence of electrode area on conditioning in vacuum-gap breakdown. In: Influence of Electrode Area on the Conditioning Effect in Vacuum. Vol. 2259. pp. 35–38, doi: 10.1117/12.174551.
URL http://dx.doi.org/10.1117/12.174551

Shioiri, T., Kamikawaji, T., Kaneko, E., Homma, M., Takahashi, H., Ohshima, I., 4 1995. Influence of electrode area on the conditioning effect in vacuum. Dielectrics and Electrical Insulation, IEEE Transactions on 2 (2), 317–320, doi: 10.1109/94.388258.

Sinclair, C. K., 2006. Dc photoemission electron guns as erl sources. Nuclear Instruments and Methods in Physics Research Section A: Accelerators, Spectrometers, Detectors and Associated Equipment 557 (1), 69 – 74, energy Recovering Linacs 2005 Proceedings of the 32nd Advanced {ICFA} Beam Dynamics Workshop on Energy Recovering Linacs 32nd Advanced {ICFA} Beam Dynamics Workshop on Energy Recovering Linacs, doi: 10.1016/j.nima.2005.10.053.
URL http://dx.doi.org/10.1016/j.nima.2005.10.053

Singla, R., Simoncig, A., Först, M., Prabhakaran, D., Cavalieri, A. L., Cavalleri, A., 8 2013. Photoinduced melting of the orbital order in $la_{0.5}sr_{1.5}mno_4$ measured with 4-fs laser pulses. Phys. Rev. B 88, 075107, doi:10.1103/PhysRevB.88.075107.
URL http://dx.doi.org/10.1103/PhysRevB.88.075107

Siwick, B., Dwyer, J., Jordan, R., Miller, R., 2004. Femtosecond electron diffraction studies of strongly driven structural phase transitions. Chemical Physics 299 (2-3), 285 – 305, ultrafast Science with X-rays and Electrons, doi: 10.1016/j.chemphys.2003.11.040.
URL http://dx.doi.org/10.1016/j.chemphys.2003.11.040

Siwick, B. J., Dwyer, J. R., Jordan, R. E., Miller, R. J. D., 2002. Ultrafast electron optics: Propagation dynamics of femtosecond electron packets. Journal of Applied Physics 92 (3), 1643–1648, doi: 10.1063/1.1487437.
URL http://dx.doi.org/10.1063/1.1487437

Siwick, B. J., Dwyer, J. R., Jordan, R. E., Miller, R. J. D., 2003. An atomic-level view of melting using femtosecond electron diffraction. Science 302 (5649), 1382–1385, doi: 10.1126/science.1090052.
URL http://dx.doi.org/10.1126/science.1090052

Siwick, B. J., Green, A. A., Hebeisen, C. T., Miller, R. J. D., May 2005. Characterization of ultrashort electron pulses by electron-laser pulse cross correlation. Opt. Lett. 30 (9), 1057–1059, doi: 10.1364/OL.30.001057.
URL http://ol.osa.org/abstract.cfm?URI=ol-30-9-1057

SLAC, 2005. Electron gamma shower (egs) 5. SLAC National Accelerator Laboratory, 2575 Sand Hill Road, Menlo Park, CA. Web. 9 Jan 2014.
URL http://rcwww.kek.jp/research/egs/egs5.html

SLAC, 2014. Lcls parameters. SLAC National Accelerator Laboratory, 2575 Sand Hill Road, Menlo Park, CA. Web. 9 Jan 2014.
URL https://portal.slac.stanford.edu/sites/lclscore_public/Accelerator_Physics_Published_Documents/LCLS-parameters.pdf

Spence, J., Weierstall, U., Chapman, H., 2012. X-ray lasers for structural and dynamic biology. Reports on Progress in Physics 75 (10), 102601.
URL http://stacks.iop.org/0034-4885/75/i=10/a=102601

Steffen, K. G., 1965. High Energy Beam Optics. Interscience.

Sternheimer, R., Berger, M., Seltzer, S., 1984. Density effect for the ionization loss of charged particles in various substances. Atomic Data and Nuclear Data Tables 30 (2), 261 – 271, doi: 10.1016/0092-640X(84)90002-0.
URL http://dx.doi.org/10.1016/0092-640X(84)90002-0

SwissFEL, 2014a. Paul Scherrer Institut, 5232 Villigen PSI, Schweiz. Web. 16. Aug 2014.
URL http://www.psi.ch/swissfel/swissfel-accelerator

SwissFEL, 2014b. Ultrafast phenomena at the nanoscale: Science opportunities at the swissfel x-ray laser. Paul Scherrer Institut, 5232 Villigen PSI, Schweiz. Web. 16. Aug 2014.
URL http://www.psi.ch/swissfel/InformationEN/SwissFEL_Science_Case_small.pdf

Todd, A., 2006. State-of-the-art electron guns and injector designs for energy recovery linacs (erl). Nuclear Instruments and Methods in Physics Research Section A: Accelerators, Spectrometers, Detectors and Associated Equipment 557 (1), 36 – 44, energy Recovering Linacs 2005 Proceedings of the 32nd Advanced {ICFA} Beam Dynamics Workshop on Energy Recovering Linacs 32nd Advanced {ICFA} Beam Dynamics Workshop on Energy Recovering Linacs, doi: 10.1016/j.nima.2005.10.087.
URL http://dx.doi.org/10.1016/j.nima.2005.10.087

Tokita, S., Hashida, M., Inoue, S., Nishoji, T., Otani, K., Sakabe, S., Nov 2010. Single-shot femtosecond electron diffraction with laser-accelerated electrons: Experimental demonstration of electron pulse compression. Phys. Rev. Lett. 105, 215004, doi: 10.1103/PhysRevLett.105.215004.
URL http://link.aps.org/doi/10.1103/PhysRevLett.105.215004

Trinh, N., May 1980. Electrode design for testing in uniform field gaps. Power Apparatus and Systems, IEEE Transactions on PAS-99 (3), 1235–1242, doi: 10.1109/TPAS.1980.319754.
URL http://dx.doi.org/10.1109/TPAS.1980.319754

Tufan, M. C., Namdar, T., Gümüs, H., 2013. Stopping power and csda range calculations for incident electrons and positrons in breast and brain tissues. Radiation and Environmental Biophysics 52 (2), 245–253, doi: 10.1007/s00411-013-0457-x.
URL http://dx.doi.org/10.1007/s00411-013-0457-x

van der Geer, S., de Loos, M., van Oudheusden, T., op 't Root, W., van der Wiel, M., Luiten, O., Apr 2006. Longitudinal phase-space manipulation of ellipsoidal electron bunches in realistic fields. Phys. Rev. ST Accel. Beams 9, 044203.
URL http://doi.org/10.1103/PhysRevSTAB.9.044203

van Oostrom, A., Augustus, L., 1982. Electrical breakdown between stainless-steel electrodes in vacuum. Vacuum 32 (3), 127–135, doi: 10.1016/0042-207X(82)80042-0.
URL http://dx.doi.org/10.1016/0042-207X(82)80042-0

van Oudheusden, T., de Jong, E. F., van der Geer, S. B., Root, W. P. E. M. O., Luiten, O. J., Siwick, B. J., 2007. Electron source concept for single-shot sub-100 fs electron diffraction in the 100 kev range. Journal of Applied Physics 102 (9), –, doi: 10.1063/1.2801027.
URL http://dx.doi.org/10.1063/1.2801027

van Oudheusden, T., Pasmans, P. L. E. M., van der Geer, S. B., de Loos, M. J., van der Wiel, M. J., Luiten, O. J., Dec 2010. Compression of subrelativistic space-charge-dominated electron bunches for single-shot femtosecond electron diffraction. Phys. Rev. Lett. 105, 264801, doi: 10.1103/PhysRevLett.105.264801.
URL http://dx.doi.org/10.1103/PhysRevLett.105.264801

Veisz, L., Kurkin, G., Chernov, K., Tarnetsky, V., Apolonski, A., Krausz, F., Fill, E., 2007. Hybrid dc-ac electron gun for fs-electron pulse generation. New Journal of Physics 9 (12), 451.
URL http://stacks.iop.org/1367-2630/9/i=12/a=451

Vogt, H., Schultz, H., 5 2011. Grundzüge des praktischen Strahlenschutzes, 6th Edition. Carl Hanser Verlag GmbH & Co. KG.

Waldecker, L., Bertoni, R., Ernstorfer, R., 2015. Compact femtosecond electron diffractometer with 100 kev electron bunches approaching the single-electron pulse duration limit. Journal of Applied Physics 117 (4), –.
URL http://scitation.aip.org/content/aip/journal/jap/117/4/10.1063/1.4906786

Wang, J., Loew, G., 1997. Field emission and rf breakdown in high-gradient room-temperature linac structures. SLAC-PUB-7684 -, –.
URL http://www.slac.stanford.edu/cgi-wrap/getdoc/slac-pub-7684.pdf

Watanabe, A., Deguchi, M., Kitabatake, M., 2001. Microscopic study of field emission from diamond particles. Diamond and Related Materials 10 (3âĂŞ7), 818 – 823, 11th

European Conference on Diamond, Diamond-like Materials, Carbon Nanotubes, Nitrides and Silicon Carbide, doi: 10.1016/S0925-9635(00)00588-4.
URL http://dx.doi.org/10.1016/S0925-9635(00)00588-4

Watanabe, A., Deguchi, M., Kitabatake, M., Kono, S., 2003. Field emission from diamond particles studied by scanning field emission microscopy. Ultramicroscopy 95 (0), 145 – 151, doi: 10.1016/S0304-3991(02)00311-X.
URL http://dx.doi.org/10.1016/S0304-3991(02)00311-X

Weninger, C., Baum, P., 2012. Temporal distortions in magnetic lenses. Ultramicroscopy 113 (0), 145–151, doi: 10.1016/j.ultramic.2011.11.018.
URL http://dx.doi.org/10.1016/j.ultramic.2011.11.018

Wijker, W., 1961. The electrical breakdown in vacuum. Applied Scientific Research, Section B 9 (1), 1–20, doi: 10.1007/BF02921887.
URL http://dx.doi.org/10.1007/BF02921887

Williamson, J., Dantus, M., Kim, S., Zewail, A., 1992. Ultrafast diffraction and molecular structure. Chemical Physics Letters 196 (6), 529 – 534, doi: 10.1016/0009-2614(92)85988-M.
URL http://dx.doi.org/10.1016/0009-2614(92)85988-M

Williamson, J., Zewail, A., 1993. Ultrafast electron diffraction. velocity mismatch and temporal resolution in crossed-beam experiments. Chemical Physics Letters 209 (1-2), 10–16, doi: 10.1016/0009-2614(93)87193-7.
URL http://dx.doi.org/10.1016/0009-2614(93)87193-7

Williamson, S., Mourou, G., Li, J. C. M., Jun 1984. Time-resolved laser-induced phase transformation in aluminum. Phys. Rev. Lett. 52, 2364–2367, doi: 10.1103/PhysRevLett.52.2364.
URL http://link.aps.org/doi/10.1103/PhysRevLett.52.2364

Winick, H. (Ed.), 1997. Fourth Generation Light Sources. Particle Accelerator Conference, Vancouver, B.C., Canada.
URL accelconf.web.cern.ch/accelconf/pac97/papers/pdf/FBC003.PDF

Worster, J., 1969. The brightness of electron beams. Journal of Physics D: Applied Physics 2 (3), 457.
URL http://stacks.iop.org/0022-3727/2/i=3/a=321

Wulff, M., Plech, A., Eybert, L., Randler, R., Schotte, F., Anfinrud, P., 2003. The realization of sub-nanosecond pump and probe experiments at the esrf. Faraday Discuss. 122, 13–26, doi: 10.1039/B202740M.
URL http://dx.doi.org/10.1039/B202740M

XFEL, 2014. European XFEL GmbH. Web. 28 July 2014.
URL http://www.xfel.eu/overview/facts_and_figures/

Yalcin, S., Gurler, O., Gultekin, A., Gundogdu, O., 2006. An analytical expression for electron elastic scattering cross section from atoms and molecules in 1.0 kev to 1.0 mev energy range. Physics Letters A 356 (2), 138 – 145, doi: 10.1016/j.physleta.2006.04.037.
URL http://dx.doi.org/10.1016/j.physleta.2006.04.037

Yang, J., Kan, K., Kondoh, T., Yoshida, Y., 2011a. Photoinjector based mev electron microscopy. In: Proceedings of DIPAC2011, Hamburg, Germany.
URL http://adweb.desy.de/mpy/DIPAC2011/papers/tupd85.pdf

Yang, J., Kan, K., Naruse, N., Murooka, Y., Yoshida, Y., Tanimura, K., Urakawa, J., 2011b. Femtosecond photoinjector and relativistic electron microscopy. In: Proceedings of IPAC2011, San Sebastian, Spain.
URL https://accelconf.web.cern.ch/accelconf/IPAC2011/papers/tupc057.pdf

Yang, J., Kan, K., Naruse, N., Yoshida, Y., Tanimura, K., Urakawa, J., 2009. 100-femtosecond mev electron source for ultrafast electron diffraction. Radiation Physics and Chemistry 78 (12), 1106–1111, aPSRC-2008, The Second Asia-Pacific Symposium on Radiation Chemistry, August 29 September 1, 2008, doi: 10.1016/j.radphyschem.2009.05.009.
URL http://dx.doi.org/10.1016/j.radphyschem.2009.05.009

Yonath, A., Saper, M., Makowski, I., Mussig, J., Piefke, J., Bartunik, H., Bartels, K., Wittmann, H., 2 1986. Characterization of single crystals of the large ribosomal particles from bacillus stearothermophilus. J. Mol. Biol. 187, 4, doi:10.1016/0022-2836(86)90342-6.
URL http://dx.doi.org/10.1016/0022-2836(86)90342-6

Zeitler, B., Dornmair, I., Gehrke, T., Titberidze, M., Maier, A., Hidding, B., Flöttmann, K., Grüner, F., 2013. Merging conventional and laser wakefield accelerators. Proc. SPIE 8779, 877904–877904–7, doi: 10.1117/12.2019339.
URL http://dx.doi.org/10.1117/12.2019339

Zhang, D., 2013. Femtosecond structural dynamics on the atomic length scale. Phd thesis, Fachbereich Physik der Universität Hamburg.
URL http://www.physnet.uni-hamburg.de/services/fachinfo/___Kurzfassungen/Dongfang___Zhang.htm

Zholents, A., Zolotorev, M., Wan, W., 2001. Generation of attosecond electron bunches. In: Proceedings of the 2001 Particle Accelerator Conference, Chicago.
URL http://epaper.kek.jp/p01/PAPERS/FOAC004.PDF

Zhu, P., Berger, H., Cao, J., Geck, J., Hidaka, Y., Kraus, R., Pjerov, S., Shen, Y., Tobey, R. I., Zhu, Y., Hill, J. P., Wang, X. J., 4 2013. Femtosecond time-resolved mev electron diffraction. arXiv:1304.5176 -, –.
URL http://arxiv.org/abs/1304.5176

PUBLICATIONS

Publications related to the content and the author of this work :

REGAE:

- 2015: Manz, S., Casandruc, A., Zhang, D., Zhong, Y.-P., Loch, R.A., Marx, A., Hasegawa, T., Chung, L., Bayesteh, Sh., Delsim-Hashemi, H., Hoffmann, M., Felber, M., Hachmann, M., Mayet, F., Hirscht, J., Keskin, S., Hada, M., Epp, S., Floettmann, K., Miller, R.J.D., Mapping Atomic Motions with Ultrabright Electrons: Towards Fundamental Limits in Space-Time Resolution. Faraday Discussions, 2015. http://dx.doi.org/10.1039/c4fd00204k.

- 2013: Zhang, D., Hada, M., Hirscht, J., Hayes, S. A., Pichugin, K., Casandruc, A., Manz, S., Gengler, R. Y. N., Seki, T., Matsuo, J., Moriena, G., Sciaini, G., and Miller, R. J. D., A femtosecond electron diffraction study: Electronically-driven ablation via highly localized electronic states. 15th European Symposium on Gas Electron Diffraction, Frauenchiemsee, Germany, June 23rd 2013, oral presentation.

- 2013: Zhang, D., Manz, S., Casandruc, A., Hirscht, J., Keskin, S., Nicholls, J., Pichugin, K., Hayes, S. A., Jangam, S., Hasegawa, T., Marx, A., Bayesteh, S., Delsim-Hashemi, H., Felber, M., Schlarb, H., Hoffmann, M., Huening, M., Gehrke, T., Mayet, F., Hachmann, M., Moriena, G., Epp, S., Hada, M., Floettmann, K. and Miller, R. J. D., REGAE: Towards Ultrafast Electron Diffraction and Dynamic Microscopy", 15th European Symposium on Gas Electron Diffraction, Frauenchiemsee, Germany, June 23rd-27th, 2013, poster presentation.

- 2012: Hada, M., Hirscht, J., Zhang, D., Manz, S., Pichugin, K., Mazurenko, D., Bayesteh, S., Delsim-Hashemi, H., Floettmann, K., Huening, M., Lederer, S., Moriena, G., Mueller, C., Sciaini, G. and Miller, R.J.D., 2012. REGAE: New Source for Atomically Resolved Dynamics. International Conference on Ultrafast Structural Dynamics, Berlin Germany, March 19-21, 2012, ISBN: 978-1-55752-939-8, Joint Poster (JT2A). http://dx.doi.org/10.1364/HILAS.2012.JT2A.47

- 2012: Zhang, D., Hirscht, J., Hada, M., Manz, S., Pichugin, K., Mazurenko, D. A., Bayesteh, S., Delsim-Hashemi, H., Floettmann, K., Huening, M., Lederer, S., Moriena, G., Mueller, C., Sciaini, G. and Miller, R. J. D., REGAE: New Source for Atomically Resolved Dynamics. Banff Meeting on Structural Dynamics, The Banff Center, Banff, Alberta, Canada, February 19th-22nd, 2012, poster presentation.

- 2011: Palmer, C., Floettmann, K., Grebenyuk, J., Hirscht, J., Kleinwaechter, T., Kuhn, M., Mehrling, T., Miller, R.J.D., Schaper, L., Schnepp, M., Schwinkendorf, J. -P,

Zeitler, B., Gruener, F. and Osterhoff, J. 2011. REGAE: New Source for Atomically Resolved Dynamics. HPL Meeting, Christmas Meeting of the High Power Laser Science Community, Didcot, U.K., December 14-16.
http://fla.desy.de/publications/2011/index_eng.html

- 2011: Hirscht, J., Mazurenko, D.A., Zhang, D., Hada, M., Bayesteh, S., Delsim-Hashemi, H., Floettmann, K., Huening, M., Lederer, S., Moriena, G., Mueller, C. and Miller, R.J.D. REGAE: New Source for Atomically Resolved Dynamics. Max Planck Evaluation Mai 2011 at the Flash experimental hall, DESY Hamburg.
https://regae.desy.de/e135097/e135132/

- 2010: Hirscht, J., Mazurenko, D.A., Zhang, D., Bayesteh, S., Delsim-Hashemi, H., Floettmann, K., Huening, M., Lederer, S., Moriena, G. and Miller, R.J.D. Relativistic Electron Gun for Atomic Exploration REGAE for femtosecond electron diffraction, 1st CFEL-Symposium 2011 at Sylt Quelle, 18.-20.03.2011.
https://regae.desy.de/e135097/e135149/

E-Gun 300:

- 2014: Hada, M., Zhang, D., Pichugin, K., Hirscht, J., Kochman, M.A., Hayes, S.A., Manz, S., Gengler, R.Y.N., Wann, D.A., Seki, T., Moriena, G., Morrison, C.A., Matsuo, J., Sciaini, G. and Miller, R.J.D., 2014. Cold ablation driven by localized forces in alkali halides. Nature Communications 5, article number: 3863. doi:10.1038/ncomms4863. Nature Publishing Group, a division of Macmillan Publishers Limited. All Rights Reserved.
http://dx.doi.org/10.1038/ncomms4863

Gas-Phase setup:

- 2015: Ishikawa, T., Hayes, S.A., Keskin, S., Corthey, G., Hada, M., Pichugin, K., Marx, A., Hirscht, J., Miller, R.J.D., Shionuma, K., Onda, K., Okimoto, Y., Koshihara, S.-Y., Yamamoto, T., Hengbo, C., Nomura, M. and Kato, R., 2015. Direct Observation of Collective Modes Coupled to a Molecular Orbital Driven Photoinduced Phase Transition. Submitted to Science.

FED-CAMM:

- 2015: Hirscht, J. High voltage feedthrough assembly, time-resolved transmission electron microscope and method of electrode manipulation in a vacuum environment. PCT 08/2015.

- 2014: Hirscht, J. High voltage feedthrough assembly, electron diffraction apparatus and method of electrode manipulation in a vacuum environment. EP 08/2014.

A STOPPING POWER & SCATTERING POWER

A.1 MASS STOPPING POWER

The terms of the sum for the mass stopping power (equation 2.12) are given by [ICRU (1984)]:

$$\left(\frac{S}{\rho}\right)_{col} = \frac{2\pi r_e^2 m_e c^2 N_A Z}{\beta^2 M_A} \cdot \left\{ ln\left[\frac{\tau^2(\tau+1)}{2\left(\frac{I}{m_e c^2}\right)^2}\right] + F(\tau) - \delta \right\} \tag{A.1}$$

and

$$\left(\frac{S}{\rho}\right)_{rad} = \frac{4r_e^2\alpha}{\beta^2} N_A \frac{Z(Z+1)}{M_A} (\tau+1) m_0 c^2 \cdot ln\left(183\, Z^{-\frac{1}{3}} + \frac{1}{18}\right). \tag{A.2}$$

In these equations, r_e denotes the radius of the electron, which is given by $e^2/\left(m_e c^2\right) = 2.818 \cdot 10^{-15}$ m, N_A means the Avogadro constant (=6.02252$\cdot$ 1o^{23} mol^{-1}), Z the atomic number, $\beta = v/c_{vac}$, M_A the molar mass of substance A, $\tau = E/\left(m_0 c^2\right)$, I the mean excitation energy, $m_0 c^2$ the rest energy of the electron. $F(\tau)$ is given by

$$F(\tau) = 1 - \beta^2 + \frac{\frac{\tau^2}{8} - (2\tau+1)\, ln2}{(\tau+1)^2}, \tag{A.3}$$

where α denotes the fine structure constant and δ the density effect correction [Sternheimer et al. (1984)]. The density effect is the polarization of a dense material. In an optically dense medium, in which the particle exceeds the speed of light (v_{light} = c/n, with n denoting the refractive index of that medium), the energy loss caused by soft collisions is observed as blue light or Čerenkov radiation.

A.2 MASS SCATTERING POWER

Analogous to the mass stopping power, a mass scattering power can be defined by [ICRU (1984)]:

$$\frac{T}{\rho} = \frac{1}{\rho}\frac{d\overline{\Theta^2}}{dl}. \tag{A.4}$$

A more exact expression evaluates the screening effects of the nucleus:

$$\frac{T}{\rho} = \pi\left(\frac{2r_e Z}{(\tau+1)\beta^2}\right)^2 \frac{N_A}{M_A}\left\{ ln\left[1+\left(\frac{\Theta_m}{\Theta_\mu}\right)^2\right] - 1 + \left[1+\left(\frac{\Theta_m}{\Theta_\mu}\right)^2\right]^{-1}\right\}, \tag{A.5}$$

with Θ_m denoting the cut-off or critical angle, beyond which elastic scattering does not occur because of the limited size of the nucleus:

$$\Theta_m = \frac{2A^{-\frac{1}{3}}}{\alpha\beta\left(\tau+1\right)} \tag{A.6}$$

Θ_μ is the screening angle, which describes a minimal angle of scattering determined by the screening of the nucleus by the orbital electrons.

$$\Theta_\mu = 1.130\frac{\alpha Z^{\frac{1}{3}}}{\beta\left(\tau+1\right)} \tag{A.7}$$

A.5 does not include electron-electron scattering, which can be included in appropriate manner by replacing Z^2 with $Z\left(Z+1\right)$. For thin absorbers, this formula is only marginally applicable. Single large-angle scattering events are majorly occurring within this regime.

B REGAE SIMULATIONS

General and REGAE simulation parameters		
Klystron		
ν	2.998	GHz (S-band)
total power	24	[MW]
max. repetition rate	50	[Hz]
Cavities		
1^{st} (photo-cathode-) cavity	1.5	cells
rf power	17	[MW]
$\Delta\ E_{max,cav_1}$ (at the photo-cathode)	110.0	[MV/m]
$\Delta\ E_{avg,cav_1}$	41.27	[MV/m]
Φ_{nom,cav_1}	0	[deg]
$\Phi_{emission,cav_1}$	35	[deg]
2^{nd} (buncher-) cavity	4.0	cells
rf power	6	[MW]
$\Delta\ E_{max,cav_2}$	25.00	[MV/m]
$\Delta\ E_{avg,cav_2}$	7.70	[MV/m]
Φ_{nom,cav_2}	-90	[deg]
Additional simulation parameters		
Laser pulse length	500	[fs]
Laser focus on photo-cathode	7	[μm,rms]
Macro-particles	1	$\cdot 10^5$
Charge	80	[fC]
ϵ_x/ϵ_y	0.8077	[nm, rms]
divergence x/y	-3.8865/-1.3241	$\cdot\ 10^{-9}$ [mrad]
$E_{kin,avg}$	5	[MeV]
Solenoids		
$B_{z,max}$ 0.551 m	0.16	[T]
$B_{z,max}$ 0.892 m	0.11	[T]

Table 15: General and additional parameters used for the ASTRA simulations of section 3.4.1. They are completed with the specification of positions of REGAE beamline elements, which are provided in Delsim-Hashemi et al. (2013).

C FED-CAMM SIMULATIONS

FED-CAMM simulation parameters and results										
Gap [mm]	2	4	6	8	10	12	14	16	18	20
Volt [keV]	30	60	90	120	150	180	210	240	270	300
# e_1^-	10^4									
ΔE_1 [eV]	0.2									
Laser pulse duration [fs]	40	35	35	35	40	35	35	40	35	35
Spot size [μm]	200	200	200	200	200	200	200	200	200	200
$\Delta t_{1mm}[fs, fwhm]$	110	106	107	103	108	103	109	111	105	108
$\Delta t_{10mm}[fs, fwhm]$	122	112	111	107	110	105	110	113	107	114
# e_1^-	10^4									
ΔE_2 [eV]	0.6									
Laser pulse duration [fs]	35	35	35	40	35	35	35	35	35	35
Spot size [μm]	200	200	200	150	200	200	150	200	200	200
$\Delta t_{1mm}[fs, fwhm]$	165	176	172	174	173	173	172	174	165	177
$\Delta t_{10mm}[fs, fwhm]$	177	181	176	178	174	175	173	176	167	180
# e_2^-	10^5									
$\Delta E_1[eV]$	0.2									
Laser pulse duration [fs]	35	35	35	35	35	35	40	35	35	35
Spot size [μm]	200	200	200	200	200	200	200	200	200	200
$\Delta t_{1mm}[fs, fwhm]$	139	134	139	148	145	152	155	164	159	136
$\Delta t_{10mm}[fs, fwhm]$	258	194	178	179	160	174	174	177	173	168
# e_2^-	10^5									
$\Delta E_2[eV]$	0.6									
Laser pulse duration [fs]	35	40	35	35	35	35	45	35	35	35
Spot size [μm]	200	200	200	200	200	200	200	200	200	200
$\Delta t_{1mm}[fs, fwhm]$	202	208	207	215	216	220	219	220	222	201
$\Delta t_{10mm}[fs, fwhm]$	308	258	240	242	229	238	234	232	234	231

Table 16: Simulated electron pulse durations for various settings of the FED-CAMM instrument, as illustrated in figure 32 and figure 33 of section 5.3.2, including statistical errors as specified at the beginning of that section.

FED-CAMM simulation parameters and results					
# e^-, ΔE	10^4, 0.2 eV				
	Field Gradient [MV/m]				
	26.3	20.0	15.0	10.0	7.5
Energy [keV]	Electron pulse duration [fs, fwhm]				
100	67.11	84.55	110.08	155.87	209.86
200	67.53	82.35	110.98	159.67	233.07
300	68.93	84.47	110.43	168.30	210.86
Std.dev.	0.78	1.05	0.37	5.20	10.71
# e^-, ΔE	10^5, 0.2 eV				
	Field Gradient [MV/m]				
	26.3	20.0	15.0	10.0	7.5
Energy [keV]	Electron pulse duration [fs, fwhm]				
100	80.47	105.59	140.51	226.20	345.39
200	83.84	111.10	150.97	271.61	382.95
300	84.06	118.80	170.09	291.87	412.22
Std.dev.	1.64	5.42	12.25	27.45	27.36

Table 17: Simulated electron pulse durations obtained for various settings of the FED-CAMM instrument, as illustrated in figure 34 and figure 35 of section 5.3.2, including statistical errors as specified at the beginning of that section.

LIST OF FIGURES

Figure 49 Comparison of worldwide FED setups with the instruments developed in this work. The big blue arrow indicates the former increase of time resolution with energy as one of the majorly changing parameters. The red dot denotes the REGAE with ≈ 5 MeV and 900 fs (fwhm) electron pulses. The green line marks the capability of the compact E-Gun 300, ranging from 690 to 250 fs (fwhm). The purple line marks the temporal resolution of the FED-CAMM instrument, ranging below 120 fs (fwhm), potentially below 70 fs (fwhm) for all applied potentials. The competitors inconsistently provide rms and fwhm specifications, mostly not specified at all. Thus many data points, especially those of a few MeV, have to be shifted by a factor of 2.355 towards longer electron pulse duration. 156

LIST OF TABLES

ACKNOWLEDGEMENTS

I thank Prof. R.J. Dwayne Miller for letting me engrave myself in the development of new and leading electron source technology, my means of contribution to his efforts in respect of molecular movies. It was my pleasure to work independently and self-directed on the development of the FED-CAMM instrument during the second half of my PhD work. This was made possible by further trust in my person, my skills and potentials, the allocation of financial resources and granted time within the employment in the Max Planck group and later Max Planck institute, the joint research center CFEL and the DESY campus in Hamburg. Within this setting I could design and build the groups' new instruments, which form the content of this work.

I thank A.Z. Rahmatian, who introduced me to the CFEL and to Prof. H.N. Chapman back in 2010. Prof. Chapman directed me to the group of Prof. Miller, thus I thank Prof. Chapman for the acquaintance of myself with Prof. Miller.

At least one person is required for a novel idea, but more than one person is required for the implementation, assuming that the idea includes more than a computer algorithm or a copious theory. The successful implementation of my own ideas in regard of all developed instruments was dependent on the contribution of many other people.

Within the administration of the MPSD, I thank Dr. Monika Kämpfe and Ute Kaluza for their kind organizational support throughout all years of my PhD work. I equally thank Dagmar Schröder-Huse, Kathja Schröder, Ulrike Krieger, Tania Hartin, Andre Hein, Diana Hoppe, Sonia Utermann, Carolin Wodars and Frauke Kleinwort. I sincerely thank Dr. Ralf Köhn and Dr. Faton Krasniqi from CFEL, Ernst Möller and Dr. Tluczykont from the University, Klaus Witt, Norbert Tesch, Wolfgang Clement, Hans-Peter Heinrich and Albrecht Leuschner from DESY and DESY D3 for their support in respect of the radiation safety work, which mostly concerned the compact setups. From the computer deck I thank Peter Johanssen, Björn Witt and Alina Mätzold for their very kind support. From the CUI I thank Claudia Busch, Heiko Kraus and once again Prof. Chapman.

Excellent infrastructural support within DESY in the sphere of REGAE was initially provided by Kurt Müller, Dietmar Ebbrecht and Jürgen Hannemann, and within CFEL by Nils Joehnke, Gisbert Mantei, Andreas Bogdan, Dietmar Pietschok and Wolfgang Steiner. Within the close proximity of the CFEL I am thankful for the continuous support of Claus Seeger and Wolfgang Weppner.

As my work is mostly experimental, I have to thank all leaders and coordinators of the workshops on DESY ground for their excellent and kind support during all projects and their numerous employees. Many thanks go to Thorsten Schlüter, Manfred Pieper and Rene Meyer, Lothar Klein and Jürgen Teichmeier, Stephan Fleig and Frank Jonas. Within these workshops I thank all employees, who were involved in manufacturing little and large amounts of parts for the new setups and who were all willing to try and test the feasibility of new manufacturing approaches using the present utilities. Many thanks go to Fernando Borges, Matthias Bötcher, Jörg Erfurth, Andrea Guss, Rolf Hansen, Dirk Liebertz, Wolfgang Menck, Wolfgang Seeck and Dmitrij Seibel. I also thank Murat Güler, Alexander Kim, Tim Lensch, Uwe Packheiser, Stephan Rath, Peter Reichenbach, Timo Sgonina and Jörg Stephan for their solid and kind support during all of the past years and projects. I thank Kurt Bohle, Jörg Dams, Tim Erke, Daniel Grosse, Jonas Hölzer, Hillmer Kosch, Bernd Krambeer, Markus Link, Gernot Mahler, Thomas Marckmann, Jan-Hendrik Meyer, Christian Reimers, Karsten Scheef and all previous and currently present trainees for their involvement in state-of-the-art scientific instrument development. Special thanks go to Mecki Meklenburg for his counseling support and fine machining skills during the installation and completion of my work in the CFEL. The same is true for the intense efforts of engineer Josef Gonschior, senior Otto Peters and Gernot Maler. I also thank Michael Plönsky-Mackenthun, again Tim Erke and others, who assisted and trained me in manufacturing and processing a few of my own instrument components as a required means to speed up manufacturing, made possible in cooperation with the workshop leaders. I thank Björn Hager, Carsten Conrad, Andreas Bremer and colleagues from ZM1 for always quickly supporting my requests with a resulting high level of customer satisfaction. From the same department I thank Cornelius Martens and Martin Lemke for their help in the REGAE project. I thank Bernd Schwitzky and his colleagues for supportive electric consultation. I especially thank Fred Knof and Ali Ashgar from the quality control department of DESY for their support. Special thanks go to Bernd Hentschel for his perfected lens winding skills that concern all compact setups. I thank Jochen Küpper, Nele Müller and Jens S. Kienitz for support and encouraging discussions about high voltage breakdown mechanisms. I thank Karol Dlugolecki and his colleagues for discussions and solid support in their labs. I thank Ottfried Geffert for his temporary computer and hardware service and Friedjof Tellkamp, who is satisfactory continuing and finishing these tasks. I thank Kim Heuck and Paul Fuchs for their instant help in cleaning prototype components. In this matter I also thank Jörg Ziegler and Klaudia Hagemann for their kind and quick support. I thank Kai Ludwig for his kind and engaged assistance. I thank Oliver Becker, Holger Meyer and Sven Gieschen for discussions and help. I thank the IPP support group around Hauke Krohn for the introduction of and training in Solid Edge and continuous support by Hauke Krohn, Ulrike Büchler and Volker Rupprecht. For the same reason, I have to thank DESY engineers Jens Tiessen, Thorsten Wohlenberg and former DESY engineer Marcus

Barenscheer for their first assistance in engineering that concerned the REGAE. I would like to thank the other group members of MVS who were especially supportive within the first projects. This is among others Christian Buhr, Stefan Holm, Sven Lederer, Lutz Lilje, Bernd Nagel, Helmut Remde, Marco Schroeder, Jens Tiessen, Peter Toedten, Torsten Wohlenberg and Antonio de Zubiaurre Wagner. I sincirely thank Susan Dexheimer and Cheng Lu for their help in the preparation of an interesting specimen system for further studies.

I thank my kind co-workers and group members for the pleasant atmosphere in and outside of work. I especially thank the elder group members which I first met in our group, namely Ryan Cooney, Raymond Gao, Hubert Jean-Ruel, Gustavo Moriena and German Sciaini. I am also grateful for the acquaintance of all those people who started with and past myself. Special thanks go to my colleague Dongfang Zhang for his support with the optical installations at the FED-CAMM. I also thank Valentyn Prokhorenko in this regard. I thank Valentyn for granting me access to machinist Wolfgang Cleophas, whom I thank for his instant assistance and the manufacturing of several parts.

I thank Jose R. Crespo Lopez-Urrutia for his initial elucidation of high voltage design considerations and further advice regarding the very important subject of radiation safety. Among the first people I met in the sphere of my work were Jutta Pelz and Benno Frensche, who were helping us with the design and construction of the envisaged new installations in the REGAE building. I thank the DESY group employees of MDI, MEA, MKK, MKS and BAU for their kind support and every other person who was involved with my work but whom I forgot to explicitly mention. Each of you has contributed in a very crucial aspect and only by your contribution my experimental work was made possible. Thus I also thank all companies for their regularly kind and occasionally outstanding customer support. For reading and commenting bits or large sections of this work, I thank Jason Biggs, Sergio Coelho, Edward Cooper, Antonia Karamatskou, Tuathan O'Shea, Philipp Pelz and R.J.Dwayne Miller.

Among the last people who were involved with my work and to whom I am thankful are the people working at the Max Planck Society, the Max Planck Innovation GmbH and associated partners. I am very thankful for your support in matters that range beyond the scope of science and in which scientists unfortunately have little or no experience.

At last I want to thank my entire family and my much loved Antonia for their long-standing support and love. This is for you.